

**Advances in Synthesis and Application of Poly(Amino Acid)s  
and Polyesters**

Jason Rowley

Submitted in accordance with the requirements for the degree of Doctor of  
Philosophy

The University of Leeds  
School of Chemistry

December 2021

The candidate confirms that the work submitted is his own, except where work which has formed part of jointly-authored publications has been included. The contribution of the candidate and the other authors to this work has been explicitly indicated below. The candidate confirms that appropriate credit has been given within the thesis where reference has been made to the work of others.

In Chapter 3, S. Chana synthesised the TiO<sub>2</sub>-NPs and characterised them. For Chapter 4, P. A. Wall synthesised and conducted an FTIR spectrum of the CND/CaNP-ABPA nanocomposite, H. Yu synthesised some of the NCA monomers used, M. J. Howard assisted with solution-state NMR analysis, D. L. Baker conducted solid-state NMR analysis, and A. Kulak conducted TGA and SEM analysis. The CNDs and CaNPs were synthesised by both D. C. Green and J. V. Rowley, whilst all polymers and nanocomposites were synthesised and characterised by J. V. Rowley. In Chapter 6, the PGI, dyed-PGI, dyed-PGI organogels, and dyed cross-linked PGI organogels were synthesised by both J. V. Rowley and P. A. Wall. The thiol-modified dyes were prepared by P. A. Wall. Characterisation was performed by both J. V. Rowley and P. A. Wall. Blue coloured, cross-linked organogels were prepared by J. V. Rowley, whilst antimicrobial testing of such was conducted by J. J. Vernon. In Chapter 7, polymers were synthesised by both J. V. Rowley and J. Exley, whilst J. V. Rowley conducted polymer characterisation. Dye deposition, leeching and simulated washing experiments were conducted by J. Exley and in-house at P&G, Longbenton, Newcastle.

This copy has been supplied on the understanding that it is copyright material and that no quotation from the thesis may be published without prior acknowledgement.

## Acknowledgements

First and foremost, I'd like to thank my PhD supervisor, Dr Paul Thornton, for developing my passion for macromolecules, for your patience and dedication, excellent feedback, and top polymer craic. You have been a good friend through my PhD journey, and I hope to keep in touch! I'd also like to thank the University of Leeds for funding via the Gunnell and Matthews Scholarship.

To Dr David Green, thank you for firstly making phosphorescent chalk, which is very entertaining to watch, and also for training me on many analytical instruments and providing guidance at the start of the CaNP work. I'd like to thank Dr Algy Kazlauciusas for SEM and DSC analysis, and thoughtful discussions. I'd also like to thank Dr Alex Kulak for TGA and SEM analysis. For helping with NMR studies, I'd like to thank Dr Mark Howard and Dr Daniel Baker, and for running lots of HPLC samples I'd like to thank Martin Huscroft and Dr Jeanine Williams. Also, I'd like to thank Dr Jon Vernon for your thorough antimicrobial testing, and Simran Chana for providing some titanium dioxide nanoparticles.

To past and present members of the Thornton group, I'd like to say thank you for thoughtful discussions and for working well as a team, specifically Dr Huayang Yu and Dr Saskia Boardman. I hope I helped previous masters students as much as they helped me develop; in particular I'd like to thank James Exley for making some very interesting PET-PEG polymers and conducting laundry tests, and Paddy Wall for stellar work on polyglobalide. I'd like to thank all those in 3.14 for your friendship and lab banter, in particular Simran Chana, Dan Patterson, David Martin, Rashmi Seneviratne, Marcos Arribas and Andrew Booth.

I'd like to also thank my family, especially Mum and Dad, for your encouragement and support. Finally, I'd like to thank my partner, Liam Robinson, for your support, care, and patience along this PhD journey.

## Abstract

The excellent mechanical and chemical resistance of many polymers leads to their persistence in the environment, and as such biodegradable alternatives are urgently sought. Additionally, many commodity polymers are coloured to add value, but common polyesters lack suitable chemical functionality to enable efficient dyeing resulting in coloured wastewater, leading to aesthetic, ecological and environmental issues. This Thesis aims to address these issues by covalently dyeing polyesters and by developing the synthesis and applications of biodegradable polymers.

Firstly, amphiphilic polysarcosine (PSar)-based polymers were synthesised presenting a terminal phosphonate functional group. The biodegradable and biocompatible amphiphilic polymers formed nanoparticles capable of encapsulating the chemotherapeutic doxorubicin and releasing the drug in acidic solutions. Fluorescent and phosphorescent calcium carbonate nanoparticles were functionalised with the PSar-based polymers via a phosphonate-oxygen-metal (P-O-M) bond. The resulting nanocomposites displayed pH-responsiveness, releasing doxorubicin in an acidic environment whilst simultaneously losing afterglow, showing promise as early-stage candidates as theranostic devices. Secondly, for the first time, stannous octoate-catalysed ring opening polymerisation of alanine anhydride was reported, initiated from poly(ethylene glycol) (PEG) methyl ether. The resulting PEG-*block*-polyalanine amphiphilic copolymers possessed high equivalence of polyalanine, and formed nanoparticles which displayed stimuli-responsiveness with respect to pH for doxorubicin release. Thirdly, the covalent grafting of thiol-modified dyes to polyglobalide, an aliphatic polyester presenting a C=C double bond within the polymer chain, is reported. The efficiently dyed polymer could also be cross-linked and swollen in organic solvents and oils. When swollen in the antimicrobial 2-phenylethanol, organogels formed which demonstrated significant antimicrobial activity. Finally, PEG-*block*-poly(ethylene terephthalate) was modified to contain an aromatic amine which could undergo *in situ* colouration, creating no coloured wastewater. The resulting coloured polyester has

application in advanced laundry formulations as optical brighteners and soil release polymers.

## Table of Contents

<b>Acknowledgements</b> .....	<b>iii</b>
<b>Abstract</b> .....	<b>iv</b>
<b>Table of Contents</b> .....	<b>vi</b>
<b>List of Figures</b> .....	<b>xi</b>
<b>List of Tables</b> .....	<b>xv</b>
<b>List of Schemes</b> .....	<b>xvi</b>
<b>Common Abbreviations</b> .....	<b>xviii</b>
<b>Chapter 1 Introduction</b> .....	<b>1</b>
1.1 Step-Growth Polymerisation Reactions .....	3
1.1.1 Poly(ethylene terephthalate) (PET) .....	4
1.1.2 Polyamides .....	7
1.1.3 Issues with step-growth polymers .....	7
1.2 Poly(amino acid)s (PAAs) .....	8
1.2.1 Introduction to PAAs .....	8
1.2.2 Synthesis of PAAs.....	9
1.2.3 Poly(amino acid) (PAA) architectures .....	11
1.3 Controlled Polymerisation Reactions.....	14
1.3.1 Chain-Growth Condensation Polymerisations (CGCP) .....	15
1.3.2 Ring-Opening Polymerisation (ROP) .....	16
1.3.3 <i>N</i> -Carboxyanhydride (NCA) ROP .....	20
1.4 Polymers as Biomaterials.....	25
1.4.1 Nanoparticles (NPs) as drug delivery vehicles .....	26
1.4.2 Hydrogels for drug delivery and tissue engineering .....	31
1.4.3 Theranostic devices .....	32
1.5 Summary and Future Outlook .....	34
1.6 Research Aims and Thesis Outline .....	35
1.7 References .....	36
<b>Chapter 2 Instrumentation, Materials and General Methods</b> .....	<b>46</b>
2.1 Instrumentation.....	46
2.1.1 Advanced Polymer Chromatography (APC).....	46
2.1.2 Centrifugation, Sample Drying and Lyophilisation.....	46
2.1.3 Dynamic Light Scattering (DLS) and Zeta Potential Analyses	46
2.1.4 Differential Scanning Calorimetry (DSC).....	47

2.1.5	Fourier-Transform Infrared Spectroscopy (FTIR).....	47
2.1.6	High-Performance Liquid Chromatography (HPLC).....	47
2.1.7	Incubation at 37 °C.....	48
2.1.8	Nuclear Magnetic Resonance (NMR) Spectroscopy.....	48
2.1.9	Powdered X-Ray Diffraction (pXRD).....	49
2.1.10	Raman Microscopy.....	49
2.1.11	Scanning Electron Microscopy (SEM).....	49
2.1.12	Thermogravimetric Analysis (TGA).....	50
2.1.13	UV-vis Spectrophotometry.....	50
2.2	Materials.....	50
2.3	General Methods.....	53
2.3.1	Synthesis of NCA monomers.....	53
2.3.2	Preparation of PBS buffer solution at pH 7.4.....	55
2.3.3	Dropping-In Method of NP Formation.....	55
2.3.4	Doxorubicin Loading and Release.....	55
2.4	References.....	58
<b>Chapter 3 Phosphonate-Terminated Amphiphilic Polymers as Biomaterials and for Metal Chelation.....</b>		<b>59</b>
	Abstract.....	59
3.1	Introduction.....	59
3.1.1	Phosphonate-containing polymers.....	59
3.1.2	Drug delivery of a hydrophobic chemotherapy drug.....	64
3.1.3	Alternatives to ubiquitous PEG in drug delivery vehicles.....	65
3.1.4	Summary.....	67
3.2	Experimental Details.....	67
3.2.1	Synthesis of HUPA-PSar polymers.....	67
3.2.2	Dox release.....	68
3.2.3	HUPA-PSar <sub>181</sub> self-assembly with TiO <sub>2</sub> -NPs to form TiO <sub>2</sub> -NCs	69
3.3	Results and Discussions.....	70
3.3.1	NCA ROP initiated from the hydroxyl group on HUPA.....	70
3.3.2	NP formation, Dox loading and release.....	74
3.3.3	HUPA-PSar conjugation with metals via P-O-M bond.....	77
3.4	Conclusions.....	79
3.5	References.....	80

<b>Chapter 4 Carbon nanodot-containing polymer-calcium carbonate nanocomposite as a theranostic doxorubicin delivery vehicle.....</b>	<b>84</b>
Preamble .....	84
Abstract .....	84
4.1 Introduction .....	85
4.1.1 Drug-delivery vehicles.....	85
4.1.2 Theranostics .....	86
4.1.3 Calcium carbonate .....	88
4.1.4 Summary.....	90
4.2 Experimental Details .....	91
4.2.1 CND/CaNP synthesis and surface-functionalisation with ABPA or HUPA.....	91
4.2.2 Nanocomposite syntheses .....	92
4.2.3 Synthesis of polymers for comparison, DLS, and for the grafting-to approach .....	93
4.2.4 Dox release study .....	95
4.2.5 Afterglow lifetime analysis (stroboscopy) .....	96
4.3 Results and Discussion .....	97
4.3.1 CND/CaNP synthesis and functionalisation .....	97
4.3.2 CND/CaNP-PAA nanocomposite synthesis .....	100
4.3.3 Nanocomposites as drug release vehicles.....	110
4.4 Conclusions.....	114
4.5 References.....	115
<b>Chapter 5 Novel route to PEG-<i>block</i>-polyalanine: tin-catalysed ring-opening polymerisation of alanine anhydride .....</b>	<b>118</b>
Abstract .....	118
5.1 Introduction .....	118
5.1.1 Problems encountered synthesising PAla via NCA ROP ....	119
5.1.2 ROP of alanine anhydride .....	119
5.1.3 PEG- <i>b</i> -PAla block copolymers.....	120
5.1.4 Summary.....	121
5.2 Experimental Details .....	122
5.2.1 Synthesis of PEG- <i>b</i> -PAla copolymers.....	122
5.2.2 Catalyst loading on kinetics investigation.....	122
5.2.3 NP formation and Dox release .....	123
5.3 Results and Discussion .....	124
5.3.1 Copolymer synthesis.....	124

5.3.2	Polymer NP formation .....	128
5.3.3	Dox release study of the polymers .....	129
5.4	Conclusions.....	131
5.5	References .....	132
<b>Chapter 6</b>	<b>Antimicrobial Dye-Conjugated Polyglobalide-Based Organogels .....</b>	<b>134</b>
	Preamble .....	134
	Abstract.....	134
6.1	Introduction.....	134
6.1.1	Polyglobalide (PGI) .....	135
6.1.2	Covalent dyeing of PGI .....	136
6.1.3	Antimicrobial Organogels .....	137
6.1.4	Summary.....	138
6.2	Experimental Details.....	138
6.2.1	Synthesis of PGI.....	138
6.2.2	Synthesis of DR1 3-mercaptopropionate (2) and DB3 3-mercaptopropionate (3).....	139
6.2.3	Dyeing of PGI with DR1 3-mercaptopropionate or DB3 3-mercaptopropionate .....	140
6.2.4	PGI organogels .....	141
6.2.5	Antimicrobial activity testing of the cross-linked organogels.....	142
6.3	Results and Discussion .....	144
6.3.1	Polymer and dye synthesis .....	144
6.3.2	Covalent conjugation of PGI with DR1 3-mercaptopropionate (2) and DB3 3-mercaptopropionate (3).....	148
6.3.3	PGI-based physical organogels.....	151
6.3.4	PGI-based cross-linked chemical organogels .....	152
6.3.5	Antimicrobial activity of the chemical organogels.....	155
6.4	Conclusions.....	157
6.5	References .....	157
<b>Chapter 7</b>	<b>Covalent colouration of an amphiphilic polyester by <i>in situ</i> chromophore creation for advanced laundry formulations.....</b>	<b>160</b>
	Preamble .....	160
	Abstract.....	160
7.1	Introduction.....	161
7.1.1	Traditional methods of dyeing PET and associated issues .....	161
7.1.2	Soil release polymers (SRPs) and optical brighteners in advanced laundry formulations .....	163

7.1.3	Summary.....	164
7.2	Experimental Details .....	165
7.2.1	Synthesis of P1 .....	165
7.2.2	Simulated dye transfer inhibition of P1 .....	166
7.2.3	Synthesis of P2: conjugation of 2-amino-3,5-dinitrothiophene to P1.....	167
7.2.4	Tests of P2 in laundry applications .....	168
7.2.5	Synthesis of P3: sulfanilamide conjugation to P1 .....	169
7.3	Results and Discussion .....	170
7.3.1	Amphiphilic PET-PEG synthesis and capability to be a SRP 170	
7.3.2	Colouration of P1 and fabric dyeing ability .....	173
7.3.3	Sulfanilamide conjugation to P1 .....	176
7.4	Conclusions.....	178
7.5	References.....	178
	<b>Concluding Remarks and Future Works.....</b>	<b>181</b>
	<b>List of Publications.....</b>	<b>183</b>

## List of Figures

<b>Figure 1.1</b> Synthesis of antimicrobial PET- <i>g</i> -EGDE-PHMG by firstly surface-functionalising PET (a) followed by covalent conjugation of EGDE-PHMG to the functionalised PET surface (b).....	<b>6</b>
<b>Figure 1.2</b> R group for 20 common proteinogenic $\alpha$ -amino acids.....	<b>9</b>
<b>Figure 1.3</b> (a) Example of a PAA, poly(Phe) which can be synthesised by protein biosynthesis, SPPS or NCA ROP. (b) Synthesis of polypeptide-polymer conjugate via SPPS-peptide synthesis followed by RAFT polymerisation.....	<b>10</b>
<b>Figure 1.4</b> Examples of an $\alpha$ -helix and $\beta$ -sheet conformation, and a micelle and vesicle polymeric nanoparticle. ....	<b>12</b>
<b>Figure 1.5</b> Co-delivery of cisplatin prodrug and paclitaxel from PLGA-PEG NP for treating lung cancer with improved efficacy to radiotherapy and traditional chemotherapy.....	<b>27</b>
<b>Figure 1.6</b> Synthesis of PBLG- <i>b</i> -PSar and PLys(Z)- <i>b</i> -PSar via sequential NCA ROP, followed by aggregation with a drug forming drug-loaded polymer micelles.....	<b>28</b>
<b>Figure 1.7</b> Polymer-metal hybrid nanocomposite examples.....	<b>30</b>
<b>Figure 1.8</b> Illustration of the subcutaneous <i>in situ</i> gel formation for cartilage regeneration.....	<b>31</b>
<b>Figure 1.9</b> Theranostic examples.....	<b>33</b>
<b>Figure 2.1</b> UV-vis calibration curve of Dox free base in PBS buffer solution at pH 7.4 and acetate buffer solution. ....	<b>56</b>
<b>Figure 2.2</b> HPLC calibration curves of Dox free base in PBS buffer solution at pH 7.4 (a) and acetate buffer solution at pH 5 (b).....	<b>57</b>
<b>Figure 3.1</b> Synthesis and self-assembly with Dox of cRGD-PEG- <i>b</i> -PTyr forming a polymeric NP.....	<b>65</b>
<b>Figure 3.2</b> (a) Some advantages and disadvantages of PEG, and (b) possible alternatives to PEG. ....	<b>66</b>
<b>Figure 3.3</b> $^1\text{H}$ NMR spectra of HUPA-PSar <sub>34</sub> (a), HUPA-PSar <sub>95</sub> (b) and HUPA-PSar <sub>181</sub> (c).....	<b>71</b>
<b>Figure 3.4</b> $^{13}\text{C}$ NMR spectra of HUPA-PSar <sub>34</sub> (a), HUPA-PSar <sub>95</sub> (b) and HUPA-PSar <sub>181</sub> (c).....	<b>72</b>
<b>Figure 3.5</b> FTIR spectra of HUPA and the HUPA-PSar polymers.....	<b>73</b>
<b>Figure 3.6</b> $^{31}\text{P}$ NMR spectra of HUPA and HUPA-PSar <sub>95</sub> .....	<b>74</b>
<b>Figure 3.7</b> (a) Hydrodynamic diameter ( $d_{\text{H}}$ ) distribution of the HUPA-PSar polymers measured by DLS, (b) relationship between equivalence and $d_{\text{H}}$ , and (c) SEM micrograph of HUPA-PSar <sub>95</sub> NPs.....	<b>76</b>
<b>Figure 3.8</b> Dox release over time for HUPA-PSar <sub>181</sub> in pH 7.4, 6 and 5 buffer solutions.....	<b>77</b>

- Figure 3.9** (a) FTIR spectra of HUPA-PSar<sub>181</sub>, TiO<sub>2</sub>-NP and TiO<sub>2</sub>-NC. (b) Turbidimetric analysis from UV-vis absorbance at 650 nm over time for TiO<sub>2</sub>-NP and TiO<sub>2</sub>-NC in DI water. (c) SEM micrographs of TiO<sub>2</sub>-NPs and (d) TiO<sub>2</sub>-NCs. .... **78**
- Figure 4.1** (a) Images of zebrafish larvae under bright field light and under UV, followed by time-resolved afterglow imaging after 72, 216 and 288 ms. (b) Illustration of porphyrin detection with afterglow reported in whole blood. .... **87**
- Figure 4.2** UV-vis (a) and FTIR spectra (b) of CNDs. .... **91**
- Figure 4.3** Raman spectrum (a), pXRD pattern (b), SEM micrograph (c), and normalised afterglow lifetime of CND/CaNPs (d). .... **98**
- Figure 4.4** (a) FTIR spectra of CND/CaNPs and ABPA- or HUPA-functionalised CND/CaNPs, and (b) an SEM micrograph of ABPA-functionalised CND/CaNPs. (c) Particle size distribution of CaNPs, ABPA-functionalised CaNPs and a CaNP-polymer nanocomposite on day zero and after four days, and (d) bar graph comparing the same. **99**
- Figure 4.5** <sup>1</sup>H NMR spectra of ABPA-PPhe<sub>8</sub>-*b*-PSar<sub>105</sub> (a), CND/CaNP-ABPA-PPhe<sub>4</sub>-*b*-PSar<sub>16</sub> (b), ABPA-PBLG<sub>22</sub>-*b*-PSar<sub>63</sub> (c), and CND/CaNP-ABPA-PBLG<sub>18</sub>-*b*-PSar<sub>16</sub> (d). .... **103**
- Figure 4.6** <sup>1</sup>H NMR spectra of CND/CaNP-HUPA-PSar<sub>82</sub> (a) and HUPA-PSar<sub>95</sub> (b). .... **104**
- Figure 4.7** <sup>13</sup>C NMR spectra of ABPA-PPhe<sub>8</sub>-*b*-PSar<sub>105</sub> (a), CND/CaNP-ABPA-PPhe<sub>4</sub>-*b*-PSar<sub>16</sub> (b), ABPA-PBLG<sub>22</sub>-*b*-PSar<sub>63</sub> (c), CND/CaNP-ABPA-PBLG<sub>18</sub>-*b*-PSar<sub>16</sub> (d), CND/CaNP-HUPA-PSar<sub>82</sub> (e), and HUPA-PSar<sub>95</sub> (f). .... **105**
- Figure 4.8** (a) Raman microscopy spectra of CND/CaNP-ABPA-PPhe<sub>4</sub>-*b*-PSar<sub>16</sub> and CND/CaNP-ABPA-PBLG<sub>18</sub>-*b*-PSar<sub>16</sub> and the dried supernatant from washing CND/CaNP-ABPA-PPhe<sub>4</sub>-*b*-PSar<sub>16</sub>. (b) FTIR spectra of CND/CaNPs, ABPA-PPhe<sub>8</sub>-*b*-PSar<sub>105</sub> free polymer, CND/CaNP-ABPA-PPhe<sub>4</sub>-*b*-PSar<sub>16</sub>, HUPA-PSar<sub>95</sub> free polymer and CND/CaNP-HUPA-PSar<sub>82</sub>. .... **106**
- Figure 4.9** <sup>1</sup>H NMR spectra of HUPA-PSar<sub>17</sub> (a) and HUPA-PSar<sub>23</sub> (b), <sup>13</sup>C NMR spectra of HUPA-PSar<sub>17</sub> (c) and HUPA-PSar<sub>23</sub> (d), and FTIR spectra of the HUPA-PSar polymers (e), CND/CaNP-HUPA-PSar nanocomposites (f) and dried supernatants (g). .... **108**
- Figure 4.10** TGA thermograms of CND/CaNPs, some CND/CaNP-polymer nanocomposites, and polymer analogues. .... **109**
- Figure 4.11** Kinetic UV-vis absorbance of CND/CaNPs and CND/CaNP-polymer nanocomposites in water over four hours. .... **111**
- Figure 4.12** (a) Cumulative amount of Dox released over time for CND/CaNP-ABPA-PPhe<sub>4</sub>-*b*-PSar<sub>16</sub> in PBS buffer solution at pH 7.4 and acetate buffer solution at pH 5. (b) Cumulative amount of Dox released over time for CND/CaNP-HUPA-PSar<sub>23</sub> in PBS buffer solution at pH 7.4 and acetate buffer solution at pH 5. .... **112**

<b>Figure 4.13</b> Images determining the presence of afterglow of CNP/CaNP-ABPA-PPhe <sub>4</sub> - <i>b</i> -PSar <sub>16</sub> in PBS buffer solution (a), CNP/CaNP-ABPA-PPhe <sub>4</sub> - <i>b</i> -PSar <sub>16</sub> following removal of solution and drying (b), and CNP/CaNP-ABPA-PPhe <sub>4</sub> - <i>b</i> -PSar <sub>16</sub> after being suspended in pH 5 acetate buffer solution (c). .....	<b>114</b>
<b>Figure 5.1</b> <sup>1</sup> H NMR spectra of the PEG(5,000)- <i>b</i> -PAla copolymers. ....	<b>125</b>
<b>Figure 5.2</b> <sup>13</sup> C NMR spectra of the PEG(5,000)- <i>b</i> -PAla copolymers. ....	<b>126</b>
<b>Figure 5.3</b> (a) FTIR spectra and (b) pXRD patterns of the PEG- <i>b</i> -PAla polymers. ....	<b>127</b>
<b>Figure 5.4</b> Equivalence over time for the synthesis of PEG(5,000)- <i>b</i> -PAla with different catalyst loadings. ....	<b>128</b>
<b>Figure 5.5</b> (a) <i>d<sub>H</sub></i> sizes of the PEG- <i>b</i> -PAla polymers determined from DLS, and (b) <i>d<sub>H</sub></i> plotted against equivalence for the copolymers. (c) SEM images of PEG(5,000)- <i>b</i> -PAla <sub>36</sub> and (d) PEG(5,000)- <i>b</i> -PAla <sub>4</sub> . ....	<b>129</b>
<b>Figure 5.6</b> Dox release study over time for PEG- <i>b</i> -PAla <sub>4</sub> and PEG- <i>b</i> -PAla <sub>20</sub> in pH 7.4 and pH 5 over 96 hours. ....	<b>131</b>
<b>Figure 6.1</b> Conjugation of alginate/soy protein via the Maillard reaction and organogel formation from the resulting aerogel by oil adsorption. ....	<b>137</b>
<b>Figure 6.2</b> <sup>1</sup> H (a) and <sup>13</sup> C (b) NMR spectra of PGI. ....	<b>144</b>
<b>Figure 6.3</b> APC chromatogram (a) and DSC thermogram (b) of PGI. ....	<b>145</b>
<b>Figure 6.4</b> (a) FTIR spectra of DR1 3-mercaptopropionate, DR1 bis(3-mercaptopropionate) and tris(3-mercaptopropionate); UV-vis absorbance spectra of (b) DR1 and DR1 3-mercaptopropionate, (c) DR1 bis(3-mercaptopropionate), and (d) DR1 tris(3-mercaptopropionate). ....	<b>146</b>
<b>Figure 6.5</b> <sup>1</sup> H NMR spectra of DR1 bis(3-mercaptopropionate) (a) and DR1 tris(3-mercaptopropionate) (b). ....	<b>147</b>
<b>Figure 6.6</b> <sup>1</sup> H NMR (a), FTIR (b) and UV-vis absorbance (c) spectra of DB3 3-mercaptopropionate. ....	<b>148</b>
<b>Figure 6.7</b> Analysis of PGI dyed with 2 and 3. <sup>1</sup> H NMR spectra of (a) 2-dyed and (b) 3-dyed PGI; (c) FTIR spectra of the dyed PGI; and (d) DSC thermogram of 2- and 3-dyed PGI. ....	<b>150</b>
<b>Figure 6.8</b> Elastic ( <i>G'</i> ) and viscous modulus ( <i>G''</i> ) against angular frequency for PGI swollen in 2-phenylethanol. ....	<b>152</b>
<b>Figure 6.9</b> (a) DSC thermogram for PGI cross-linked with EDT. (b) Average elastic ( <i>G'</i> ) and viscous ( <i>G''</i> ) modulus against angular frequency for PGI cross-linked with EDT and swollen in 2-phenylethanol. ....	<b>153</b>
<b>Figure 6.10</b> (a) SEM micrograph of PGI cross-linked with EDT. (b) 3-dyed PGI cross-linked with EDT and dispersed in 2-phenylethanol. (c) Average elastic ( <i>G'</i> ) and viscous ( <i>G''</i> ) modulus against angular frequency for PGI cross-linked with EDT, covalently dyed with 3 and swollen in 2-phenylethanol. ....	<b>154</b>
<b>Figure 6.11</b> Antimicrobial activities of the dyed and non-dyed cross-linked PGI organogels in 2-phenylethanol. ....	<b>156</b>

- Figure 7.1** Diagrams showing (a) the difference between dyeing polyester fabric using a disperse dye, and (b) dyeing polyester fabric with a disperse dye coupled to a SRP. ....**164**
- Figure 7.2** Calibration curves for known concentrations of pure unreacted/monomeric dye precursors for a conventional polymer-dye (a) and P2 (b). ....**168**
- Figure 7.3** Conventional (a) vs. aniline-containing SRP (P1) (b). ....**170**
- Figure 7.4**  $^1\text{H}$  NMR spectra (a), FTIR spectra (b), and APC chromatogram (c) of P1. ....**171**
- Figure 7.5** The colour difference,  $\Delta E$ , of various fabrics before and after simulated washing with an indigo dye bleed in the absence (control) and presence of P1. ....**173**
- Figure 7.6**  $^1\text{H}$  NMR (a), FTIR (b), and UV-vis absorbance spectra (c) of P2. ....**174**
- Figure 7.7** UV-vis absorbance spectra of the media outside the dialysis membrane for conventional and this novel approach. ....**175**
- Figure 7.8** (a) Graph comparing the consistency of dye deposition onto cotton and polyester for a commercial unmodified polymer-dye and P2. (b) Graph comparing the consistency of the shading across a mixed washing load containing cotton, polycotton and polyester. ....**176**
- Figure 7.9** UV-vis absorbance (a), FTIR (b), and  $^1\text{H}$  NMR (c) spectra of P3. ....**177**

## List of Tables

<b>Table 1.1</b> Comparison of the different methods of synthesising PAAs. ....	<b>11</b>
<b>Table 1.2</b> Comparison between common NCA ROP mechanisms.....	<b>25</b>
<b>Table 2.1</b> Chemicals used and their supplier.....	<b>51</b>
<b>Table 3.1</b> Calculated and actual equivalence values, and polymer nanoparticle dimensions.....	<b>71</b>
<b>Table 4.1</b> Summary of nanocomposite materials synthesised.....	<b>101</b>
<b>Table 4.2</b> Comparison between the integrals of initiator protons to polymer protons to calculate polymer equivalents and molecular weight. ....	<b>102</b>
<b>Table 4.3</b> Summary of TGA data. ....	<b>110</b>
<b>Table 5.1</b> List of polymers synthesised with their expected and actual equivalence of Ala. ....	<b>125</b>
<b>Table 5.2</b> Hydrodynamic diameters ( $d_H$ ) and PDI values of the PEG(5,000)- <i>b</i> -PAla polymers measured by DLS. ....	<b>129</b>
<b>Table 5.3</b> Dox loading content and efficiency for PEG- <i>b</i> -PAla <sub>4</sub> and PEG- <i>b</i> -PAla <sub>20</sub> . ....	<b>130</b>
<b>Table 6.1</b> Minimum weight percentage of PGI required to form a self-supporting organogel in various continuous phases.....	<b>151</b>
<b>Table 6.2</b> PGI:EDT ratio, weight loss % of PGI in the organogels formed, and the solvent loss rate of the organogels created in THF or 2-phenylethanol. ....	<b>153</b>

## List of Schemes

<b>Scheme 1.1</b> Example of a chain-growth (a) and step-growth (b) polymerisation reaction.....	<b>2</b>
<b>Scheme 1.2.</b> An example of a (a) homopolymer, (b) heteropolymer (copolymer), (c) block copolymer, (d) graft copolymer and (e) star (co)polymer.....	<b>3</b>
<b>Scheme 1.3</b> Two-step synthesis of PET from DMT, whereby the first step is transesterification (a) and the second a polycondensation (b). The direct esterification of terephthalic acid with EG to synthesise PET (c). .....	<b>5</b>
<b>Scheme 1.4</b> Synthesis of Nylon-6,6 via step-growth polycondensation. ....	<b>7</b>
<b>Scheme 1.5</b> Random NCA ROP copolymerisation and deprotection (a) and block NCA ROP copolymerisation and deprotection (b) of Lys and Aib. ....	<b>13</b>
<b>Scheme 1.6</b> (a) CGCP polymerisation reactions based on substituent effects or (b) by intramolecular transfer of catalyst.....	<b>15</b>
<b>Scheme 1.7</b> Reaction scheme of the ROP of nylon-6 from $\epsilon$ -caprolactam..	<b>16</b>
<b>Scheme 1.8</b> (a) The synthesis of poly( $\epsilon$ -caprolactam/glycolide)-PEG catalysed by Sn(Oct) <sub>2</sub> . (b) The synthesis of P $\gamma$ BL catalysed by an f-block catalyst or a 'superbase'.....	<b>18</b>
<b>Scheme 1.9</b> (a) Synthesis of PEG-PPMT via enzymatic ROP. (b) Enzymatic synthesis of hexamethylene furanoate or hexamethylene terephthalate oligomers followed by (c) enzymatic ROP and depolymerisation. ....	<b>19</b>
<b>Scheme 1.10</b> (a) Synthesis of amino acid NCAs via Leuchs method and (b) Fuchs-Farthing approach.....	<b>21</b>
<b>Scheme 1.11</b> General reaction scheme for the ROP of NCAs. ....	<b>22</b>
<b>Scheme 1.12</b> NCA ROP via the NAM. ....	<b>22</b>
<b>Scheme 1.13</b> NCA ROP via the AMM. ....	<b>23</b>
<b>Scheme 1.14</b> Reaction scheme for the synthesis of PEtOx- <i>b</i> -PBLG, followed by post-polymerisation deprotection to form PEtOx- <i>b</i> -PLG and conjugation of SN38 chemotherapeutic, forming a polymer-drug conjugate. ....	<b>29</b>
<b>Scheme 1.15</b> NCA ROP of BLG-NCA from PEG-NH <sub>2</sub> (a) followed by post-polymerisation end-group functionalisation with OSM-NHS (b). ....	<b>32</b>
<b>Scheme 3.1</b> Example of phosphonates and bisphosphonates.....	<b>60</b>
<b>Scheme 3.2</b> Reaction scheme for copolymerisation of vinylidene fluoride and (dimethoxyphosphoryl)methyl 2-(trifluoromethyl)acrylate, and subsequent hydrolysis. ....	<b>61</b>
<b>Scheme 3.3</b> Poly(ethylenimine methylenephosphonate) and diethylenetriamine penta(methylene phosphonic acid). ....	<b>62</b>
<b>Scheme 3.4</b> Phosphonate-containing monomers for binding to hydroxyapatite. ....	<b>62</b>

<b>Scheme 3.5</b> Reaction scheme for the self-assembly of HUPA on TiO <sub>2</sub> (a) and the subsequent polymerisation of MPC from the hydroxy group of HUPA (b). Synthesis of TiO-antimicrobial polymer hybrid composite (c). .....	<b>64</b>
<b>Scheme 3.6</b> Reaction scheme for the synthesis of PBLG- <i>b</i> -PSar from a dendrimer to form an amphiphilic star copolymer. ....	<b>67</b>
<b>Scheme 3.7</b> Reaction scheme for the acid-catalysed initiation (a) followed by base-catalysed propagation (b) of HUPA and Sar-NCA to synthesise HUPA-PSar <sub><i>n</i></sub> via hydroxyl-initiated NCA ROP.....	<b>68</b>
<b>Scheme 3.8.</b> Self-assembly of HUPA-PSar <sub>181</sub> with TiO <sub>2</sub> -NPs to form TiO <sub>2</sub> -NCs.....	<b>78</b>
<b>Scheme 4.1</b> Representative scheme of the surface modification of calcite particles. ....	<b>90</b>
<b>Scheme 4.2</b> Surface-functionalising CND/CaNPs with ABPA or HUPA. ....	<b>98</b>
<b>Scheme 4.3</b> Grafting-from approach to yield nanocomposites CND/CaNP-ABPA-PPh <sub>e4</sub> - <i>b</i> -PSar <sub>16</sub> and CND/CaNP-ABPA-PBLG <sub>18</sub> - <i>b</i> -PSar <sub>16</sub> (a), and CND/CaNP-HUPA-PSar <sub>82</sub> (b). ....	<b>100</b>
<b>Scheme 5.1</b> Synthesis of alanine anhydride (a) and the synthesis of poly(lactide- <i>co</i> -Ala) (b).....	<b>120</b>
<b>Scheme 5.2</b> Reaction scheme for the Sn(Oct) <sub>2</sub> -catalysed synthesis of PEG- <i>b</i> -PAla. ....	<b>125</b>
<b>Scheme 6.1</b> (a) Conversion of DR1 into thiol-bearing DR1 and (b) covalent conjugation of DR1 to linseed oil. ....	<b>136</b>
<b>Scheme 6.2</b> Reaction scheme for the CALB-catalysed ROP of globalide to synthesise PGI.....	<b>139</b>
<b>Scheme 6.3</b> Reaction scheme for the Steglich esterification of DB3 with 3-mercaptopropionic acid to afford DB3 3-mercaptopropionate.....	<b>140</b>
<b>Scheme 6.4</b> Thiol-ene coupling of PGI with 2 or 3 to yield PGI that is dyed red or blue.....	<b>141</b>
<b>Scheme 7.1</b> Step-growth polymerisation process for the synthesis of SWPU-DB60.....	<b>162</b>
<b>Scheme 7.2</b> Reaction scheme for the step-growth synthesis of P1.....	<b>166</b>
<b>Scheme 7.3</b> Reaction scheme for the colouration of P1 to yield P2. ....	<b>167</b>
<b>Scheme 7.4</b> Reaction scheme for the conjugation of sulfanilamide to P1 forming P3. ....	<b>169</b>

## Common Abbreviations

Ala – Alanine	MWCO – Molecular weight cut-off
APC – Advanced polymer chromatography	NCA – <i>N</i> -Carboxyanhydride
CDCl <sub>3</sub> – Deuterated chloroform	NMR – Nuclear magnetic resonance
C.I. – Colour Index	NP – Nanoparticle
Đ – Dispersity	PAA – Poly(amino acid)
Da – Daltons	PAla – Polyalanine
DCM – Dichloromethane	PBLG – Poly( $\gamma$ -benzyl-L-glutamate)
$d_H$ – Hydrodynamic diameter	PBS – Phosphate buffered saline
DI – Deionised	PDI – Polydispersity index
DLS – Dynamic light scattering	PEG – Poly(ethylene glycol)
DMF – <i>N,N</i> -Dimethylformamide	PET – Poly(ethylene terephthalate)
DMSO – Dimethyl sulfoxide	PLys(Z) – Poly(lysine- $\epsilon$ - <i>N</i> -benzyloxycarbonyl)
DoP – Degree of Polymerisation	PPhe - Polyphenylalanine
Dox – Doxorubicin	PSar – Polysarcosine
DSC – Differential scanning calorimetry	pXRD – Powder X-ray diffraction
FDA – Food and Drug Administration	RB – Round-bottomed
FTIR – Fourier transform infra-red	ROP – Ring-opening polymerisation
HPLC – High-performance liquid chromatography	r.p.m. – Revolutions per minute
M <sub>n</sub> – Number average molecular weight	SEM – Scanning electron microscopy
M <sub>w</sub> – Mass average molecular weight	THF – Tetrahydrofuran
	UV – Ultra-violet
	$\zeta$ – Zeta potential

# Chapter 1

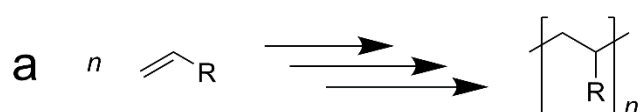
## Introduction

This Thesis describes the synthesis of polymers via step-growth and ring-opening polymerisations. Metal-catalysed and enzyme-catalysed ring-opening polymerisations (ROPs) are utilised, as well as ROP of cyclic amino acids, *N*-carboxyanhydrides (NCAs). The efficient colouration of some of the polymers is discussed to add-value, reduce environmental impact, and demonstrate functionality of the polymer. Also, the use of some of the materials as antimicrobial gels or drug delivery vehicles is demonstrated. The following introduction is a review of the literature surrounding these topics as a grounding for the Chapters which follow.

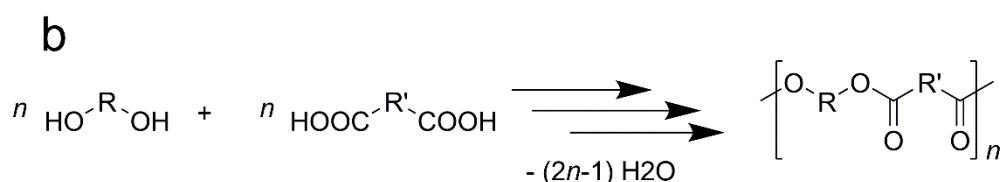
Polymers are molecules of relatively high molecular mass made up of repeat units (monomers) either covalently bonded together or held together by hydrogen bonds, van der Waals forces, etc. Polymers can have different properties depending on many variables such as the monomer(s) used to create the polymer, chain end groups, protecting groups, chain length and degree of cross-linking.<sup>1</sup> The monomer can be the same molecule repeating to create a homopolymer or the monomer units can be different to yield a heteropolymer (copolymer). These properties allow polymers to have applications in packaging, paints and coatings, building and construction, electronics, automotive components, medicine, adhesives, and energy production amongst other applications.<sup>2</sup>

Naturally occurring polymers exist, such as cellulose and natural rubber, as well as synthetic polymers. Naturally occurring polymers can also be synthetically altered to increase their applications; for example cellulose, which consists of a linear chain of D-glucose units, can have a synthetic polymer, poly(butyl acrylate), grafted from the reactive hydroxyl group on D-glucose to yield a fire-retardant biomaterial.<sup>3</sup>

Synthetic polymers are synthesised by two main reaction mechanisms: step-growth or chain-growth polymerisations.<sup>4</sup> Chain-growth polymerisation reactions most frequently require a reactive functional group (such as ethylene) on the monomer which transfers its reactive character to a propagating species, forming a high molecular weight ( $M_w$ ) polymer early in the process and the yield gradually increasing with monomer conversion (Scheme 1.1a).<sup>5</sup> Step-growth polymerisation reactions, however, require monomers with at least two reactive functional groups to react together firstly forming a dimer, then tetramer, etc., with the  $M_w$  rising steadily with monomer conversion (Scheme 1.1b).<sup>6</sup> Classification of the polymers produced may be by their response to thermal treatment, where thermoplastics melt when heated, and solidify when cooled, whilst thermoset polymers do not melt but irreversibly decompose at high temperatures. In terms of the thermal classification of polymers, step-growth reactions may give either thermosets or thermoplastics whilst chain-growth reactions only give thermoplastics.<sup>4</sup>



Chain-growth polymerisation

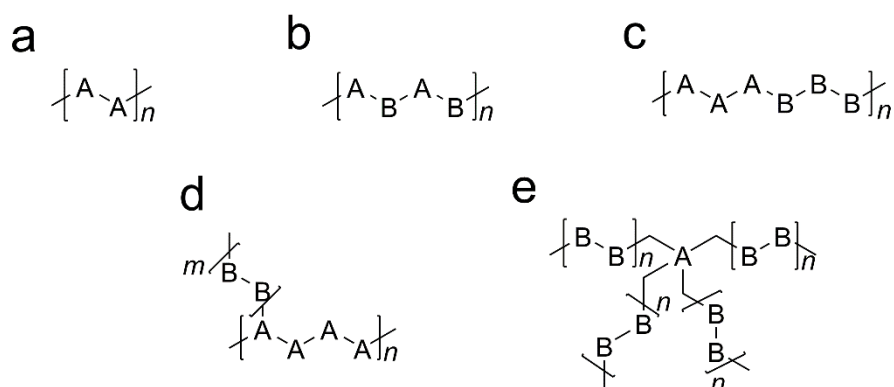


Step-growth polymerisation

**Scheme 1.1** Example of a chain-growth (a) and step-growth (b) polymerisation reaction.

Most polymers synthesised globally are commodity polymers used in everyday life, such as polyethylene, and are synthesised industrially by chain-growth or step-growth polymerisation reactions.<sup>2,5,7</sup> Controlling chain-growth polymerisation reactions allows complex macromolecular structures to be synthesised, such as block copolymers, graft copolymers, star (co)polymers and many more (Scheme 1.2).<sup>1</sup> Chain-growth polymers may also feature branching

and cross-linking, whilst branching may be conducted in step-growth polymerisation reactions *in situ* by including a monomer of more than two reactive functional groups.<sup>5</sup>



**Scheme 1.2.** An example of a (a) homopolymer, (b) heteropolymer (copolymer), (c) block copolymer, (d) graft copolymer and (e) star (co)polymer. A and B represent repeat units.

Conventional step-growth polymerisation reactions, discussed in more detail in Section 1.1, provide little control over  $M_w$  or architecture.<sup>8</sup> Such control over  $M_w$  and architecture is termed ‘living’ or controlled polymerisation reactions and are discussed in more detail in Sections 1.2 and 1.3. Examples of polymers synthesised via step-growth polymerisations or controlled polymerisation reactions as biomaterials are described in Section 1.4.

## 1.1 Step-Growth Polymerisation Reactions

The first example of a polymer synthesised via step-growth polymerisation was Bakelite, formed by the condensation of phenyl and formaldehyde in 1909.<sup>9</sup> It wasn’t until the 1930s, however, that Carothers and Flory elucidated the principles of step-growth polymerisation reactions.<sup>10</sup> Since then, step-growth polymerisation reactions have been a major industrial interest, producing commodity polymers such as polyesters and polyamides.<sup>11</sup> Polyesters are typically synthesised by reaction of dibasic acids and diols whilst polyamides are synthesised by the reaction of dibasic acids and diamines.

### 1.1.1 Poly(ethylene terephthalate) (PET)

Poly(ethylene terephthalate) (PET) is an aliphatic-aromatic, semicrystalline, thermoplastic polyester widely used in packaging food and beverages, moulding components, fibres, films and textiles.<sup>12</sup> PET is widely used because of its excellent properties, such as high thermal stability, good barrier properties, excellent transparency, high tensile strength and easy processability.<sup>13</sup> In 2018, the demand for PET in Europe was approximately four million tonnes, equal to 7.7% of all polymers.<sup>14</sup>

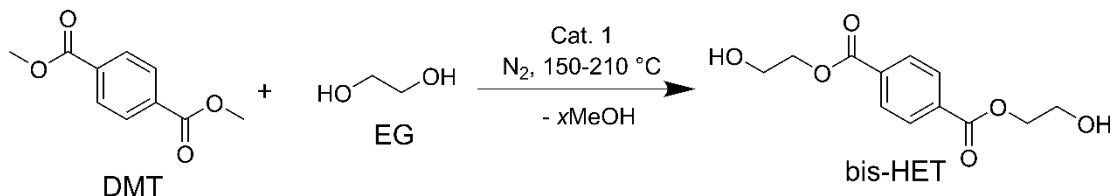
#### 1.1.1.1 Industrial synthesis of PET

The original industrial synthesis of PET involved a two-step reaction in the melt between dimethyl terephthalate (DMT) and ethylene glycol (EG).<sup>15-17</sup> Firstly, a transesterification reaction converts the methyl ester groups of DMT into bis(2-hydroxyethyl)terephthalate (bis-HET) or oligomers (Scheme 1.3a). This step is catalysed with a metal (Mn, Zn, Ca or Mg) acetate, and conducted in an inert atmosphere at temperatures between 150 and 210 °C. Once all the methanol is distilled off, the temperature is then increased to between 270 and 280 °C and a high vacuum applied. These conditions, with antimony trioxide catalyst, synthesise PET by polycondensation (Scheme 1.3b).<sup>18</sup>

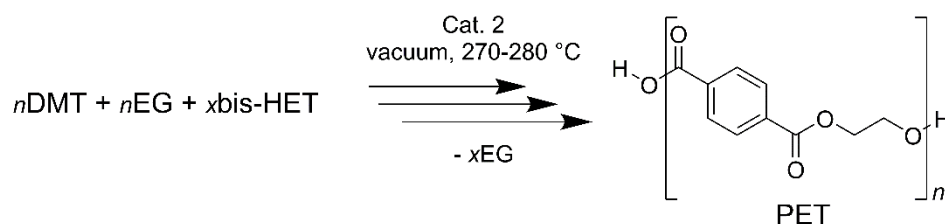
Alternatively, terephthalic acid and EG may polymerise in a direct esterification of terephthalic acid and EG, followed by polycondensation (Scheme 1.3c).<sup>19</sup> Terephthalic acid here self-catalyses the esterification, releasing water, but terephthalic acid does not easily dissolve in EG.<sup>20</sup> To overcome the solubility issue, a monomer feed is required. Both methods are still used in industry today, although direct esterification is more frequently conducted due to the rapid esterification of the pre-polymer and not needing to recycle methanol.<sup>21</sup> If a very high  $M_w$  (i.e. >100,000 Da) is required for more rugged applications, such as automotive components, the polymer is subjected to a third, solid-state polymerisation at a high temperature (200-240 °C) for 10-30 h.<sup>22</sup> This third step

is to reactivate the catalyst trapped in the polymer to react new and unreacted monomer with the polymer chain ends, which are still available for propagation.<sup>18</sup>

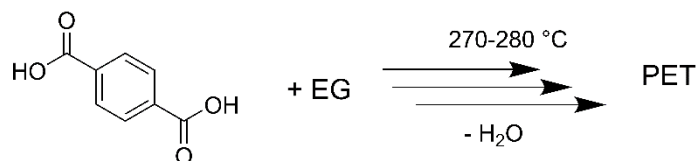
**a** Transesterification



**b** Polycondensation



**c** Direct Esterification



**Scheme 1.3** Two-step synthesis of PET from DMT, whereby the first step is transesterification (a) and the second a polycondensation (b). The direct esterification of terephthalic acid with EG to synthesise PET (c). Cat. 1 = Mn, Zn, Ca or Mg acetate; Cat. 2 = antimony trioxide.<sup>18</sup>

### 1.1.1.2 Advanced uses of PET

Contamination and infection from microorganisms is a big concern in areas such as healthcare, water purification systems, medical devices, hospitals, dental equipment, food storage, packaging and household sanitation.<sup>23-25</sup> Conferring antimicrobial activity on a materials surface helps in the battle against microbial contamination and infection.<sup>26</sup> PET is relatively cheap, moderately biocompatible and has excellent mechanical properties so is used in heart valves, catheters, implants and sutures.<sup>27</sup> Thus, PET is an attractive material to impart antimicrobial activity to, and researchers have done so by chemically modifying PET, surface coating PET, or by blending antimicrobial agents with PET.<sup>28</sup>

One example of work to impart antimicrobial activity to PET is that by Cao and colleagues, who firstly modified an antimicrobial polymer, polyhexamethylene guanidine hydrochloride (PHMG), to have an epoxy terminal group, ethylene glycol diglycidyl ether-PHMG (EGDE-PHMG).<sup>29</sup> PET was surface-functionalised by aminolysis (Figure 1.1a) to present primary amine groups on the surface from which the epoxy group of EGDE-PHMG can react, covalently surface-functionalising PET with the antimicrobial polymer (Figure 1.1b). Antimicrobial activity of above 99.99% inhibition of *Escherichia coli* and *Staphylococcus aureus* was reported, rendering the product extremely promising as an antimicrobial material.

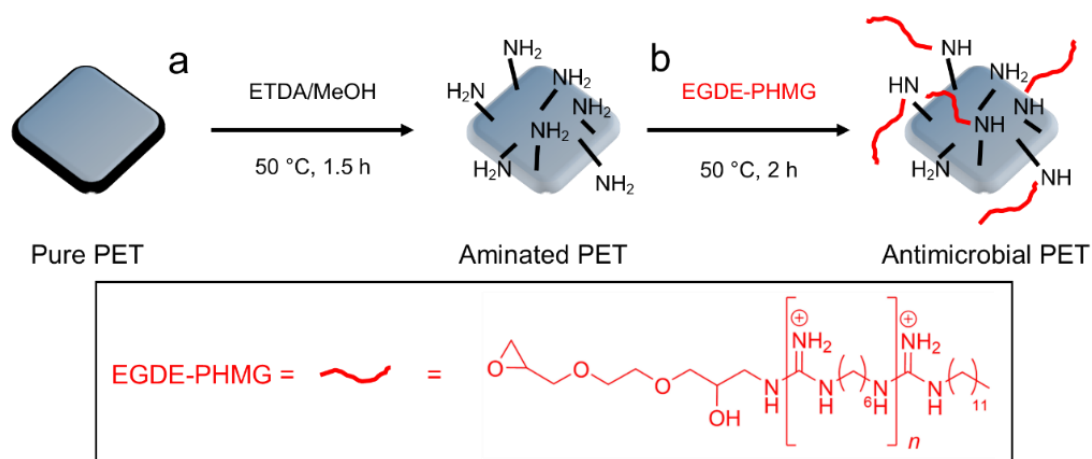
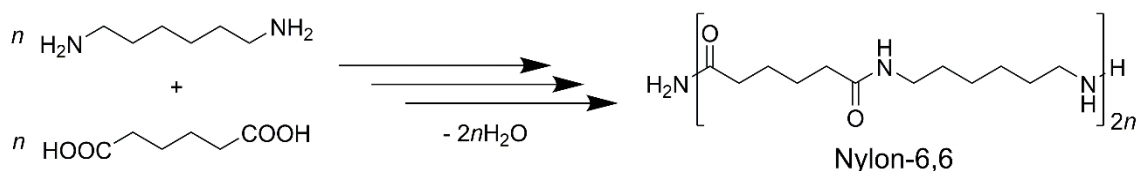


**Figure 1.1** Synthesis of antimicrobial PET-g-EGDE-PHMG by firstly surface-functionalising PET (a) followed by covalent conjugation of EGDE-PHMG to the functionalised PET surface (b).<sup>29</sup> ETDA = ethylenediamine.

Another interesting advanced use for PET is as a soil release agent in advanced laundry formulations.<sup>30</sup> Soil release agents aid the diffusion of water into the soil-fabric interface, decrease soil adsorption onto fabric surfaces, and reduce soil redeposition onto fabrics in the wash.<sup>31-35</sup> In order to do this, the polymer must be amphiphilic, and so hydrophobic PET may be created with hydrophilic poly(ethylene glycol) (PEG) to form an amphiphilic block copolymer architecture.

### 1.1.2 Polyamides

Polyamides possess useful properties such as heat resistance, abrasion resistance, high impact and tensile strength, and electrical insulation.<sup>36</sup> Such properties make polyamides useful in many industries, including the textile, automotive, and electrical industries.<sup>37</sup> The first commercial polyamide was Nylon-6,6, developed by Carothers in the 1930s by the step-growth polycondensation reaction between adipic acid and hexanediamine (Scheme 1.4).<sup>38-41</sup>



**Scheme 1.4** Synthesis of Nylon-6,6 via step-growth polycondensation.<sup>37</sup>

### 1.1.3 Issues with step-growth polymers

As previously discussed, polymers synthesised via step-growth polymerisation reactions provide little control over  $M_w$  or architecture. A method of overcoming this limitation is discussed in more detail in Section 1.3.1. It is also prudent to raise the increasing environmental issues surrounding most commodity polymers produced by step-growth, and indeed chain-growth, reactions. Often the starting materials are from crude oil, a valuable natural non-renewable resource, and the excellent mechanical and chemical resistant properties of the materials produced lead to their persistence in the environment.<sup>2,42-44</sup> Much research has been conducted in reducing the environmental burden of polymers on the environment, such as alternatives to commodity polymers or improving recycling.<sup>45-47</sup> Additionally, many commodity polymers are coloured in order to add value to the product, but polymers such as PET lack suitable chemical functionality to enable efficient dyeing.<sup>48</sup> To overcome this, the dyeing of PET is conducted in an excess of disperse dyes, requires auxiliaries, and produces coloured wastewater, creating acute aesthetic, ecological and environmental problems.<sup>49-52</sup>

## 1.2 Poly(amino acid)s (PAAs)

### 1.2.1 Introduction to PAAs

Many biological functions are performed by proteins which are made of polypeptides, natural polymers of L- $\alpha$ -amino acids (1, Figure 1.2). There are hundreds of amino acids, but those which are used in polypeptides are called proteinogenic and all have the same L-stereochemical series, therefore the L- will be omitted hereafter, unless the particular amino acid is an anomaly.<sup>53</sup> Figure 1.2 shows the structure of 20 common proteinogenic amino acids.

As can be seen in Figure 1.2, even just 20 common proteinogenic amino acids have many different specific characteristics such as being hydrophilic/hydrophobic, acidic/basic and/or polar/non-polar. When polymerised, the R-groups impart this chemical functionality onto the PAA backbone, which subsequently give the PAAs different properties or allows for the attachment of different moieties to modify the chemical or physical properties of the polymer post-polymerisation.<sup>55</sup>

These proteinogenic and many other non-proteinogenic amino acids are the monomers which make up polypeptides and PAAs. Polypeptides are long specific sequences of amino acids, and many of these polypeptides together self-assemble to form proteins. PAAs can be long chains of the same amino acid (homopolypeptides), or long chains of different amino acids, but crucially are not usually in a specific sequence like polypeptides.<sup>54</sup>

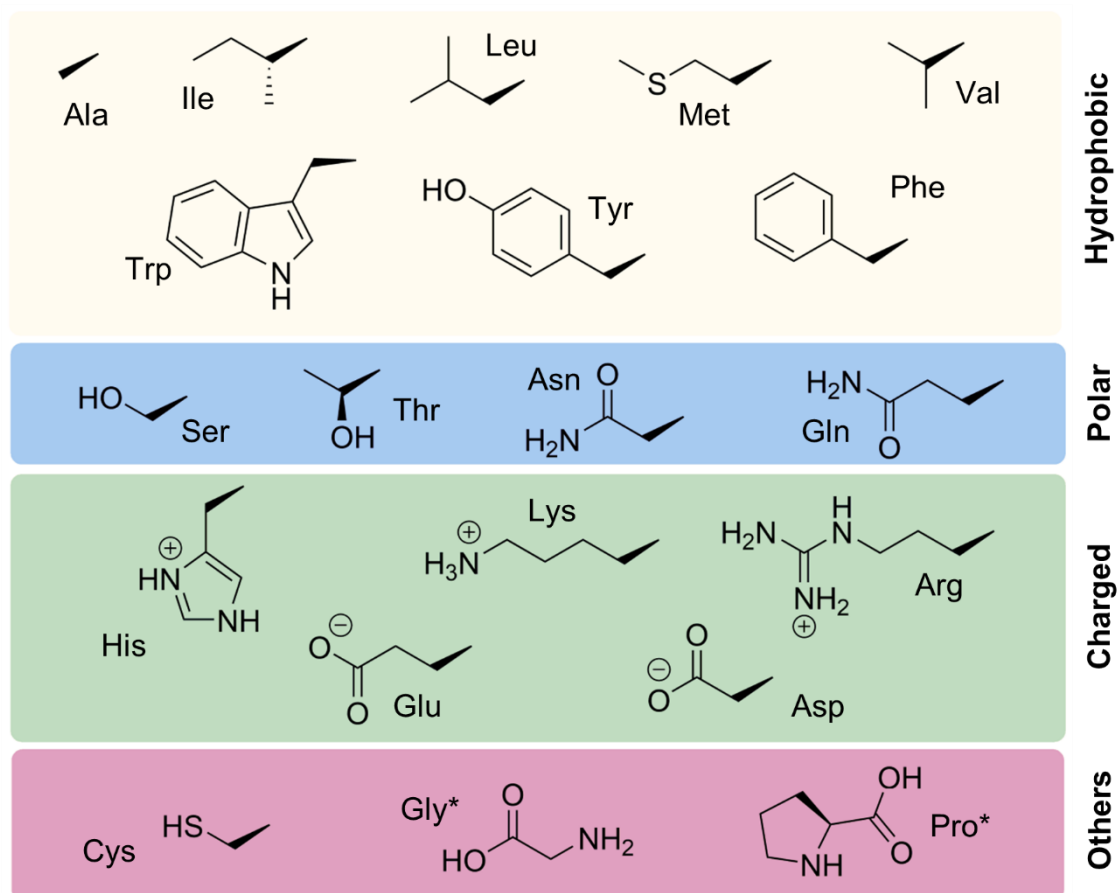
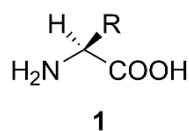


**Figure 1.2** R group for 20 common proteinogenic  $\alpha$ -amino acids. \*For Gly and Pro the whole  $\alpha$ -amino acid structure is shown whereas for the rest just the R group on 1 is shown.

### 1.2.2 Synthesis of PAAs

In synthetic chemistry, homopolypeptides (polypeptides of one  $\alpha$ -amino acid, and PAAs of one  $\alpha$ -amino acid) can be synthesised by solid-phase peptide synthesis (SPPS),  $\alpha$ -amino acid NCA ROP (Section 1.3.3), or *in vitro* by protein biosynthesis (Figure 1.3a). Synthetic polypeptides are useful as some natural polypeptides are difficult to isolate, and many more amino acids than those shown in Figure 1.2 can be included.<sup>56-57</sup>

Although SPPS offers precise control over monomer sequence and chain length, its maximum chain length is restricted to approximately 50 amino acid units.<sup>58</sup> Whilst SPPS is a well-established procedure, NCA ROP synthesises PAAs of high  $M_w$  in a shorter sequence time that possess narrow polydispersity with sophisticated architectures, retained chirality and with high yields.<sup>59</sup> NCA ROP does, however, lack precise control over the monomer sequence and chain length. Biosynthetic methods yield longer still polypeptides with high  $M_w$ , precise chain length and monomer sequence, but production is not trivial, specialist equipment not typically found in synthetic chemistry laboratories are required, and the procedure is time and cost intensive.<sup>57,60-61</sup> Table 1.1 summarises the differences between the three PAA synthetic methods.

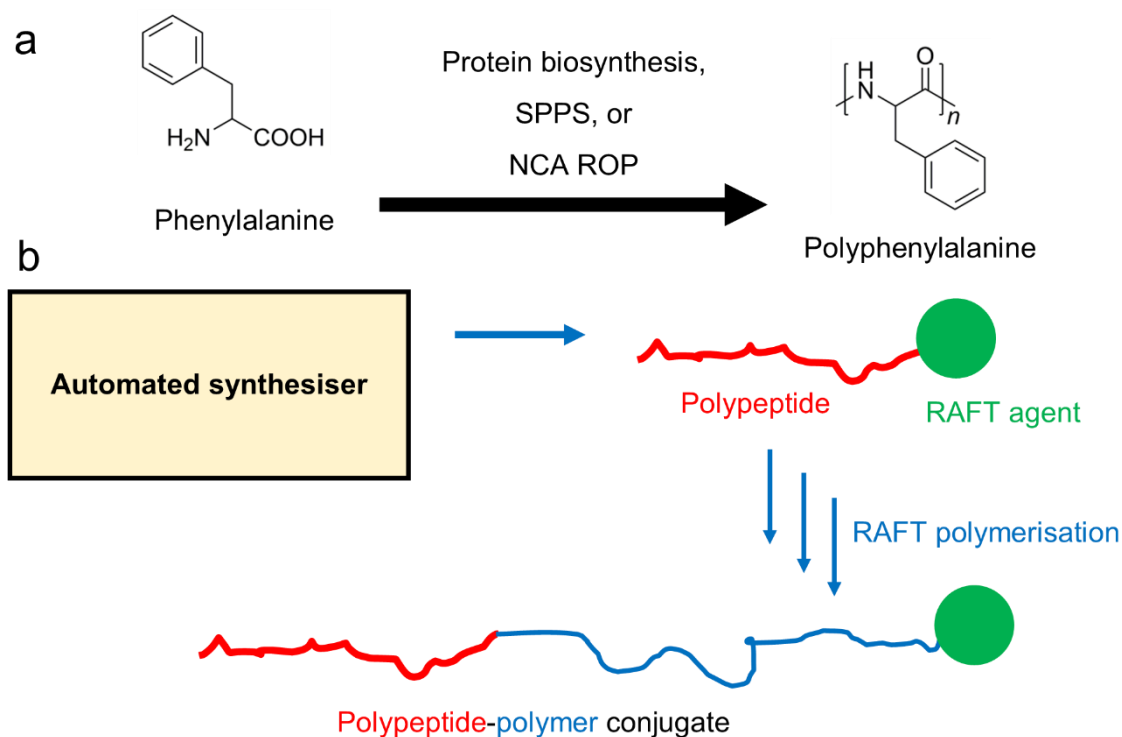


**Figure 1.3** (a) Example of a PAA, poly(Phe) which can be synthesised by protein biosynthesis, SPPS or NCA ROP. (b) Synthesis of polypeptide-polymer conjugate via SPPS-peptide synthesis followed by RAFT polymerisation.

**Table 1.1** Comparison of the different methods of synthesising PAAs.

<b>PAA synthetic procedure</b>	<b>Advantages</b>	<b>Disadvantages</b>
Protein biosynthesis	Very high $M_w$ ; precision of monomer sequence.	Experimentation not trivial; requires specialised equipment.
SPPS	Precise control over monomer sequence.	Chain length is typically restricted to 50 monomer units.
NCA ROP	High $M_w$ ; high yields; sophisticated architectures may be produced.	Imprecise control over monomer sequence.

These methods can be combined with other controlled polymerisation techniques (Section 1.3) to synthesise well-defined hybrid PAA-synthetic polymer conjugates.<sup>62</sup> For example, Chen and co-workers synthesised a series of peptide-reversible addition-fragmentation chain-transfer (peptide-RAFT) agents by automated SPPS.<sup>63</sup> These peptide-RAFT agents then went on to form peptide-polymer conjugates via RAFT polymerisation, which have potential use as a gene delivery system (Figure 1.3b).

### 1.2.3 Poly(amino acid) (PAA) architectures

#### 1.2.3.1 Secondary structure and self-assembly

The properties of a particular polypeptide, and as such its use, are determined by the primary amino acid sequence. Each individual amino acids influence over the structure is weak, but added together they give polypeptides a secondary structure, such as an  $\alpha$ -helix or  $\beta$ -sheet (Figure 1.4, left).<sup>64</sup>

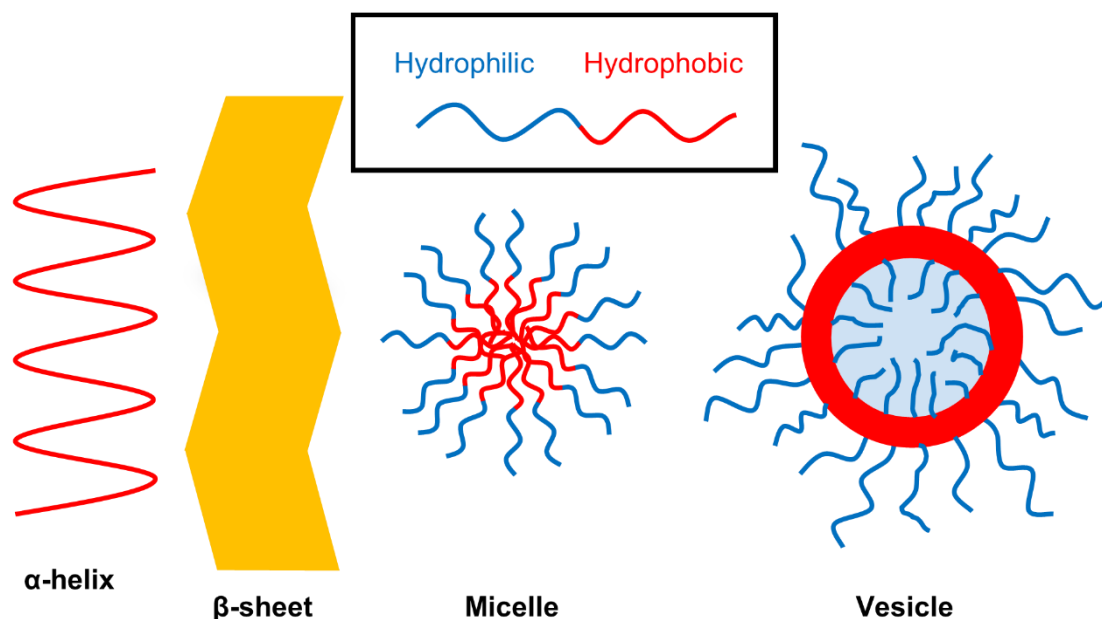


**Figure 1.4** Examples of an  $\alpha$ -helix and  $\beta$ -sheet conformation (left), and a micelle and vesicle polymeric nanoparticle (right).

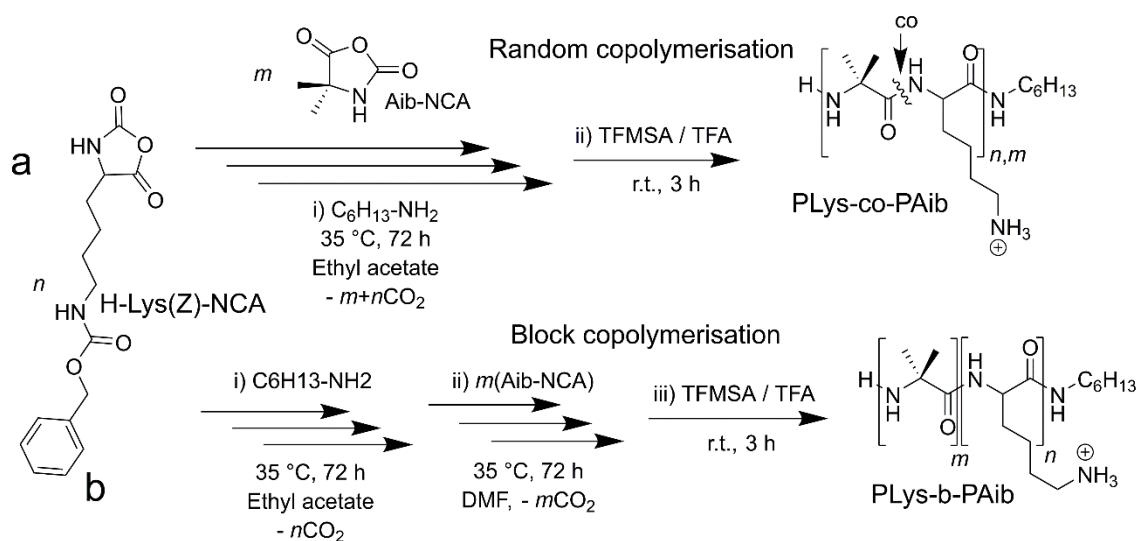
PAAs can be synthesised to form many different architectures, such as those described in Scheme 1.2. A very important and useful characteristic of PAAs is their ability to self-assemble into discrete structures, such as  $\alpha$ -helix or  $\beta$ -sheets conformations (like polypeptides), or nanoparticles (NPs) such as micelles and vesicles (Figure 1.4, right).<sup>65-67</sup> This self-assembly comes about and is maintained by hydrophilic-hydrophobic interactions,  $\pi$ - $\pi$  stacking, hydrogen bonds and electrostatic interactions.<sup>68-72</sup>

### 1.2.3.2 Block and random copolymers

Block copolymers (Scheme 1.2c) can be synthesised by NCA ROP of  $\alpha$ -amino acids by firstly polymerising one NCA to completion and then using this PAA as a macroinitiator for sequential NCA ROP.<sup>70,73-75</sup> There is no theoretical limit to the number of blocks there can be.<sup>76</sup> NCA ROP can be combined with other polymerisation techniques to create the first or second block.<sup>77-78</sup> For example, Sang and colleagues firstly synthesised a hydrophilic, PEG-functionalised thermoresponsive poly(*N*-isopropylacrylamide), poly(NIPAM-co-PEG) with a terminal primary amine.<sup>79</sup> From this terminal primary amine, poly( $\gamma$ -benzyl-L-glutamate) (PBLG) was polymerised via NCA ROP to add a hydrophobic block

onto poly(NIPAM-co-PEG), forming an amphiphilic copolymer with potential application as a drug delivery vehicle.

Random (or statistical) copolymers consist of two or more amino acid monomer units statistically spread throughout the polymer chain based on monomer reaction kinetics.<sup>80-81</sup> Huang *et al.* synthesised a random co-PAA of PBLG and polylysine (PLys) via NCA ROP.<sup>82</sup> The random copolymer self-assembled into aggregates and it was found that the surface charge of the aggregates was greatly dependent on the solution pH because the carbonyl and amino groups could be deprotonated or protonated, respectively, to become charged. This pH-responsiveness was manipulated and demonstrated as a potential drug delivery vehicle. Recently, another PBLG-co-PLys random copolymer with 10% BLG and 90% Lys was found to have remarkable antimicrobial activity against multi-drug resistant bacteria *in vivo* and *in vitro*.<sup>83</sup> In addition, Tarasenko and colleagues synthesised a series of random and block co-PAA of Lys and  $\alpha$ -aminoisobutyric acid (Aib) via NCA ROP (Scheme 1.5).<sup>84</sup> They found that the block copolymers formed vesicles whilst the random copolymers formed micelles, expanding our understanding of such nano-sized biomaterials for drug delivery and tissue engineering applications.



**Scheme 1.5** Random NCA ROP copolymerisation and deprotection (a) and block NCA ROP copolymerisation and deprotection (b) of Lys and Aib. TFMSA = trifluoromethanesulfonic acid.<sup>84</sup>

### 1.2.3.3 PAAs as biomaterials

Various biomaterials may be produced using PAAs as they mimic many properties of polypeptides such as excellent biocompatibility, biodegradability (when in non-monomeric form) to non-toxic products *in vivo* and versatility of structures and functionalities.<sup>80,85-86</sup> Polypeptides can also be combined with synthetic polymers as polypeptide-polymer hybrid materials, retaining the excellent properties of polypeptides and adding the features of the synthetic polymers, such as enhanced solubility in desired solvents and improved processability.<sup>87</sup> Typically, PAAs synthesised via NCA ROP are useful as antimicrobial agents,<sup>88-91</sup> for tissue engineering,<sup>92-94</sup> for drug/gene delivery<sup>95-97</sup> and for protein/peptide mimicking.<sup>98-99</sup>

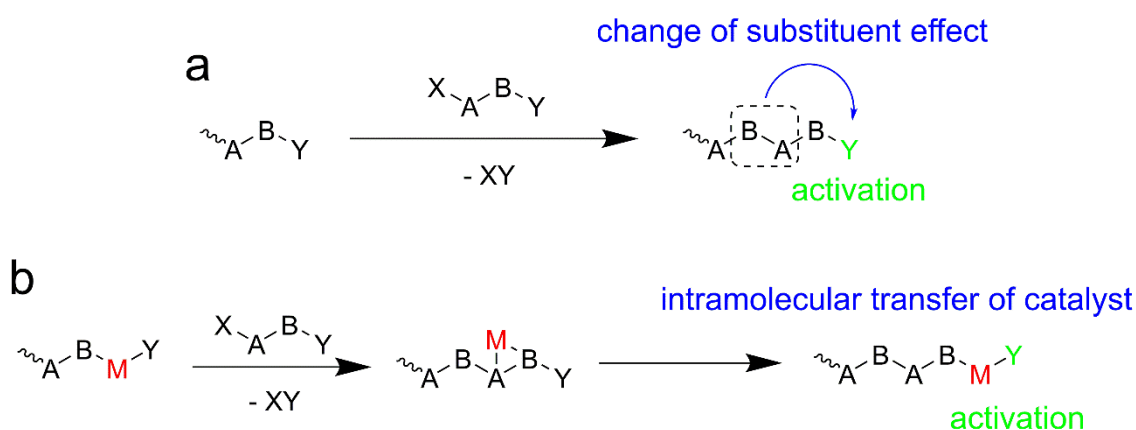
## 1.3 Controlled Polymerisation Reactions

When materials are used in humans, such as for drug delivery and for other important applications, it is vital to know the dimensions and architectures of the materials. Controlled (also termed 'living') polymerisation techniques produce polymers of known and consistent  $M_w$ . Controlled polymerisation processes theoretically have no side reactions and the only terminating step should be when all the monomer is consumed.<sup>100</sup>

Controlled polymerisation techniques are generally chain-growth polymerisation reactions and examples include chain-growth condensation polymerisations (CGCP) (Section 1.3.1); anionic polymerisations;<sup>101</sup> radical controlled polymerisation techniques including atom-transfer radical polymerisation (ATRP),<sup>100</sup> reversible addition-fragmentation chain-transfer polymerisation (RAFT)<sup>102</sup> and nitroxide-mediated polymerisation (NMP);<sup>103</sup> and ROPs (Section 1.3.2) including the ROP of NCAs (Section 1.3.3).<sup>104</sup>

### 1.3.1 Chain-Growth Condensation Polymerisations (CGCP)

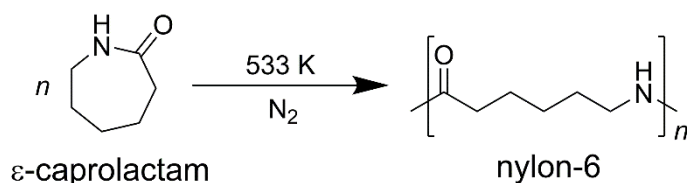
It was previously stated in Section 1.1.3 that an issue with step-growth polymerisation reactions is they provide little control over  $M_w$  or architecture. However, if the propagating polymer end group can be made more reactive than the monomer itself, the step-growth polymerisation reaction may be transferred to a chain-growth reaction.<sup>8</sup> During condensation polymerisations the propagating chain end group is stable and not a reactive radical or ion, so CGCPs demonstrate controlled polymerisation behaviour.<sup>105</sup> Indeed, proteins, DNA and RNA are perfectly monodisperse and produced by a CGCP mechanism *in vivo*.<sup>106-108</sup> CGCP can be conducted synthetically by one of two ways: either enhance the reactivity of the polymer end group (Y) by a substituent effect induced by B-A bond formation between the monomer and polymer (Scheme 1.6a),<sup>109</sup> or activate the polymer end group using a metal catalyst (M) (Scheme 1.6b).<sup>110-111</sup> Thus the scope of condensation polymerisation reactions opens-up to more advanced applications, such as biomaterials and electronics, because the reaction can be controlled, forming complex polymer architectures with defined  $M_w$  and narrow dispersity ( $\mathcal{D}$ ).



**Scheme 1.6** (a) CGCP polymerisation reactions based on substituent effects or (b) by intramolecular transfer of catalyst.<sup>8</sup> A and B are monomers, X and Y are polymer end groups, and M is a metal catalyst.

### 1.3.2 Ring-Opening Polymerisation (ROP)

ROP is as the name suggests: the polymerisation of cyclic monomers. Many conventional polymerisation reactions generally occur by the conversion of a multiple bond to a single bond. For ROPs, however, the driving force is generally ring strain and associated sterics. As a good indication that sterics are involved, strain-free six-membered rings generally don't polymerise via ROP.<sup>112</sup> One of the earliest commercially available synthetic polymers was nylon-6,6, patented by DuPont in September 1938, and its initial synthesis described in Section 1.1.2.<sup>40</sup> In order not to infringe this initial patent, nylon-6 instead of nylon-6,6 was developed by the ROP of  $\epsilon$ -caprolactam (Scheme 1.7).



**Scheme 1.7** Reaction scheme of the ROP of nylon-6 from  $\epsilon$ -caprolactam.

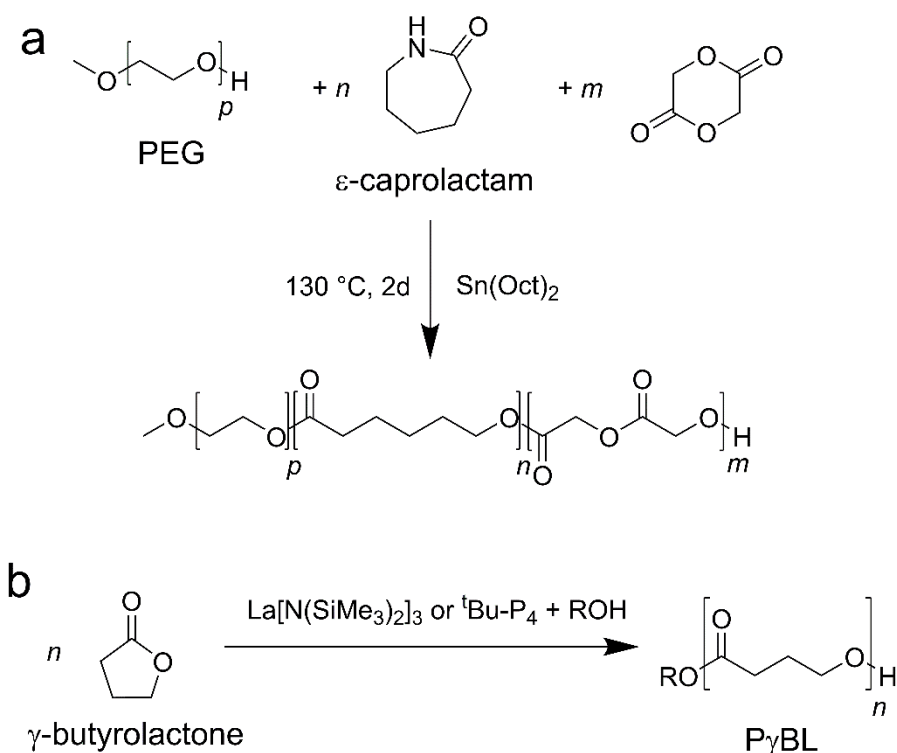
Although the nylon example above is an anionic ROP mechanism, there are more ROP mechanisms a polymer chemist can utilise, such as cationic or radical ROP.<sup>113</sup> Metal catalysts (Section 1.3.2.1) and enzymes (Section 1.3.2.2) are also frequently utilised for ROPs, as well as the self-catalysed ROP of NCAs, discussed in detail in Section 1.3.3.

#### 1.3.2.1 Metal-catalysed ROP

Recently, Sun *et al.* synthesised a block copolymer of poly( $\epsilon$ -caprolactam/glycolide) and PEG using ROP with PEG as a macroinitiator and  $\text{Sn}(\text{Oct})_2$  as a catalyst (Scheme 1.8a).<sup>114</sup> The block copolymer formed NPs in aqueous solution and exhibited high drug loading properties with prolonged drug release and therefore is a promising candidate as a drug delivery system.  $\text{Sn}(\text{Oct})_2$  is the most frequently used catalyst for the ROP of cyclic diesters

because it is reactive and has low toxicity.<sup>115</sup> There are always concerns of using metals in any reaction due to toxicological concerns, however Sn(Oct)<sub>2</sub> has been approved by the American Food and Drug Administration (FDA) for use in foods and pharmaceuticals.<sup>116-117</sup>

$\gamma$ -Butyrolactone was once thought to be “non-polymerisable” because of the lack of ring strain in the cyclic lactone.<sup>118</sup> This perceived “non-polymerisability” was unfortunate because  $\gamma$ -butyrolactone can be sourced from a renewable feedstock and poly( $\gamma$ -butyrolactone) (P $\gamma$ BL), an aliphatic polyester, would likely be biodegradable and have properties making it suitable to replace non-degradable commodity polymers from non-renewable sources.<sup>119-123</sup> In 2016, Hong and Chen first successfully synthesised P $\gamma$ BL via ROP catalysed by an f-block metal catalyst (lanthanum),<sup>124</sup> then soon after used a strong base organocatalyst to synthesise P $\gamma$ BL (Scheme 1.8b).<sup>125</sup> The ‘superbase’ *tert*-Bu-P<sub>4</sub> forms a H-bonding paired complex with an alcohol initiator (ideally BnOH or Ph<sub>2</sub>CHOH) which goes on to polymerise P $\gamma$ BL with 90% monomer conversion in four hours to high M<sub>w</sub>. The recyclability of the prepared aliphatic polyester back to its monomer was demonstrated by heating the polymer at 260 °C for one hour.

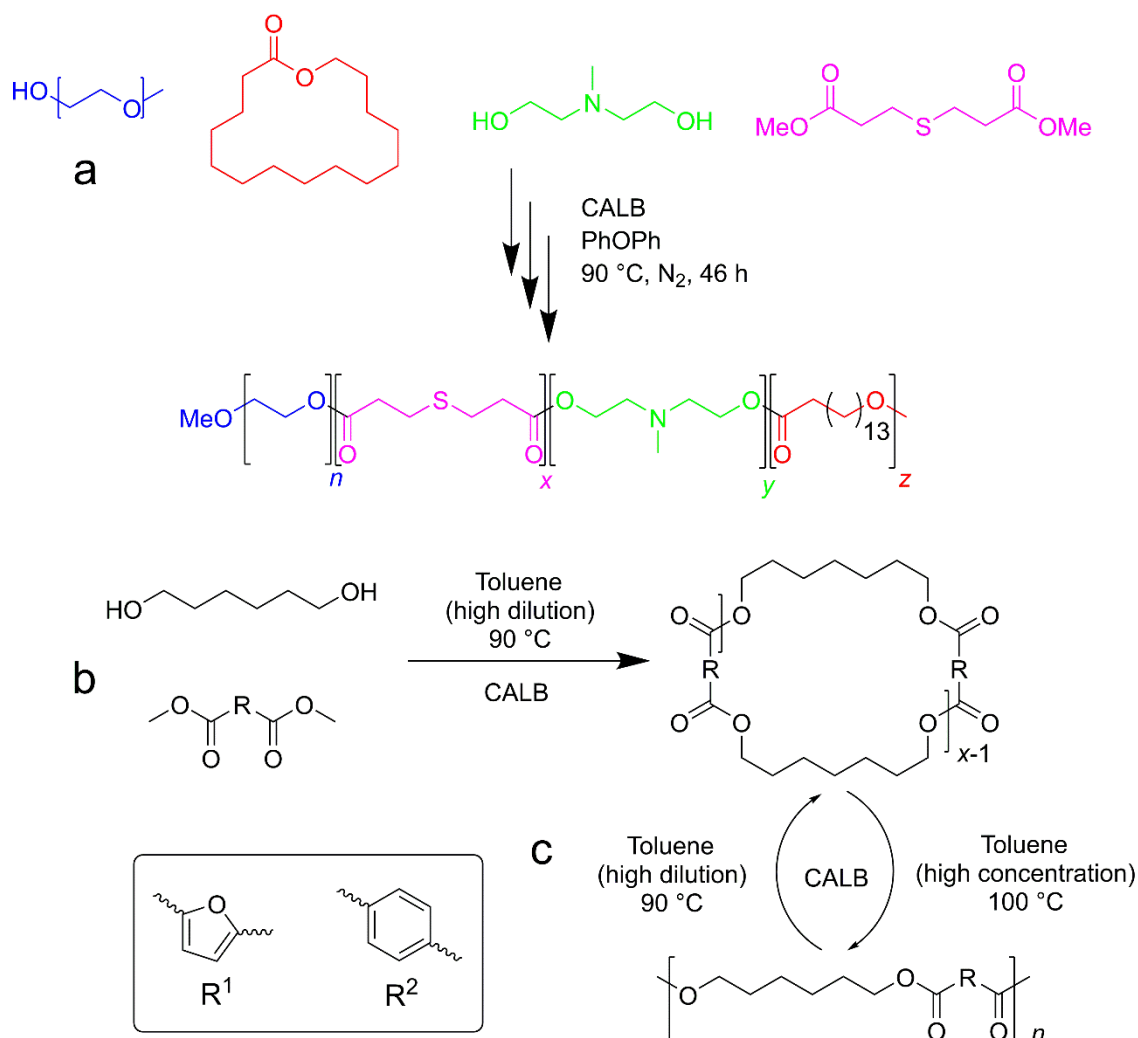


**Scheme 1.8** (a) The synthesis of poly( $\epsilon$ -caprolactam/glycolide)-PEG catalysed by Sn(Oct)<sub>2</sub>.<sup>114</sup> (b) The synthesis of P $\gamma$ BL catalysed by an f-block catalyst or a ‘superbase’.<sup>124-125</sup>

### 1.3.2.2 Enzymatic ROP

Enzymes are recyclable, non-toxic, and when immobilised on a support can easily be collected by filtration after the polymerisation reaction. When used to catalyse polymerisation reactions, enzymes operate under mild conditions with remarkable efficiency, and as such are a ‘greener’ alternative to metal catalysts for ROPs.<sup>126-128</sup> A recent review on immobilised *Candida antarctica* lipase B (CALB or Novozym 435) -mediated ROP reactions by Lu and colleagues<sup>129</sup> highlights the many applications of enzymatic ROP in biomaterials, including drug and gene delivery,<sup>130</sup> antimicrobial polymers,<sup>131</sup> and tissue engineering.<sup>132</sup> For example, in 2019 Gong and co-workers used CALB to synthesise the copolymer PEG-*b*-poly( $\omega$ -pentadecalactone-*co*-*N*-methyldiethanolamine-*co*-3,3'-thiodipropionate) (PEG-PPMT) (Scheme 1.9a).<sup>133</sup> This copolymer self-assembles into NPs in aqueous solutions because of the outer hydrophilic PEG layer and inner hydrophobic lactone core, contains amino and thioether moieties for pH and reactive oxygen species dual stimuli-responsiveness, and contains ester linkages

that ensure the biodegradability of the PPMT block. The authors demonstrated the anti-cancer efficacy of chemotherapy drug-loaded PEG-PPMT NPs *in vivo* using the dual stimuli-responsiveness.



**Scheme 1.9** (a) Synthesis of PEG-PPMT via enzymatic ROP.<sup>133</sup> (b) Enzymatic synthesis of hexamethylene furanoate (R<sup>1</sup>) or hexamethylene terephthalate (R<sup>2</sup>) oligomers followed by (c) enzymatic ROP and depolymerisation.<sup>139</sup>

Enzymatic ROP is not only useful for the creation of biomaterials, but also for the synthesis of polymers to potentially replace some commodity polymers.<sup>127</sup> As discussed in Section 1.1.3, there is a need to replace many commodity polymers with polymers from a renewable resource that may be biodegradable. Aliphatic polyesters have significant potential to replace some commodity polymers in applications ranging from packaging to personal care products owing to their degradability, biocompatibility, and the monomers can be sourced from

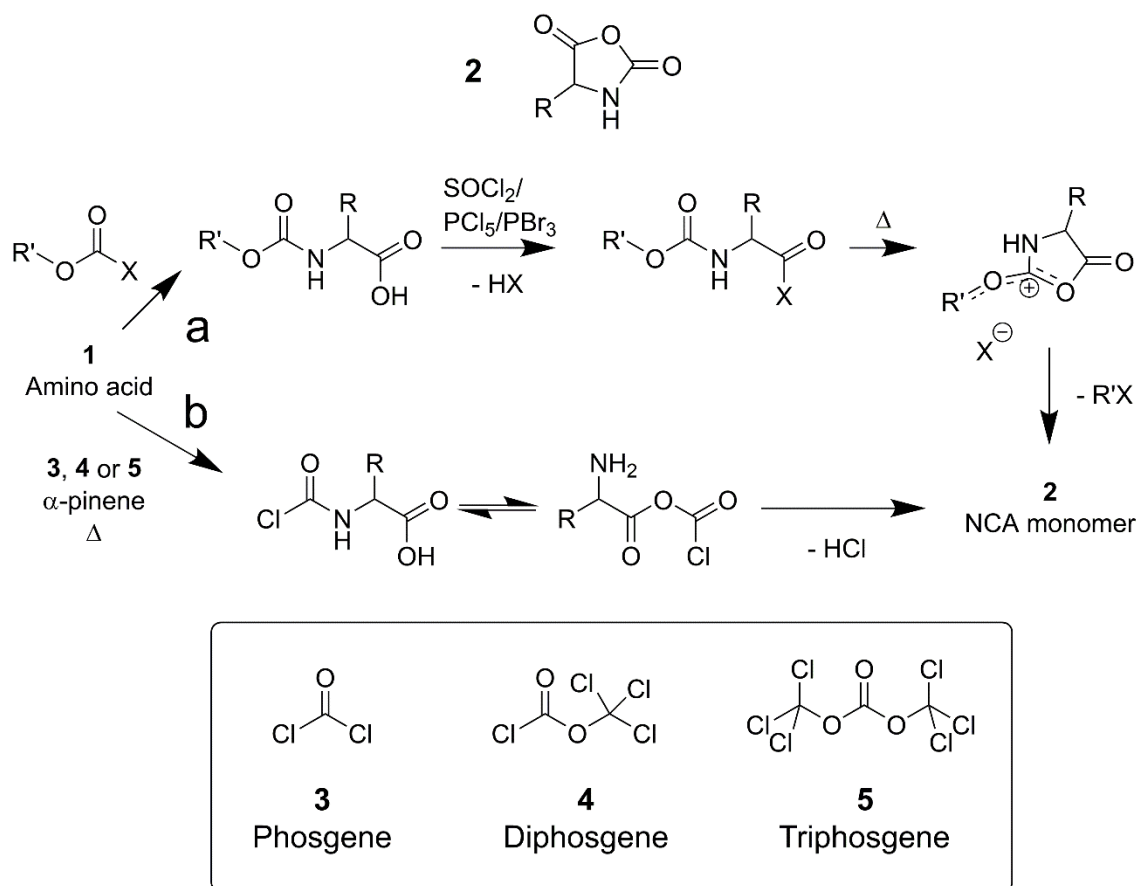
renewable resources.<sup>134-138</sup> Flores *et al.* were innovative with their use of CALB, using the enzyme to catalyse the oligomerisation of hexamethylene furanoate ( $R^1$ ) or hexamethylene terephthalate ( $R^2$ ) with 1,6-hexanediol (Scheme 1.9b).<sup>139</sup> The researchers then demonstrated CALB-mediated ROP of the cyclic oligomers, forming semicrystalline polymers, as well as the depolymerisation back to cyclic oligomers using CALB at different concentrations (Scheme 1.9c). In this work, Flores and co-workers demonstrate a material which can be continuously polymerised and depolymerised, thus forming a 'circular economy'.

### 1.3.3 N-Carboxyanhydride (NCA) ROP

In this Thesis, the ROP of NCAs to synthesise PAAs is frequently used and so is discussed in more detail in this Section.

#### 1.3.3.1 History of NCAs

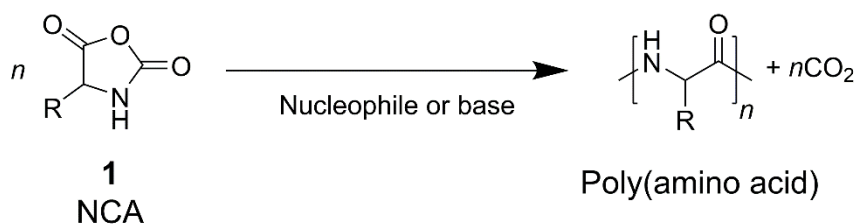
NCAs (**2**, Scheme 1.10) are heterocycles with an anhydride group, an amine group and a >CHR group whereby the R group can be a plethora of functional groups. Between 1906 and 1908, Hermann Leuchs *et al.* first described the synthesis and properties of NCAs, then termed Leuchs's anhydrides.<sup>140-142</sup> It was not until the 1920s, however, that Curtius *et al.*<sup>143-145</sup> and Wessely *et al.*<sup>146-153</sup> reported NCAs to synthesise high molecular weight PAAs, using primary amines, alcohol or water as initiators.<sup>59,154</sup> Leuchs' approach (Scheme 1.10a) used chlorinating agents such as thionyl chloride, and then developed phosphorous halides instead to improve reactivity. Another early synthesis method, the Fuchs-Farthing approach (Scheme 1.10b), is relatively straightforward and yields pure NCA monomers with good yields and no racimisation.<sup>87</sup>



**Scheme 1.10** (a) Synthesis of amino acid NCAs via Leuchs method and (b) Fuchs-Farthing approach. R' = alkyl or benzyl, X = Cl or Br.<sup>87</sup>

### 1.3.3.2 NCA ROP mechanisms

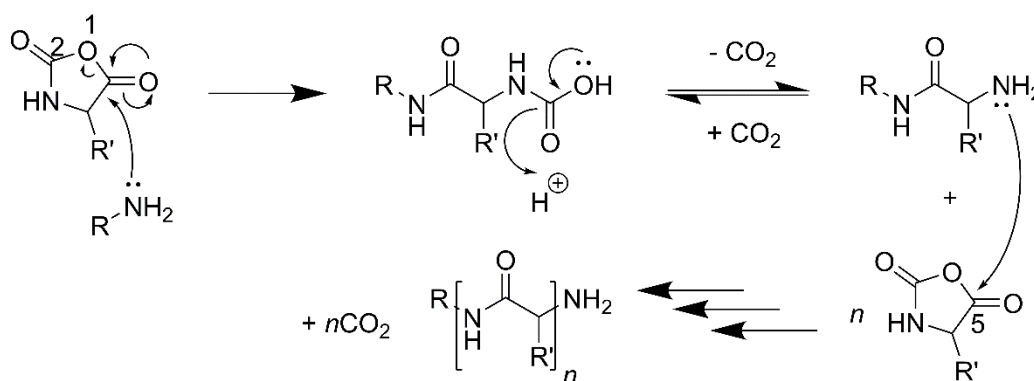
From the NCA, simple and straightforward ROP can occur, initiated from a nucleophile or base (Scheme 1.11).<sup>54</sup> There are two main mechanisms for the ROP of NCAs: the normal amine mechanism (NAM) and the activated monomer mechanism (AMM), discussed in Sections 1.3.3.2.1 and 1.3.3.2.2, respectively. More recently, however, many other NCA ROP mechanisms and techniques have been developed, discussed in Section 1.3.3.2.3.



**Scheme 1.11** General reaction scheme for the ROP of NCAs.

### 1.3.3.2.1 Normal amine mechanism (NAM)

Typical NCA ROP initiators are simple small molecules with a primary amine, secondary amine or alcohol functional groups. These small molecule initiators can initiate NCA ROP via the NAM because they are nonionic and possess at least one mobile hydrogen atom (Scheme 1.12).<sup>54,59</sup> The NAM starts by nucleophilic attack of the C-5 (carbonyl) position, opening the ring and forming an unstable intermediate by proton transfer.<sup>59,155</sup>  $\text{CO}_2$  is released revealing a primary amine which goes on to propagate NCA ROP.

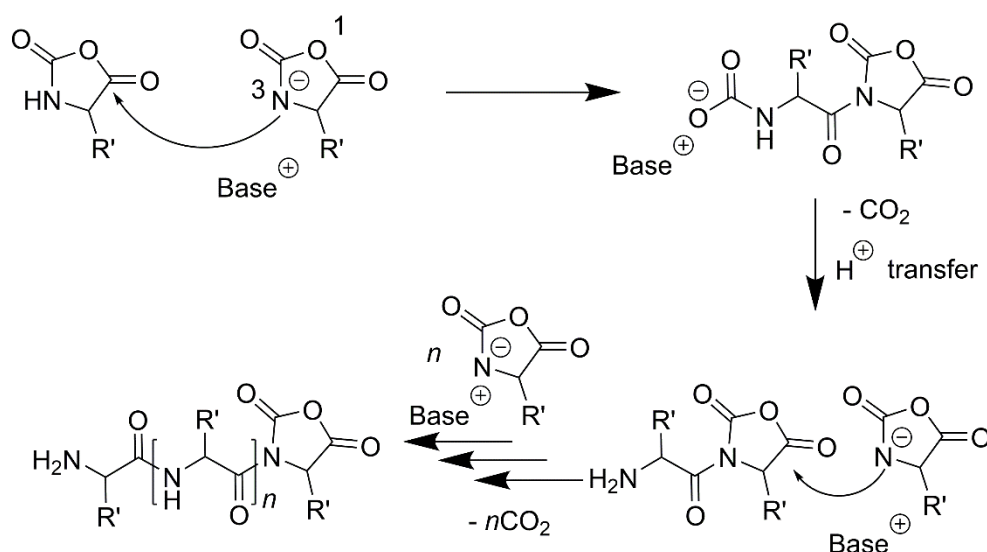


**Scheme 1.12** NCA ROP via the NAM.<sup>59</sup>

### 1.3.3.2.2 Activated monomer mechanism (AMM)

The AMM uses a base to initiate NCA ROP. Such bases are typically tertiary amines and metal alkoxides which abstract the proton from the  $>\text{NH}$  group in the NCA.<sup>54,59</sup> As can be seen in Scheme 1.13, the base or alkoxide acts more like a catalyst than an initiator because it catalyses the formation of NCA anions. These

NCA anions go on to initiate chain propagation which in turn generates another NCA anion.<sup>80,156</sup>



**Scheme 1.13** NCA ROP via the AMM.<sup>54</sup>

One important note here is that such polymerisation reactions can switch back and forth between the NAM and AMM. This switch can occur many times in a polymerisation system, for example a propagating step in one mechanism is a side reaction in another, and *vice versa*.<sup>157</sup> It is also prudent to mention the limitation of NCA ROP is the presence of side reactions such as premature chain termination and chain transfer.<sup>156</sup> These side reactions are brought about by impurities, such as the by-products of NCA synthesis or water, which reduce the actual PAA chain length and increase the dispersity.<sup>54</sup> The most common method of purifying NCA monomers is recrystallisation, however Kramer and Deming describe a more effective purification of NCA monomers, regardless of how synthesised, by flash column chromatography.<sup>158</sup>

### 1.3.3.2.3 Summary of developments in NCA ROP

To avoid unwanted side-reactions, extensive work mostly by Deming and co-workers has used transition metal complexes as catalysts for NCA ROP.<sup>156,159</sup> Although the use of transition metals provides fewer side reactions, a further

purification step of removing the metal is required. Work by Hadjichristidis *et al.* synthesised PAAs via the NAM of NCA ROP in a high vacuum with bespoke sophisticated apparatus.<sup>160-161</sup> In 2007, Lu and Cheng discovered the organosilicon-amine initiator hexamethyldisilazane (HMDS) produced PBLG from BLG-NCA with surprisingly excellent control over the  $M_w$  and very low dispersity.<sup>162</sup> More recently, Wu and colleagues used lithium-HMDS (LiHMDS) to generate large PAAs of narrow dispersity and excellent control over  $M_w$ , significantly faster than traditional NAM NCA ROP and without the need for anhydrous conditions.<sup>163</sup>

NCA ROP has also been initiated by light,<sup>164</sup> Al-Schiff base complexes,<sup>165</sup> amine-borane Lewis pairs,<sup>166</sup> or by ammonium salts.<sup>167-168</sup> Other catalysts for NCA ROP have included rare earth metals,<sup>169</sup> fluorinated alcohol<sup>170</sup> and a thiourea organocatalyst<sup>171</sup> whilst the influence a flow of nitrogen,<sup>172</sup> low dielectric solvents,<sup>65,173</sup> emulsions,<sup>174</sup> and low temperatures<sup>155,175</sup> have also been investigated. NAM is traditionally the most frequently used method of NCA ROP because of its simplicity and well-defined mechanism, however as can be seen above there are many avenues a polymer chemist can take when designing PAA syntheses. Table 1.2 gives a comparison between some different NCA ROP mechanisms.

**Table 1.2** Comparison between common NCA ROP mechanisms.

<b>NCA ROP mechanism</b>	<b>Advantages</b>	<b>Disadvantages</b>
NAM	Relatively straightforward; high $M_w$ ; complex architectures.	Very pure monomer required for controlled synthesis; slow.
AMM		
Transition-metal catalysed	Greater control over $M_w$ than NAM or AMM; narrower dispersity.	Additional purification step to remove metal required; very high $M_w$ cannot be obtained.
High vacuum technique	Lowest dispersity; greatest control over $M_w$ .	Requires bespoke apparatus; laborious; slow.
Organosilicon amines	Very narrow dispersity; fast; doesn't require anhydrous conditions.	Less reactive NCAs unsuitable.

## 1.4 Polymers as Biomaterials

As previously discussed in Section 1.1.1.2, imparting antimicrobial activity to PET for potential application as a biomaterial for use in heart valves and sutures, for example, may be done. There are other examples of the materials discussed having use as a biomaterial, for example NPs as drug delivery vehicles, and these are discussed in Section 1.4.1. The polymers may also form hydrogels, and their use in drug delivery and tissue engineering is discussed in Section 1.4.2. Of particular potential clinical application are theranostic devices which combine therapeutics and diagnostics in one device (material), and these are discussed in Section 1.4.3.

### 1.4.1 Nanoparticles (NPs) as drug delivery vehicles

Nanoscale drug delivery vehicles are intended to prevent harmful side effects, enhance the amount of drugs at the required zone of interest, minimise drug degradation and loss, and increase drug bioavailability.<sup>176</sup> Pharmacokinetics is used to describe the adsorption, distribution, metabolism and excretion of a compound, thus drug delivery vehicles are intended to improve the pharmacokinetics of drugs.<sup>177</sup> Drug delivery vehicles can be used to treat, or improve treatment, of many diseases, including cancer,<sup>178</sup> glaucoma,<sup>179</sup> Parkinson's disease,<sup>180</sup> chronic pain,<sup>181</sup> fungal infection,<sup>182</sup> diabetes,<sup>183</sup> or asthma;<sup>184</sup> and for the prevention of diseases such as restricting Human immunodeficiency virus (HIV) proliferation or delivering vaccines.<sup>185-187</sup> Although some drug delivery vehicles simply release the drug slowly over a prolonged period of time,<sup>188</sup> drug delivery vehicles typically release their cargo in a stimuli-responsive manner.<sup>189</sup> Stimuli may include light, enzymes, ultrasonic radiation, magnetisation, or changes to redox potential, pH, temperature, or combinations thereof.<sup>190-192</sup>

#### 1.4.1.1 Amphiphilic polymeric micelles for drug delivery

Amphiphilic polymers may self-assemble into micelles whereby in aqueous solutions the hydrophilic ends of the polymers point outwards, and the hydrophobic ends are packed inside. If this self-assembly occurs in the presence of hydrophobic drug molecules, the drug may be loaded within the core or corona of the micelle and can thus be used in drug/gene delivery.<sup>193-196</sup> One amphiphilic copolymer of particular interest is poly(D,L-lactic-co-glycolic acid)-*b*-PEG (PLGA-PEG), whereby PLGA serves as the hydrophobic block, and PEG the hydrophilic block.<sup>197</sup> PLGA-PEG has approval for use in medicine by the FDA, and when decorated with tumour-targeting moieties, and encapsulating the hydrophobic chemotherapeutic Pt-based prodrug of cisplatin, a remarkable improvement in cisplatin's therapeutic ability against prostate cancer was observed.<sup>198-199</sup> More recently, Tian *et al.* describe the co-delivery of cisplatin and another chemotherapeutic, paclitaxel, using PLGA-PEG to treat lung cancer (Figure

1.5).<sup>200</sup> The authors demonstrate their co-delivery strategy has superior reduction in tumour growth rates compared to conventional chemoradiotherapy.

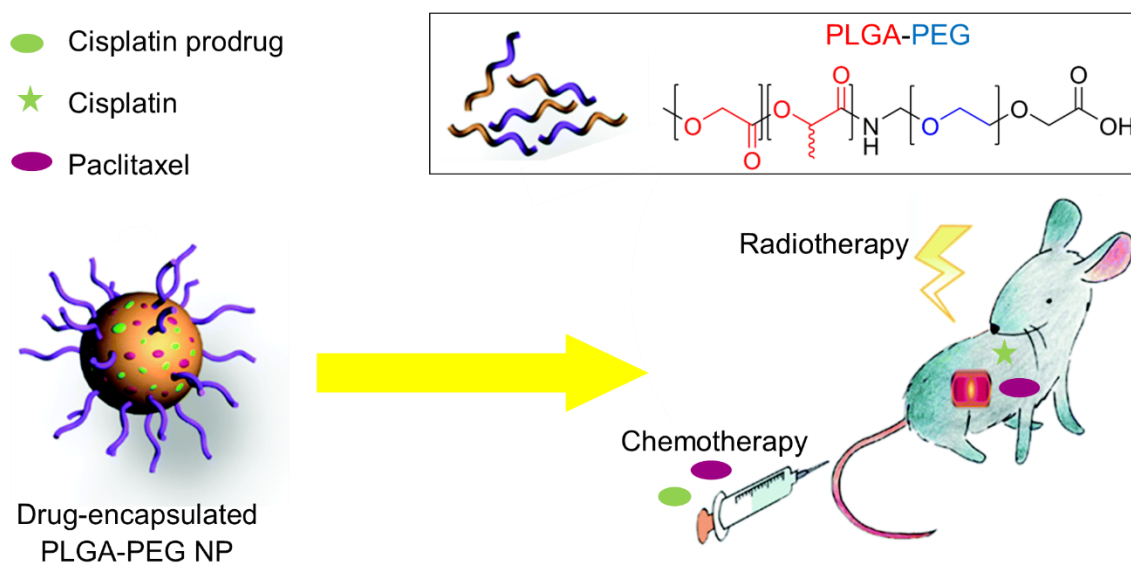


**Figure 1.5** Co-delivery of cisplatin prodrug and paclitaxel from PLGA-PEG NP for treating lung cancer with improved efficacy to radiotherapy and traditional chemotherapy. Adapted from Ref. 200 with permission from The Royal Society of Chemistry.

PEG is often used to initiate NCA ROP from one of its terminal OH or NH<sub>2</sub> groups, combining the excellent properties of PAAs with the biocompatibility, hydrophilicity and diverse sizes and architectures of readily available PEG.<sup>201-203</sup> However, several potential safety concerns have risen from the repeated use of PEG.<sup>204</sup> It is reported that PEG can cause tissue accumulation, hypersensitivity, an immunological response, accelerated blood clearance, and generates antibodies under certain conditions *in vivo*.<sup>205-207</sup> Additionally, PEG is not biodegradable and so alternatives to its use is sought by researchers.<sup>208-210</sup> Polysarcosine (PSar, poly(*N*-methyl glycine)), is a promising alternative to PEG due to its high water solubility, non-ionic character, stability *in vivo*, resistance to protein adsorption, and non-immunogenicity.<sup>211-213</sup> Birke and co-workers synthesised a range of PBLG-*b*-PSar and PLys(Z)-*b*-PSar amphiphilic block copolymers via sequential NCA ROP (Figure 1.6).<sup>214</sup> The polymers formed micelles in aqueous solution and a hydrophobic enzyme inhibition drug, used in the treatment of some cancers, was loaded. The micelles increased the drugs bioavailability, thus the polymeric micelles are a potential drug delivery vehicle.

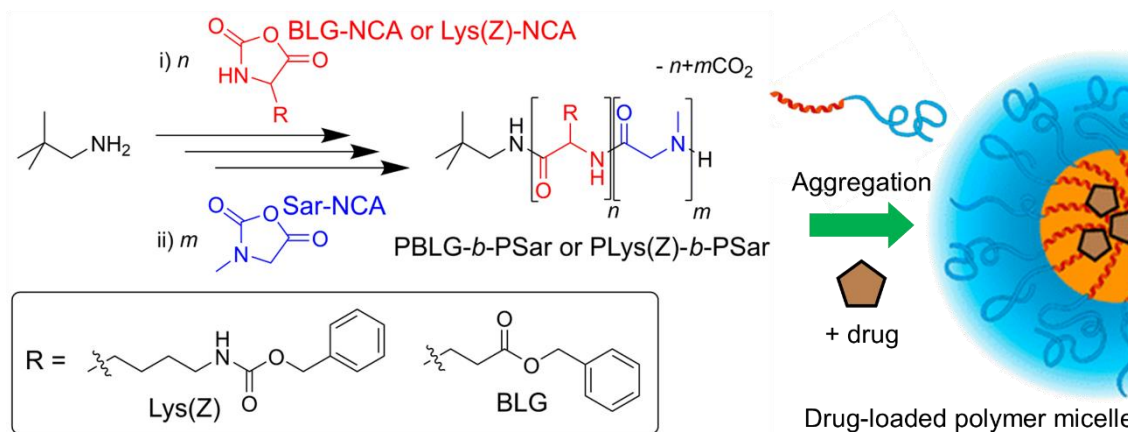


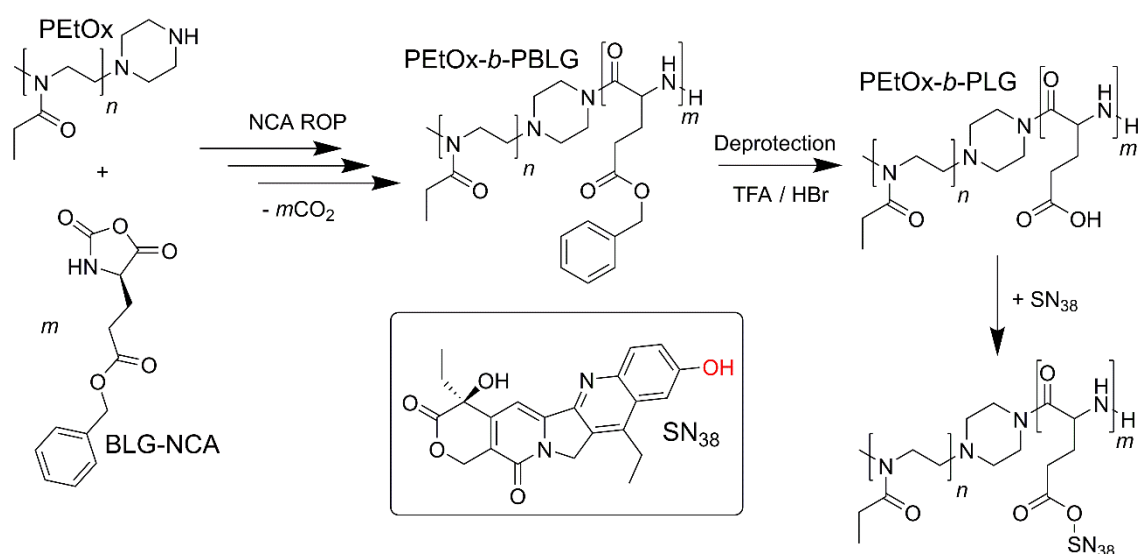
**Figure 1.6** Synthesis of PBLG-*b*-PSar and PLys(Z)-*b*-PSar via sequential NCA ROP, followed by aggregation with a drug forming drug-loaded polymer micelles. Reprinted (adapted) with permission from Ref. 214. Copyright 2014 American Chemical Society.

#### 1.4.1.2 Polymer-therapeutic conjugates

Drug delivery vehicles often have their payload loaded inside the material but loading of the drug can be challenging and lead to loss of valuable drug molecules. Drug loss can be prevented by covalently bonding the therapeutic to the polymer, either by initiating NCA ROP from a drug molecule or attaching therapeutic molecules to a polymer chain.<sup>75</sup> Zhang *et al.* synthesised PEG-*b*-PBLG amphiphilic block copolymers which the chemotherapy drug docetaxel was able to conjugate with through a disulphide bond.<sup>215</sup> The copolymer-drug conjugates formed micelles in aqueous solution and the authors demonstrated their redox sensitivity, releasing more docetaxel in the presence of a glutathione analogue, D,L-dithiothreitol, than without, thus a promising effective cancer therapy.

Synthesised polymers can also be functionalised post-polymerisation with therapeutics. In 2019, Salmanpour and colleagues synthesised poly(2-ethyl-2-oxazoline)-*b*-PBLG (PEtOx-*b*-PBLG) by using PEtOx as a macroinitiator for NCA ROP of BLG-NCA (Scheme 1.14).<sup>216</sup> The PBLG block required deprotection post-polymerisation to remove the benzyl ester protecting group to present a carboxylic acid functional group on the polymer chain. From these carboxylic acid functional groups, SN38, an FDA-approved drug to treat colorectal cancers, was

conjugated to the amphiphilic block copolymer via carbodiimide mediated esterification between the carboxylic acid alcohol and the alcohol group on SN38, coloured red in Scheme 1.14. SN38 is poorly water soluble and is susceptible to hydrolytic degradation but included in this polymer-drug conjugate the pharmacokinetics of the drug are improved, and the ester linkage between the polymer and drug is thought to be broken when the polymer-drug reaches the slightly more acidic tumour environment. Consequentially, this polymer-drug conjugate and others are potentially efficient drug delivery systems for therapeutics of poor water solubility.



**Scheme 1.14** Reaction scheme for the synthesis of PETox-*b*-PBLG, followed by post-polymerisation deprotection to form PETox-*b*-PLG and conjugation of SN38 chemotherapeutic, forming a polymer-drug conjugate.<sup>216</sup>

#### 1.4.1.3 Inorganic nanoparticle-polymer hybrid materials

Hybrid materials combine the properties of two distinct materials together, such as a block copolymer where one block is a PAA and the other a polyester or a polymer-inorganic material nanocomposite, for example.<sup>87</sup> In 2016, Luo *et al.* decorated a silica-coated gold nanorod with a Pt(IV) complex, a photosensitiser NP, tumour-targeting ligands, and PEG chains for a tri-synergistic tumour therapy system (Figure 1.7a).<sup>217</sup> The silica coating was used to improve biocompatibility, hold a high volume of photosensitiser NP which can selectively kill cancer cells,

and provides an easy surface for the Pt(IV) complex to be adhered and convert to a Pt(II) complex within the reducing environment of a tumour and imparting cell death. The photosensitiser NP was modified with tumour-targeting conjugated PEG, whereby PEG aided the long-term circulation of the nanocomposite system whilst the tumour-targeting moieties improved the chemotherapeutic efficacy.

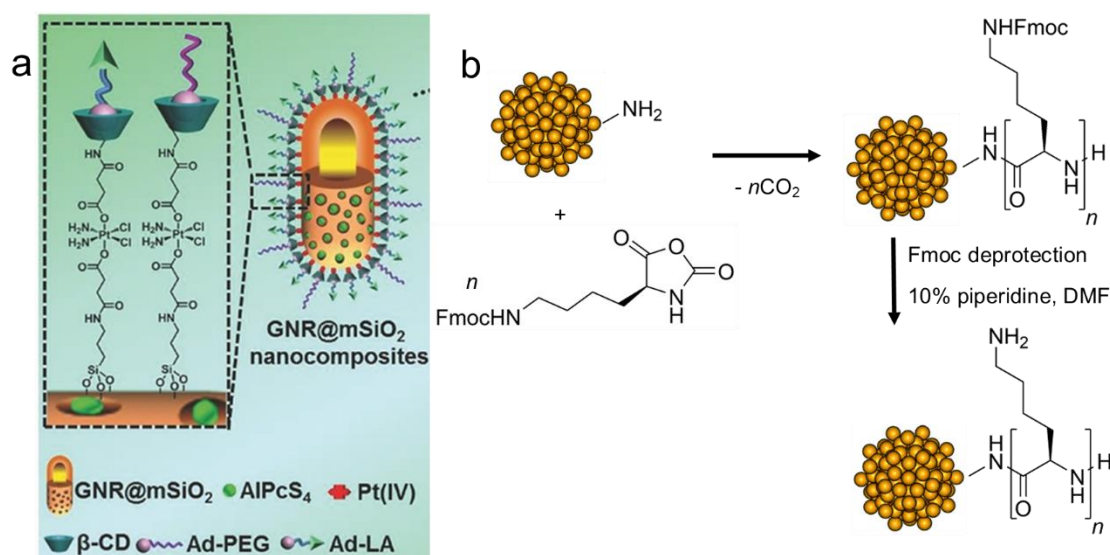


**Figure 1.7** Polymer-metal hybrid nanocomposite examples. (a) Silica-coated gold nanorod (GNR) with a photosensitiser NP, decorated with a Pt(IV) complex, tumour-targeting moieties and PEG solubilising agents.<sup>217</sup> Photosensitisers = AIPcS<sub>4</sub> and β-CD and tumour-targeting moieties adamantane (Ad) and lactobionic acid (LA). © 2016 WILEY-VCH Verlag GmbH & Co. KGaA, Weinheim. (b) Synthesis of PLys-Au<sub>144</sub> hybrid nanocomposite via NCA ROP – published by the Royal Society of Chemistry.<sup>218</sup>

NCA ROP can be initiated from an inorganic material ('grafted-from'), or a PAA can self-assemble around, or bind to, an inorganic material, ('grafting-to').<sup>219</sup> Grafting PAAs with inorganic material is often utilised to improve the biocompatibility of the inorganic material, such as multiwalled carbon nanotubes.<sup>220</sup> Grafting from does not necessarily need to be from an inorganic material or macroinitiator, it can be from biologically active molecules to improve their biodistribution, for example.<sup>75</sup> Guryanov and colleagues grafted PLys from Au<sub>144</sub> nanoclusters, forming a hybrid biocompatible star-like nanocomposite which the authors suggest can be used to prepare very stable drug delivery vehicles (Figure 1.7b).<sup>218</sup>

### 1.4.2 Hydrogels for drug delivery and tissue engineering

Hydrogels are water-swollen networks of polymer, transforming polymer chemistry to 3D.<sup>221</sup> Recently, Lee *et al.* developed a hydrogel based on hyaluronic acid and chitosan which demonstrates temperature-dependant sol-gel transitions with tuneable mechanical properties (Figure 1.8).<sup>222</sup> The material offers good cell binding affinity, biocompatibility, and shows promising application as an injectable scaffold system for cartilage regeneration.

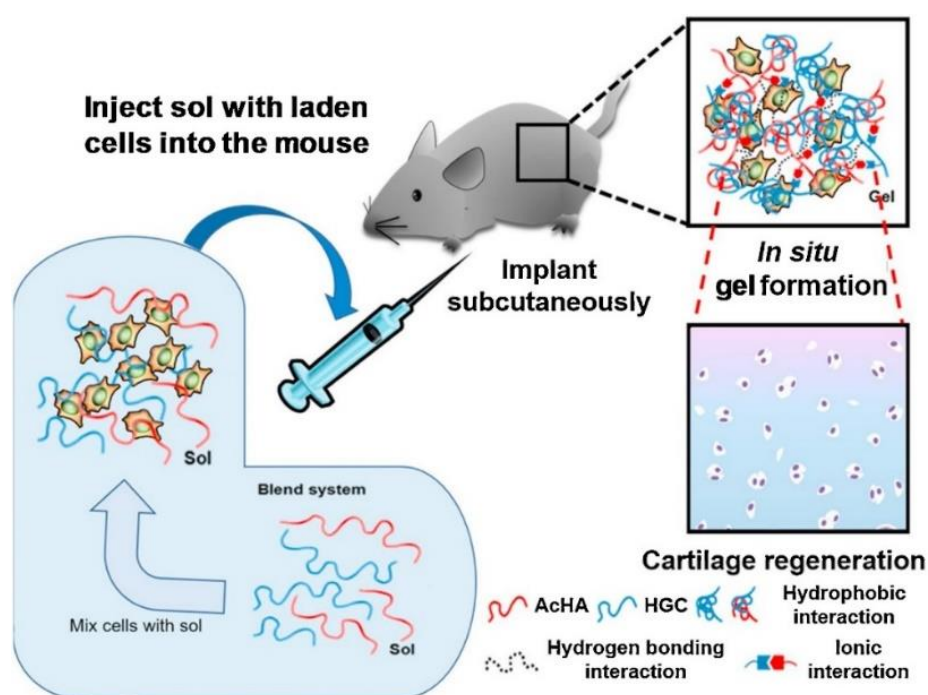
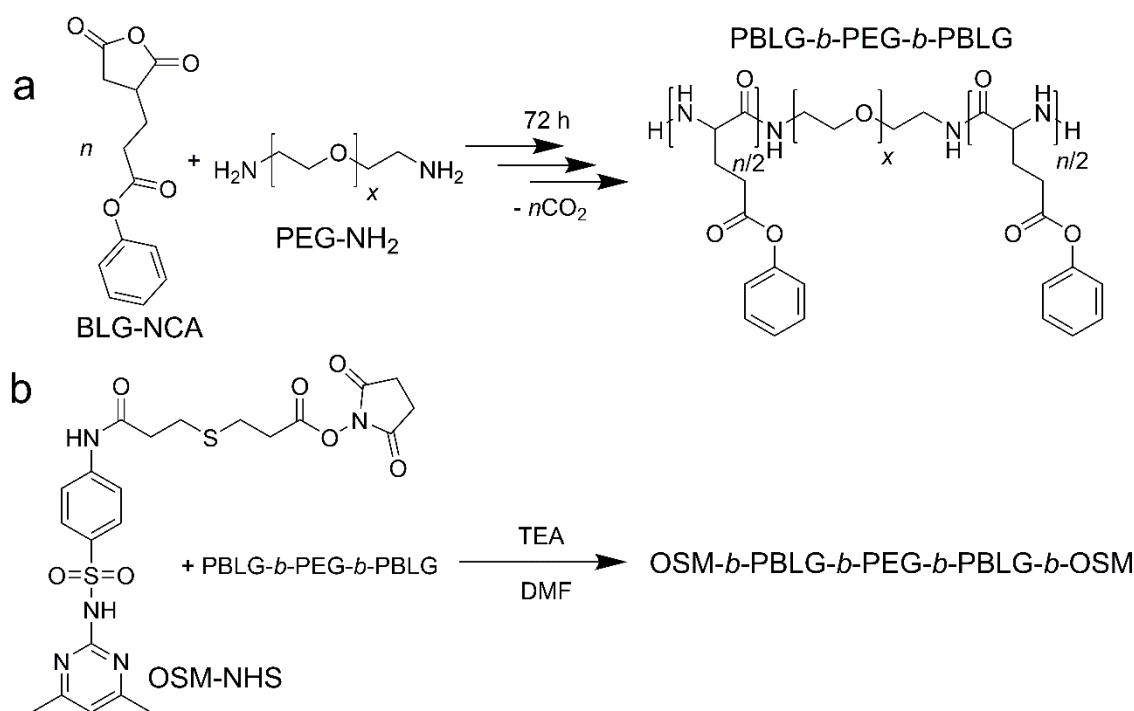


**Figure 1.8** Illustration of the subcutaneous *in situ* gel formation for cartilage regeneration. Reprinted from Ref. 222, copyright (2020), with permission from Elsevier.

When the polymer involved in the hydrogel is a PAA, the hydrogel has inherent biocompatibility, biodegradability, multiple functionalities from the different  $\alpha$ -amino acids and tuneable architectures.<sup>93</sup> There is interest in hydrogels from PAAs for tissue engineering, antibacterial coatings, 3D cell scaffolds and drug/gene delivery.<sup>223-224</sup> Turabee and colleagues synthesised a PBLG-*b*-PEG block copolymer via NCA ROP of BLG-NCA from the terminal  $\text{NH}_2$  groups on PEG-amine (Scheme 1.15a).<sup>225</sup> Post-polymerisation functionalisation of the chain end group using *N*-hydroxy succinimide ester activated oligo(sulfamethazine)

(OSM-NHS) resulted in a penta-block copolymer (Scheme 1.15b). The PBLG blocks imparted temperature responsiveness, OSM blocks pH-responsiveness and PEG provided pliability and lowers inflammation at the site of implantation. The copolymer formed a gel *in situ* on subcutaneous administration due to changes in pH and temperature and was reported to release proteins.



**Scheme 1.15** NCA ROP of BLG-NCA from PEG-NH<sub>2</sub> (a) followed by post-polymerisation end-group functionalisation with OSM-NHS (b).<sup>225</sup> TEA = triethylamine.

### 1.4.3 Theranostic devices

Theranostics is a combination of diagnosis and therapy and aims for early diagnosis, accurate imaging, precise treatment and real-time monitoring of treatment efficacy.<sup>226-228</sup> In 2019, Scialabba *et al.* decorated carbon nanodots (CNDs), fluorescent nanoparticles of carbon, with biotin, a tumour-targeting moiety, linked via PEG chains (Figure 1.9a).<sup>229</sup> The CNDs the researchers used are able to convert near-infrared radiation into heat, coupled with biotin's tumour-targeting ability induces local hyperthermia inside tumours. Additionally, the NPs could be loaded with the chemotherapeutic drug, irinotecan, and its release

triggered by the near-infrared-triggered photothermal ablation of the tumour mass. An *in vivo* bioimaging ability of the NPs was also demonstrated, and as the NPs target and selectively kill tumours, the system has a high potential as an efficient theranostic tool.

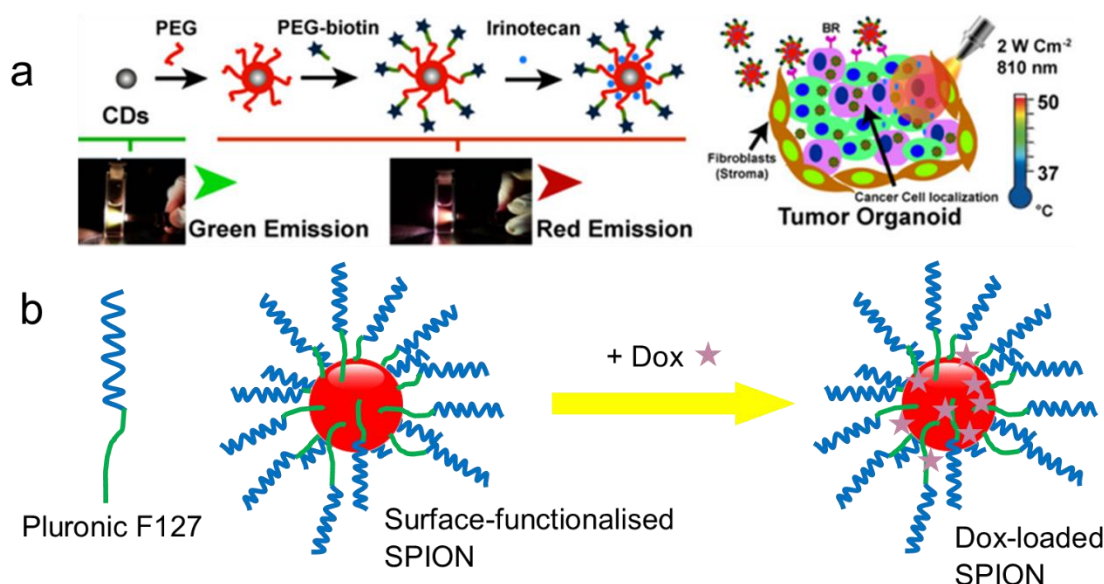


**Figure 1.9** Theranostic examples. (a) Biotin-decorated CDs through a PEG linker for the tumour-targeted release of the chemotherapeutic irinotecan and *in vivo* bioimaging ability as a theranostic tool. Reprinted (adapted) with permission from Ref. 229. Copyright (2019) American Chemical Society. (b) Surface-functionalisation of a SPION with Pluronic F127, followed by Dox loading for targeted Dox delivery and simultaneous MRI imaging.<sup>230</sup>

Recent work by Salunkhe and co-workers uses magnetic NPs of iron oxide to induce localised hyperthermia for a theranostic device.<sup>230</sup> The researchers synthesised high magnetic moment superparamagnetic iron oxide NPs (SPIONs), followed by conjugation with an amphiphilic copolymer of hydrophobic poly(propylene oxide) and hydrophilic poly(ethylene oxide) (Pluronic F27) (Figure 1.9b). The surface-functionalisation of SPIONs allowed them to form micelles and significantly enhanced their dispersion stability in aqueous media. Additionally, the chemotherapeutic doxorubicin (Dox) was attached via electrostatic linking. Magnetic resonance imaging (MRI) of the tumour site induces localised hyperthermia at the tumour site and this increase in temperature also released Dox, providing a targeted chemotherapeutic. Additionally, MRI imaging of the

tumour site allows visualisation of the NPs tumour efficacy, thus a potential theranostic device.

## 1.5 Summary and Future Outlook

Polymers are essential for modern life and commodity polymers dominate the market. PET is a commodity polymer synthesised via step-growth polycondensation and has wide-ranging applications including packaging, textiles, antimicrobial biomaterials and advanced laundry formulations. There are environmental issues with the continued use of commodity polymers, whose monomers are often sourced from non-renewable crude oil and the persistence in the environment of the polymer leads to pollution of the oceans. Pollution of the waterways in coloured effluent from the inefficient colouring of polymers is also of concern. Efforts to overcome these issues have been made, such as biodegradable replacements, monomers from renewable resources, and advances in the dyeing processes. However, much work is still to be done to make the polymer industry more environmentally friendly and sustainable.

Controlled polymerisation techniques such as ROPs allow polymers to be synthesised with control over  $M_w$ , narrow dispersity and with complex architectures. ROP of cyclic macrolactones catalysed by the FDA-approved  $\text{Sn}(\text{Oct})_2$  or enzymes provide biodegradable aliphatic polyesters as potential alternatives to some commodity polymers. NCA ROP allows PAAs to be synthesised in a reliable way with high  $M_w$ , low dispersity and with a plethora of architectures and functionalities. The prepared PAAs may form discrete structures, such as  $\alpha$ -helix,  $\beta$ -sheets, micelles or vesicles from many polymer architectures such as block, graft or random copolymers.

Biocompatible and highly functional polymers such as PAAs and PEG allow innovative biomaterials to be synthesised for the treatment of diseases including cancer. Amphiphilic block copolymers may self-assemble to form micellar NPs for drug delivery applications. Research into stimuli-responsive NPs also allow

the targeted delivery of chemotherapeutics to tumour cells, improving the pharmacokinetics and hence reducing debilitating side-effects. Much research is also focused on these polymers as hydrogels for drug delivery or tissue engineering applications. Hybrid materials are also of intense interest, combining two useful properties into one material leads to impressive and potentially game-changing innovations, such as theranostic photothermal-initiated drug release and simultaneous bioimaging. Although promising, much work is still required in developing these treatments as limitations in clinical translation is a continuous and pressing issue.

## **1.6 Research Aims and Thesis Outline**

This Thesis aims to address some of the issues highlighted above: polymers contributing to pollution and improving the pharmacokinetics of chemotherapy drugs. Specifically, work presented aims to reduce the contribution of polymers to pollution by the formation of highly functional biodegradable polymers for drug delivery or tissue engineering, forming biodegradable polymers to improve the aqueous compatibility of metal NPs and chemotherapy drugs, and to develop more efficient polymer dyeing methods to add value, improve colourfastness and reduce dye effluent pollution. Polymers developed include PAAs because of their biodegradability, biocompatibility, variety of properties available and versatility of structure, and polyesters because of their proliferation in industry.

Chapter 3 describes the synthesis of a biodegradable amphiphilic PAA which self-assembles into a polymeric NP and can uptake and selectively release a chemotherapeutic to acidic environments. The PAA possesses a terminal phosphonate functional group which can bond with metal NPs to improve their aqueous compatibility. Chapter 4 continues this work by developing the phosphonate-terminated PAA to graft-to, or self-assemble with, a fluorescent and phosphorescent NP. The formed nanocomposites possess stimuli-responsiveness with respect to pH, releasing a loaded chemotherapeutic to acidic environments and simultaneously losing afterglow which provides a possible theranostic material. In Chapter 5, a novel route to PAAs is explored:

the ROP of cyclic dipeptide alanine anhydride catalysed by  $\text{Sn}(\text{Oct})_2$  and initiated by PEG monomethyl ether. The afforded amphiphilic block copolymer possessing a large polyalanine equivalence, high semi-crystallinity, and pH-responsiveness. The material has potential application as a drug delivery vehicle or with optimisation may replace some commodity polymers.

Chapter 6 describes the straightforward and permanent colouration of polyglobalide, a potentially biodegradable polyester. The dyed polyglobalide was cross-linked to enable its use in high-temperature applications to potentially replace some commodity polymers, and dyeing adds value. Swelling in 2-phenylethanol allows the materials to be simple and cost-effective antimicrobial gels. In Chapter 7, an amphiphilic poly(ether-ester) was modified to present a handle for efficient covalent dyeing without coloured wastewater. The method described may be used for commodity polyesters or the reported modified polymer has potential utilisation in advanced laundry formulations.

## 1.7 References

1. J. W. Nicholson, *The Chemistry of Polymers*, Royal Society of Chemistry, Cambridge, U.K., 2012.
2. M. Mishra, ed., *Encyclopedia of Polymer Applications*, CRC Press, Boca Raton, Florida U.S.A., 2019.
3. D. K. Jena and P. K. Sahoo, *Journal of Applied Polymer Science*, 2018, **135**, 45968.
4. J. W. Nicholson, *The Chemistry of Polymers*, Royal Society of Chemistry, London, U.K., 5th edn., 2017.
5. S. Koltzenburg, M. Maskos and O. Nuyken, *Polymer Chemistry*, Springer Nature, Berlin, Germany, 2017.
6. S. Fakirov, in *Fundamentals of Polymer Science for Engineers*, Wiley-VCH, Weinheim, Germany, 2017, ch. 9, pp. 221-240.
7. R. Geyer, J. R. Jambeck and K. L. Law, *Science Advances*, 2017, **3**, e1700782.
8. T. Yokozawa and Y. Ohta, *Chemical Reviews*, 2016, **116**, 1950-1968.
9. D. Crespy, M. Bozonnet and M. Meier, *Angewandte Chemie International Edition*, 2008, **47**, 3322-3328.
10. B. M. Mandal, *Fundamentals of polymerization*, World Scientific, Singapore, 2013.
11. G. Yilmaz and Y. Yagci, *Progress in Polymer Science*, 2020, **100**, 101178.
12. D. Kang, R. Auras and J. Singh, *Resources, Conservation and Recycling*, 2017, **116**, 45-52.

13. S. Zekriardehani, S. A. Jabarin, D. R. Gidley and M. R. Coleman, *Macromolecules*, 2017, **50**, 2845-2855.
14. PlasticsEurope, *Plastics - The Facts 2019*, [https://www.plasticseurope.org/application/files/1115/7236/4388/FINAL\\_web\\_version\\_Plastics\\_the\\_facts2019\\_14102019.pdf](https://www.plasticseurope.org/application/files/1115/7236/4388/FINAL_web_version_Plastics_the_facts2019_14102019.pdf), (accessed 11/06/2020, 2020).
15. US2130948, 1938.
16. W. H. Carothers, *Journal of the American Chemical Society*, 1929, **51**, 2548-2559.
17. W. H. Carothers and J. A. Arvin, *Journal of the American Chemical Society*, 1929, **51**, 2560-2570.
18. M. V. Pergal and M. Balaban, in *Polyethylene Terephthalate: Uses, Properties and Degradation*, ed. N. A. Barber, Nova Science Publishers, New York, U.S.A., 2017, ch. 1, pp. 1-102.
19. J. Scheirs and T. E. Long, *Modern polyesters: chemistry and technology of polyesters and copolyesters*, Wiley, Chichester, U.K., 2003.
20. K. Pang, R. Kotek and A. Tonelli, *Progress in Polymer Science*, 2006, **31**, 1009-1037.
21. S. Mandal and A. Dey, in *Recycling of Polyethylene Terephthalate Bottles*, eds. S. Thomas, A. Rane, K. Kanny, A. V.K and M. G. Thomas, William Andrew Publishing, Oxford, U.K., 2019, ch. 1, pp. 1-22.
22. H. K. Webb, J. Arnott, R. J. Crawford and E. P. Ivanova, *Polymers*, 2013, **5**, 1-18.
23. E.-R. Kenawy, S. D. Worley and R. Broughton, *Biomacromolecules*, 2007, **8**, 1359-1384.
24. A. Muñoz-Bonilla and M. Fernández-García, *Progress in Polymer Science*, 2012, **37**, 281-339.
25. X. Ding, A. Wang, W. Tong and F.-J. Xu, *Small*, 2019, **15**, 1900999.
26. L. Cen, K. G. Neoh and E. T. Kang, *Langmuir*, 2003, **19**, 10295-10303.
27. S. del Hoyo-Gallego, L. Pérez-Álvarez, F. Gómez-Galván, E. Lizundia, I. Kuritka, V. Sedlarik, J. M. Laza and J. L. Vila-Vilela, *Carbohydrate Polymers*, 2016, **143**, 35-43.
28. W. Cao, D. Wei, A. Zheng and Y. Guan, *European Polymer Journal*, 2019, **118**, 231-238.
29. W. Cao, D. Wei, Y. Jiang, S. Ye, A. Zheng and Y. Guan, *Journal of Materials Science*, 2019, **54**, 2699-2711.
30. US10351802, 2019.
31. E. Kissa, in *Detergency: Theory and Technology*, eds. W. G. Cutler and E. Kissa, Marcel Dekker Inc., New York, USA, 1986, vol. 20, ch. 5, pp. 333-370.
32. B. S. Butola, in *Polyesters and Polyamides*, eds. B. L. Deopura, R. Alagirusamy, M. Joshi and B. Gupta, Woodhead Publishing, Cambridge, UK, 2008, ch. 12, pp. 325-353.
33. A. Valentini, S. Bakalis, K. Gkatzionis, G. Palazzo, N. Cioffi, C. D. Franco, E. Robles, A. Brooker and M. M. Britton, *Industrial & Engineering Chemistry Research*, 2019, **58**, 14839-14847.
34. T. M. R. Miranda, J. Santos and G. M. B. Soares, *IOP Conference Series: Materials Science and Engineering*, 2017, **254**, 032005.
35. J. V. Rowley, J. Exley, H. Yu, G. S. Mircale, A. S. Hayward and P. D. Thornton, *Chemical Communications*, 2020, **56**, 6360-6363.
36. A. Douka, S. Vouyiouka, L.-M. Papaspyridi and C. D. Papaspyrides, *Progress in Polymer Science*, 2018, **79**, 1-25.

37. M. Winnacker and B. Rieger, *Macromolecular Rapid Communications*, 2016, **37**, 1391-1413.
38. W. H. Carothers and G. J. Berchet, *Journal of the American Chemical Society*, 1930, **52**, 5289-5291.
39. W. H. Carothers, *Chemical Reviews*, 1931, **8**, 353-426.
40. US2130523, 1938.
41. J. K. Smith and D. A. Hounshell, *Science*, 1985, **229**, 436-442.
42. Y. Zhu, C. Romain and C. K. Williams, *Nature*, 2016, **540**, 354-362.
43. A.-C. Albertsson and M. Hakkarainen, *Science*, 2017, **358**, 872-873.
44. I. A. Kane, M. A. Clare, E. Miramontes, R. Wogelius, J. J. Rothwell, P. Garreau and F. Pohl, *Science*, 2020, **368**, 1140-1145.
45. K. Hamad, M. Kaseem, M. Ayyoob, J. Joo and F. Deri, *Progress in Polymer Science*, 2018, **85**, 83-127.
46. J.-B. Zhu, E. M. Watson, J. Tang and E. Y.-X. Chen, *Science*, 2018, **360**, 398-403.
47. J. M. Garcia and M. L. Robertson, *Science*, 2017, **358**, 870-872.
48. T. Salem, S. Uhlmann, M. Nitschke, A. Calvimontes, R.-D. Hund and F. Simon, *Progress in Organic Coatings*, 2011, **72**, 168-174.
49. A. D. Broadbent, *Basic Principles of Textile Colouration*, Society of Dyers and Colourists, Bradford, U.K., 2001.
50. T. Hussain, M. Tausif and M. Ashraf, *Journal of Cleaner Production*, 2015, **108**, 476-483.
51. S. M. Burkinshaw, K. Liu and G. Salihu, *Dyes and Pigments*, 2019, **171**, 106367.
52. A. Murcia-Salvador, J. A. Pellicer, M. I. Fortea, V. M. Gómez-López, M. I. Rodríguez-López, E. Núñez-Delicado and J. A. Gabaldón, *Polymers*, 2019, **11**, 1003.
53. J. Jones, *Amino Acid and Peptide Synthesis*, Oxford University Press, Oxford, U.K., 2nd edn., 2002.
54. M. Khuphe and P. D. Thornton, in *Engineering of Biomaterials for Drug Delivery Systems*, ed. A. Parambath, Woodhead Publishing, 2018, ch. 7, pp. 199-228.
55. T. Saxena, L. Karumbaiah and C. M. Valmikinathan, in *Natural and Synthetic Biomedical Polymers*, eds. S. G. Kumbar, C. T. Laurencin and M. Deng, Elsevier, Oxford, 2014, pp. 43-65.
56. M. A. Gauthier and H.-A. Klok, *Chemical Communications*, 2008, **23**, 2591-2611.
57. U. Glebe, B. Santos de Miranda, P. van Rijn and A. Boker, in *Bio-Synthetic Hybrid Materials and Bionanoparticles: A Biological Chemical Approach Towards Material Science*, The Royal Society of Chemistry, 2015, pp. 1-29.
58. S. Cavalli, F. Albericio and A. Kros, *Chemical Society Reviews*, 2010, **39**, 241-263.
59. J. Huang and A. Heise, *Chemical Society Reviews*, 2013, **42**, 7373-7390.
60. A. D. Silverman, A. S. Karim and M. C. Jewett, *Nature Reviews Genetics*, 2020, **21**, 151-170.
61. A. Rasines Mazo, S. Allison-Logan, F. Karimi, N. J.-A. Chan, W. Qiu, W. Duan, N. M. O'Brien-Simpson and G. G. Qiao, *Chemical Society Reviews*, 2020, **49**, 4737-4834.
62. M. A. Qadir, M. Martin and P. T. Hammond, *Chemistry of Materials*, 2014, **26**, 461-476.

63. C. Chen, F. Kong, X. Wei and S. H. Thang, *Chemical Communications*, 2017, **53**, 10776-10779.
64. D. W. P. M. Lowik, E. H. P. Leunissen, M. van den Heuvel, M. B. Hansen and J. C. M. van Hest, *Chemical Society Reviews*, 2010, **39**, 3394-3412.
65. Z. Song, H. Fu, R. Baumgartner, L. Zhu, K.-C. Shih, Y. Xia, X. Zheng, L. Yin, C. Chipot, Y. Lin and J. Cheng, *Nature Communications*, 2019, **10**, 5470.
66. A. I. Triftaridou, F. Chécot and I. Iliopoulos, *Macromolecular Chemistry and Physics*, 2010, **211**, 768-777.
67. E. C. Izgu, A. Björkbom, N. P. Kamat, V. S. Lelyveld, W. Zhang, T. Z. Jia and J. W. Szostak, *Journal of the American Chemical Society*, 2016, **138**, 16669-16676.
68. R. Jones, *Nature Nanotechnology*, 2008, **3**, 699-700.
69. H. Lu, J. Wang, Y. Bai, J. W. Lang, S. Liu, Y. Lin and J. Cheng, *Nature Communications*, 2011, **2**, 206.
70. M. Khuphe, C. S. Mahon and P. D. Thornton, *Biomaterials Science*, 2016, **4**, 1792-1801.
71. A. Kumar, W. Pisula and K. Müllen, *Journal of Applied Polymer Science*, 2018, **135**, 46750.
72. Y. Ding, M. Cai, Z. Cui, L. Huang, L. Wang, X. Lu and Y. Cai, *Angewandte Chemie International Edition*, 2018, **57**, 1053-1056.
73. J. Fan, R. Li, X. He, K. Seetho, F. Zhang, J. Zou and K. L. Wooley, *Polymer Chemistry*, 2014, **5**, 3977-3981.
74. G. J. M. Habraken, A. Heise and P. D. Thornton, *Macromolecular Rapid Communications*, 2012, **33**, 272-286.
75. M. Khuphe, A. Kazlauciusas, M. Huscroft and P. D. Thornton, *Chemical Communications*, 2015, **51**, 1520-1523.
76. T. Higashihara and R. Faust, *Reactive and Functional Polymers*, 2009, **69**, 429-434.
77. M. Levit, N. Zashikhina, A. Dobrodumov, A. Kashina, I. Tarasenko, E. Panarin, S. Fiorucci, E. Korzhikova-Vlakh and T. Tennikova, *European Polymer Journal*, 2018, **105**, 26-37.
78. X. He, J. Wu and C. Gao, *RSC Advances*, 2020, **10**, 5747-5757.
79. X. Sang, Q. Yang, Q. Wen, L. Zhang and C. Ni, *Materials Science and Engineering: C*, 2019, **98**, 910-917.
80. N. Hadjichristidis, H. Iatrou, M. Pitsikalis and G. Sakellariou, *Chemical Reviews*, 2009, **109**, 5528-5578.
81. D. Mavrogiorgis, P. Bilalis, A. Karatzas, D. Skoulas, G. Fotinogiannopoulou and H. Iatrou, *Polymer Chemistry*, 2014, **5**, 6256-6278.
82. Y. Huang, Z. Tang, X. Zhang, H. Yu, H. Sun, X. Pang and X. Chen, *Biomacromolecules*, 2013, **14**, 2023-2032.
83. W. Jiang, X. Xiao, Y. Wu, W. Zhang, Z. Cong, J. Liu, S. Chen, H. Zhang, J. Xie, S. Deng, M. Chen, Y. Wang, X. Shao, Y. Dai, Y. Sun, J. Fei and R. Liu, *Biomaterials Science*, 2020, **8**, 739-745.
84. I. Tarasenko, N. Zashikhina, I. Guryanov, M. Volokitina, B. Biondi, S. Fiorucci, F. Formaggio, T. Tennikova and E. Korzhikova-Vlakh, *RSC Advances*, 2018, **8**, 34603-34613.
85. M. Zhao, Z. Fan, Z. Yang, J. Xu, C. Zheng, Y. Yue, H. Liu and K. Deng, *Journal of Polymer Research*, 2017, **24**, 174.
86. R. Baumgartner, H. Fu, Z. Song, Y. Lin and J. Cheng, *Nature Chemistry*, 2017, **9**, 614-622.

87. C. Deng, J. Wu, R. Cheng, F. Meng, H.-A. Klok and Z. Zhong, *Progress in Polymer Science*, 2014, **39**, 330-364.
88. M. Xiong, Z. Han, Z. Song, J. Yu, H. Ying, L. Yin and J. Cheng, *Angewandte Chemie International Edition*, 2017, **56**, 10826-10829.
89. M. W. Lee, M. Han, G. V. Bossa, C. Snell, Z. Song, H. Tang, L. Yin, J. Cheng, S. May, E. Luijten and G. C. L. Wong, *ACS Nano*, 2017, **11**, 2858-2871.
90. Z. Y. Ong, N. Wiradharma and Y. Y. Yang, *Advanced Drug Delivery Reviews*, 2014, **78**, 28-45.
91. C. Zhou, X. Qi, P. Li, W. N. Chen, L. Mouad, M. W. Chang, S. S. J. Leong and M. B. Chan-Park, *Biomacromolecules*, 2010, **11**, 60-67.
92. K. Zhang, S. Yan, G. Li, L. Cui and J. Yin, *Biomaterials*, 2015, **71**, 24-34.
93. X. Zhou and Z. Li, *Advanced Healthcare Materials*, 2018, **7**, 1800020.
94. N. Cui, J. Qian, J. Wang, C. Ji, W. Xu and H. Wang, *RSC Advances*, 2016, **6**, 73699-73708.
95. Z. Song, R. A. Mansbach, H. He, K.-C. Shih, R. Baumgartner, N. Zheng, X. Ba, Y. Huang, D. Mani, Y. Liu, Y. Lin, M.-P. Nieh, A. L. Ferguson, L. Yin and J. Cheng, *Nature Communications*, 2017, **8**, 92.
96. Y. Hou, Y. Zhou, H. Wang, R. Wang, J. Yuan, Y. Hu, K. Sheng, J. Feng, S. Yang and H. Lu, *Journal of the American Chemical Society*, 2018, **140**, 1170-1178.
97. X. Wu, Y. Wu, H. Ye, S. Yu, C. He and X. Chen, *Journal of Controlled Release*, 2017, **255**, 81-93.
98. T. J. Deming, *Progress in Polymer Science*, 2007, **32**, 858-875.
99. M. N. Zhou, C. S. Delaveris, J. R. Kramer, J. A. Kenkel, E. G. Engleman and C. R. Bertozzi, *Angewandte Chemie International Edition*, 2018, **57**, 3137-3142.
100. R. F. Storey, in *Fundamentals of Controlled/Living Radical Polymerization*, The Royal Society of Chemistry, 2013, ch. 2, pp. 60-77.
101. M. Ciftci, Y. Yoshikawa and Y. Yagci, *Angewandte Chemie International Edition*, 2017, **56**, 519-523.
102. G. Moad, E. Rizzardo and S. H. Thang, in *Fundamentals of Controlled/Living Radical Polymerization*, The Royal Society of Chemistry, 2013, ch. 6, pp. 205-249.
103. X. G. Qiao, P. Y. Dugas, B. Charleux, M. Lansalot and E. Bourgeat-Lami, *Polymer Chemistry*, 2017, **8**, 4014-4029.
104. R. B. Grubbs and R. H. Grubbs, *Macromolecules*, 2017, **50**, 6979-6997.
105. T. Yokozawa and Y. Ohta, *Chemical Communications*, 2013, **49**, 8281-8310.
106. S. Ramakrishnan, *Resonance*, 2017, **22**, 355-368.
107. A. Kornberg, *Science*, 1960, **131**, 1503-1508.
108. A. Travers, *Nature*, 1976, **263**, 641-646.
109. T. Sanji, K. Nose, J. Kakinuma and T. Iyoda, *Polymer Chemistry*, 2016, **7**, 7116-7125.
110. S. Ye, S. Cheng, A. A. Pollit, M. W. Forbes and D. S. Seferos, *Journal of the American Chemical Society*, 2020, **142**, 11244-11251.
111. J. Lee, H. Park, S.-H. Hwang, I.-H. Lee and T.-L. Choi, *Macromolecules*, 2020, **53**, 3306-3314.
112. O. Nuyken and S. Pask, *Polymers*, 2013, **5**, 361.
113. A. Tardy, J. Nicolas, D. Gigmes, C. Lefay and Y. Guillemeuf, *Chemical Reviews*, 2017, **117**, 1319-1406.

114. X. Sun, X. Liu, C. Li, Y. Wang, L. Liu, F. Su and S. Li, *Journal of Applied Polymer Science*, 2018, **135**, 45732.
115. S. Kaihara, S. Matsumura, A. G. Mikos and J. P. Fisher, *Nature Protocols*, 2007, **2**, 2767-2771.
116. D. C. Batiste, M. S. Meyersohn, A. Watts and M. A. Hillmyer, *Macromolecules*, 2020, **53**, 1795-1808.
117. H. R. Kricheldorf and S. M. Weidner, *European Polymer Journal*, 2019, **119**, 37-44.
118. K. N. Houk, A. Jabbari, H. K. Hall and C. Alemán, *The Journal of Organic Chemistry*, 2008, **73**, 2674-2678.
119. J. J. Bozell and G. R. Petersen, *Green Chemistry*, 2010, **12**, 539-554.
120. T. Werpy and G. Petersen, *Top Value Added Chemicals from Biomass: Volume I -- Results of Screening for Potential Candidates from Sugars and Synthesis Gas*, U. S. D. o. Energy Report DOE/GO-102004-1992, National Renewable Energy Lab., CO, USA, 2004.
121. S. Moins, P. Loyer, J. Odent and O. Coulembier, *RSC Advances*, 2019, **9**, 40013-40016.
122. C. Zhang, in *Biodegradable Polyesters*, ed. S. Fakirov, John Wiley & Sons, Weinheim, Germany, 2015, ch. 1, pp. 1-24.
123. H. Tsuji, M. Nishikawa, Y. Osanai and S. Matsumura, *Macromolecular Rapid Communications*, 2007, **28**, 1651-1656.
124. M. Hong and E. Y. X. Chen, *Nature Chemistry*, 2016, **8**, 42-49.
125. M. Hong and E. Y.-X. Chen, *Angewandte Chemie International Edition*, 2016, **55**, 4188-4193.
126. J. A. Wilson, Z. Ates, R. L. Pflughaupt, A. P. Dove and A. Heise, *Progress in Polymer Science*, 2019, **91**, 29-50.
127. J. Engel, A. Cordellier, L. Huang and S. Kara, *ChemCatChem*, 2019, **11**, 4983-4997.
128. A. Kundys, E. Białecka-Florjańczyk, A. Fabiszewska and J. Małajowicz, *Journal of Polymers and the Environment*, 2018, **26**, 396-407.
129. Y. Lu, Q. Lv, B. Liu and J. Liu, *Biomaterials Science*, 2019, **7**, 4963-4983.
130. Y. Chen, M. Su, Y. Li, J. Gao, C. Zhang, Z. Cao, J. Zhou, J. Liu and Z. Jiang, *ACS Applied Materials & Interfaces*, 2017, **9**, 30519-30535.
131. Y. Xiao, J. Pan, D. Wang, A. Heise and M. Lang, *Biomacromolecules*, 2018, **19**, 2673-2681.
132. Y.-H. Tsou, X.-Q. Zhang, X. Bai, H. Zhu, Z. Li, Y. Liu, J. Shi and X. Xu, *Advanced Functional Materials*, 2018, **28**, 1802607.
133. Y.-h. Gong, M. Shu, J.-h. Xie, C. Zhang, Z. Cao, Z.-z. Jiang and J. Liu, *Journal of Materials Chemistry B*, 2019, **7**, 651-664.
134. J. V. Rowley, P. Wall, H. Yu, G. Tronci, D. A. Devine, J. J. Vernon and P. D. Thornton, *ACS Applied Polymer Materials*, 2020, **2**, 2927-2933.
135. G. Becker and F. R. Wurm, *Chemical Society Reviews*, 2018, **47**, 7739-7782.
136. I. Grizzi, H. Garreau, S. Li and M. Vert, *Biomaterials*, 1995, **16**, 305-311.
137. G. Guidotti, M. Soccio, V. Siracusa, M. Gazzano, E. Salatelli, A. Munari and N. Lotti, *Polymers*, 2017, **9**, 724.
138. M. Claudino, I. van der Meulen, S. Trey, M. Jonsson, A. Heise and M. Johansson, *Journal of Polymer Science Part A: Polymer Chemistry*, 2012, **50**, 16-24.
139. I. Flores, A. Martínez de Ilarduya, H. Sardon, A. J. Müller and S. Muñoz-Guerra, *ACS Applied Polymer Materials*, 2019, **1**, 321-325.
140. H. Leuchs, *Ber. Dtsch. Chem. Ges.*, 1906, **39**, 857-861.

141. H. Leuchs and W. Manasse, *Ber. Dtsch. Chem. Ges.*, 1907, **40**, 3235-3249.
142. H. Leuchs and W. Geiger, *Ber. Dtsch. Chem. Ges.*, 1908, **41**, 1721-1726.
143. T. Curtius and W. Sieber, *Ber. dtsch. Chem. Ges. A/B*, 1921, **54**, 1430-1437.
144. T. Curtius and W. Sieber, *Ber. dtsch. Chem. Ges. A/B*, 1922, **55**, 1543-1558.
145. T. Curtius, K. Hochschwender, H. Meier, W. Lehmann, A. Benckiser, M. Schenck, W. Wirbatz, J. Gaier and W. Mühlhäusser, *J. Prakt. Chem.*, 1930, **125**, 211-302.
146. F. Wessely, *Z. Physiol. Chem.*, 1925, **146**, 72-90.
147. F. Wessely and F. Sigmund, *Z. Physiol. Chem.*, 1926, **159**, 102-119.
148. F. Sigmund and F. Wessely, *Z. Physiol. Chem.*, 1926, **157**, 91-105.
149. F. Wessely and M. John, *Z. Physiol. Chem.*, 1927, **170**, 38-43.
150. F. Wessely and J. Mayer, *Monatshefte für Chemie und verwandte Teile anderer Wissenschaften*, 1928, **50**, 439-448.
151. F. Wessely, K. Riedl and H. Tuppy, *Monatshefte für Chemie und verwandte Teile anderer Wissenschaften*, 1950, **81**, 861-872.
152. F. Wessely and W. Swoboda, *Monatshefte für Chemie und verwandte Teile anderer Wissenschaften*, 1951, **82**, 621-627.
153. K. Schlögl, F. Wessely and G. Korger, *Monatshefte für Chemie und verwandte Teile anderer Wissenschaften*, 1952, **83**, 845-864.
154. H. R. Kricheldorf, *Angewandte Chemie International Edition*, 2006, **45**, 5752-5784.
155. G. J. M. Habraken, M. Peeters, C. H. J. T. Dietz, C. E. Koning and A. Heise, *Polymer Chemistry*, 2010, **1**, 514-524.
156. T. J. Deming, *Journal of Polymer Science Part A: Polymer Chemistry*, 2000, **38**, 3011-3018.
157. T. J. Deming, in *Peptide Hybrid Polymers*, eds. H.-A. Klok and H. Schlaad, Springer-Verlag, Berlin, Germany, 2006, vol. 202, pp. 1-18.
158. J. R. Kramer and T. J. Deming, *Biomacromolecules*, 2010, **11**, 3668-3672.
159. T. J. Deming and S. A. Curtin, *Journal of the American Chemical Society*, 2000, **122**, 5710-5717.
160. T. Aliferis, H. Iatrou and N. Hadjichristidis, *Biomacromolecules*, 2004, **5**, 1653-1656.
161. D. L. Pickel, N. Politakos, A. Avgeropoulos and J. M. Messman, *Macromolecules*, 2009, **42**, 7781-7788.
162. H. Lu and J. Cheng, *Journal of the American Chemical Society*, 2007, **129**, 14114-14115.
163. Y. Wu, D. Zhang, P. Ma, R. Zhou, L. Hua and R. Liu, *Nature Communications*, 2018, **9**, 5297.
164. T. Stukenkemper, J. F. G. A. Jansen, C. Lavilla, A. A. Dias, D. F. Brougham and A. Heise, *Polymer Chemistry*, 2017, **8**, 828-832.
165. A. Bhaw-Luximon, D. Jhurry, J. Belleney and V. Goury, *Macromolecules*, 2003, **36**, 977-982.
166. H. Zhang, Y. Nie, X. Zhi, H. Du and J. Yang, *Chemical Communications*, 2017, **53**, 5155-5158.
167. C. D. Vacogne and H. Schlaad, *Chemical Communications*, 2015, **51**, 15645-15648.
168. I. Conejos-Sánchez, A. Duro-Castano, A. Birke, M. Barz and M. J. Vicent, *Polymer Chemistry*, 2013, **4**, 3182-3186.

169. H. Peng, J. Ling and Z. Shen, *Journal of Polymer Science Part A: Polymer Chemistry*, 2012, **50**, 1076-1085.
170. W. Zhao, Y. Lv, J. Li, Z. Feng, Y. Ni and N. Hadjichristidis, *Nature Communications*, 2019, **10**, 3590.
171. W. Zhao, Y. Gnanou and N. Hadjichristidis, *Polymer Chemistry*, 2015, **6**, 6193-6201.
172. J. Zou, J. Fan, X. He, S. Zhang, H. Wang and K. L. Wooley, *Macromolecules*, 2013, **46**, 4223-4226.
173. Z. Song, H. Fu, J. Wang, J. Hui, T. Xue, L. A. Pacheco, H. Yan, R. Baumgartner, Z. Wang, Y. Xia, X. Wang, L. Yin, C. Chen, J. Rodríguez-López, A. L. Ferguson, Y. Lin and J. Cheng, *Proceedings of the National Academy of Sciences*, 2019, **116**, 10658-10663.
174. J. Jacobs, D. Pavlović, H. Prydderch, M.-A. Moradi, E. Ibarboure, J. P. A. Heuts, S. Lecommandoux and A. Heise, *Journal of the American Chemical Society*, 2019, **141**, 12522-12526.
175. W. Vayaboury, O. Giani, H. Cottet, A. Deratani and F. Schué, *Macromolecular Rapid Communications*, 2004, **25**, 1221-1224.
176. Z. Ahmad, A. Shah, M. Siddiq and H.-B. Kraatz, *RSC Advances*, 2014, **4**, 17028-17038.
177. S. A. Saghir and R. A. Ansari, in *Reference Module in Biomedical Sciences*, Elsevier, 2018, DOI: <https://doi.org/10.1016/B978-0-12-801238-3.62154-2>.
178. M. Khuphe and P. D. Thornton, *Macromolecular Chemistry and Physics*, 2018, **219**, 1800352.
179. Y. Ikuta, S. Aoyagi, Y. Tanaka, K. Sato, S. Inada, Y. Koseki, T. Onodera, H. Oikawa and H. Kasai, *Scientific Reports*, 2017, **7**, 44229.
180. M. Qu, Q. Lin, L. Huang, Y. Fu, L. Wang, S. He, Y. Fu, S. Yang, Z. Zhang, L. Zhang and X. Sun, *Journal of Controlled Release*, 2018, **287**, 156-166.
181. M. Khanal, S. V. Gohil, E. Kuyinu, H.-M. Kan, B. E. Knight, K. M. Baumbauer, K. W. H. Lo, J. Walker, C. T. Laurencin and L. S. Nair, *Acta Biomaterialia*, 2018, **74**, 280-290.
182. M. A. Hutnick, S. Ahsanuddin, L. Guan, M. Lam, E. D. Baron and J. K. Pokorski, *Biomacromolecules*, 2017, **18**, 379-385.
183. S. Sarkar, D. Das, P. Dutta, J. Kalita, S. B. Wann and P. Manna, *Carbohydrate Polymers*, 2020, 116594.
184. J. Li, H. Zheng, L. Qin, E.-Y. Xu, L. Yang, L. Zhang, X. Zhang, L. Fan, M. Beck-Broichsitter, U. Muenster, L. Chen, Y. Zhang and S. Mao, *Acta Biomaterialia*, 2019, **96**, 505-516.
185. M. Li, M. Zhao, Y. Fu, Y. Li, T. Gong, Z. Zhang and X. Sun, *Journal of Controlled Release*, 2016, **228**, 9-19.
186. B. Singh, S. Maharjan, K.-H. Cho, L. Cui, I.-K. Park, Y.-J. Choi and C.-S. Cho, *International Journal of Biological Macromolecules*, 2018, **110**, 54-64.
187. U. Roy, V. Drozd, A. Durygin, J. Rodriguez, P. Barber, V. Atluri, X. Liu, T. G. Voss, S. Saxena and M. Nair, *Scientific Reports*, 2018, **8**, 1603.
188. C. M. Santamaria, A. Woodruff, R. Yang and D. S. Kohane, *Materials Today*, 2017, **20**, 22-31.
189. M. Khuphe, N. Ingram and P. D. Thornton, *Nanoscale*, 2018, **10**, 14201-14206.
190. J. Zhu, Y. Niu, Y. Li, Y. Gong, H. Shi, Q. Huo, Y. Liu and Q. Xu, *Journal of Materials Chemistry B*, 2017, **5**, 1339-1352.

191. S. S. Said, S. Campbell and T. Hoare, *Chemistry of Materials*, 2019, **31**, 4971-4989.
192. H. Yu, N. Ingram, J. V. Rowley, D. C. Green and P. D. Thornton, *Chemistry – A European Journal*, 2020, **26**, 13352-13358.
193. K. A. Dill and P. J. Flory, *Proceedings of the National Academy of Sciences*, 1981, **78**, 676-680.
194. K. Kataoka, A. Harada and Y. Nagasaki, *Advanced Drug Delivery Reviews*, 2001, **47**, 113-131.
195. S. Takae, K. Miyata, M. Oba, T. Ishii, N. Nishiyama, K. Itaka, Y. Yamasaki, H. Koyama and K. Kataoka, *Journal of the American Chemical Society*, 2008, **130**, 6001-6009.
196. G. Kwon, M. Naito, M. Yokoyama, T. Okano, Y. Sakurai and K. Kataoka, *Journal of Controlled Release*, 1997, **48**, 195-201.
197. T. C. Johnstone, K. Suntharalingam and S. J. Lippard, *Chemical Reviews*, 2016, **116**, 3436-3486.
198. S. Dhar, N. Kolishetti, S. J. Lippard and O. C. Farokhzad, *Proceedings of the National Academy of Sciences*, 2011, **108**, 1850-1855.
199. J. Li, R. M. Stayshich and T. Y. Meyer, *Journal of the American Chemical Society*, 2011, **133**, 6910-6913.
200. J. Tian, Y. Min, Z. Rodgers, K. M. Au, C. T. Hagan, M. Zhang, K. Roche, F. Yang, K. Wagner and A. Z. Wang, *Journal of Materials Chemistry B*, 2017, **5**, 6049-6057.
201. K. Miyata, R. J. Christie and K. Kataoka, *Reactive and Functional Polymers*, 2011, **71**, 227-234.
202. F. M. Veronese and G. Pasut, *Drug Discovery Today*, 2005, **10**, 1451-1458.
203. H. A. Mohamed, M. Khuphe, S. J. Boardman, S. Shepherd, R. M. Phillips, P. D. Thornton and C. E. Willans, *RSC Advances*, 2018, **8**, 10474-10477.
204. S. Abbina and A. Parambath, in *Engineering of Biomaterials for Drug Delivery Systems*, ed. A. Parambath, Woodhead Publishing, 2018, ch. 14, pp. 363-376.
205. A. C. Engler, X. Ke, S. Gao, J. M. W. Chan, D. J. Coady, R. J. Ono, R. Lubbers, A. Nelson, Y. Y. Yang and J. L. Hedrick, *Macromolecules*, 2015, **48**, 1673-1678.
206. K. Knop, R. Hoogenboom, D. Fischer and U. S. Schubert, *Angewandte Chemie International Edition*, 2010, **49**, 6288-6308.
207. J. Leal, X. Peng, X. Liu, D. Arasappan, D. C. Wylie, S. H. Schwartz, J. J. Fullmer, B. C. McWilliams, H. D. C. Smyth and D. Ghosh, *Journal of Controlled Release*, 2020, **322**, 457-469.
208. D. Russo, A. de Angelis, C. J. Garvey, F. R. Wurm, M.-S. Appavou and S. Prevost, *Biomacromolecules*, 2019, **20**, 1944-1955.
209. Y. Zhu, A. Poma, L. Rizzello, V. M. Gouveia, L. Ruiz-Perez, G. Battaglia and C. K. Williams, *Angewandte Chemie International Edition*, 2019, **58**, 4581-4586.
210. M. Debayle, E. Balloul, F. Dembele, X. Xu, M. Hanafi, F. Ribot, C. Monzel, M. Coppey, A. Fragola, M. Dahan, T. Pons and N. Lequeux, *Biomaterials*, 2019, **219**, 119357.
211. K. Son, M. Ueda, K. Taguchi, T. Maruyama, S. Takeoka and Y. Ito, *Journal of Controlled Release*, 2020, **322**, 209-216.
212. B. Weber, A. Birke, K. Fischer, M. Schmidt and M. Barz, *Macromolecules*, 2018, **51**, 2653-2661.

213. H. Yu, N. Ingram, J. V. Rowley, S. Parkinson, D. C. Green, N. J. Warren and P. D. Thornton, *Journal of Materials Chemistry B*, 2019, **7**, 4217-4223.
214. A. Birke, D. Huesmann, A. Kelsch, M. Weillbacher, J. Xie, M. Bros, T. Bopp, C. Becker, K. Landfester and M. Barz, *Biomacromolecules*, 2014, **15**, 548-557.
215. P. Zhang, H. Zhang, W. He, D. Zhao, A. Song and Y. Luan, *Biomacromolecules*, 2016, **17**, 1621-1632.
216. M. Salmanpour, G. Yousefi, S. M. Samani, S. Mohammadi, M. H. Anbardar and A. Tamaddon, *European Journal of Pharmaceutical Sciences*, 2019, **136**, 104941.
217. G.-F. Luo, W.-H. Chen, Q. Lei, W.-X. Qiu, Y.-X. Liu, Y.-J. Cheng and X.-Z. Zhang, *Advanced Functional Materials*, 2016, **26**, 4339-4350.
218. I. Guryanov, F. Polo, E. V. Ubyvovk, E. Korzhikova-Vlakh, T. Tennikova, A. T. Rad, M.-P. Nieh and F. Maran, *Chemical Science*, 2017, **8**, 3228-3238.
219. T. Borase and A. Heise, *Advanced Materials*, 2016, **28**, 5725-5731.
220. Y. Yao, W. Li, S. Wang, D. Yan and X. Chen, *Macromolecular Rapid Communications*, 2006, **27**, 2019-2025.
221. S. R. Caliri and J. A. Burdick, *Nature Methods*, 2016, **13**, 405-414.
222. E. J. Lee, E. Kang, S.-W. Kang and K. M. Huh, *Carbohydrate Polymers*, 2020, **244**, 116432.
223. B. S. McAvan, M. Khuphe and P. D. Thornton, *European Polymer Journal*, 2017, **87**, 468-477.
224. E. Liarou, S. Varlas, D. Skoulas, C. Tsimblouli, E. Sereti, K. Dimas and H. Iatrou, *Progress in Polymer Science*, 2018, **83**, 28-78.
225. M. H. Turabee, T. Thambi, H. T. T. Duong, J. H. Jeong and D. S. Lee, *Biomaterials Science*, 2018, **6**, 661-671.
226. X. Chen and S. T. C. Wong, in *Cancer Theranostics*, eds. X. Chen and S. Wong, Academic Press, Oxford, 2014, ch. 1, pp. 3-8.
227. W. Tang, W. Fan, J. Lau, L. Deng, Z. Shen and X. Chen, *Chemical Society Reviews*, 2019, **48**, 2967-3014.
228. J. Zhang, L. Ning, J. Huang, C. Zhang and K. Pu, *Chemical Science*, 2020, **11**, 618-630.
229. C. Scialabba, A. Sciortino, F. Messina, G. Buscarino, M. Cannas, G. Roscigno, G. Condorelli, G. Cavallaro, G. Giammona and N. Mauro, *ACS Applied Materials & Interfaces*, 2019, **11**, 19854-19866.
230. A. Salunkhe, V. Khot, S. I. Patil, S. A. M. Tofail, J. Bauer and N. D. Thorat, *ACS Applied Bio Materials*, 2020, **3**, 2305-2313.

## **Chapter 2**

### **Instrumentation, Materials and General Methods**

#### **2.1 Instrumentation**

##### **2.1.1 Advanced Polymer Chromatography (APC)**

APC was conducted on a Waters Acquity APC system using a bed of three Acquity columns (XT 125, XT 200 and XT450) that were all 150 mm in length, had an internal diameter of 4.6 mm, and contained particles of 2.5  $\mu\text{m}$  in diameter with different pore sizes dependant on the column. THF was used as the mobile phase at a flow rate of 0.5 mL  $\text{min}^{-1}$ , column temperature was set to 40  $^{\circ}\text{C}$  and detection was by refractive index measurement. The APC instrument was calibrated against standard poly(methyl methacrylate) samples in THF. Instrument control, calibration, data acquisition and data processing was conducted on Waters Empower 3 software.

##### **2.1.2 Centrifugation, Sample Drying and Lyophilisation**

Samples collected by centrifugation were done so in disposable centrifuge tubes (2 x or 4 x 15 mL) in a Hermle Z326 K centrifuge at 0  $^{\circ}\text{C}$ . Samples dried in a vacuum oven were done so in a Fiestreem vacuum oven equipped with a variable temperature control unit and pressure gauge. Lyophilisation was conducted in a Thermoelectron Heto Powerdry LLI500 freeze-dryer.

##### **2.1.3 Dynamic Light Scattering (DLS) and Zeta Potential Analyses**

DLS analyses were carried out using a Malvern Zetasizer Nano ZSP instrument with a 4 mW He-Ne laser operating at a wavelength of 633 nm and an Avalanche

photodiode detector. A non-invasive backscatter-optic arrangement was used to collect the light scattered at  $173^\circ$ . Prior to analysis, the samples were equilibrated for two minutes then analysed at  $25^\circ\text{C}$  in disposable 12 mm polystyrene cuvettes. Measurements were performed in triplicate. Data was processed via the cumulative analysis of the experimental correlation function; then the diameter of the particles was computed from the diffusion coefficients using the Stokes-Einstein equation.

Zeta potential analyses were conducted on the same instrument in disposable folded capillary zeta cells at  $25^\circ\text{C}$ . Samples were dissolved in DI water and no background electrolyte was added.

#### **2.1.4 Differential Scanning Calorimetry (DSC)**

DSC curves were collected using a TA Instruments DSC Q20 instrument with a heating rate of  $10^\circ\text{C min}^{-1}$  and an inert gas flow of  $\text{N}_2$  at a rate of  $50\text{ mL min}^{-1}$ .

#### **2.1.5 Fourier-Transform Infrared Spectroscopy (FTIR)**

FTIR spectra were obtained with a Perkin Elmer Spectrum One spectrometer fitted with a Specac Golden Gate attenuated total reflectance attachment. Spectra were obtained between  $4000\text{ cm}^{-1}$  and  $550\text{ cm}^{-1}$  at  $1\text{ cm}^{-1}$  intervals, accumulated over 100 runs. Data acquisition, instrument control and automatic background deletion was handled by the Spectrum software.

#### **2.1.6 High-Performance Liquid Chromatography (HPLC)**

HPLC analyses were run on a  $\text{C}_{18}$  column (Ascentis Express  $\text{C}_{18}$ ,  $2.7\text{ }\mu\text{m}$  particle size,  $50\text{ mm} \times 2.1\text{ mm}$ ) over five minutes. The mobile phase was

water/acetonitrile (60:40 v/v) with 0.1% trifluoroacetic acid and a flow rate of 0.5 mL min<sup>-1</sup>.

### **2.1.7 Incubation at 37 °C**

Samples which were incubated at 37 °C were done so in beakers in a Cleaver Scientific Ltd Stirring Water Bath maintained at 37.0 °C.

### **2.1.8 Nuclear Magnetic Resonance (NMR) Spectroscopy**

<sup>1</sup>H, <sup>13</sup>C and <sup>31</sup>P NMR spectra at 400 MHz, 100 MHz and 202 MHz, respectively, were recorded on a two-channel Bruker AV3HD NMR spectrometer operating at 9.4 T and equipped with a 5 mm BBO probe. <sup>1</sup>H and <sup>13</sup>C NMR spectra at 500 MHz and 125 MHz, respectively, were recorded on a Bruker AV4 NEO 11.75 T 500 MHz spectrometer fitted with a 5 mm Bruker DCH cryoprobe. <sup>1</sup>H NMR spectra conducted at 600 MHz were recorded on a JEOL ECA600 series II spectrometer equipped with a 5 mm z-pfg BB/1H Royal probe operating Delta 5.0 software. Cross-polarisation magic-angle spinning (MAS) (solid-state) <sup>13</sup>C NMR spectra were obtained on a Bruker AVANCE II 400 MHz spectrometer with a double-bearing MAS probe head (BL4 type) and a Bruker MAS II control unit. Samples for MAS were packed into 4 mm diameter zirconium rotor tubes. Measurement parameters included a <sup>13</sup>C resonant frequency of ~100.6 MHz, 90° proton pulse length of 2.5 μs, a 2 ms contact time, 5 s delay time and a spinning speed of 10 kHz. Chemical shifts (in ppm) were referenced to a tetramethylsilane standard which has a chemical shift of 0 ppm. All samples were run at 298 K and NMR spectra were analysed on the MestReNova software; all Bruker spectrometers were operated using TOPSPIN software.

### **2.1.9 Powdered X-Ray Diffraction (pXRD)**

The X-ray diffraction pattern of powdered samples was conducted on a Bruker D2 Phaser (LYNXEYE detector) whereby powdered samples were deposited onto a silicon wafer. Data was obtained between  $2\theta = 10^\circ$  to  $75^\circ$  over 20 minutes on spinning samples. Instrument control, data acquisition and conversion were conducted in DIFFRAC.SUITE software package. A  $K\alpha_2$  strip was performed on the data.

### **2.1.10 Raman Microscopy**

Raman microscopy was conducted on glass substrates using a Reinshaw in Via Raman Microscope (785 nm laser) with a 50x objective and MS20 encoded sample stage. Data acquisition was undertaken with Reinshaw WiRE 3.4 with a laser intensity of 0.1% under three accumulated acquisitions between  $1200\text{ cm}^{-1}$  and  $100\text{ cm}^{-1}$ .

### **2.1.11 Scanning Electron Microscopy (SEM)**

For solution-state analyses, samples were dissolved in solvent and placed onto an SEM glass cover slip then left to dry. Once dried, the cover slip was mounted on an SEM stub using conductive tape. Solid samples were mounted directly on an SEM stub using conductive tape. All samples were sputter-coated with a film of gold using a Quorum Q150RS sputter-coater, powered by a 20 mA current. SEM analyses were then loaded into a JEOL JSM-6610LV SEM from Oxford Instruments, equipped with a field emission electron gun as an electron source. The accelerating voltage was varied between 5-15 kV and the working distance varied between 10 mm and 17 mm.

### **2.1.12 Thermogravimetric Analysis (TGA)**

TGA was conducted on a TA Instruments SDT Q600 simultaneous TGA/DSC instrument from room temperature to 900 °C at a constant ramp rate of 5 °C min<sup>-1</sup> and with a N<sub>2</sub> flow rate of 100 mL min<sup>-1</sup>.

### **2.1.13 UV-vis Spectrophotometry**

UV-vis spectrophotometric analyses were conducted using a dual beam Varian Cary 50 UV-vis spectrophotometer equipped with a xenon pulse lamp. Qualitative samples were analysed in quartz cuvettes against a blank sample in triplicate. Dox calibration curves and quantification of Dox concentration samples were conducted in disposable poly(methyl methacrylate) samples against a blank sample in triplicate. Instrument control and data acquisition were conducted using Varian Cary WinUV 3.0 software. For optical density (OD<sub>600</sub>) measurements to estimate viable bacterial counts in antimicrobial activity testing, a Jenway 6305 spectrophotometer was used at 600 nm.

## **2.2 Materials**

All chemicals were used as received unless otherwise stated. A list of chemicals used and their supplier is provided in Table 2.1.

**Table 2.1** Chemicals used and their supplier.

<b>Chemical</b>	<b>Supplier</b>	<b>Chemical</b>	<b>Supplier</b>
Acetate buffer solution	ACROS	Acetic acid	Merck
Alanine anhydride	ChemCruz	Aluminium oxide	ACROS
2-Amino-3,5-dinitrothiophene	ChemCruz	4-Aminobutylphosphonic acid	Merck
Antimony trioxide	Alfa Aesar	2,2'-Azobis(2-methylpropionitrile)	Merck
BLG	Fluorochem	Brain heart infusion broth	Oxoid
1-Butyl-3-methylimidazolium tetrafluoroborate	Merck	Butylated hydroxytoluene	Merck
Calcium acetate monohydrate	Merck	Calcium carbonate	Merck
CDCl <sub>3</sub>	Merck	Chloroform	Merck
C.I. disperse blue 3	ChemCruz	C.I. disperse red 1	Merck
Colombia blood agar	Oxoid	Corn oil	Tesco
DCM	VWR	Dialysis tubing (benzylated)	Merck
<i>N-N</i> -Dicyclohexylcarbodiimide	Alfa Aesar	Diethyl ether	Fisher
Dimethyl terephthalate	Merck	4-Dimethylaminopyridine	ACROS
1,4-Dioxane	Merck	DMF	Fisher
DMSO- <i>d</i> <sub>6</sub>	Eurisotop	Dox·HCl	Fluorochem
Ethanol	VWR	<i>N</i> -Ethyl-diisopropylamine	Alfa Aesar

Table 2.1 continued...

Ethylene glycol	Alfa Aesar	2-2'- (Ethylenedioxy)diethanethiol	Merck
Folic acid	Merck	Globalide	Symrise
HCl (33%)	Fisher	Hexane	Merck
11-Hydroxyundecylphosphonic acid	Alfa Aesar	Linseed oil	Merck
Lipase B (CALB)	Merck	3-Mercaptopropionic acid	Merck
Methanesulfonic acid	Alfa Aesar	Methanol	Fisher
MgSO <sub>4</sub>	Merck	NaHCO <sub>3</sub>	Fisher
Olive oil	Tesco	5% Oxalated horse blood	Oxoid
PBS tablets at pH 7.4	Merck	PEG monomethyl ether	Merck
L-Phenylalanine	ACROS	<i>N</i> - Phenyldiethanolamine	Alfa Aesar
2-Phenylethanol	Merck	α-Pinene	Merck
2-Propanol	VWR	Propionic acid	Alfa Aesar
Safflower oil	Merck	Sarcosine	Alfa Aesar
Sn(Oct) <sub>2</sub>	Merck	Sodium hydroxide	Merck
Sodium nitrite	Merck	Sulfanilamide	Alfa Aesar
Sulfuric acid	Fisher	THF	Fisher
Titanium (IV) isopropoxide	Merck	Triethylamine	Fluorochem
Triphosgene	Fluorochem		

## 2.3 General Methods

### 2.3.1 Synthesis of NCA monomers

#### 2.3.1.1 Synthesis of sarcosine-NCA (Sar-NCA)

Sar-NCA was prepared from a previously reported procedure with adaptations.<sup>1</sup> Sar (4.0 g, 44.9 mmol) and  $\alpha$ -pinene (14.0 g, 102.8 mmol) were added to anhydrous THF (60 mL) under N<sub>2</sub> and the mixture refluxed under N<sub>2</sub> for 30 minutes. Triphosgene (8.0 g, 27.0 mmol) was dissolved in anhydrous THF (20 mL) and added dropwise to the refluxing reaction mixture. After four hours, refluxing of the yellow-brown solution was stopped and the volume reduced on a rotary evaporator to yield a brown oil which was further dried in a vacuum oven at room temperature overnight.

The dried yellow-brown residue was redissolved in THF (30 mL), and the solution precipitated by adding dropwise to ice-cold hexane (150 mL). To aid precipitation, the mixture was stored at -18 °C for one hour before the Sar-NCA was collected by vacuum filtration, dried *in vacuo* then recrystallised twice in THF/hexane (1:5 v/v) to yield Sar-NCA as off-white crystals (yield 2.6 g, 49.5%). <sup>1</sup>H NMR (400 MHz, CDCl<sub>3</sub>,  $\delta$  ppm):  $\delta$  4.05 ppm (s, 2H, >N-CH<sub>2</sub>-COO-) and  $\delta$  2.99 ppm (s, 3H, >NCH<sub>3</sub>). FTIR  $\nu_{\text{max}}$  (solid): 1847 cm<sup>-1</sup> (m, anhydride) and 1760 cm<sup>-1</sup> (s, tertiary amine).

#### 2.3.1.2 Synthesis of L-phenylalanine-NCA (Phe-NCA)

Phe-NCA was synthesised as reported previously.<sup>2</sup> Briefly, Phe (5.00 g, 30.3 mmol) was weighed into a 3-necked RB flask which had been dried in an oven and flushed with N<sub>2</sub>. Under a stream of N<sub>2</sub>,  $\alpha$ -pinene (4.03 g, 29.6 mmol) and anhydrous THF (80 mL) were added to the reaction mixture and refluxed for 30 minutes. Triphosgene (4.02 g, 13.5 mmol) was dissolved in anhydrous THF (20

mL) and added dropwise to the reaction mixture using a dropping funnel and refluxed under N<sub>2</sub> for three hours. The Phe-NCA was reduced to dryness on a rotary evaporator, redissolved in THF (15 mL) and precipitated by added dropwise to ice-cold hexane (300 mL). The THF/hexane mixture was left in the freezer for 15 minutes to aid precipitation and the Phe-NCA collected by vacuum filtration and recrystallised three times in THF/hexane (1:9 v/v) yielding a white amorphous powder. Yield: 4.11 g (71 %). <sup>1</sup>H NMR (400 MHz, CDCl<sub>3</sub>, δ ppm): δ 7.12-7.31 (m, 5H, aromatic), δ 5.46 (s, 1H, >NH), δ 4.46 (dd, 1H, CH<sub>2</sub>CH(COO-)NH-), δ 3.08 (dd, 2H, PhCH<sub>2</sub>C(COO-)NH-). FTIR  $\nu_{\max}$  (solid): 3356 cm<sup>-1</sup> (m, phenyl), 1837 cm<sup>-1</sup> (m, cyclic conjugated anhydride), 1770 cm<sup>-1</sup> (s, secondary amide).

### 2.3.1.3 Synthesis of $\gamma$ -benzyl-L-glutamate-NCA (BLG-NCA)

A similar method to that described above was used (Section 2.3.1.2). Briefly, BLG (10.0 g, 42.1 mmol) and  $\alpha$ -pinene (19.2 g, 140.9 mmol) were dissolved in anhydrous THF (80 mL). The solution was heated to reflux then a solution of triphosgene (15.0 g, 50.5 mmol) in anhydrous THF (20 mL) was added dropwise through a dropping funnel. The reaction solution was refluxed for four hours and the monomer precipitated into ice-cold hexane (100 mL). BLG-NCA was collected by centrifuge and dried in a vacuum oven at room temperature. Yield: 7.99 g (72%). <sup>1</sup>H NMR (300 MHz, DMSO-*d*<sub>6</sub>, δ ppm): δ 9.09 (s, 1H), δ 7.42-7.30 (m, 5H), δ 5.10 (s, 2H), 4.52-4.42 (m, 1H), δ 2.55 (s, 2H), δ 2.11-2.01 (m, 1H), δ 1.93 (td, *J* = 15.1, 7.6 Hz, 1H). FTIR  $\nu_{\max}$  (solid): 3252 & 3331 cm<sup>-1</sup> (amide N-H), 3088 cm<sup>-1</sup> (aromatic), 2858 & 2932 cm<sup>-1</sup> (alkane C-H), 1859 & 1880 cm<sup>-1</sup> (anhydride C=O), 1720 & 1773 cm<sup>-1</sup> ester C=O), 1606 cm<sup>-1</sup> (amide C=O), 1583 cm<sup>-1</sup> (aromatic C=C).

### **2.3.2 Preparation of PBS buffer solution at pH 7.4**

PBS buffer solution at pH 7.4 was prepared by adding a PBS buffer tablet to the required amount of DI water as stated on the instructions to reach pH 7.4. The tablet was dissolved by stirring and the pH of the solution checked.

### **2.3.3 Dropping-In Method of NP Formation**

The dropping-in method (nanoprecipitation) was utilised for the formation of NPs.<sup>3-5</sup> The polymer in question was dissolved in an organic solvent (DMF, chloroform, for example) and added dropwise to an aqueous solution (DI water, PBS buffer solution, for example) under vigorous stirring. The organic solvent was removed by solvent evaporation for low boiling point solvents or by dialysis for high boiling point solvents, leaving NPs in aqueous solution.

### **2.3.4 Doxorubicin Loading and Release**

#### **2.3.4.1 Preparation of Dox free base**

Dox·HCl (3 mg, 5  $\mu$ mol) was dissolved in chloroform (3 mL) with triethylamine (20  $\mu$ L, 15 mg, 143  $\mu$ mol). The red coloured solution was stirred in a closed vial in the dark at room temperature for four hours before being either used or stored in the freezer as a stock solution of Dox free base in chloroform.

#### **2.3.4.2 Dox UV-vis calibration**

The Dox calibration on UV-vis was performed as reported previously.<sup>6</sup> Briefly, known concentrations of Dox free base (from Section 2.3.4.1) in PBS buffer solution at pH 7.4 or acetate buffer solution at pH 5 were prepared and transferred

to disposable poly(methyl methacrylate) cuvettes. The samples were analysed on UV-vis whereby the absorbance at 498 nm was observed for samples in PBS buffer solution or 502 nm for samples in acetate buffer solution. The data was plotted, and a calibration curve was determined by line of best fit (Figure 2.1). Dox concentration can thus be calculated from Equation (2.1) for samples in PBS buffer solutions at pH 7.4 and Equation (2.2) for samples in acetate buffer solutions.

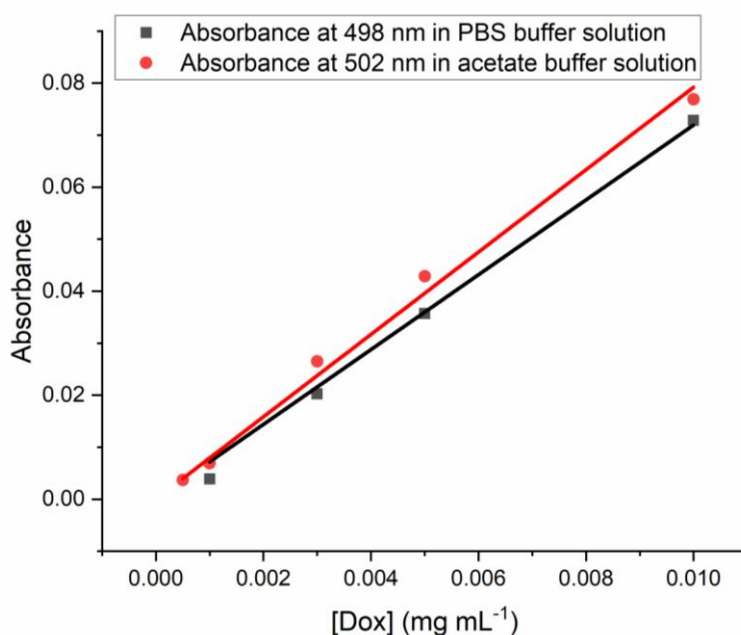


**Figure 2.1** UV-vis calibration curve of Dox free base in PBS buffer solution at pH 7.4 and acetate buffer solution.

$$[Dox] = \frac{7.19 \pm 0.12}{UV - vis\ abs.\ @\ 498\ nm} \quad (2.1)$$

$$[Dox] = \frac{7.92 \pm 0.18}{UV - vis\ abs.\ @\ 502\ nm} \quad (2.2)$$

### 2.3.4.3 Dox HPLC calibration

Known concentrations of Dox free base (Section 2.3.4.1) in PBS buffer solution at pH 7.4 or in acetate buffer solution at pH 5 were prepared and transferred to HPLC sample vials. The samples were analysed on HPLC as per Section 2.1.6 and using conditions previously optimised to detect Dox.<sup>7</sup> A calibration curve was produced using the area of the Dox peak (eluting at 0.5 min) vs concentration (Figure 2.2). Dox concentration can thus be calculated from Equation (2.3) for samples in PBS buffer solution at pH 7.4 and Equation (2.4) for samples in acetate buffer solution at pH 5.

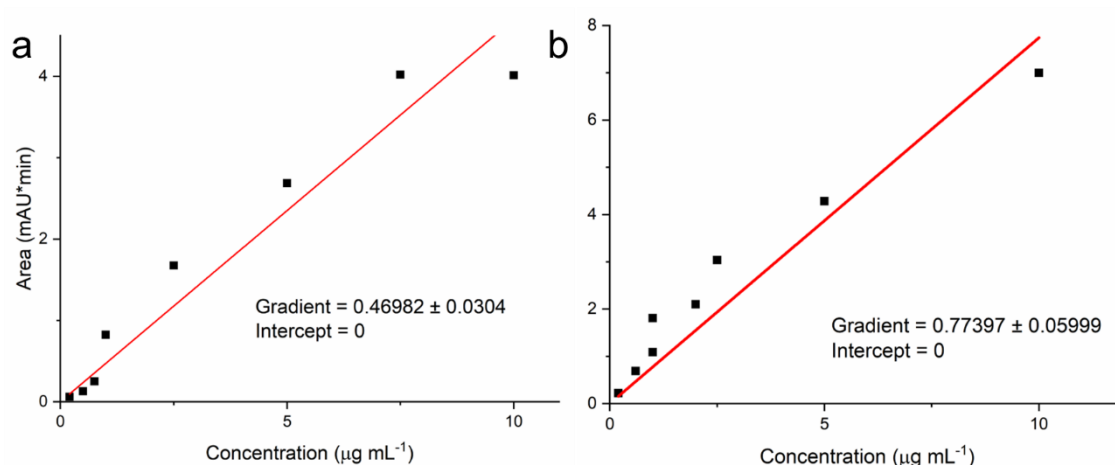


**Figure 2.2** HPLC calibration curves of Dox free base in PBS buffer solution at pH 7.4 (a) and acetate buffer solution at pH 5 (b).

$$[Dox] = \frac{0.469 \pm 0.030}{\text{Area of Dox peak on HPLC}} \quad (2.3)$$

$$[Dox] = \frac{0.774 \pm 0.060}{\text{Area of Dox peak on HPLC}} \quad (2.4)$$

#### 2.3.4.4 Dox loading content and efficiency calculations

Drug loading content is calculated from Equation (2.5) and drug loading efficiency is calculated from Equation (2.6).

$$\text{Drug loading content} = 100\% * \frac{\text{Mass of drug in NP}}{\text{Initial mass of NP}} \quad (2.5)$$

$$\text{Drug loading efficiency} = 100\% * \frac{\text{Mass of drug in NP}}{\text{Mass of drug in feed}} \quad (2.6)$$

## 2.4 References

1. M. Khuphe, C. S. Mahon and P. D. Thornton, *Biomaterials Science*, 2016, **4**, 1792-1801.
2. G. J. M. Habraken, M. Peeters, C. H. J. T. Dietz, C. E. Koning and A. Heise, *Polymer Chemistry*, 2010, **1**, 514-524.
3. S. Schubert, J. J. T. Delaney and U. S. Schubert, *Soft Matter*, 2011, **7**, 1581-1588.
4. J. Nicolas, S. Mura, D. Brambilla, N. Mackiewicz and P. Couvreur, *Chemical Society Reviews*, 2013, **42**, 1147-1235.
5. Y. Zhang, Z. Yang, X. Zheng, L. Chen and Z. Xie, *Journal of Materials Chemistry B*, 2020, **8**, 5305-5311.
6. H. Yu, N. Ingram, J. V. Rowley, S. Parkinson, D. C. Green, N. J. Warren and P. D. Thornton, *Journal of Materials Chemistry B*, 2019, **7**, 4217-4223.
7. K. Alhareth, C. Vauthier, C. Gueutin, G. Ponchel and F. Moussa, *Journal of Chromatography B*, 2012, **887-888**, 128-132.

## Chapter 3

# Phosphonate-Terminated Amphiphilic Polymers as Biomaterials and for Metal Chelation

### Abstract

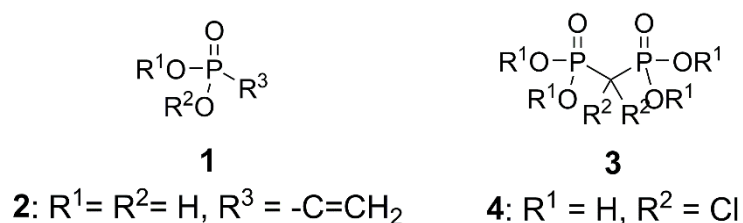
Poor pharmacokinetics of chemotherapy drugs leads to adverse side effects, whereas drug delivery vehicles which can target tumour sites are sought to reduce such adverse side effects. Polymeric nanoparticles of 11-hydroxyundecylphosphonic acid (HUPA) -initiated polysarcosine were synthesised, as confirmed by DLS and SEM analyses, which were able to uptake the hydrophobic chemotherapeutic drug, doxorubicin. An ester link between the polymer and HUPA afforded the nanoparticles stimuli-responsiveness to pH, releasing only 35% doxorubicin in physiological pH (7.4), but releasing 72% and 80% in pH 6 and 5 buffer solutions, respectively. Tumours present a more acidic environment to healthy tissue, therefore the targeted delivery of doxorubicin to acidic solutions may allow these biodegradable and biocompatible polymers to be used as targeted drug delivery vehicles to improve the pharmacokinetics of hydrophobic chemotherapy drugs. Additionally, these polymers can form P-O-M bonds, as demonstrated by greatly improving the aqueous compatibility of titanium dioxide nanoparticles, and thus are suitable as potentially biodegradable and biocompatible P-O-M bond-forming polymers for dental adhesion, drug delivery or metal chelators.

### 3.1 Introduction

#### 3.1.1 Phosphonate-containing polymers

The phosphonate functional group (Scheme 3.1, **1**) is tetrahedral with a central phosphorus atom and P=O, P-OR<sup>1</sup>, P-OR<sup>2</sup> and P-R<sup>3</sup> groups whereby the R<sup>3</sup>

group is an alkyl or aryl group. Phosphonic acids have protons for R<sup>1</sup> and R<sup>2</sup>. A phosphonate dimer, bisphosphonates (**3**), can also be prepared and are a class of drug used to treat osteoporosis.<sup>1</sup> For example, clodronic acid (**4**) is a bisphosphonate molecule used to treat osteoporosis whereby it binds to bone mineral sites.<sup>2</sup> **4** binds to bone mineral sites because phosphonates and bisphosphonates have strong affinity for metal centres, forming a P-O-M bond with a general formula shown in Equation (3.1).<sup>3-6</sup>



**Scheme 3.1** Example of phosphonates and bisphosphonates.

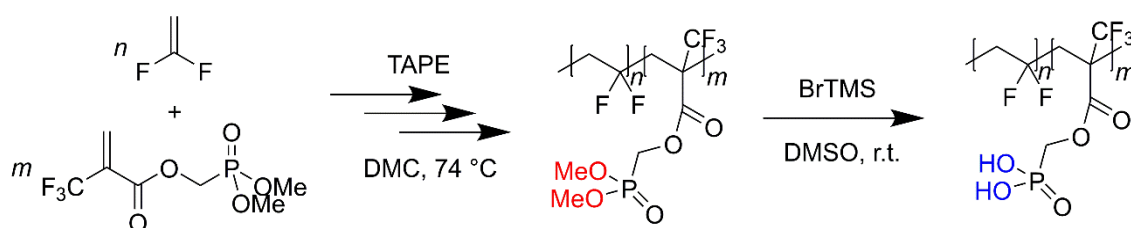


This useful ability to ligate metal ions through a P-O-M bond allows polymers containing phosphonate groups to have useful applications, such as in corrosion inhibition,<sup>7</sup> fuel cells,<sup>8</sup> metal chelators,<sup>9</sup> adhesives in dentistry<sup>10</sup> and as biomaterials.<sup>6,11</sup> For example, vinylphosphonic acid (**2**) is a phosphonate functional group-containing monomer which when polymerised forms poly(vinylphosphonic acid) (PVPA).<sup>12-13</sup> PVPA is used in flame retardants,<sup>14-15</sup> fuel cells,<sup>16-18</sup> metal chelators,<sup>19-21</sup> dental adhesives,<sup>22-23</sup> tissue engineering,<sup>24</sup> and as a drug delivery vehicle.<sup>25-28</sup>

### 3.1.1.1 Phosphonate-containing polymers for metal chelation

Industry uses the P-O-M bond forming ability of phosphonates for waste water treatment,<sup>29</sup> crude oil production<sup>30</sup> and industrial equipment cleaning.<sup>31</sup> Banerjee *et al.* reported the copolymerisation of vinylidene fluoride and a phosphonate-containing monomer, (dimethoxyphosphoryl)methyl 2-(trifluoromethyl)acrylate,

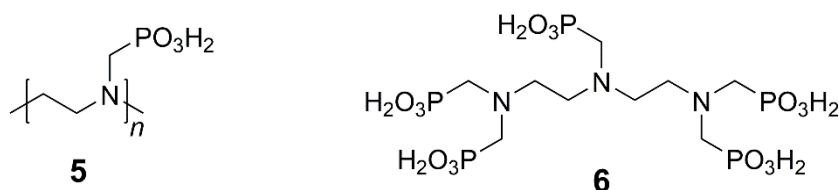
by radical copolymerisation (Scheme 3.2).<sup>32</sup> The formed polymer was hydrophobic, but subsequent hydrolysis of the phosphate monoester groups resulted in the generation of phosphonic acid groups which imparted hydrophilicity and even superhydrophilicity to the copolymer, depending on the monomer ratios and degree of hydrolysis. The authors included this hydrophilic polymer into a formulation for coating a steel surface and demonstrated excellent corrosion resistance due in part to the phosphonic acid adhering to the steel plate.



**Scheme 3.2** Reaction scheme for copolymerisation of vinylidene fluoride and (dimethoxyphosphoryl)methyl 2-(trifluoromethyl)acrylate, and subsequent hydrolysis.<sup>32</sup> TAFE = tert-amyl peroxy-2-ethylhexanoate; DMC = dimethyl carbonate; BrTMS = bromotrimethylsilane.

Rare Earth elements are critical for modern technology and their extraction from waste streams a potentially lucrative endeavour.<sup>33</sup> Phosphonate-containing polymers can be effective as metal scavengers due to their high affinity for target elements and low cost.<sup>34-35</sup> Recently, Archer and co-workers synthesised poly(ethylenimine methylenephosphonate) (Scheme 3.3, **5**) and studied its rare Earth chelating properties.<sup>36</sup> The authors used isothermal titration calorimetry to quantitatively measure the formation and dissociation of complexes, discovering the metals coordinate with multiple phosphonate units on either the same, or neighbouring polymer chains; remaining metal coordination sites were filled with solvent molecules. Interestingly, Archer and colleagues studied a small molecule structurally analogous to **5** (diethylenetriamine penta(methylene phosphonic

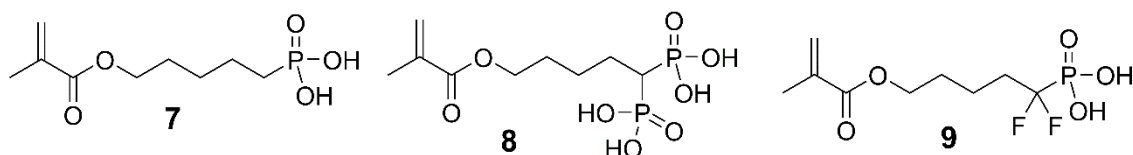
acid), **6**) and found binding more favourable to the polymer, with the polymer requiring slightly fewer phosphonate units on average to bind each metal ion.



**Scheme 3.3** Poly(ethylenimine methylenephosphonate) and diethylenetriamine penta(methylene phosphonic acid).

### 3.1.1.2 Phosphonate-containing polymers as biomaterials

Materials used in dental treatment must conform to strict requirements, such as having high light and discolouration stability in the oral environment, very low toxicity, no mutagenic or carcinogenic potential, and excellent mechanical properties.<sup>37</sup> Polymers with phosphonate groups can meet these applications and provide an anchor to calcium on dentin, thus making them suitable as dental adhesives.<sup>38-41</sup> Catel *et al.* synthesised phosphonic acid (**7**), bisphosphonic acid (**8**) and difluoromethylphosphonic acid (**9**) monomers which were demonstrated to bind to hydroxyapatite, a major component of bone and teeth.<sup>42</sup> The monomers are designed to photopolymerise *in situ* during dental treatment in an adhesive formulation. The authors found that their inclusion in commercial dental adhesive formulations lead to significantly higher adhesion and improve adhesive durability, therefore are great candidates to enter adhesive dental formulations.

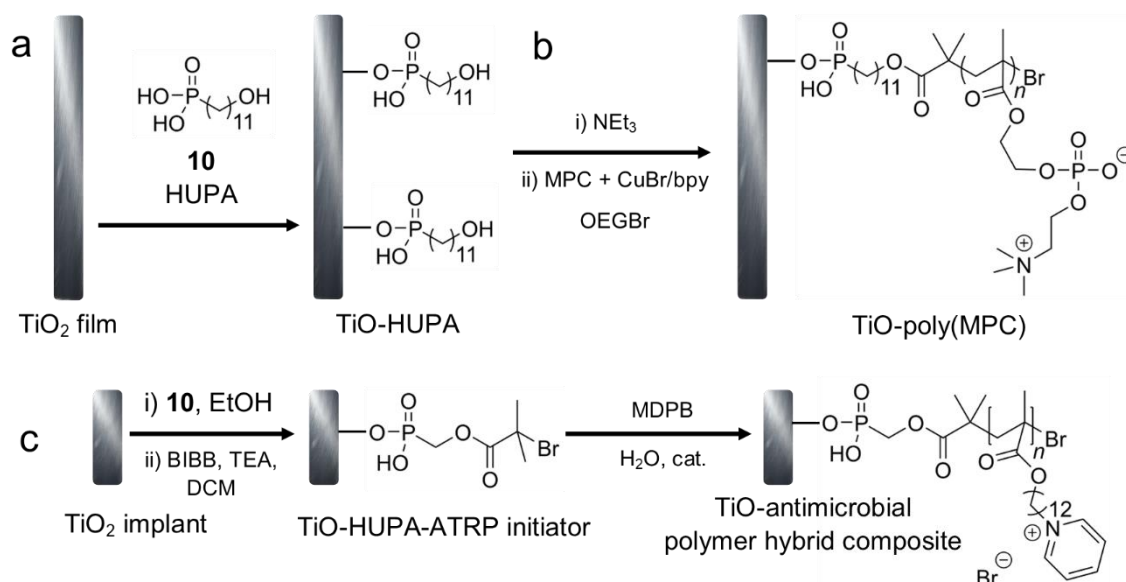


**Scheme 3.4** Phosphonate-containing monomers for binding to hydroxyapatite.

### 3.1.1.3 Hybrid materials from phosphonate-containing molecules binding to a metal and initiating a polymerisation

A phosphonate-containing molecule can initially be adhered to a metal surface through a P-O-M bond and subsequently used as an initiator for polymerisations. The resulting hybrid material (Section 1.4.1.3) combines a metal with a polymer via the P-O-M bond forming ability of the phosphonate functional group. For example, Zhao and colleagues self-assembled 11-hydroxyundecylphosphonic acid (HUPA) (**10**) onto the surface of a TiO<sub>2</sub> film forming an organic linking layer on the TiO<sub>2</sub> film and presenting a hydroxyl group for further functionalisation (Scheme 3.5a).<sup>43</sup> From this hydroxyl group, 2-methacryloyloxyethyl phosphorylcholine (MPC) was polymerised forming a TiO-poly(MPC) hybrid composite material (Scheme 3.5b). The modified TiO surface was effective at inhibiting platelet adhesion *in vivo*, thus improving the physiological stability of the TiO<sub>2</sub>. Antimicrobial polymers (Section 1.1.1.2) can also be grafted from the HUPA layer on a HUPA-coated TiO<sub>2</sub> implant to form an antimicrobial coating. For example, Clevenger patented a method of attaching an atom-transfer radical polymerisation (ATRP) initiator to TiO-functionalised HUPA (Scheme 3.5c).<sup>44</sup> From this, an antimicrobial polymer, poly(12-methacryloyloxydodecylpyridinium bromide) (poly(MDPB)), was polymerised via ATRP to form a TiO-antimicrobial polymer hybrid composite material.

Metallic pigments offer a metallic or pearlescent lustre to a surface, but the metal ions in such paint formulations can react with water, acids or bases in the formulation, causing discolouration or surface defects.<sup>45</sup> Phosphonate-containing molecules, such as HUPA, have also been demonstrated to improve the passivation, adhesion and dispersion of a metal pigment in a formulation.<sup>46</sup> Phosphonate-containing molecules bound to metal that initiate polymerisations may also be used to create protective coatings, ionomer resins, flame retardant materials, electronics and drug delivery vehicles.<sup>47</sup>



**Scheme 3.5** Reaction scheme for the self-assembly of HUPA on TiO<sub>2</sub> (a) and the subsequent polymerisation of MPC from the hydroxy group of HUPA (b).<sup>43</sup> Synthesis of TiO-antimicrobial polymer hybrid composite (c).<sup>44</sup> BIBB =  $\alpha$ -bromoisobutyryl bromide; bpy = 2,2'-bipyridine; cat. = CuBr and pentamethyldiethylenetriamine; OEGBr = oligomeric methoxy PEG 2-bromoisobutyrate; TEA = triethylamine.

### 3.1.2 Drug delivery of a hydrophobic chemotherapy drug

Doxorubicin (Dox) is a widely used chemotherapeutic and has therapeutic activity against a wide range of tumours.<sup>48</sup> Dox and other chemotherapeutic drugs have poor pharmacokinetics, interacting with healthy tissue as well as cancerous tissue, thus causing unpleasant and debilitating side effects.<sup>49-50</sup> Tumours have a more acidic environment than healthy cells and so if the chemotherapeutic can be loaded within a polymeric system and released only when it reaches this lower pH, the pharmacokinetics are greatly improved (Section 1.4.1).<sup>51-53</sup>

There are many examples of polymer-based drug delivery vehicles created for the delivery of Dox.<sup>52,54-56</sup> A cyclic arginine-glycine-aspartic (cRGD) tripeptide has been explored to improve a NPs affinity for, and uptake in, cancerous cells.<sup>57-59</sup> In 2019, Gu and co-workers synthesised a PEG-*b*-polytyrosine amphiphilic block copolymer via NCA ROP, followed by conjugation of cRGD to PEG (cRGD-PEG-*b*-PTyr) (Figure 3.1).<sup>60</sup> Self-assembly of the amphiphilic block copolymer with Dox formed a small polymeric NP of 70 nm. As can be seen in Figure 3.1, the NP had

an inner core with Dox and PTyr with PEG forming a hydrophilic shell, presenting cRGD on the outside for the NP to be adhered to, and taken in by, cancerous cells. Dox release in this instance was triggered by an enzyme, proteinase K, degrading PTyr. Gu and colleagues demonstrated the cRGD-conjugated NPs had 2.8 times better antitumour activity than non-cRGD-conjugated NPs, and overall cRGD-PEG-*b*-PTyr exhibited over five times better targeted delivery of Dox than clinically used liposomal Dox. Although extremely promising work, the material still includes PEG, which has issues and alternatives are desirable (Section 3.1.3).

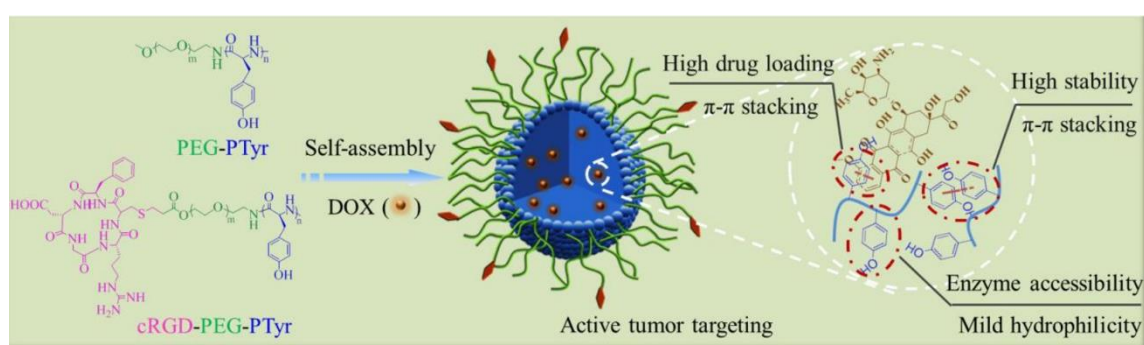


**Figure 3.1** Synthesis and self-assembly with Dox of cRGD-PEG-*b*-PTyr forming a polymeric NP. Reprinted from Ref. 60, copyright (2019), with permission from Elsevier.

### 3.1.3 Alternatives to ubiquitous PEG in drug delivery vehicles

PEG is a very useful and readily available polymer found in many products from surfactants to drugs. As seen above and in Section 1.4.1, PEG is frequently used in drug delivery vehicles to enhance drug solubilisation, increase efficacy and improve pharmacokinetics.<sup>61</sup> Unfortunately there are a few issues with PEG, such as it is not biodegradable and higher  $M_w$  PEG can cause significant tissue accumulation *in vivo* (Figure 3.2a).<sup>62-64</sup> Alternative polymers to overcome all or some of the problems with PEG in drug delivery have been reported, such as poly(2-oxazoline),<sup>65</sup> polyglycerols,<sup>66</sup> polyzwitterions,<sup>67</sup> polyacrylamides<sup>68</sup> and polyvinylpyrrolidones (Figure 3.2b).<sup>69</sup>

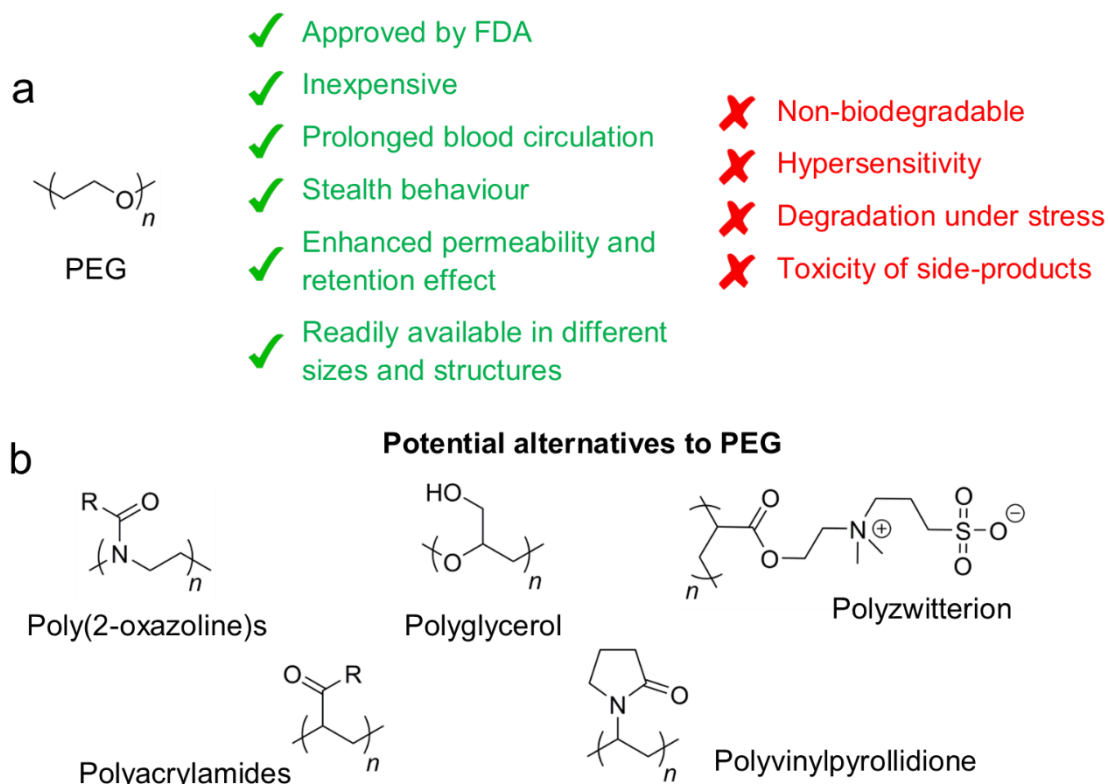
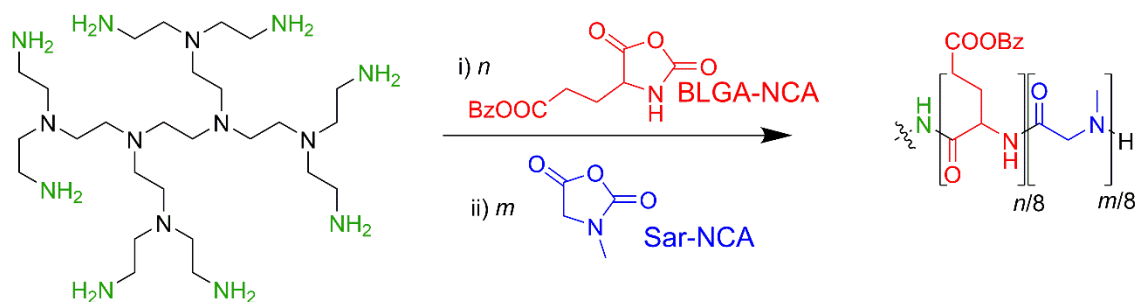


**Figure 3.2** (a) Some advantages and disadvantages of PEG, and (b) possible alternatives to PEG.<sup>63</sup>

Poly(amino acid)s (PAAs) are also promising alternatives to PEG due to their biocompatibility and biodegradability, as discussed in Section 1.2.1.<sup>70-72</sup> Specifically, polypeptoids, structural mimics of PAAs but with an *N*-substituted glycine unit, are very promising replacements to PEG because they are hydrophilic, biodegradable and biocompatible with enhanced physiological stability to PAAs.<sup>73-77</sup> Specifically, polysarcosine (PSar) is a nonionic polypeptoid and is a very promising replacement of PEG because it is biodegradable, highly hydrophilic, and has enhanced physiological stability than PAAs.<sup>78</sup> Recently, Skoulas *et al.* synthesised a PAA-*b*-polypeptoid amphiphilic star copolymer of PBLG-*b*-PSar via sequential NCA ROP (Section 1.2.3) (Scheme 3.6).<sup>79</sup> The authors demonstrated this material as a potential drug delivery vehicle through the mucus and epithelial barriers, typically a difficult drug delivery route but very advantageous for localised, non-invasive drug delivery to target tissues.<sup>80-84</sup>



**Scheme 3.6** Reaction scheme for the synthesis of PBLG-*b*-PSar from a dendrimer to form an amphiphilic star copolymer.<sup>79</sup>

### 3.1.4 Summary

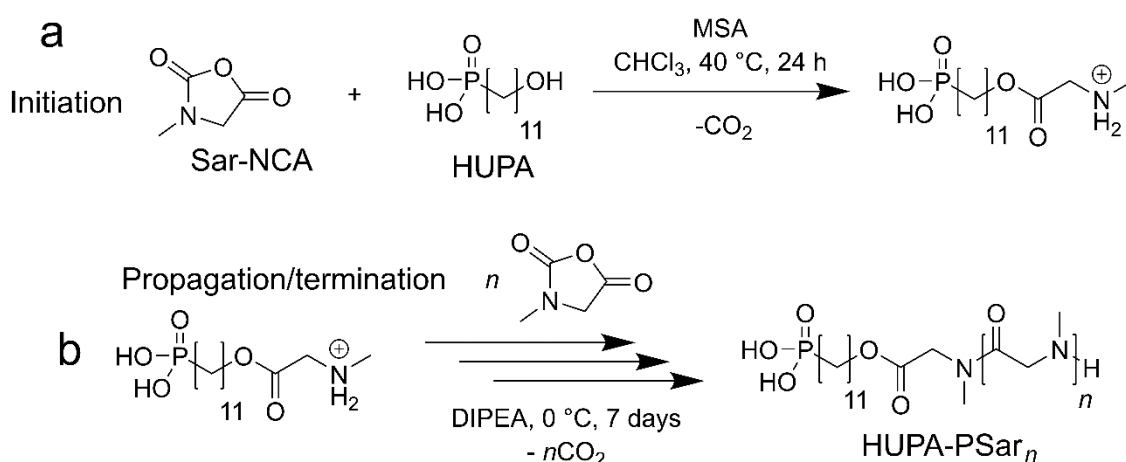
Polymers containing the phosphonate functional group have many useful applications because of their ability to form P-O-M bonds. Herein, the synthesis of two HUPA-PSar polymers is described which have a terminal phosphonate group to bind to metal ions, and a hydrophilic, biodegradable and biocompatible polymer which is an alternative to ubiquitous PEG. The polymers synthesised are amphiphilic and thus can form NPs whereby a drug can be loaded and released to improve the drug's pharmacokinetics. Additionally, the polymers may bind to materials with metals to improve their aqueous dispersibility, biocompatibility or corrosion resistance, for example, through a P-O-M bond.

## 3.2 Experimental Details

### 3.2.1 Synthesis of HUPA-PSar polymers

Three amphiphilic, phosphonate-terminated polymers were synthesised, HUPA-PSar<sub>34</sub>, HUPA-PSar<sub>95</sub> and HUPA-PSar<sub>181</sub> (Scheme 3.7), using a previously reported procedure with modifications.<sup>54,85</sup> Briefly, into an oven-dried and N<sub>2</sub>-flushed Schlenk tube, Sar-NCA (from Section 2.3.1.1) was weighed and suspended in anhydrous chloroform (10 mL). Methanesulfonic acid (0.01 g, 0.11 mmol, 3 eq.) and HUPA (0.01 g, 0.04 mmol, 1 eq.) were added to the Schlenk tube and the acid-catalysed initiation reaction stirred at 40 °C with a flow of N<sub>2</sub>

(Scheme 3.7a). After 24 hours, the initiation reaction was complete and *N*-ethyl-diisopropylamine (0.27 g, 2.09 mmol, 52 eq.) added to propagate the polymerisation reaction (Scheme 3.7b). The reaction solution was stirred at 0 °C with a flow of N<sub>2</sub> for four days after which FTIR spectroscopy confirmed the reaction had reached completion by the loss of anhydride peak from Sar-NCA. The polymer solution was added dropwise to ice-cold diethyl ether (1:5 v/v) and the polymer collected by centrifugation (4,000 r.p.m., 15 minutes), washed by dialysis (2,000 Da MWCO) against DI water and lyophilised.



**Scheme 3.7** Reaction scheme for the acid-catalysed initiation (a) followed by base-catalysed propagation (b) of HUPA and Sar-NCA to synthesise HUPA-PSar<sub>*n*</sub> via hydroxyl-initiated NCA ROP. MSA = methanesulfonic acid; DIPEA = *N*-ethyl-diisopropylamine.

### 3.2.2 Dox release

A solution of polymer (10 mg) in chloroform (1 mL) was prepared and added dropwise to vigorously stirred PBS buffer solution at pH 7.4 (8 mL) simultaneously with Dox free base in chloroform (from Section 2.3.4.1, 3 mL, 1 mg mL<sup>-1</sup>). The Dox free base and polymer solution was stirred in the open in the dark overnight for the chloroform to evaporate.

Unloaded Dox was removed by dialysis (2,000 Da MWCO) against DI water for 24 hours. The amount of Dox loaded was determined by analysing an aliquot of

the solution outside the dialysis tubing by UV-vis spectrophotometry, using the calibration described in Section 2.3.4.2. Three 1 mL aliquots were then taken from the red coloured Dox-loaded NP solution inside the dialysis tubing and transferred to separate dialysis tubing. One of the aliquots was dialysed against fresh PBS buffer solution at pH 7.4, another dialysed against acetate buffer solution at pH 6, and the final aliquot dialysed against acetate buffer solution at pH 5. The dialysis was conducted with gentle stirring in the dark at 37 °C. At regular time intervals, aliquots of the buffer solutions outside the dialysis tubing were taken and analysed by UV-vis spectrophotometry to determine how much Dox had been released.

### **3.2.3 HUPA-PSar<sub>181</sub> self-assembly with TiO<sub>2</sub>-NPs to form TiO<sub>2</sub>-NCs**

Firstly, TiO<sub>2</sub>-NPs were synthesised by adding acetic acid (20 mL), 1-butyl-3-methylimidazolium tetrafluoroborate (500 µL) and DI water (1.25 mL) to a RB flask fitted with a stirrer bar. Titanium (IV) isopropoxide (500 µL) was then added with stirring. The reagents were stirred for a further five minutes, sonicated for 30 s, sealed in a hydrothermal bomb and heated to 200 °C for 24 h. TiO<sub>2</sub>-NPs were then washed with DI water, sonicated and collected by centrifugation (4,500 r.p.m., 30 minutes). This washing and collection step was repeated until acetic acid was removed, and a final washing, sonicating, centrifugating and decanting was performed with ethanol. The washed TiO<sub>2</sub>-NPs were allowed to dry in the open overnight (yield = 0.136 g).

Secondly, HUPA-PSar<sub>181</sub> (5 mg) and the TiO<sub>2</sub>-NPs prepared above (5 mg) were weighed in a glass vial and suspended in DI water (5 mL) with the aid of an ultrasonic bath. The TiO<sub>2</sub>-NCs were collected by centrifugation (4,000 rpm, 30 mins), washed with DI water and chloroform before being dried in the open. Turbidimetric analyses involved suspending the sample in DI water (either TiO<sub>2</sub>-NPs or TiO<sub>2</sub>-NCs, 5 mg in 5 mL DI water) with the aid of an ultrasonic bath and transferring the milky white suspension to a quartz cuvette. The sample was loaded into a UV-vis spectrophotometer and the absorbance at 650 nm recorded every 60 s for 60 h.

## 3.3 Results and Discussions

### 3.3.1 NCA ROP initiated from the hydroxyl group on HUPA

#### 3.3.1.1 HUPA-PSar synthesis and characterisation

Phosphonate-terminated amphiphilic polymers, HUPA-PSar<sub>34</sub>, HUPA-PSar<sub>95</sub> and HUPA-PSar<sub>181</sub> were synthesised as per Scheme 3.7. This reaction scheme is different to conventional NCA ROP (Section 1.3.3.2) because it features a polypeptoid initiated from a hydroxyl group, thus providing an ester linkage between the initiator (HUPA) and polymer (PSar). <sup>1</sup>H NMR spectroscopy was conducted to confirm polymer synthesis whereby the 14 protons corresponding to the middle seven CH<sub>2</sub> groups in the HUPA alkyl chain were observed between 1.1 and 1.4 ppm (Figure 3.3). The peaks between 2.7 and 3.1 ppm are attributed to the CH<sub>3</sub> protons on PSar whilst the peaks between 3.9 and 4.4 ppm correspond with the CH<sub>2</sub> protons in PSar. Calculated and expected Sar equivalences are provided in Table 3.1 where the actual Sar equivalence was calculated from the comparison between the 14 protons from the middle seven CH<sub>2</sub> groups on the HUPA alkyl chain and the CH<sub>3</sub> and CH<sub>2</sub> groups in PSar. <sup>13</sup>C NMR spectroscopy further confirmed polymer synthesis whereby the peak at 36 ppm corresponds with the CH<sub>3</sub> group on PSar, the peak at 50 ppm corresponds with the CH<sub>2</sub> group on PSar, whilst the peak at 168 ppm corresponds with the carbonyl C=O group on PSar (Figure 3.4).

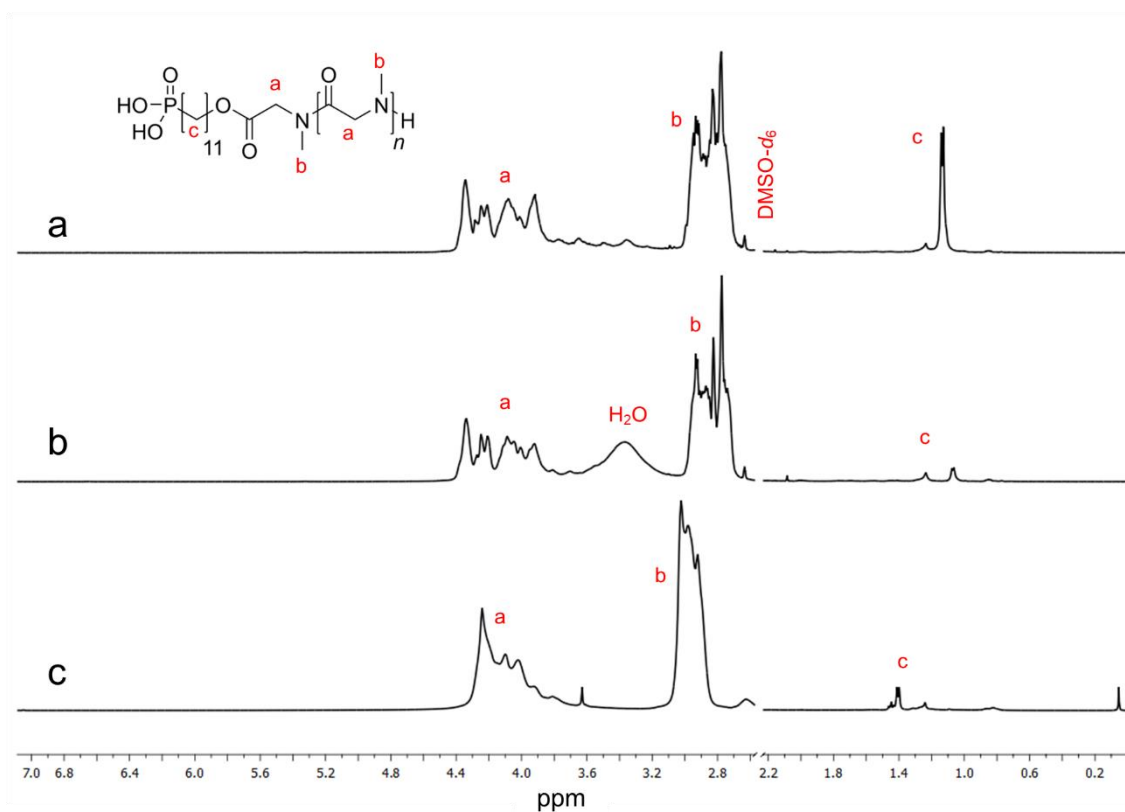


**Figure 3.3**  $^1\text{H}$  NMR spectra of HUPA-PSar<sub>34</sub> (a), HUPA-PSar<sub>95</sub> (b) (500 MHz, DMSO- $d_6$ ) and HUPA-PSar<sub>181</sub> (c) (500 MHz,  $\text{CDCl}_3$ ).

**Table 3.1** Calculated and actual equivalence values, and polymer nanoparticle dimensions.

Polymer	Equivalence		$d_H$ (nm) <sup>b</sup>	PDI <sup>b</sup>	$\zeta$ (mV) <sup>b</sup>
	Theoretical	Observed <sup>a</sup>			
HUPA-PSar <sub>34</sub>	51	34	267	0.416	11.7 ± 4.40
HUPA-PSar <sub>95</sub>	102	95	162	0.393	23.4 ± 5.06
HUPA-PSar <sub>181</sub>	244	181	141	0.267	23.4 ± 4.53

<sup>a</sup> Determined from  $^1\text{H}$  NMR analysis. <sup>b</sup> Determined from DLS analysis of 1.0 mg mL<sup>-1</sup> aqueous solutions in triplicate.

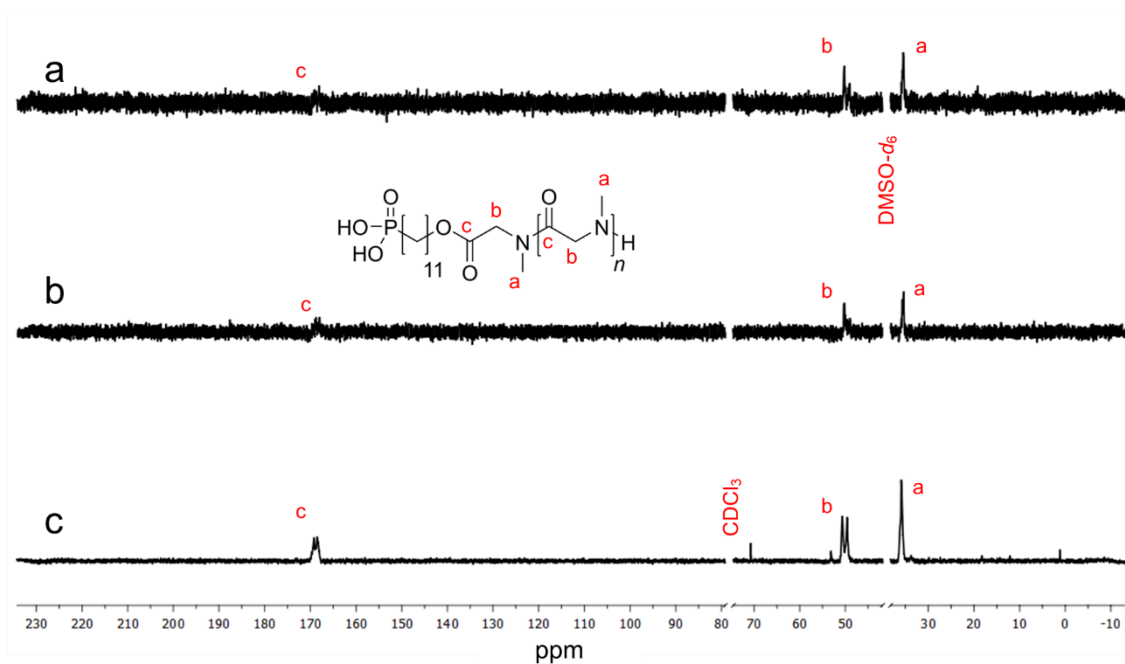


**Figure 3.4**  $^{13}\text{C}$  NMR spectra of HUPA-PSar<sub>34</sub> (a), HUPA-PSar<sub>95</sub> (b) (126 MHz, DMSO-*d*<sub>6</sub>) and HUPA-PSar<sub>181</sub> (c) (126 MHz, CDCl<sub>3</sub>).

FTIR spectroscopy was also used to confirm polymer synthesis (Figure 3.5). HUPA features a broad -OH peak at  $3183\text{ cm}^{-1}$ , CH<sub>2</sub> vibrational modes at  $2917\text{ cm}^{-1}$ ,  $2849\text{ cm}^{-1}$  and  $1467\text{ cm}^{-1}$ , and PO-H stretching bands at  $2353\text{ cm}^{-1}$  in its FTIR spectrum. The HUPA-PSar polymers also have CH<sub>2</sub> vibrational modes at  $2989\text{ cm}^{-1}$  and  $1495\text{ cm}^{-1}$ , but additionally an amide peak at  $1640\text{ cm}^{-1}$ . The presence of both CH<sub>2</sub> peaks (from HUPA) and a strong amide peak in the polymers is further evidence for the polymerisation of PSar initiated from HUPA.

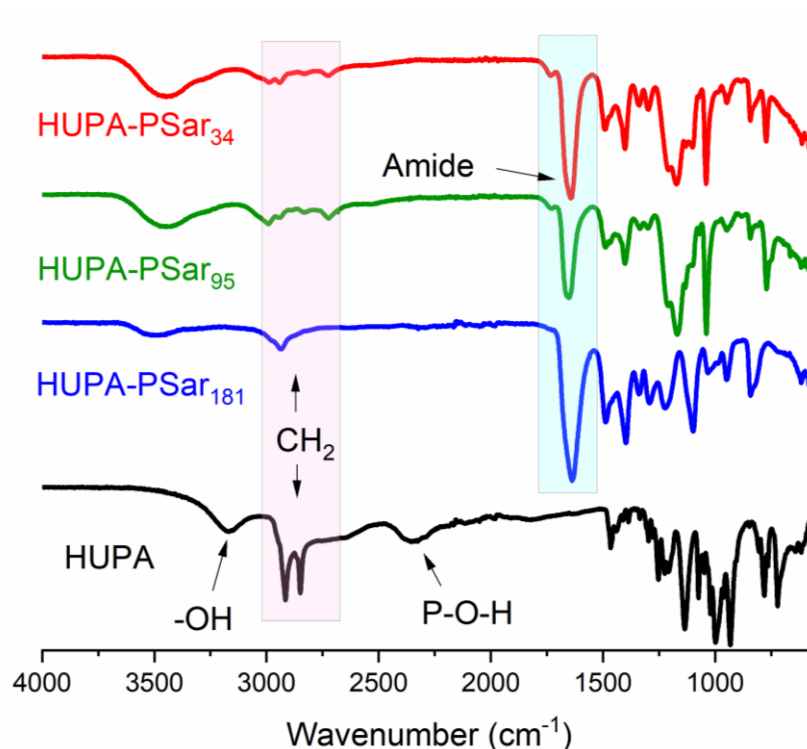


**Figure 3.5** FTIR spectra of HUPA and the HUPA-PSar polymers.

### 3.3.1.2 Evidence for hydroxyl-initiated polymerisation rather than phosphonate-initiated

Acid-catalysed initiation and base-catalysed propagation is an effective way of synthesising PAAs from hydroxyl groups. HUPA, however, has a phosphonate group and a hydroxyl group. As described in Section 3.1.1, the phosphonic acid group contains a P=O bond and two P-OH bonds; to determine if the polymerisation occurs from the terminal hydroxyl group or a P-OH group on the phosphonate,  $^{31}\text{P}$  NMR spectroscopy was carried out. As shown in Figure 3.6, HUPA has a single  $^{31}\text{P}$  NMR peak at 29.2 ppm whilst HUPA-PSar<sub>95</sub> has a single peak at 27.3 ppm. Because these peaks are so close and both within the phosphonate group  $^{31}\text{P}$  NMR range, it is evidence for the polymerisation being conducted from the hydroxyl group of HUPA rather than the P-OH groups. Further, if the polymerisation were to have occurred from the phosphonate group, forming one P-O-C bond (phosphate monoester), there would be a  $^{31}\text{P}$  peak shift from 29 ppm to between 0 and 10 ppm, which is not observed. If the polymerisation occurred from both P-OH groups, it would form two P-O-C bonds

(phosphate diester) and a  $^{31}\text{P}$  peak between 0 and -5 ppm would be anticipated.<sup>86-88</sup>

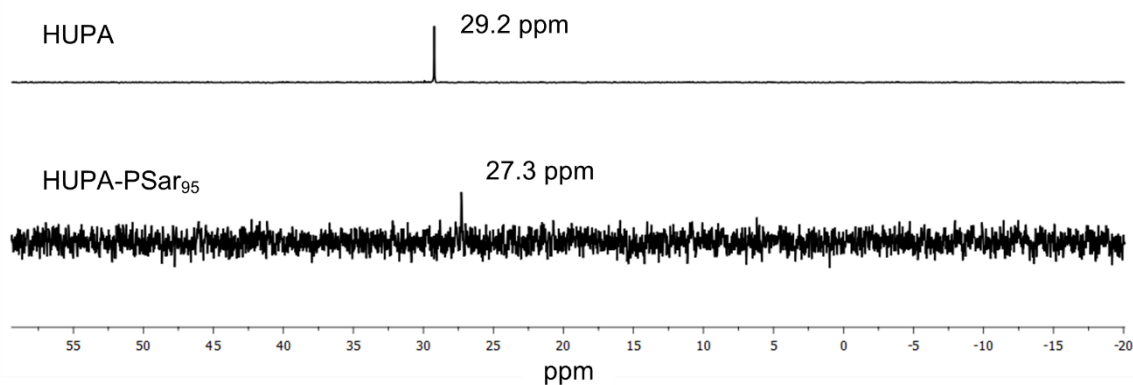


**Figure 3.6**  $^{31}\text{P}$  NMR spectra of HUPA and HUPA-PSar<sub>95</sub> (202 MHz, DMSO-*d*<sub>6</sub>).

As well as the  $^{31}\text{P}$  NMR spectroscopy results, a very strong broad peak in the polymers FTIR spectrum between 1050-970  $\text{cm}^{-1}$ , which would correspond to a P-O-C stretch, would be observed if NCA ROP had occurred from the P-OH group.<sup>89</sup> Because this peak does not appear in the FTIR spectrum of any HUPA-PSar polymer (Figure 3.5), it can be concluded that the polymerisation exclusively occurred from the hydroxyl group on HUPA and not from a P-OH group. NMR spectroscopies and FTIR spectroscopy have confirmed successful HUPA-PSar polymer synthesis. The amphiphilic polymers' ability to self-assemble into a NP was then investigated.

### 3.3.2 NP formation, Dox loading and release

#### 3.3.2.1 HUPA-PSar NP formation

The dropping-in method for NP formation was used (Section 2.3.3) and DLS analysis revealed the polymers form NPs with hydrodynamic diameters ( $d_H$ ) of 267, 162 and 141 nm for HUPA-PSar<sub>34</sub>, HUPA-PSar<sub>95</sub> and HUPA-PSar<sub>181</sub>, respectively (Table 3.1 and Figure 3.7a). The NPs displayed PDI values of 0.416,

0.393 and 0.267 for HUPA-PSar<sub>34</sub>, HUPA-PSar<sub>95</sub> and HUPA-PSar<sub>181</sub>, respectively (Table 3.1). Zeta potential values ( $\zeta$ ) give an indication on the stability of NPs because charged particles repel each other whereas neutral NPs may be more likely to aggregate. HUPA-PSar<sub>34</sub>, HUPA-PSar<sub>95</sub> and HUPA-PSar<sub>181</sub> had  $\zeta$  values of  $11.7 \pm 4.40$ ,  $23.4 \pm 5.06$  and  $23.4 \pm 4.53$  mV, respectively, indicating the NPs have a slight positive charge and thus all are more likely to form stable NPs in solution (Table 3.1). To further probe the long-term stability of HUPA-PSar<sub>95</sub>, the DLS sample was retained after initial analysis. After 45 days the sample had a  $d_H$  of 157.3 nm and PDI of 0.297, closely matching the values obtained with fresh NPs and thus indicating these NPs are stable for a month in solution. Interestingly, as the equivalence of Sar increases, the  $d_H$  also increases in a linear manner; plotting the values graphically potentially allows for the prediction of  $d_H$  from Sar equivalence (Figure 3.7b).<sup>79</sup> The smaller  $d_H$  and PDI values, and higher  $\zeta$  values as the Sar equivalence increases may be ascribed to the larger hydrophilic polymer block resisting polymer aggregation, whilst enhancing polymer-water interactions.

SEM microscopy of HUPA-PSar<sub>95</sub> confirmed NP formation (Figure 3.7c), and the particle size is close to that calculated by DLS ( $162 \pm 75$  nm,  $n=71$ , Figure 3.7c, inset). Small, stable NPs with low PDI values are required for drug delivery vehicles, as discussed in Section 1.3. The small  $d_H$  and PDI of HUPA-PSar<sub>181</sub> made this NP the best candidate to progress to a drug delivery study, where the ester link between the HUPA macroinitiator and PSar chain may be exploited to impart a degree of pH-stimuli-responsiveness.

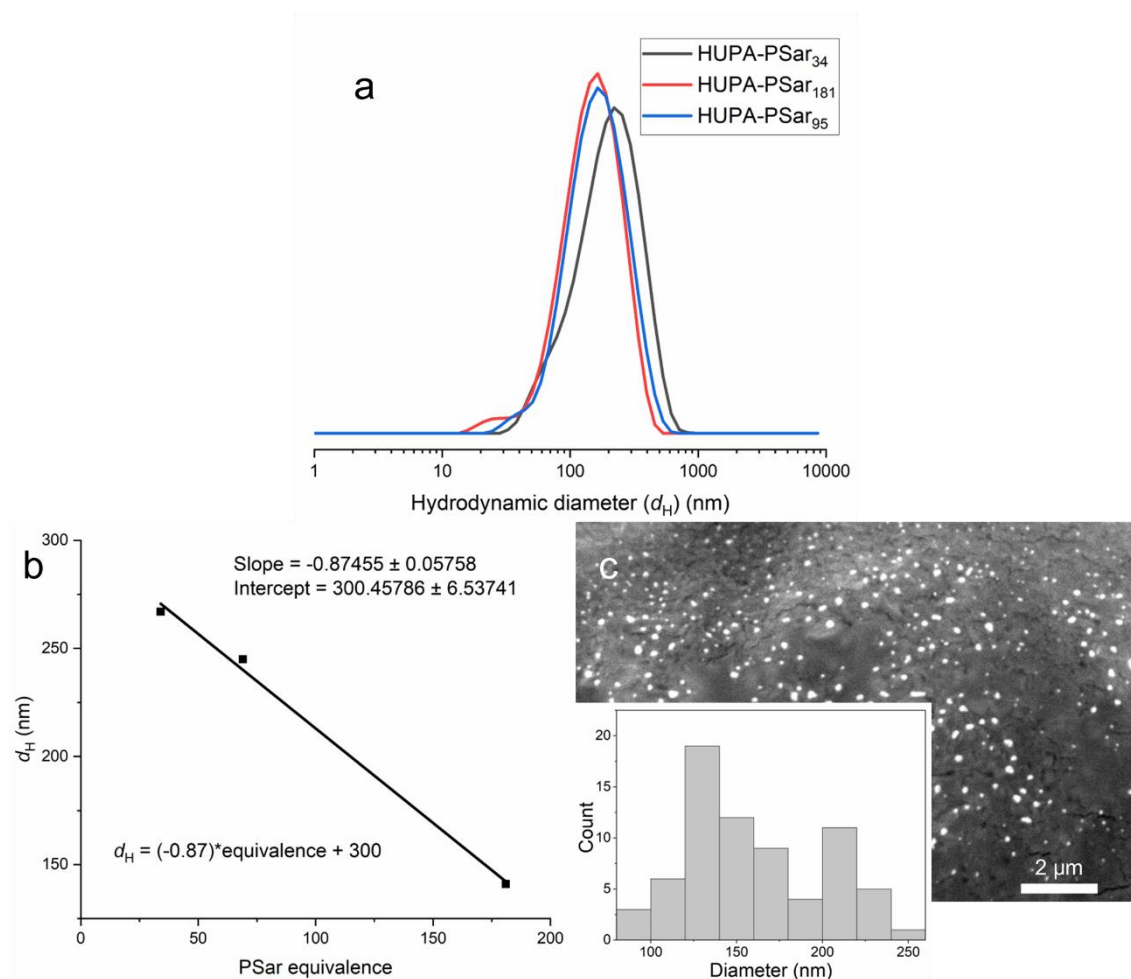


**Figure 3.7** (a) Hydrodynamic diameter ( $d_H$ ) distribution of the HUPA-PSar polymers measured by DLS, (b) relationship between equivalence and  $d_H$ , and (c) SEM micrograph of HUPA-PSar<sub>95</sub> NPs (scale bar is 2  $\mu\text{m}$ ; inset: particle size histogram ( $n=71$ )).

### 3.3.2.2 Dox loading and release of the HUPA-PSar NPs

The pH-responsiveness of HUPA-PSar<sub>181</sub> was investigated with a Dox release study in pH 7.4, 6 and 5 buffer solutions. Dox was loaded into the NPs with a loading content of 3% (calculated from Equation (2.5)) and loading efficiency of 20% by mass (calculated from Equation (2.6)). The release of Dox in PBS buffer solution at pH 7.4 and in acetate buffer solutions at pH 6 and 5 was then assayed for 168 hours using UV-vis spectrophotometry (Figure 3.8). Stimuli-responsiveness with respect to pH was demonstrated; only 35% Dox was released to pH 7.4 buffer solution after 168 h whereas 72% and 80% Dox was released into pH 6 and pH 5 buffer solutions, respectively. The low amount of Dox released to physiological pH (7.4) and high amount released to acidic

environments renders HUPA-PSar<sub>181</sub> a possible drug delivery vehicle which may enhance the pharmacokinetics of Dox for the effective, targeted treatment of tumours.

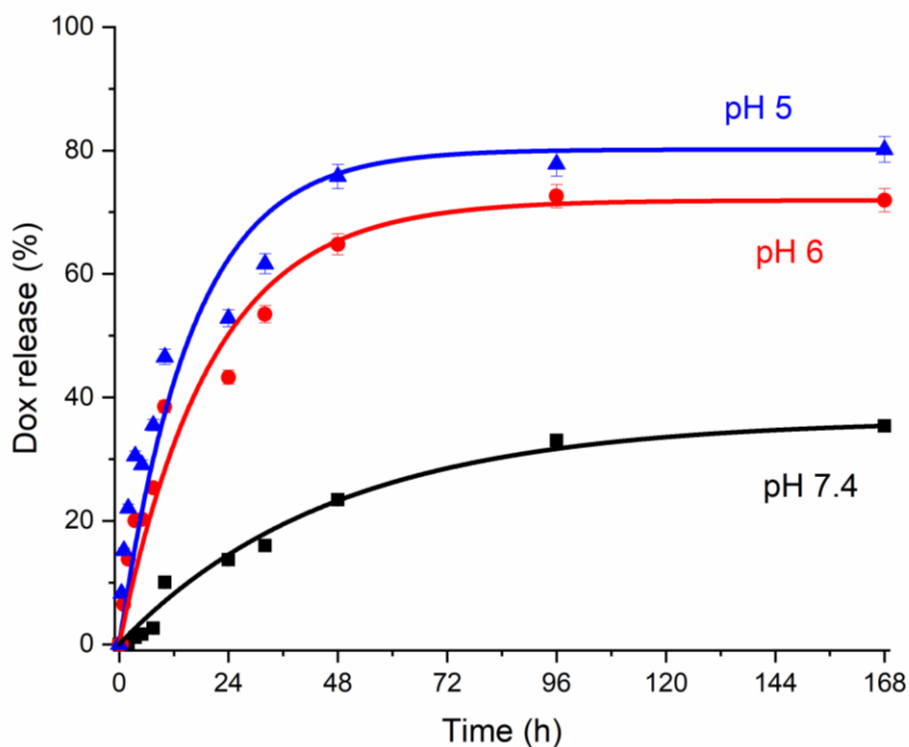
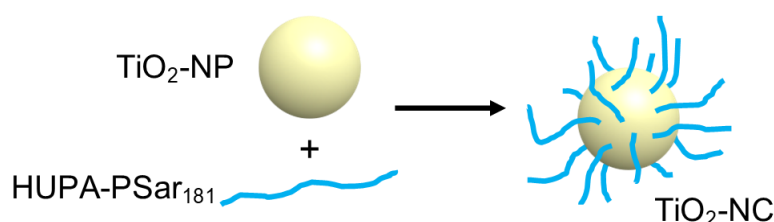


**Figure 3.8** Dox release over time for HUPA-PSar<sub>181</sub> in pH 7.4, 6 and 5 buffer solutions.

### 3.3.3 HUPA-PSar conjugation with metals via P-O-M bond

To demonstrate another potential application of the amphiphilic block copolymers produced, HUPA-PSar<sub>181</sub> was coordinated to titanium dioxide NPs (TiO<sub>2</sub>-NPs) yielding a TiO<sub>2</sub>-NP-polymer nanocomposite, TiO<sub>2</sub>-NC (Scheme 3.8). Figure 3.9a shows that after washing and drying, the FTIR spectrum corresponding to the TiO<sub>2</sub>-NC contains the same characteristic peaks that are present in the spectra corresponding to both TiO<sub>2</sub>-NPs and HUPA-PSar<sub>181</sub>. Notably, the characteristic C-H peak at 2921 cm<sup>-1</sup> is included in the polymer and nanocomposite FTIR spectra but not in the TiO<sub>2</sub>-NP spectrum, indicating polymer conjugation to TiO<sub>2</sub>-NPs. The dispersion stability of TiO<sub>2</sub>-NPs in water is somewhat limited and restricts their use in applications that require long-term storage in aqueous

formulations without dispersants. Figure 3.9b shows the bare  $\text{TiO}_2$ -NPs have poor aqueous compatibility; 50% of the  $\text{TiO}_2$ -NPs aggregated after 25 h, and complete aggregation was observed after 60 h. Conversely,  $\text{TiO}_2$ -NCs, remained as a homogeneous dispersion for much longer and after 60 h approximately 50% of the  $\text{TiO}_2$ -NCs remained in suspension.



**Scheme 3.8.** Self-assembly of HUPA-PSar<sub>181</sub> with  $\text{TiO}_2$ -NPs to form  $\text{TiO}_2$ -NCs.

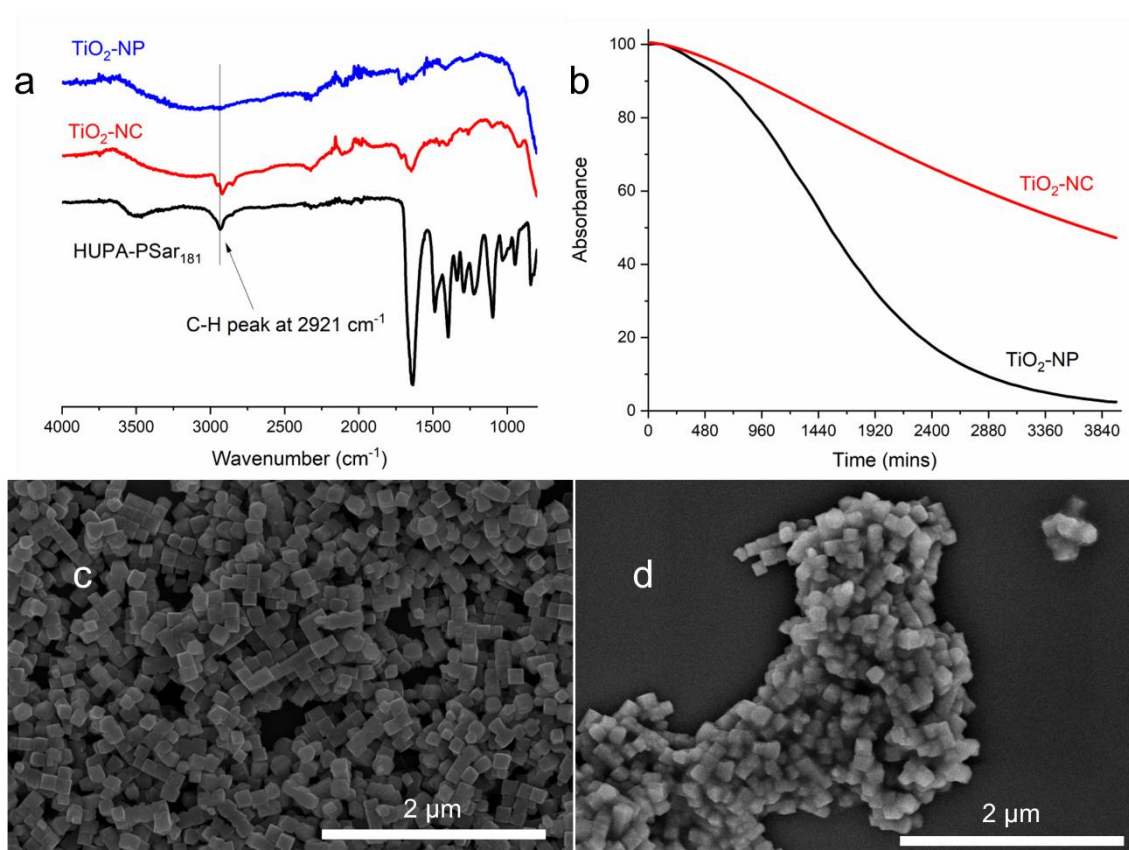


**Figure 3.9** (a) FTIR spectra of HUPA-PSar<sub>181</sub>,  $\text{TiO}_2$ -NP and  $\text{TiO}_2$ -NC. (b) Turbidimetric analysis from UV-vis absorbance at 650 nm over time for  $\text{TiO}_2$ -NP and  $\text{TiO}_2$ -NC in DI water. (c) SEM micrographs of  $\text{TiO}_2$ -NPs and (d)  $\text{TiO}_2$ -NCs (both scale bars are  $2\text{ }\mu\text{m}$ ).

TiO<sub>2</sub>-NPs and TiO<sub>2</sub>-NCs both have cuboid shapes and similar particle sizes of  $125 \pm 13$  nm and  $124 \pm 18$  nm ( $n=54$ ), respectively, as determined by SEM microscopy (Figure 3.9c-d). Interestingly, the bare TiO<sub>2</sub>-NPs have sharp and well-defined edges, whilst TiO<sub>2</sub>-NCs have shadowed edges, i.e., a 'halo' effect, indicating the NPs are coated with an organic material. FTIR, UV-vis and SEM analysis confirmed polymer conjugation to the TiO<sub>2</sub>-NPs, and this polymer conjugation was demonstrated to improve the aqueous compatibility of TiO<sub>2</sub>-NPs by 50% over 60 h.

### 3.4 Conclusions

HUPA, a long alkyl chain with a terminal phosphonate functional group on one end and a hydroxyl group on the other was used to initiate ROP of Sar-NCA. <sup>1</sup>H and <sup>13</sup>C NMR spectroscopies were used to confirm the synthesis of HUPA-PSar polymers, whilst <sup>31</sup>P NMR showed NCA ROP was initiated from the hydroxyl group of HUPA rather than a P-OH group. The polymers are amphiphilic whereby the HUPA provides hydrophobicity and PSar hydrophilicity, and formed stable NPs in aqueous solution with  $d_H$  of 262, 162 and 141 nm for HUPA-PSar<sub>34</sub>, HUPA-PSar<sub>95</sub> and HUPA-PSar<sub>181</sub>, respectively. NCA ROP initiated from a hydroxyl group here provides an ester link between HUPA and PSar which is susceptible to acid hydrolysis. Dox was loaded into HUPA-PSar<sub>181</sub> NPs and its subsequent release over time assayed by UV-vis spectrophotometry. Stimuli-responsiveness was observed with the NP only releasing 35% Dox over 168 h but releasing 72% and 80% Dox at pH 6 and 5, respectively, after 168 h. HUPA-PSar<sub>181</sub> therefore shows promise as a biodegradable and biocompatible, stimuli-responsive drug delivery vehicle to improve the pharmacokinetics of hydrophobic chemotherapy drugs, which does not use the non-biodegradable PEG. Additionally, the polymers may form P-O-M bonds, and the aqueous compatibility of TiO<sub>2</sub>-NPs was improved by self-assembly with HUPA-PSar<sub>181</sub>. Almost all the TiO<sub>2</sub>-NPs crashed out of suspension after 60 h whereas approximately 50% of the TiO<sub>2</sub>-NCs remained homogeneous after 60 h. This ability to form P-O-M bonds allows these biodegradable polymers to be useful for applications including

corrosion inhibition, fuel cells, metal chelators, dental adhesives and in biomaterials.

### 3.5 References

1. S. K. Ramasamy, A. P. Kusumbe, M. Schiller, D. Zeuschner, M. G. Bixel, C. Milia, J. Gamrekelashvili, A. Limbourg, A. Medvinsky, M. M. Santoro, F. P. Limbourg and R. H. Adams, *Nature Communications*, 2016, **7**, 13601.
2. J. R. Green, *The Oncologist*, 2004, **9**, 3-13.
3. A. Clearfield, in *Metal Phosphonate Chemistry: From Synthesis to Applications*, eds. A. Clearfield and K. D. Demadis, The Royal Society of Chemistry, Cambridge, U.K., 2012, ch. 1, pp. 1-44.
4. L. A. Vermeulen and M. E. Thompson, *Nature*, 1992, **358**, 656-658.
5. G. K. H. Shimizu, R. Vaidhyanathan and J. M. Taylor, *Chemical Society Reviews*, 2009, **38**, 1430-1449.
6. P. Bhanja, J. Na, T. Jing, J. Lin, T. Wakihara, A. Bhaumik and Y. Yamauchi, *Chemistry of Materials*, 2019, **31**, 5343-5362.
7. B. Zhang, L. Zhang, F. Li, W. Hu and P. M. Hannam, *Corrosion Science*, 2010, **52**, 3883-3890.
8. B. Date, J. Han, S. Park, E. J. Park, D. Shin, C. Y. Ryu and C. Bae, *Macromolecules*, 2018, **51**, 1020-1030.
9. W. Yang, H.-R. Tian, J.-P. Li, Y.-F. Hui, X. He, J. Li, S. Dang, Z. Xie and Z.-M. Sun, *Chemistry – A European Journal*, 2016, **22**, 15451-15457.
10. T. Gencoglu, F. D. Duman, K. Olcay, H. Y. Acar and D. Avci, *Journal of Polymer Science Part A: Polymer Chemistry*, 2018, **56**, 2739-2751.
11. S. Altuncu, F. Demir Duman, U. Gulyuz, H. Yagci Acar, O. Okay and D. Avci, *European Polymer Journal*, 2019, **113**, 155-164.
12. L. Macarie and G. Ilia, *Progress in Polymer Science*, 2010, **35**, 1078-1092.
13. L. Seiler, J. Loiseau, F. Leising, P. Boustingorry, S. Harrisson and M. Destarac, *Polymer Chemistry*, 2017, **8**, 3825-3832.
14. M. Yilmaz, A. Akar, N. Köken and N. Kızılcan, *Journal of Applied Polymer Science*, 2020, 49023.
15. S. J. Kim and J. Jang, *Fibers and Polymers*, 2017, **18**, 2328-2333.
16. Y. Hori, T. Suetake, Y. Shiota, K. Yoshizawa, Y. Shigeta, T. Ida and M. Mizuno, *ACS Applied Polymer Materials*, 2020, **2**, 1561-1568.
17. M. Tsuksamoto, K. Ebata, H. Sakiyama, S. Yamamoto, M. Mitsuishi, T. Miyashita and J. Matsui, *Langmuir*, 2019, **35**, 3302-3307.
18. E. Yilmaz and E. Can, *Journal of Polymer Science Part B: Polymer Physics*, 2018, **56**, 558-575.
19. D. Yuan, S. Zhang, Z. Xiang, Y. He, Y. Wang, Y. Liu, X. Zhao, X. Zhou and Q. Zhang, *ACS Applied Materials & Interfaces*, 2019, **11**, 24512-24522.
20. Z. Zheng, M. Mounsamy, N. Lauth-de Viguierie, Y. Coppel, S. Harrisson, M. Destarac, C. Mingotaud, M. L. Kahn and J.-D. Marty, *Polymer Chemistry*, 2019, **10**, 145-154.
21. J. B. Nichols, A. J. McQuillan and S. C. Moratti, *Colloids and Surfaces A: Physicochemical and Engineering Aspects*, 2017, **530**, 38-45.

22. Y. Zheng, L. Liu, L. Xiao, Q. Zhang and Y. Liu, *Colloids and Surfaces B: Biointerfaces*, 2019, **173**, 591-598.
23. X. Solimando, Y. Catel, N. Moszner, J.-J. Robin and S. Monge, *Polymer Chemistry*, 2020, **11**, 3237-3250.
24. S. Y. Kim and J.-S. Park, *Journal of Applied Polymer Science*, 2014, 131.
25. C. Zhang, Y. Liu, Z. Liu, H. Zhang, Q. Cheng and C. Yang, *Langmuir*, 2017, **33**, 2133-2140.
26. S. B. Sengel and N. Sahiner, *European Polymer Journal*, 2016, **75**, 264-275.
27. V. Baldim, N. Bia, A. Grailot, C. Loubat and J.-F. Berret, *Advanced Materials Interfaces*, 2019, **6**, 1801814.
28. K. Gharbi, F. Salles, P. Mathieu, C. Amiens, V. Collière, Y. Coppel, K. Philippot, L. Fontaine, V. Montembault, L. S. Smiri and D. Ciuculescu-Pradines, *New Journal of Chemistry*, 2017, **41**, 11898-11905.
29. Z. Amjad, *Int. J. Corros. Scale Inhib.*, 2015, **4**, 75-84.
30. S. J. Dyer, C. E. Anderson and G. M. Graham, *Journal of Petroleum Science and Engineering*, 2004, **43**, 259-270.
31. P. Pang, Y. Deslandes, S. Raymond, G. Pleizier and P. Englezos, *Industrial & Engineering Chemistry Research*, 2001, **40**, 2445-2451.
32. S. Banerjee, M. Wehbi, A. Manseri, A. Mehdi, A. Alaaeddine, A. Hachem and B. Ameduri, *ACS Applied Materials & Interfaces*, 2017, **9**, 6433-6443.
33. J. J. M. Nelson and E. J. Schelter, *Inorganic Chemistry*, 2019, **58**, 979-990.
34. D. Gomes Rodrigues, S. Monge, S. Pellet-Rostaing, N. Dacheux, D. Bouyer and C. Faur, *Chemical Engineering Journal*, 2019, **371**, 857-867.
35. X. Zhu and S. D. Alexandratos, *Chemical Engineering Science*, 2015, **127**, 126-132.
36. W. R. Archer, A. Fiorito, S. L. Heinz-Kunert, P. L. MacNicol, S. A. Winn and M. D. Schulz, *Macromolecules*, 2020, **53**, 2061-2068.
37. N. Moszner and Y. Catel, in *Phosphorus-Based Polymers: From Synthesis to Applications*, eds. S. Monge and G. David, The Royal Society of Chemistry, Cambridge, U.K., 2014, ch. 8, pp. 151-166.
38. Ö. Doğan and M. Öner, *Langmuir*, 2006, **22**, 9671-9675.
39. WO 02/02057, 2002.
40. D. Avci and L. J. Mathias, *Journal of Polymer Science Part A: Polymer Chemistry*, 2002, **40**, 3221-3231.
41. Y. K. Kim, L.-s. Gu, T. E. Bryan, J. R. Kim, L. Chen, Y. Liu, J. C. Yoon, L. Breschi, D. H. Pashley and F. R. Tay, *Biomaterials*, 2010, **31**, 6618-6627.
42. Y. Catel, V. Besse, A. Zulauf, D. Marchat, E. Pfund, T.-N. Pham, D. Bernache-Assolant, M. Degrange, T. Lequeux, P.-J. Madec and L. Le Pluart, *European Polymer Journal*, 2012, **48**, 318-330.
43. Y. Zhao, Q. Tu, J. Wang, Q. Huang and N. Huang, *Applied Surface Science*, 2010, **257**, 1596-1601.
44. US10390533 B2, 2019.
45. US 5429674, 1995.
46. US 9139715 B2, 2015.
47. R. Boissezon, J. Muller, V. Beaugeard, S. Monge and J.-J. Robin, *RSC Advances*, 2014, **4**, 35690-35707.
48. K. Chettab, J.-L. Mestas, M. Lafond, D. E. Saadna, C. Lafon and C. Dumontet, *Molecular Pharmaceutics*, 2017, **14**, 441-447.
49. A. M. Wagner, D. S. Spencer and N. A. Peppas, *Journal of Applied Polymer Science*, 2018, **135**, 46154.

50. Y. H. Bae and K. Park, *Journal of Controlled Release*, 2011, **153**, 198-205.
51. M. Khuphe, N. Ingram and P. D. Thornton, *Nanoscale*, 2018, **10**, 14201-14206.
52. M. Khuphe and P. D. Thornton, *Macromolecular Chemistry and Physics*, 2018, **219**, 1800352.
53. S. Manchun, C. R. Dass and P. Sriamornsak, *Life Sciences*, 2012, **90**, 381-387.
54. H. Yu, N. Ingram, J. V. Rowley, D. C. Green and P. D. Thornton, *Chemistry – A European Journal*, 2020, **26**, 13342-13358.
55. H. Yu, J. V. Rowley, D. C. Green and P. D. Thornton, *Materials Advances*, 2020, **1**, 1293-1300.
56. P. Wei, G. Gangapurwala, D. Pretzel, M. N. Leiske, L. Wang, S. Hoepfner, S. Schubert, J. C. Brendel and U. S. Schubert, *Biomacromolecules*, 2019, **20**, 130-140.
57. X. Yu, Y. Song, Y. Di, H. He, D. Fu and C. Jin, *Scientific Reports*, 2016, **6**, 31539.
58. Y. Wang, K. Zhou, G. Huang, C. Hensley, X. Huang, X. Ma, T. Zhao, B. D. Sumer, R. J. DeBerardinis and J. Gao, *Nature Materials*, 2014, **13**, 204-212.
59. L. Martínez-Jothar, S. Doukeridou, R. M. Schiffelers, J. Sastre Torano, S. Oliveira, C. F. van Nostrum and W. E. Hennink, *Journal of Controlled Release*, 2018, **282**, 101-109.
60. X. Gu, Y. Wei, Q. Fan, H. Sun, R. Cheng, Z. Zhong and C. Deng, *Journal of Controlled Release*, 2019, **301**, 110-118.
61. I. Ekladios, Y. L. Colson and M. W. Grinstaff, *Nature Reviews Drug Discovery*, 2019, **18**, 273-294.
62. A. C. Engler, X. Ke, S. Gao, J. M. W. Chan, D. J. Coady, R. J. Ono, R. Lubbers, A. Nelson, Y. Y. Yang and J. L. Hedrick, *Macromolecules*, 2015, **48**, 1673-1678.
63. K. Knop, R. Hoogenboom, D. Fischer and U. S. Schubert, *Angewandte Chemie International Edition*, 2010, **49**, 6288-6308.
64. S. Abbina and A. Parambath, in *Engineering of Biomaterials for Drug Delivery Systems*, ed. A. Parambath, Woodhead Publishing, 2018, ch. 14, pp. 363-376.
65. H. Bludau, A. E. Czapar, A. S. Pitek, S. Shukla, R. Jordan and N. F. Steinmetz, *European Polymer Journal*, 2017, **88**, 679-688.
66. M. Calderón, M. A. Quadir, S. K. Sharma and R. Haag, *Advanced Materials*, 2010, **22**, 190-218.
67. J. Wang, S. Yuan, Y. Zhang, W. Wu, Y. Hu and X. Jiang, *Biomaterials Science*, 2016, **4**, 1351-1360.
68. Y. Qi and A. Chilkoti, *Current Opinion in Chemical Biology*, 2015, **28**, 181-193.
69. N. Hadesfandiari and A. Parambath, in *Engineering of Biomaterials for Drug Delivery Systems*, ed. A. Parambath, Woodhead Publishing, 2018, ch. 13, pp. 345-361.
70. M. Khuphe and P. D. Thornton, in *Engineering of Biomaterials for Drug Delivery Systems*, ed. A. Parambath, Woodhead Publishing, 2018, ch. 7, pp. 199-228.
71. G. J. M. Habraken, A. Heise and P. D. Thornton, *Macromolecular Rapid Communications*, 2012, **33**, 272-286.
72. J. Huang, G. Habraken, F. Audouin and A. Heise, *Macromolecules*, 2010, **43**, 6050-6057.

73. B. A. Chan, S. Xuan, A. Li, J. M. Simpson, G. L. Sternhagen, T. Yu, O. A. Darvish, N. Jiang and D. Zhang, *Biopolymers*, 2018, **109**, e23070.
74. J. Ulbricht, R. Jordan and R. Luxenhofer, *Biomaterials*, 2014, **35**, 4848-4861.
75. S. M. Miller, R. J. Simon, S. Ng, R. N. Zuckermann, J. M. Kerr and W. H. Moos, *Drug Development Research*, 1995, **35**, 20-32.
76. S. M. Miller, R. J. Simon, S. Ng, R. N. Zuckermann, J. M. Kerr and W. H. Moos, *Bioorganic & Medicinal Chemistry Letters*, 1994, **4**, 2657-2662.
77. H. Yu, N. Ingram, J. V. Rowley, S. Parkinson, D. C. Green, N. J. Warren and P. D. Thornton, *Journal of Materials Chemistry B*, 2019, **7**, 4217-4223.
78. Y. Hu, Y. Hou, H. Wang and H. Lu, *Bioconjugate Chemistry*, 2018, **29**, 2232-2238.
79. D. Skoulas, V. Stuetgen, R. Gaul, S.-A. Cryan, D. J. Brayden and A. Heise, *Biomacromolecules*, 2020, **21**, 2455-2462.
80. A. Urtti, *Advanced Drug Delivery Reviews*, 2006, **58**, 1131-1135.
81. B. C. Tang, J. Fu, D. N. Watkins and J. Hanes, *Biomaterials*, 2010, **31**, 339-344.
82. K. J. Whaley, J. Hanes, R. Shattock, R. A. Cone and D. R. Friend, *Antiviral Research*, 2010, **88**, S55-S66.
83. H. M. Abdelaziz, M. Gaber, M. M. Abd-Elwakil, M. T. Mabrouk, M. M. Elgohary, N. M. Kamel, D. M. Kabary, M. S. Freag, M. W. Samaha, S. M. Mortada, K. A. Elkhodairy, J.-Y. Fang and A. O. Elzoghby, *Journal of Controlled Release*, 2018, **269**, 374-392.
84. M. Ghadiri, P. M. Young and D. Traini, *Pharmaceutics*, 2019, **11**, 113.
85. Š. Gradišar, E. Žagar and D. Pahovnik, *ACS Macro Letters*, 2017, **6**, 637-640.
86. P. Sannigrahi and E. Ingall, *Geochem Trans*, 2005, **6**, 52-52.
87. J. Köhler, H. Keul and M. Möller, *Chemical Communications*, 2011, **47**, 8148-8150.
88. M. Jimenez, N. Lesaffre, S. Bellayer, R. Dupretz, M. Vandenbossche, S. Duquesne and S. Bourbigot, *RSC Advances*, 2015, **5**, 63853-63865.
89. G. Socrates, *Infrared and Raman Characteristic Group Frequencies*, Wiley, Chichester, U.K., 3rd edn., 2001.

## Chapter 4

### Carbon nanodot-containing polymer-calcium carbonate nanocomposite as a theranostic doxorubicin delivery vehicle

#### Preamble

This Chapter is based on work published as: J. V. Rowley, P. A. Wall, H. Yu, M. J. Howard, D. L. Baker, A. Kulak, D. C. Green and P. D. Thornton, "Triggered and monitored drug release from bifunctional hybrid nanocomposites", *Polymer Chemistry*, 2022, **13** (1), 100-108.

#### Abstract

Carbon nanodot-containing calcium carbonate nanoparticles were coated with poly(amino acid)s, and the resulting nanocomposites capable of encapsulating a chemotherapeutic drug and displaying afterglow. The poly(amino acid) component enhanced nanoparticle dispersion in aqueous solution, and can be designed to be acid-cleavable to enable the chemotherapeutic, doxorubicin, to be released by the incorporation of an ester link within the polymer chain. The composited carbon nanodots offer fluorescence and brief afterglow to the nanocomposites at physiological pH, but the afterglow is lost when encountering acidic solutions (pH 5). The loss of drug molecules, and fluorescence and phosphorescence provided by the carbon nanodots, in acidic environments ensures the reported materials show promise as early-stage candidates as theranostic devices to acidic environments such as tumours.

## 4.1 Introduction

### 4.1.1 Drug-delivery vehicles

Tumours present a more acidic environment than normal tissue and utilisation of this property by drug delivery vehicles presents an attractive method of targeting tumours and reducing side-effects associated with chemotherapy (Section 1.4.1).<sup>1</sup> Poly(amino acid)s (PAAs) are particularly well suited for use as drug delivery vehicles because of their tailorable functionality and excellent biocompatibility, as discussed in Section 1.2.1.<sup>2</sup> When synthesised via NCA ROP, PAAs of narrow dispersity are produced, whilst polymer degradation results in the reformation of non-toxic amino acids and the absence of toxic side-products, essential for use *in vivo*.<sup>3-5</sup> Amphiphilic diblock PAAs, where one block is a hydrophobic PAA and the other block is a hydrophilic PAA, may be synthesised via NCA ROP and self-assemble to form micelles.<sup>6</sup> PAA-based NPs may be stimuli-responsive for controlled payload release, such as those examples described in Section 1.2.3.3.

Polymer-coated inorganic NPs are a class of nanocomposite that have the potential to be used for the encapsulation, and subsequent controlled release of, guest molecules.<sup>7</sup> As discussed in Section 1.4.1.3, NCA ROP can be initiated from an inorganic material ('grafted-from'), or a PAA can self-assemble around, or bind to, an inorganic material ('grafting-to'). Therapeutic-loaded nanocomposites have great potential as drug delivery vehicles whereby the polymeric shell enhances NP biodistribution and biocompatibility, and prevents premature drug metabolism.<sup>8</sup> A stimuli-responsive polymeric shell may act as an actuator for controlled and targeted drug release in response to a target stimulus, such as those stimuli described in Section 1.4. Such controlled release enables reduced drug dosage, which consequently mitigates side-effects caused by interactions between non-target cells and the therapeutic molecule.<sup>9</sup> Polymer-coated inorganic NPs that possess a stimuli-responsive, degradable, and non-cytotoxic polymeric shell are therefore highly desirable as potential drug delivery vehicles.

### 4.1.2 Theranostics

Drug delivery is often the primary function of stimuli-responsive materials, but the ability to track and trace their distribution and function *in vivo* is also desirable. The convergence of diagnostics and therapy in clinical science is called 'theranostics'.<sup>10</sup> Fluorescent moieties and NPs are currently used for bioimaging, as they report immediately and can be detected precisely using inexpensive and commonly available microscopic and spectroscopic methods.<sup>11</sup>

Quantum dots (QDs) are nano-scale semiconducting particles which provide stable, sharp and bright fluorescence. They have uses in light-emitting devices,<sup>12</sup> solar cells<sup>13</sup> and for fluorescent labelling.<sup>14</sup> Unfortunately, however, QDs are inherently cytotoxic due to the presence of heavy metals, therefore for any biological application, the QDs must be encapsulated or modified in such a way as to inhibit their cytotoxicity.<sup>15</sup> On the contrary, fluorescent carbon nanodots (CNDs) express biocompatibility, low toxicity, chemical stability, good photoluminescence, and ease of synthesis.<sup>16</sup> Consequentially, CNDs are used for a wide-range of applications including bioimaging,<sup>17</sup> drug delivery,<sup>18</sup> light-emitting devices<sup>19</sup> and as photocatalysts.<sup>20-21</sup>

Certain CNDs may be composited with a polymer such as poly(vinyl alcohol),<sup>22</sup> polyurethane,<sup>23</sup> or an inorganic host material.<sup>24</sup> Once suspended within some of these host materials, CNDs display bimodal fluorescence and persistent afterglow which is visible after the removal of the stimulation source, even at room temperature. In bioimaging, the ability to image with the excitation laser switched off helps to eliminate noise due to short-lived autofluorescence common to biomolecules and live cells;<sup>25-26</sup> and thus in theory, time-resolved afterglow imaging provides access to more sensitive imaging and detection methods.<sup>27</sup> Recently, Zhou *et al.* demonstrated fast, convenient and low cost phosphorescent NPs for afterglow bioimaging in both living cells and in zebrafish larvae.<sup>28</sup> Figure 4.1a shows the zebrafish larvae under a bright light and a UV light, and when the UV source is removed afterglow is observed and fades over time, providing bioimaging with a high signal-to-noise ratio and sensitivity. Moreover, afterglow

imaging may be conducted *ex vivo*, for example recent work by Yuan and colleagues were able to detect very low levels of phosphorescent porphyrin in blood samples (<0.246 ppm) by amplifying the afterglow signal with an afterglow reporter molecule (Figure 4.1b).<sup>29</sup>

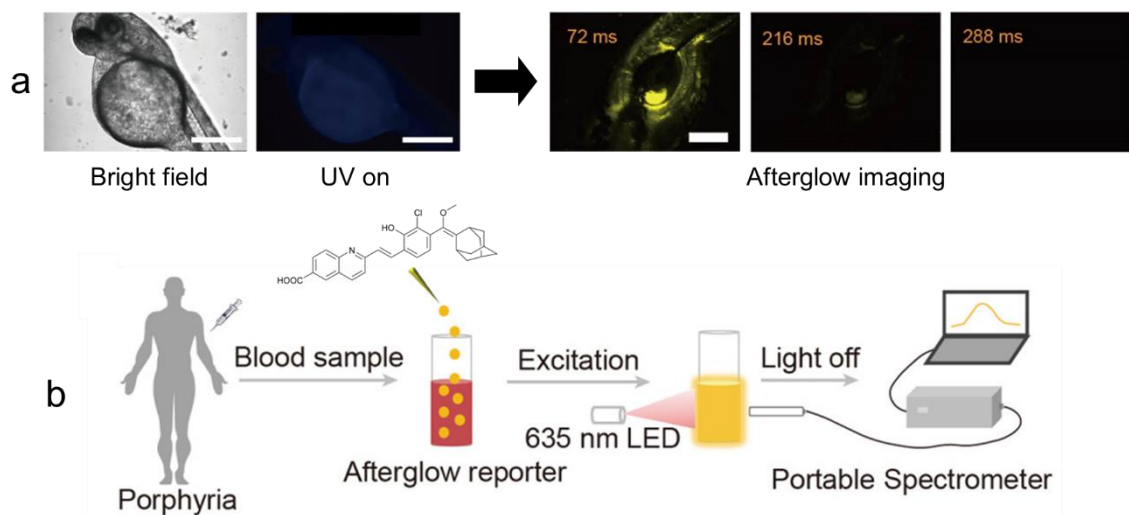
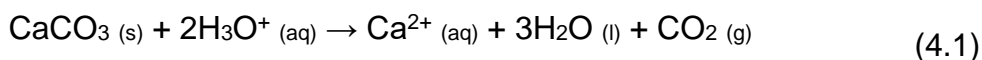


**Figure 4.1** (a) Images of zebrafish larvae under bright field light and under UV, followed by time-resolved afterglow imaging after 72, 216 and 288 ms. Reprinted (adapted) with permission from ref. 28. (b) Illustration of porphyrin detection with afterglow reported in whole blood. Reprinted (adapted) with permission from ref. 29. Both (a) and (b) are copyright 2021 American Chemical Society.

The targeted delivery of chemotherapeutics is an effective treatment for cancerous tumours as it reduces side-effects from the interaction of a drug molecule with healthy tissue. When the ability of this tumour-targeting action is visualised in real time using readily-available bioimaging, clinicians can monitor treatment progress and change their treatment strategy accordingly. CNs display afterglow when composited within a host material, so are well suited for reporting the degradation of their afterglow-activating host since their release into the external environment eliminates their afterglow behaviour. Tumours present an acidic environment, so if the host material for CNs were degraded by the acidic pH, the loss of afterglow would be indicative of the material interacting with tumour cells.

### 4.1.3 Calcium carbonate

Calcium carbonate, CaCO<sub>3</sub>, is a mineral found in abundance in nature and is an attractive inorganic biomaterial thanks to its biocompatibility. CaCO<sub>3</sub> mainly exists in three polymorphs (crystal structures): calcite, aragonite and vaterite, where calcite is the more thermodynamically stable<sup>30</sup> but vaterite is the most common in nature.<sup>31</sup> As it is found in nature and even in drinking water (it is the main component of lime scale<sup>32</sup>), CaCO<sub>3</sub> is environmentally benign and safe for use *in vivo*, relatively cheap to purchase, and easy to handle. As such, CaCO<sub>3</sub> has found use in biomaterials due to its sensitivity to acidic environments. When CaCO<sub>3</sub> is in an acidic environment it degrades into Ca<sup>2+</sup>, water and CO<sub>2</sub> gas (Equation (4.1)). This CO<sub>2</sub> gas can be clearly seen on ultrasound imaging. For example, recently Keum *et al.*<sup>31</sup> used this useful property of CaCO<sub>3</sub> to coat stents with CaCO<sub>3</sub>. Normal stents just use mechanical strength to keep the blood vessel open, but when coated in CaCO<sub>3</sub>, CO<sub>2</sub> gas was released. The CO<sub>2</sub> gas dissolves fat (plaques) thus clearing the blockage of fat. They could also watch the evolution of CO<sub>2</sub> live using ultrasound imaging.



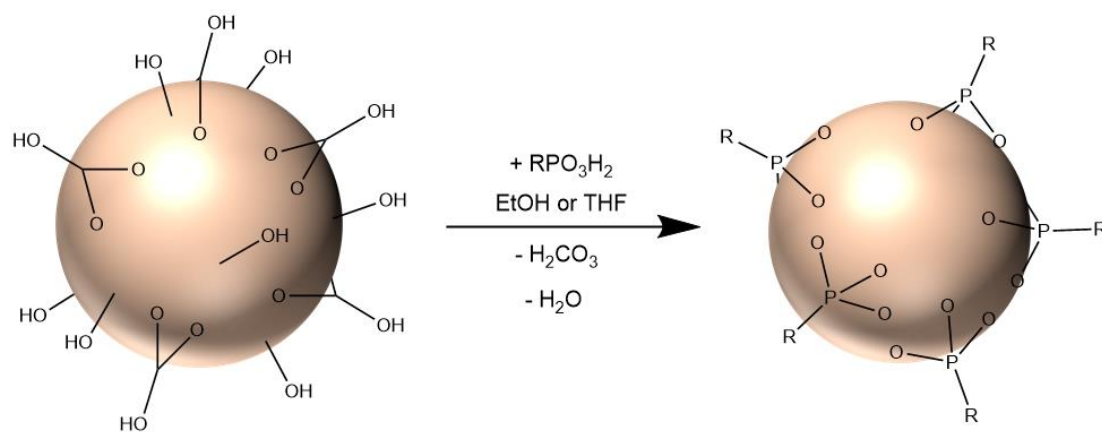
#### 4.1.3.1 CND/CaNP NPs

Recently, persistent afterglow from CNDs was achieved when they were incorporated into CaCO<sub>3</sub> NPs (CaNP), where the dense internal environment of the inorganic crystal promoted long-lifetime afterglow.<sup>24</sup> CaNPs with CNDs incorporated within (CND/CaNPs) may thus be utilised in bioimaging, however, bare CaNPs typically aggregate and recrystallise in aqueous solution and therefore require stabilisation.<sup>33</sup>

#### 4.1.3.2 Surface modification of CaNPs

Surface functionalisation of CaNPs with fatty acids,<sup>34</sup> an organotitanate coupling agent<sup>35</sup> or organosilanes<sup>36</sup> have been shown to increase the compatibility and stability of CaNP dispersions in non-aqueous media. In contrast, there are only a few examples of enhanced stability of CaNP suspensions in aqueous media. Dong *et al.* developed a stable PEG-modified CaNP nanocomposite loaded with Dox and a photosensitiser, where payload release was triggered by reduced solution pH and *in situ* monitoring was enabled by magnetic resonance imaging (MRI).<sup>37</sup> Although the material shows great promise as a theranostic agent, PEG is associated with the production of anti-PEG antibodies and accelerated blood clearance (Section 3.1.3).<sup>38</sup> Additionally, MRI is a resource-intensive technique for *in situ* monitoring of drugs, therefore alternative materials are sought to improve the compatibility of CaNPs with aqueous media and providing a means for tracking the NP *in vivo*.

Phosphonic acids can be used to modify the surface of metal oxides, such as silica nanoparticles in water,<sup>39</sup> via a P-O-M bond. Phosphonic acids have also been used with CaCO<sub>3</sub><sup>40</sup> but the surface functionalisation in terms of degree of grafting was little known until in 2012, El Malti *et al.* grafted phosphonate onto the surface of calcite particles where they observed a dense phosphonate monolayer on the surface of the calcite particle (Scheme 4.1).<sup>41</sup> Since then, more studies have been carried out on the surface modification of CaCO<sub>3</sub> using phosphonic acids<sup>42-44</sup> but more work is still required.



**Scheme 4.1** Representative scheme of the surface modification of calcite particles.<sup>41</sup>

#### 4.1.4 Summary

This Chapter describes the grafting of PAAs to CND/CaNPs which exhibit both fluorescence and afterglow. The resulting nanocomposite comprises a polymer shell which aids their dispersion in water, and provides the mechanism through which drug molecule entrapment and release is achieved. PAA coatings were achieved by both direct polymer growth from a functionalised CND/CaNP surface (grafting-from), and grafting pre-formed PAAs to CND/CaNPs through non-covalent interactions (grafting-to). The latter enabled straightforward polymer characterisation, and in both cases polymers that contained ester linking groups were grafted onto CND/CaNPs, rendering the polymer shell susceptible to acid-catalysed hydrolysis. Finally, the potential application of the nanocomposites as theranostic devices was initially assessed by observing the pH-controlled retention and release of the chemotherapeutic drug Dox, and the pH-responsive afterglow behaviour investigated.

## 4.2 Experimental Details

### 4.2.1 CND/CaNP synthesis and surface-functionalisation with ABPA or HUPA

CND/CaNPs were synthesised via the carbonation method as reported previously.<sup>24</sup> Briefly, CNDs were synthesised by suspending folic acid in DI water and adding NaOH until dissolution occurred. The folic acid solution was heated to 200 °C in a hydrothermal bomb for twelve hours to yield a stock solution of folic acid-derived CNDs. A UV-vis spectrum was obtained showing two plateaus at 258 nm and 323 nm (Figure 4.2a), and an FTIR spectrum of lyophilised CNDs was also obtained: 3250 cm<sup>-1</sup> (bm, OH and NH), 1659 cm<sup>-1</sup> (m, C=O) and 1579 cm<sup>-1</sup> (s, NH) (Figure 4.2b). Separately, CaCO<sub>3</sub> was heated in a furnace at 900 °C for 16 h to decompose to CaO. The CaO (0.44 g) was added to degassed and distilled DI water (50 mL) with vigorous stirring for 16 h to produce Ca(OH)<sub>2</sub>. N<sub>2</sub> and CO<sub>2</sub> (3:1 v/v) were bubbled through the stirring Ca(OH)<sub>2</sub> suspension at a rate of 1 L min<sup>-1</sup> whilst an aliquot of the CND stock solution (2 mL) was added to the mixture. The gas flow was continued until the pH reached 7 when the CND/CaNPs were collected by centrifugation (8,000 r.p.m., 10 min), washed with ethanol and dried.

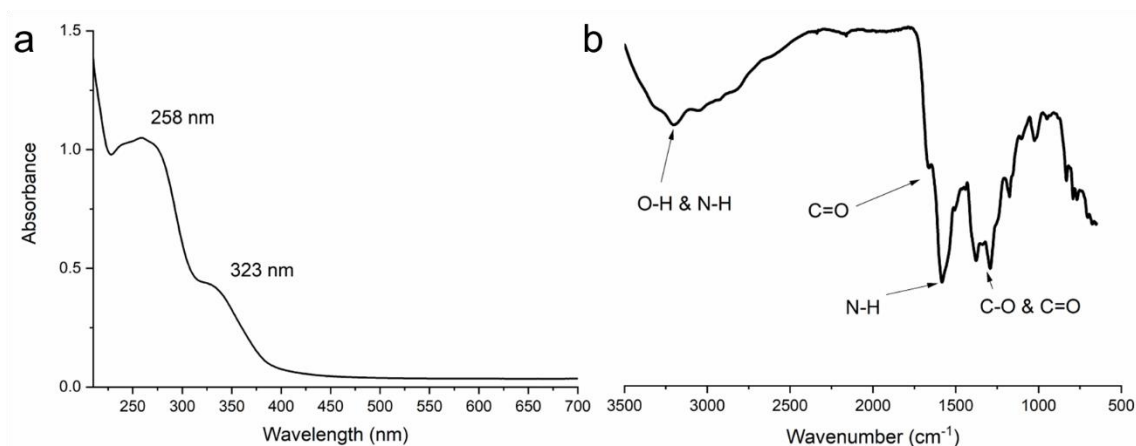


**Figure 4.2** UV-vis (a) and FTIR spectra (b) of CNDs.

CND/CaNPs (5 mg) and 4-aminobutylphosphonic acid (ABPA) (5 mg, 0.03 mmol) or 11-hydroxyundecylphosphonic acid (HUPA) (5 mg, 0.20 mmol) were weighed into a glass vial and suspended in DI water (5 mL) with the aid of an ultrasonic bath. The ABPA- or HUPA-functionalised CND/CaNPs were collected by centrifugation, washed with DI water and ethanol, and dried in an oven at 50 °C.

## 4.2.2 Nanocomposite syntheses

### 4.2.2.1 Synthesis of CND/CaNP-ABPA-PPhe<sub>4</sub>-*b*-PSar<sub>16</sub> and CND/CaNP-ABPA-PBLG<sub>18</sub>-*b*-PSar<sub>16</sub>: the grafting-from approach

As a representative example, ABPA-functionalised CND/CaNPs (0.26 g CND/CaNPs and 0.06 g, 0.4 mmol, 1 eq. ABPA) were suspended in anhydrous DMF (20 mL) and added to an oven-dried, N<sub>2</sub>-flushed Schlenk tube. The NCA (L-phenylalanine (Phe)-NCA: 0.37 g, 2.0 mmol, 5 eq. or  $\gamma$ -benzyl-L-glutamate (BLG)-NCA: 1.77 g, 6.7 mmol, 23 eq., from Sections 2.3.1.2 and 2.3.1.3, respectively) were dissolved in anhydrous DMF (20 mL) and also added to the Schlenk tube. The polymerisation was stirred at room temperature with a flow of N<sub>2</sub> until FTIR spectroscopy determined that all NCA had reacted due to the absence of peaks corresponding to the anhydride group of the NCA monomer (typically five days). Sarcosine (Sar)-NCA (from Section 2.3.1.1) was then dissolved in anhydrous DMF (10 mL), added to the Schlenk tube and stirred at room temperature with a flow of N<sub>2</sub>. Once FTIR spectroscopy determined that all NCA had reacted (also typically five days), the reaction mixture was reduced to dryness and the resulting solid washed three times in chloroform (centrifugation for 30 minutes at 4,500 r.p.m.). The nanocomposites were collected and dried in a vacuum oven at 45 °C.

### 4.2.2.2 Synthesis of CND/CaNP-HUPA-PSar<sub>32</sub>: the grafting-from approach

The NCA ROP initiated from a hydroxyl group was carried out as reported previously, with modifications,<sup>45</sup> and similarly to that reported in Chapter 3. HUPA-functionalised CND/CaNPs (0.02 g CND/CaNPs and 0.02 g, 0.08 mmol, 1 eq. HUPA) were suspended in anhydrous DMF (25 mL) in a Schlenk tube. The milky-white coloured solution was stirred under N<sub>2</sub> before Sar-NCA (0.44 g, 3.81 mmol, 48 eq.) was added. Methanesulfonic acid in anhydrous DMF solution (0.02 mg mL<sup>-1</sup>, 1 mL) was added to the Schlenk tube and the reaction stirred under N<sub>2</sub> at 40 °C for 24 h. After initiation, the polymerisation underwent propagation by cooling to 0 °C before *N*-ethyl-diisopropylamine in anhydrous DMF (12.5 mg mL<sup>-1</sup>, 2 mL) was added. After stirring at 0 °C with a flow of N<sub>2</sub> for six days, the polymerisation reaction was finished as FTIR spectroscopy determined that Sar-NCA was no longer present. The nanocomposite was collected by vacuum, washed three times in chloroform (centrifugation for 30 minutes each time at 4,500 r.p.m.) and dried in a vacuum oven at 45 °C.

#### **4.2.2.3 Synthesis of CND/CaNP-HUPA-PSar<sub>17</sub> and CND/CaNP-HUPA-PSar<sub>23</sub>: the grafting-to approach**

Into a sample vial, the HUPA-PSar polymer (Section 3.2.1, 150 mg) and CND/CaNPs (50 mg) were weighed and suspended in DI water (10 mL) with the aid of an ultrasonic bath for one hour. The nanocomposites were collected by centrifugation (4,500 r.p.m., 30 mins.), washed with DI water three times, washed with ethanol three times, washed with chloroform three times, and dried in a vacuum oven at 45 °C.

### **4.2.3 Synthesis of polymers for comparison, DLS, and for the grafting-to approach**

#### **4.2.3.1 Synthesis of ABPA-PPhe<sub>8</sub>-*b*-PSar<sub>105</sub> and ABPA-PBLG<sub>22</sub>-*b*-PSar<sub>63</sub>**

ABPA-PPhe<sub>8</sub>-*b*-PSar<sub>105</sub>: briefly, ABPA (10 mg, 0.07 mmol, 1 eq.) and Phe-NCA (25 mg, 0.13 mmol, 2 eq.) were dissolved in anhydrous DMF (20 mL) and stirred at room temperature with a flow of N<sub>2</sub> until FTIR analysis determined there was no more Phe-NCA remaining. Sar-NCA (455 mg, 3.96 mmol, 57 eq.) was dissolved in anhydrous DMF (7 mL) and added to the reaction mixture with stirring and a flow of N<sub>2</sub> at room temperature. Once all of the Sar-NCA had been exhausted, as determined by FTIR analysis, the amphiphilic block copolymer was precipitated and washed in ice-cold diethyl ether (200 mL), collected by centrifuge (4,500 r.p.m., 15 mins.), dialysed against DI water (2,000 Da MWCO) and lyophilised (yield 62%). ABPA-PBLG<sub>22</sub>-*b*-PSar<sub>63</sub> was synthesised in a similar way: briefly, ABPA (10.6 mg, 0.07 mmol, 1 eq.) was dissolved in anhydrous DMF (20 mL) and BLG-NCA (0.45 g, 1.72 mmol, 25 eq.) in anhydrous DMF (10 mL) added. After ten days, Sar-NCA (0.80 g, 6.93 mmol, 99 eq.) in anhydrous DMF (10 mL) was added to the reaction mixture. After eleven days the polymer was precipitated in diethyl ether, collected by centrifuge, dialysed and lyophilised (yield 64%).

#### 4.2.3.2 Synthesis of HUPA-PSar polymers HUPA-PSar<sub>93</sub>, HUPA-PSar<sub>17</sub> and HUPA-PSar<sub>23</sub>

HUPA-PSar<sub>95</sub>: into a N<sub>2</sub>-flushed, oven-dried Schlenk tube, Sar-NCA (0.47 g, 4.07 mmol, 102 eq.) was dissolved in anhydrous chloroform (10 mL) with stirring. Methanesulfonic acid (0.01 g, 0.12 mmol, 3 eq.) was added together with HUPA (0.01 g, 0.04 mmol, 1 eq.) and the reaction mixture stirred with a flow of N<sub>2</sub> at 40 °C for 24 h. Propagation was then started by cooling the reaction mixture to 0 °C and adding *N*-ethyl-diisopropylamine (0.27 g, 2.09 mmol, 52 eq.). After being stirred at 0 °C with a flow of N<sub>2</sub> for four days the polymerisation reaction was complete as determined by FTIR spectroscopy. The polymer was precipitated by adding dropwise into ice-cold diethyl ether (1:5 v/v), collected by centrifuge, dialysed and lyophilised (yield 84%). HUPA-PSar<sub>17</sub> and HUPA-PSar<sub>23</sub> were synthesised in the same manner as HUPA-PSar<sub>95</sub> above.

#### 4.2.3.3 Synthesis of CaNP-ABPA-PBLG<sub>18</sub>-*b*-PSar<sub>16</sub> with no CNDs, and DLS analysis of such

CaNPs were synthesised as above (Section 4.2.1) but without the CND solution being added. The CaNPs were collected by centrifugation, washed and dried. FTIR  $\nu_{\max}$  (solid): 1396  $\text{cm}^{-1}$  (s), 872  $\text{cm}^{-1}$  (s) and 712  $\text{cm}^{-1}$  (m). Surface-functionalisation and polymer grafting of these CaNPs was conducted in the same manner as that described for the nanocomposite including CNDs (Section 4.2.2.1). CaNP-ABPA was synthesised by suspending CaNPs (5 mg) and ABPA (5 mg) in DI water with the aid of an ultrasonic bath. These were then washed and dried. CaNP-ABPA-PBLG<sub>18</sub>-*b*-PSar<sub>16</sub> was synthesised by suspending ABPA-functionalised CaNPs in anhydrous DMF and adding BLG-NCA in anhydrous DMF. After seven days FTIR spectroscopy determined there was no more monomer remaining, so Sar-NCA was added in anhydrous DMF. After a further seven days Sar-NCA had been consumed too and the nanocomposite collected *in vacuo*, washed and dried. FTIR  $\nu_{\max}$  (solid): 3301  $\text{cm}^{-1}$  (w, N-H), 2934  $\text{cm}^{-1}$  (w, C-H), 1646  $\text{cm}^{-1}$  (m, amide) and 1415  $\text{cm}^{-1}$  (m, calcite).

For DLS analysis, the samples were added to a volume of PBS buffer solution at pH 7.4 to form a 0.1  $\text{mg mL}^{-1}$  suspension. Samples were suspended by placing in an ultrasonic bath for 15 minutes prior to analysis. DLS analyses were conducted in triplicate. The CaNP-polymer nanocomposite suspension was retained and re-suspended and analysed four days later by DLS.

#### 4.2.4 Dox release study

To load the nanocomposites (3 mg) with Dox, the nanocomposites were firstly added to DMF (1 mL). PBS buffer solution at pH 7.4 (10 mL) was stirred vigorously whilst the nanocomposite in DMF solution was added dropwise simultaneously with the Dox free base in chloroform solution (Section 2.3.4.1). The mixture was stirred vigorously overnight in the dark for the chloroform to evaporate, and the Dox-loaded nanocomposites transferred to dialysis tubing

(2,000 Da MWCO) and dialysed in the dark against PBS buffer solution at pH 7.4 at 37 °C until the excess Dox was removed. The concentration of Dox in the solution outside the dialysis tubing was quantified by HPLC against a calibration curve of known concentrations (Section 2.3.4.3). Dox loading efficiency was calculated from Equation (2.6).

After dialysis, the solutions inside the dialysis tubing were split in two, with half dialysed against fresh PBS buffer solution at pH 7.4, and the other half dialysed against acetate buffer solution at pH 5, both at 37 °C in the dark. Aliquots were taken at various time intervals and analysed by HPLC for cumulative Dox release quantification. The buffer solutions outside the dialysis tubing were replaced with fresh buffer solutions after each analysis by HPLC.

#### **4.2.5 Afterglow lifetime analysis (stroboscopy)**

Afterglow lifetimes were estimated using a stroboscopic method. Videos of afterglow were obtained with a Canon EOS 7D SLR camera in video mode (25 fps) with a Canon ER 100 mm f/2.8 Macro USM lens. Whilst being recorded, the samples were irradiated with UV light at 365 nm, and the UV lamp switched off after a few seconds. The video recording continued for a few seconds after the UV lamp was switched off in order to capture afterglow. Individual frames of the video were obtained using VirtualDub software, and the frames analysed in ImageJ software. Afterglow lifetimes were obtained by plotting the mean grey values against time with a 0.04 s interval.

## 4.3 Results and Discussion

### 4.3.1 CND/CaNP synthesis and functionalisation

CND-loaded CaNPs (CND/CaNPs) were produced using a carbonation method to near-complete yields. Raman microscopy and pXRD confirmed that the CND/CaNPs produced were of the calcite polymorph of  $\text{CaCO}_3$  (Figure 4.3a-b). Near-spherical NPs were synthesised with average diameters of  $54 \pm 14$  nm as determined by SEM analysis (Figure 4.3c, averaged over 126 particles), and which was in suitable agreement with the value obtained from analysing the pXRD pattern with the Scherrer equation ( $62 \pm 8$  nm, Equation ((4.2)).<sup>46</sup> The CND/CaNPs displayed bright blue fluorescence under UV radiation (365 nm) and a green afterglow visible for  $\sim 1$  s ( $\tau = \sim 0.25$  s) after the excitation source was removed (Figure 4.3d).

$$Particle\ size\ (nm) = \frac{K\lambda}{\beta \cos \theta} \quad (4.2)$$

ABPA and HUPA were used to prepare CND/CaNP surfaces for modification by NCA ROP.<sup>41</sup> Both molecules feature phosphonic acid groups which interact with the CaNP, whilst the amine or hydroxyl groups act as an initiator for subsequent ROP (Scheme 4.2). Following functionalisation, the CND/CaNPs were washed with water and ethanol to remove excess ABPA or HUPA. FTIR analysis confirmed successful functionalisation of the CND/CaNPs; the distinctive bands of calcite were found at  $1397\text{ cm}^{-1}$ ,  $871\text{ cm}^{-1}$  and  $713\text{ cm}^{-1}$ , in the spectra of ABPA- and HUPA-functionalised CND/CaNPs (Figure 4.4a). Additionally, HUPA-functionalised CND/CaNPs possess C-H stretching peaks at  $2924\text{ cm}^{-1}$  and  $2850\text{ cm}^{-1}$  corresponding with the eleven  $\text{CH}_2$  groups of HUPA. SEM analysis of the surface-functionalised CND/CaNPs showed that their morphology and dimensions are not altered by surface-functionalisation (Figure 4.4b).

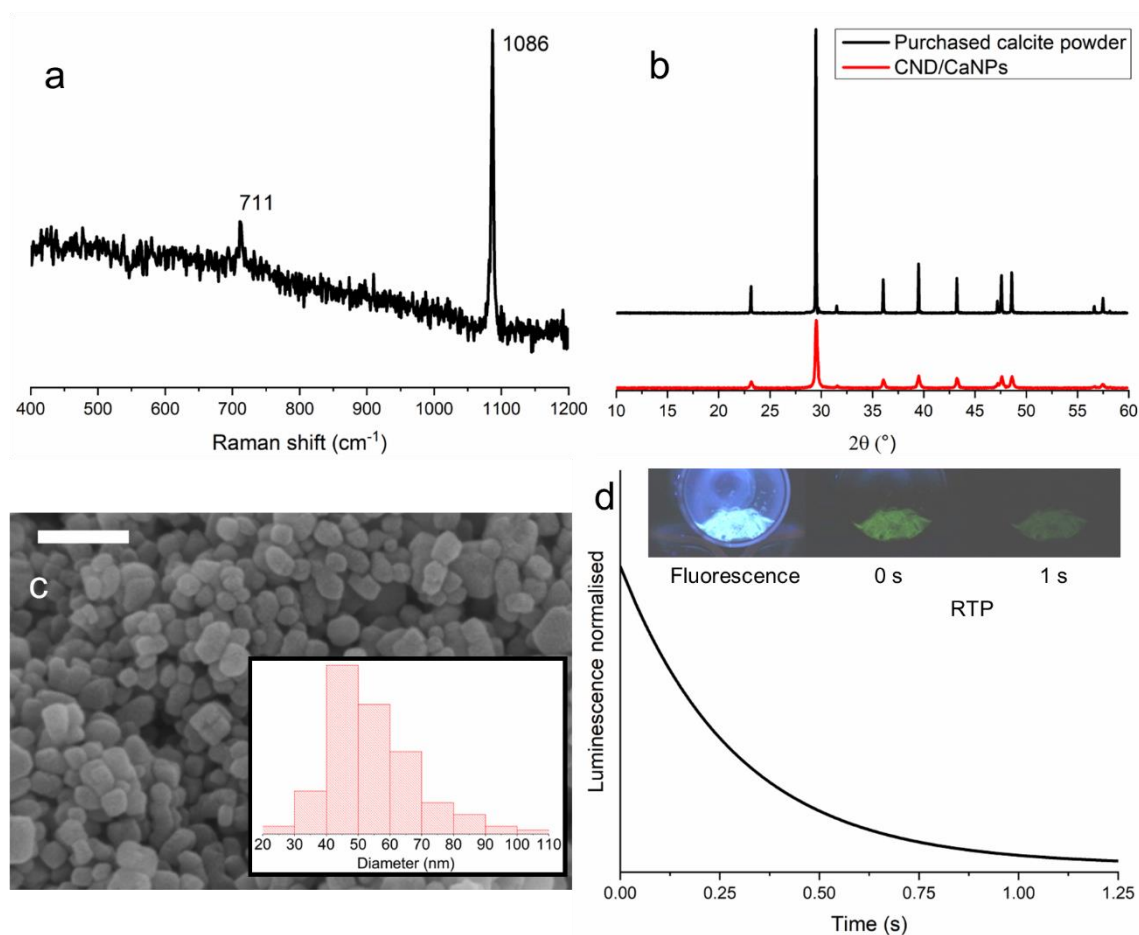
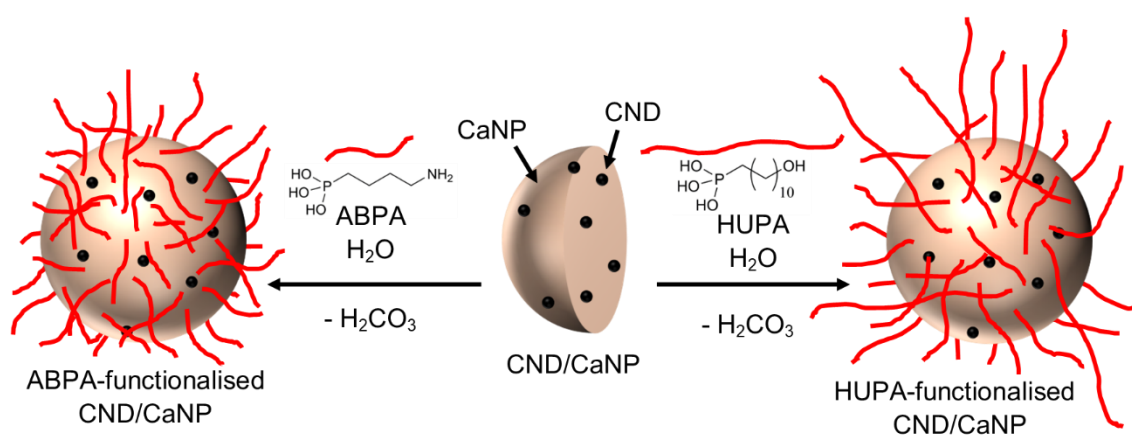


**Figure 4.3** Raman spectrum (a), pXRD pattern (b), SEM micrograph (c, inset: particle diameter distribution from this micrograph calculated from 126 particles), and normalised afterglow lifetime of CND/CaNPs (d, inset: photos of blue fluorescence and green afterglow after irradiating at 365 nm).



**Scheme 4.2** Surface-functionalising CND/CaNPs with ABPA or HUPA.

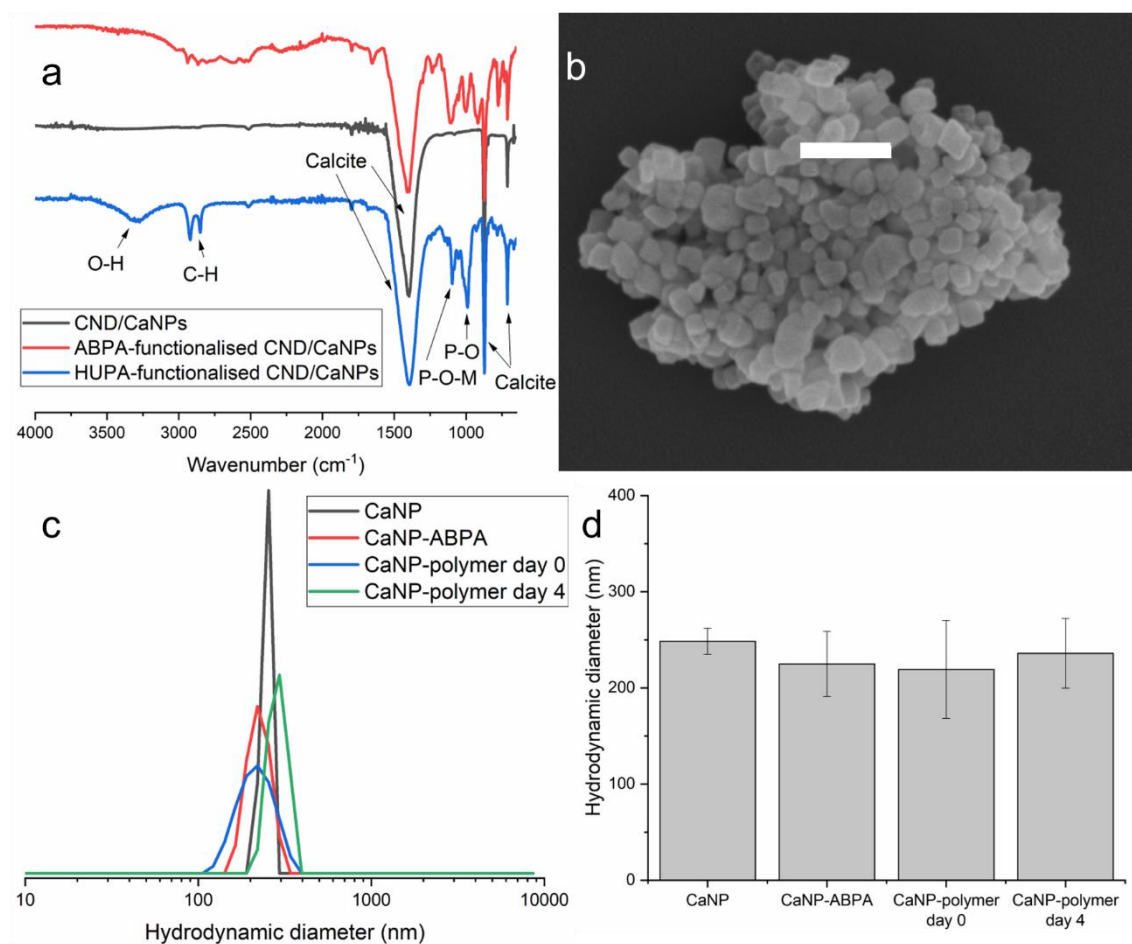


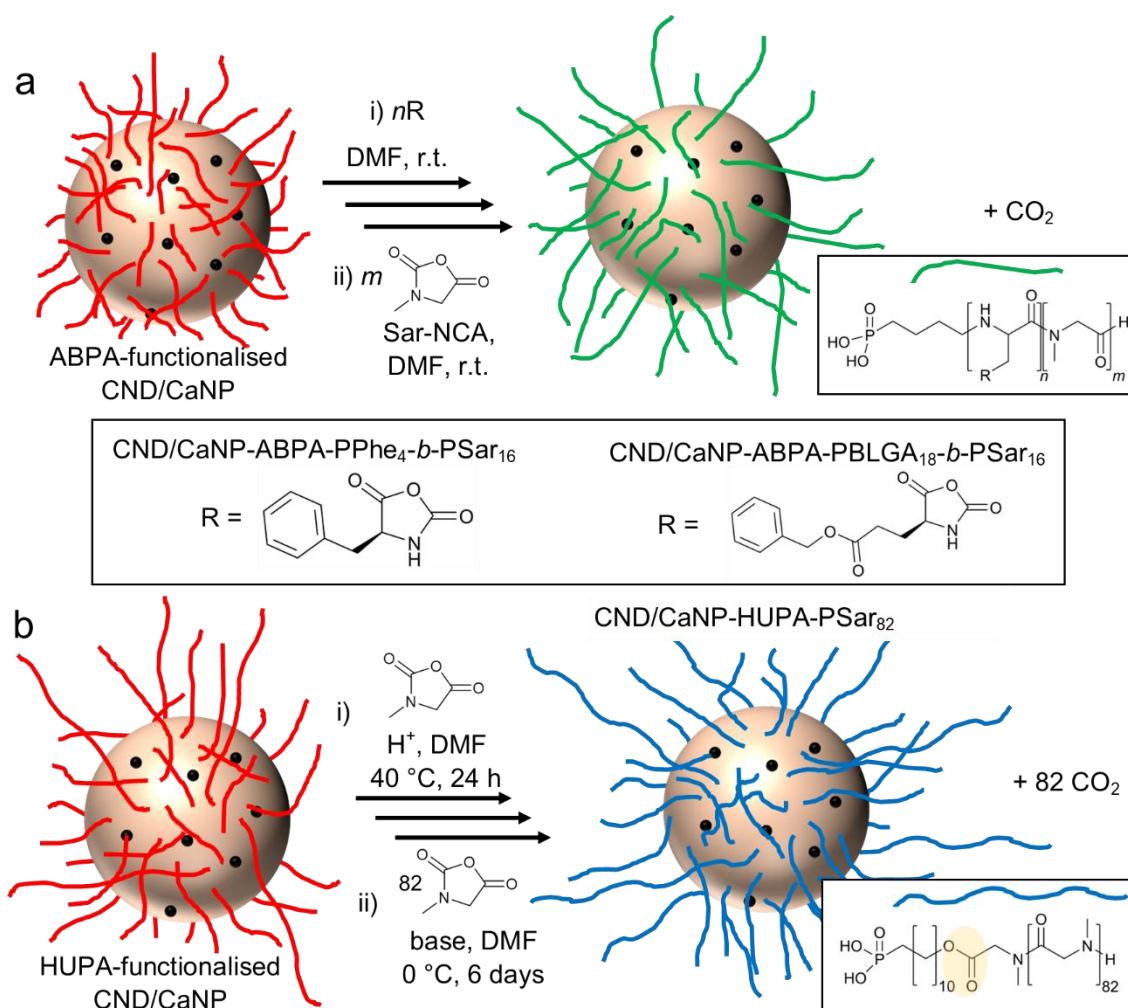
**Figure 4.4** (a) FTIR spectra of CND/CaNPs and ABPA- or HUPA-functionalised CND/CaNPs, and (b) an SEM micrograph of ABPA-functionalised CND/CaNPs (scale bar is 200 nm). (c) Particle size distribution of CaNPs, ABPA-functionalised CaNPs and a CaNP-polymer nanocomposite on day zero and after four days, and (d) bar graph comparing the same.

DLS analysis is frequently utilised to measure the size distribution profile of NPs in solution using the collective scattered light intensity fluctuations by all particles over time.<sup>47</sup> Fluorescence, however, causes interference and noise, therefore DLS is generally not considered an appropriate sizing technique for fluorescent samples, such as CND/CaNPs.<sup>48</sup> Nonetheless, the size of non-functionalised and functionalised NPs in suspension was assessed using CaNPs which were not composited with CNDs, and thus did not fluoresce. Non-functionalised and ABPA-functionalised CaNPs possess hydrodynamic diameters of  $248.4 \pm 13.65$  nm and  $224.9 \pm 33.86$  nm, respectively, in PBS buffer solution at pH 7.4 (Figure 4.4c). Figure 4.4d shows that the hydrodynamic diameter of the CaNP does not change once functionalised with ABPA.

### 4.3.2 CND/CaNP-PAA nanocomposite synthesis

#### 4.3.2.1 Nanocomposite synthesis via the 'grafting-from' approach

Initially, amphiphilic block copolymers consisting of hydrophobic PPhe or PBLG and hydrophilic PSar (CND/CaNP-ABPA-PPhe<sub>4</sub>-*b*-PSar<sub>16</sub> and CND/CaNP-ABPA-PBLG<sub>18</sub>-*b*-PSar<sub>16</sub>) were synthesised via simple, catalyst-free, sequential NCA ROP from ABPA-functionalised CND/CaNPs (grafting-from approach, Scheme 4.3a, Section 1.4.1.3).



**Scheme 4.3** Grafting-from approach to yield nanocomposites CND/CaNP-ABPA-PPhe<sub>4</sub>-*b*-PSar<sub>16</sub> and CND/CaNP-ABPA-PBLG<sub>18</sub>-*b*-PSar<sub>16</sub> (a), and CND/CaNP-HUPA-PSar<sub>82</sub> (b). The ester link which renders CND/CaNP-HUPA-PSar<sub>82</sub> more susceptible to acid hydrolysis is highlighted in yellow.

PSar was also grafted from HUPA-functionalised CND/CaNPs (CND/CaNP-HUPA-PSar<sub>82</sub>) to yield an amphiphilic block copolymer in which the alkane chain of HUPA acted as the hydrophobic component. NCA ROP proceeded from the hydroxyl group of HUPA, producing an ester link (highlighted in yellow in Scheme 4.3b) within the block copolymer chain that may be exploited for acid-mediated polymer cleavage and subsequent guest molecule release (Scheme 4.3b). The nanocomposites produced by the grafting-from approach are summarised in Table 4.1, entries 1-3.

**Table 4.1** Summary of nanocomposite materials synthesised.

	<b>Approach</b>	<b>Material</b>
<b>1</b>	Grafting-from	CND/CaNP-ABPA-PPhe <sub>4</sub> - <i>b</i> -PSar <sub>16</sub>
<b>2</b>	Grafting-from	CND/CaNP-ABPA-PBLG <sub>18</sub> - <i>b</i> -PSar <sub>16</sub>
<b>3</b>	Grafting-from	CND/CaNP-HUPA-PSar <sub>82</sub>
<b>4</b>	Grafting-to	CND/CaNP-HUPA-PSar <sub>17</sub>
<b>5</b>	Grafting-to	CND/CaNP-HUPA-PSar <sub>23</sub>

#### 4.3.2.2 Characterisation of nanocomposites from the grafted-from approach

<sup>1</sup>H NMR spectra were obtained to characterise polymeric surface coatings in comparison with spectra from similar unbound polymers, in terms of structure and monomer repeat units, formed in the absence of CND/CaNPs. Prior to all analyses, the CND/CaNP-polymer nanocomposites were suspended and extensively washed in chloroform, and then collected as a pellet by centrifugation. The supernatants were combined, dried, and the composition also analysed. Successful polymer grafting is indicated by the presence of both polymer and CND/CaNP in the pellet, whereas unbound polymer was present in the supernatant. This ensures that all the peaks assigned to the polymer arise from the CND/CaNP-conjugated polymer, as opposed to unbound polymer. Comparing the integrals of the protons with protons corresponding to the initiator

(ABPA or HUPA) with the protons corresponding to the polymer allowed for quantification of polymer equivalents, and hence average polymer  $M_w$  values to be determined. These calculations are provided in Table 4.2, and more thorough analysis of the spectra provided below.

**Table 4.2** Comparison between the integrals of initiator protons to polymer protons to calculate polymer equivalents and molecular weight.

Polymer or nanocomposite	Initiator		Polymer			Equivalence	$M_w$ (kg mol <sup>-1</sup> )
	Label	Integral	Label	Integral	# of H atoms		
ABPA-PPhe <sub>8</sub> - <i>b</i> -PSar <sub>105</sub>	d	6	a	37.58	5	8	8.8
ABPA-PPhe <sub>8</sub> - <i>b</i> -PSar <sub>105</sub>			c	314.70	3	105	
CND/CaNP-ABPA-PPhe <sub>4</sub> - <i>b</i> -PSar <sub>16</sub>	d	6	a	20.53	5	4	1.9
CND/CaNP-ABPA-PPhe <sub>4</sub> - <i>b</i> -PSar <sub>16</sub>			c	47.79	3	16	
ABPA-PBLG <sub>22</sub> - <i>b</i> -PSar <sub>63</sub>	d	6	a	109.06	5	22	9.4
ABPA-PBLG <sub>22</sub> - <i>b</i> -PSar <sub>63</sub>			c	187.92	3	63	
CND/CaNP-ABPA-PBLG <sub>18</sub> - <i>b</i> -PSar <sub>16</sub>	d	6	a	89.72	5	18	5.2
CND/CaNP-ABPA-PBLG <sub>18</sub> - <i>b</i> -PSar <sub>16</sub>			c	46.93	3	16	
HUPA-PSar <sub>95</sub>	c	14	b	286.23	3	95	7.0
CND/CaNP-HUPA-PSar <sub>82</sub>	c	14	b	246.95	3	82	6.1

Figure 4.5a-b display the <sup>1</sup>H NMR spectra of both bound nanocomposite CND/CaNP-ABPA-PPhe<sub>4</sub>-*b*-PSar<sub>16</sub> and an unbound polymer analogue ABPA-PPhe<sub>8</sub>-*b*-PSar<sub>105</sub>. Each spectrum featured a peak between 7.34 and 7.12 ppm which was assigned to the aromatic groups of the PPhe block. The peak between 4.50 and 3.92 ppm corresponds to the proton of the amide group present in both polymer blocks, and peaks between 2.90 and 2.73 ppm correspond to the protons of the methyl group bonded to the tertiary amine of each PSar repeat unit. The <sup>1</sup>H NMR spectra of CND/CaNP-ABPA-PBLG<sub>18</sub>-*b*-PSar<sub>16</sub> and the unbound polymer analogue ABPA-PBLG<sub>22</sub>-*b*-PSar<sub>63</sub> both contained an aromatic peak between 7.37 and 7.20 ppm corresponding with the aromatic protons of the PBLG block (Figure 4.5c-d). The peak between 5.12 and 5.00 ppm corresponds to the non-aromatic protons of the benzyl protecting group of each BLG repeat unit, and peaks between 2.95 and 2.71 ppm correspond to the methyl group of each PSar

repeat unit. This analysis, following extensive material washing, confirms that both PPhe<sub>4</sub>-*b*-PSar<sub>16</sub> and PBLG<sub>18</sub>-*b*-PSar<sub>16</sub> are bound to the CND/CaNPs.

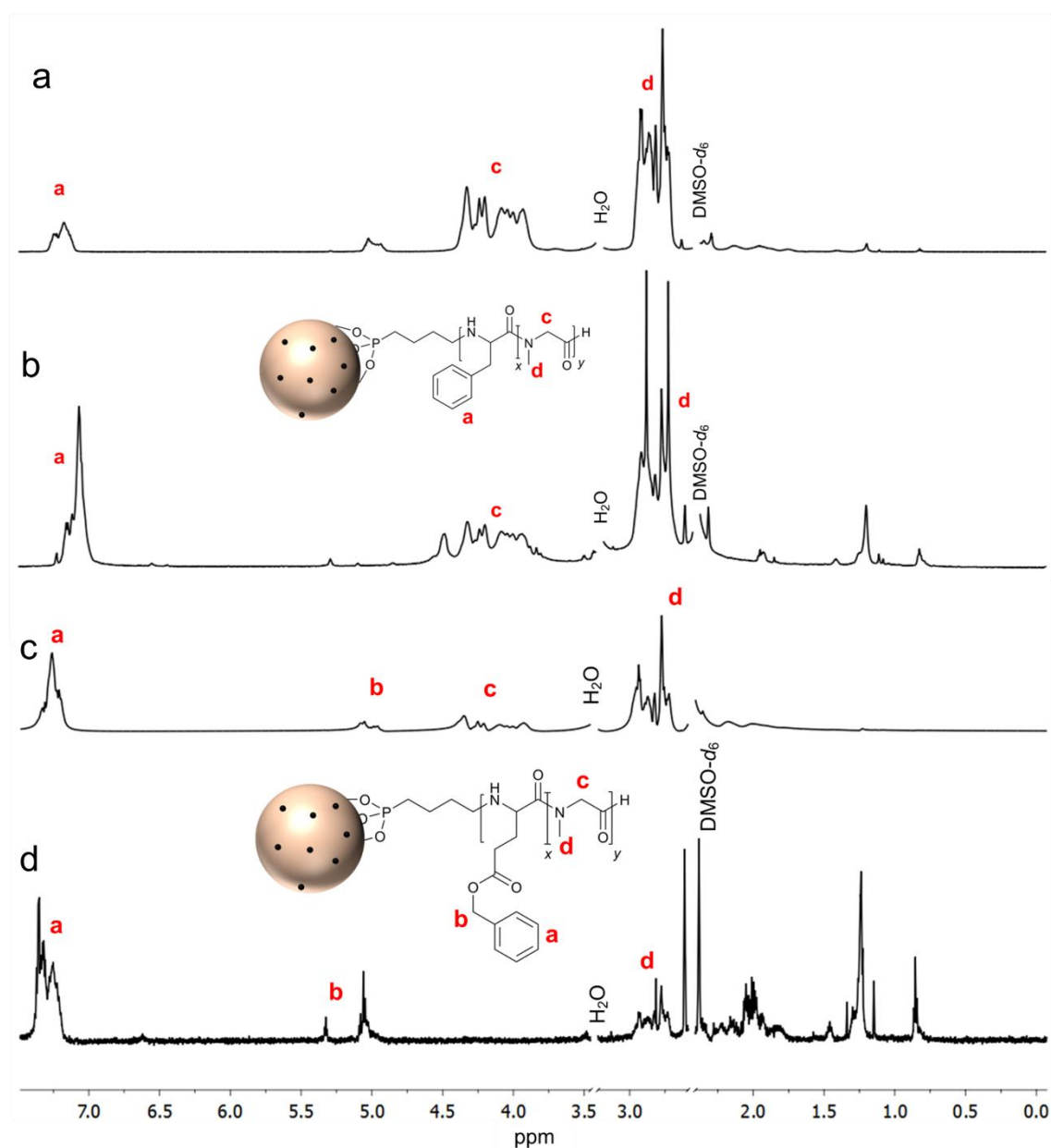


**Figure 4.5**  $^1\text{H}$  NMR spectra of ABPA-PPhe<sub>8</sub>-*b*-PSar<sub>105</sub> (a, 500 MHz, DMSO-*d*<sub>6</sub>), CND/CaNP-ABPA-PPhe<sub>4</sub>-*b*-PSar<sub>16</sub> (b, 600 MHz, DMSO-*d*<sub>6</sub>), ABPA-PBLG<sub>22</sub>-*b*-PSar<sub>63</sub> (c, 500 MHz, DMSO-*d*<sub>6</sub>), and CND/CaNP-ABPA-PBLG<sub>18</sub>-*b*-PSar<sub>16</sub> (d, 600 MHz, DMSO-*d*<sub>6</sub>). Key peaks corresponding to PAA protons denoted.

PSar grafting from HUPA-modified CND/CaNPs was also confirmed by  $^1\text{H}$  NMR spectroscopy, with unbound HUPA-PSar<sub>95</sub> used as a reference (Figure 4.6). Both spectra contained a peak between 4.33 and 3.92 ppm corresponding to the CH<sub>2</sub> group of the Sar repeat unit, a peak between 2.92 and 2.73 ppm corresponding

to the methyl group of the Sar repeat unit, and peaks between 1.24 and 1.07 ppm corresponding with the CH<sub>2</sub> groups in HUPA.

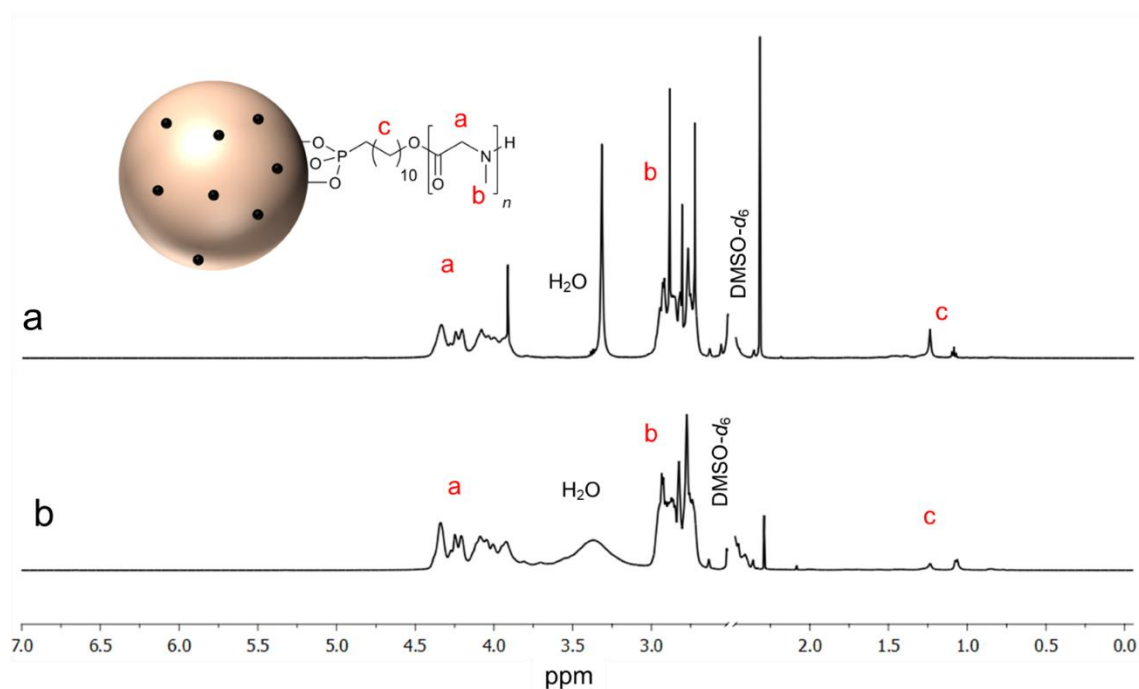


**Figure 4.6** <sup>1</sup>H NMR spectra of CND/CaNP-HUPA-PSar<sub>82</sub> (a) and HUPA-PSar<sub>95</sub> (b) (500 MHz, DMSO-*d*<sub>6</sub>).

<sup>13</sup>C NMR spectroscopy also confirmed successful nanocomposite synthesis (Figure 4.7). <sup>13</sup>C NMR peaks corresponding to the polymeric component are present in all spectra. In contrast, the peak at 168.21 ppm, corresponding to calcite,<sup>49</sup> appears exclusively in the spectra obtained from CND/CaNP-polymer nanocomposites.

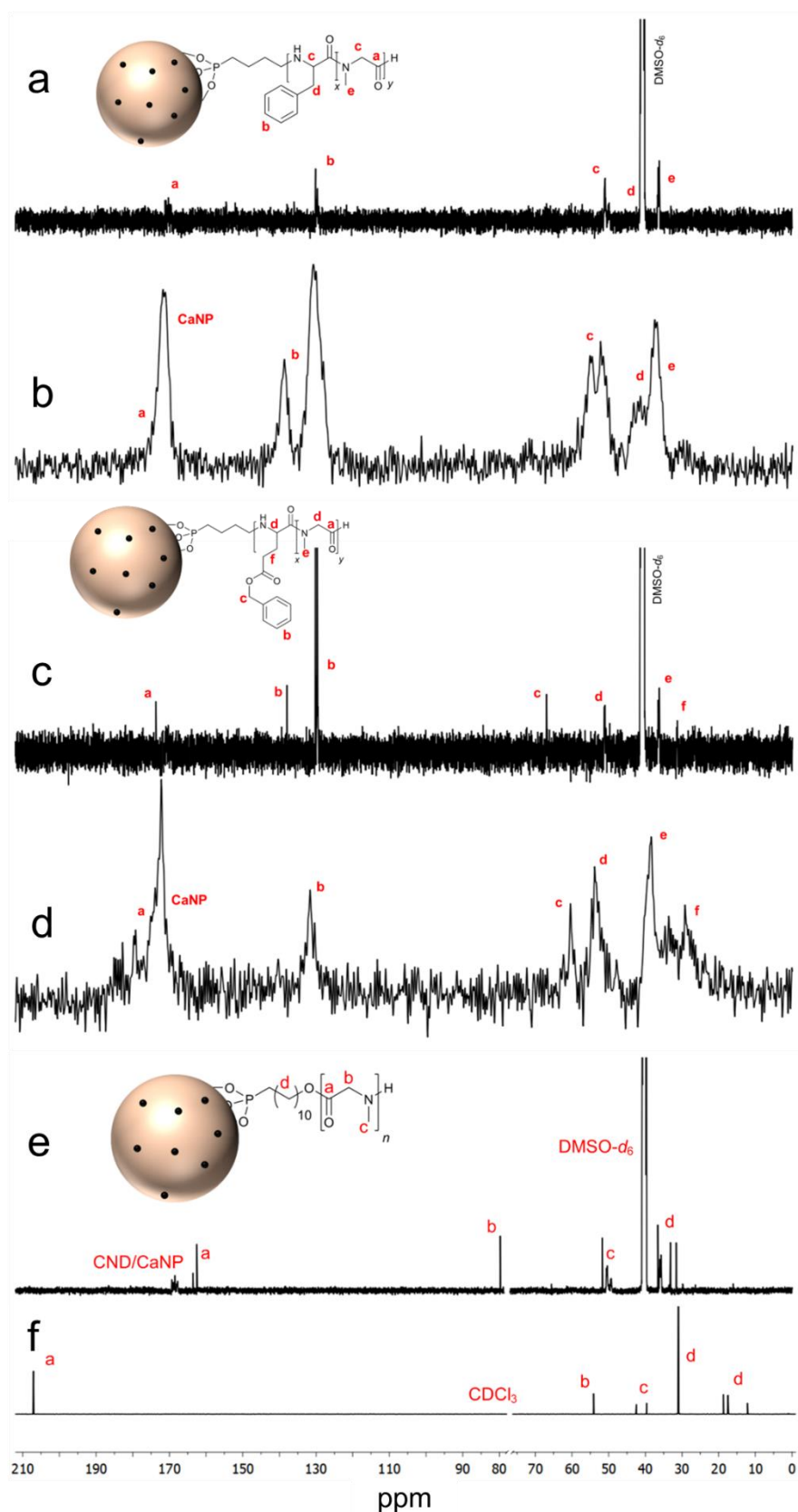


**Figure 4.7**  $^{13}\text{C}$  NMR spectra of ABPA-PPhe<sub>8</sub>-*b*-PSar<sub>105</sub> (a, 125 MHz, DMSO-*d*<sub>6</sub>), CND/CaNP-ABPA-PPhe<sub>4</sub>-*b*-PSar<sub>16</sub> (b, 100 MHz, solid-state), ABPA-PBLG<sub>22</sub>-*b*-PSar<sub>63</sub> (c, 125 MHz, DMSO-*d*<sub>6</sub>), CND/CaNP-ABPA-PBLG<sub>18</sub>-*b*-PSar<sub>16</sub> (d, 100 MHz, solid-state), CND/CaNP-HUPA-PSar<sub>82</sub> (e, 125 MHz, DMSO-*d*<sub>6</sub>), and HUPA-PSar<sub>95</sub> (f, 125 MHz, DMSO-*d*<sub>6</sub>).

As shown in Figure 4.3a, calcite features characteristic peaks at  $1086\text{ cm}^{-1}$  and  $711\text{ cm}^{-1}$  in its Raman spectrum. Raman spectra obtained from these CND/CaNP-polymer nanocomposites also contained these peaks, in addition to a characteristic aromatic peak at  $1002\text{ cm}^{-1}$  which suggests that polymer grafting caused no structural changes to the calcite core (Figure 4.8a, i-ii). The dried supernatant from the washing process revealed a Raman spectra comparable to those obtained from free polymer and featured no peaks corresponding to calcite, further confirming that chloroform washing successfully removed unbound polymer from polymer-grafted CND/CaNPs (Figure 4.8a, iii).

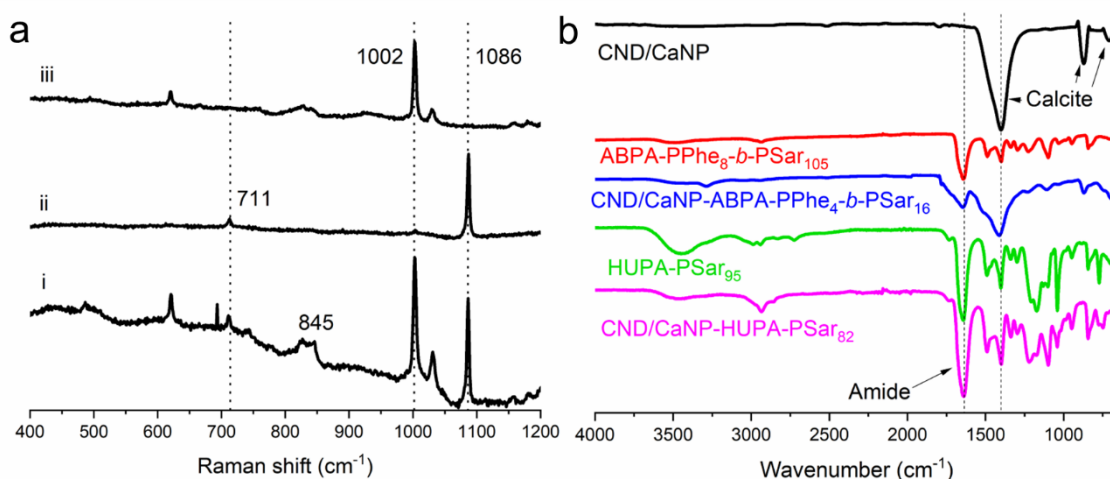


**Figure 4.8** (a) Raman microscopy spectra of CND/CaNP-ABPA-PPhe<sub>4</sub>-b-PSar<sub>16</sub> (i) and CND/CaNP-ABPA-PBLG<sub>18</sub>-b-PSar<sub>16</sub> (ii) and the dried supernatant from washing CND/CaNP-ABPA-PPhe<sub>4</sub>-b-PSar<sub>16</sub> (iii). (b) FTIR spectra of CND/CaNPs, ABPA-PPhe<sub>8</sub>-b-PSar<sub>105</sub> free polymer, CND/CaNP-ABPA-PPhe<sub>4</sub>-b-PSar<sub>16</sub>, HUPA-PSar<sub>95</sub> free polymer and CND/CaNP-HUPA-PSar<sub>82</sub>.

FTIR spectroscopy was used for additional characterisation of the CND/CaNP-polymer nanocomposites (Figure 4.8b). The spectra of all materials revealed the characteristic calcite peaks at  $1397\text{ cm}^{-1}$ ,  $871\text{ cm}^{-1}$  and  $713\text{ cm}^{-1}$ , and an amide peak in the spectra of polymer-grafted NPs. Once more, thorough washing with chloroform prior to FTIR, Raman and  $^{13}\text{C}$  NMR analyses confirmed that the polymer remains grafted to the CND/CaNPs.

#### 4.3.2.3 Synthesis and characterisation of nanocomposites from the grafting-to approach

The capability of PAAs featuring a terminal phosphonate group to graft to CND/CaNPs via ionic interactions was then investigated: the grafting-to approach (Section 1.4.1.3). For the grafting-to approach, the polymers were synthesised and then self-assembled with the CND/CaNPs, forming P-O-M bonds between the polymers and CND/CaNPs, whereas the grafting-from approach involved firstly self-assembling CND/CaNPs with the polymer initiator (ABPA or HUPA), and then subsequent NCA ROP. Two phosphonate-bearing PSar polymers were synthesised via NCA ROP initiated from the hydroxyl group of HUPA: HUPA-PSar<sub>17</sub> and HUPA-PSar<sub>23</sub>. <sup>1</sup>H NMR (Figure 4.9a-b), <sup>13</sup>C NMR (Figure 4.9c-d) and FTIR (Figure 4.9e) spectroscopies confirmed successful polymer synthesis. This grafting-to approach enables straightforward polymer analysis by NMR spectroscopy prior to grafting, as the polymers are soluble in common NMR solvents (e.g. DMSO-*d*<sub>6</sub> and CDCl<sub>3</sub>) before being grafted to an inorganic NP. The polymers were then introduced to CND/CaNPs as an aqueous solution and suspended using an ultrasonic bath. After one hour, the nanocomposite samples were processed and analysed as described above (Table 4.1, entries 4-5). FTIR spectra of both chloroform-washed nanocomposites featured characteristic broad peaks attributed to calcite (1397 cm<sup>-1</sup>, 871 cm<sup>-1</sup> and 713 cm<sup>-1</sup>) and the amide from the polymer (1634 cm<sup>-1</sup>, Figure 4.9f) confirming nanocomposite self-assembly. Meanwhile, FTIR analysis indicated that unbound polymer was washed away and retained in the chloroform supernatant, as expected (Figure 4.9g).

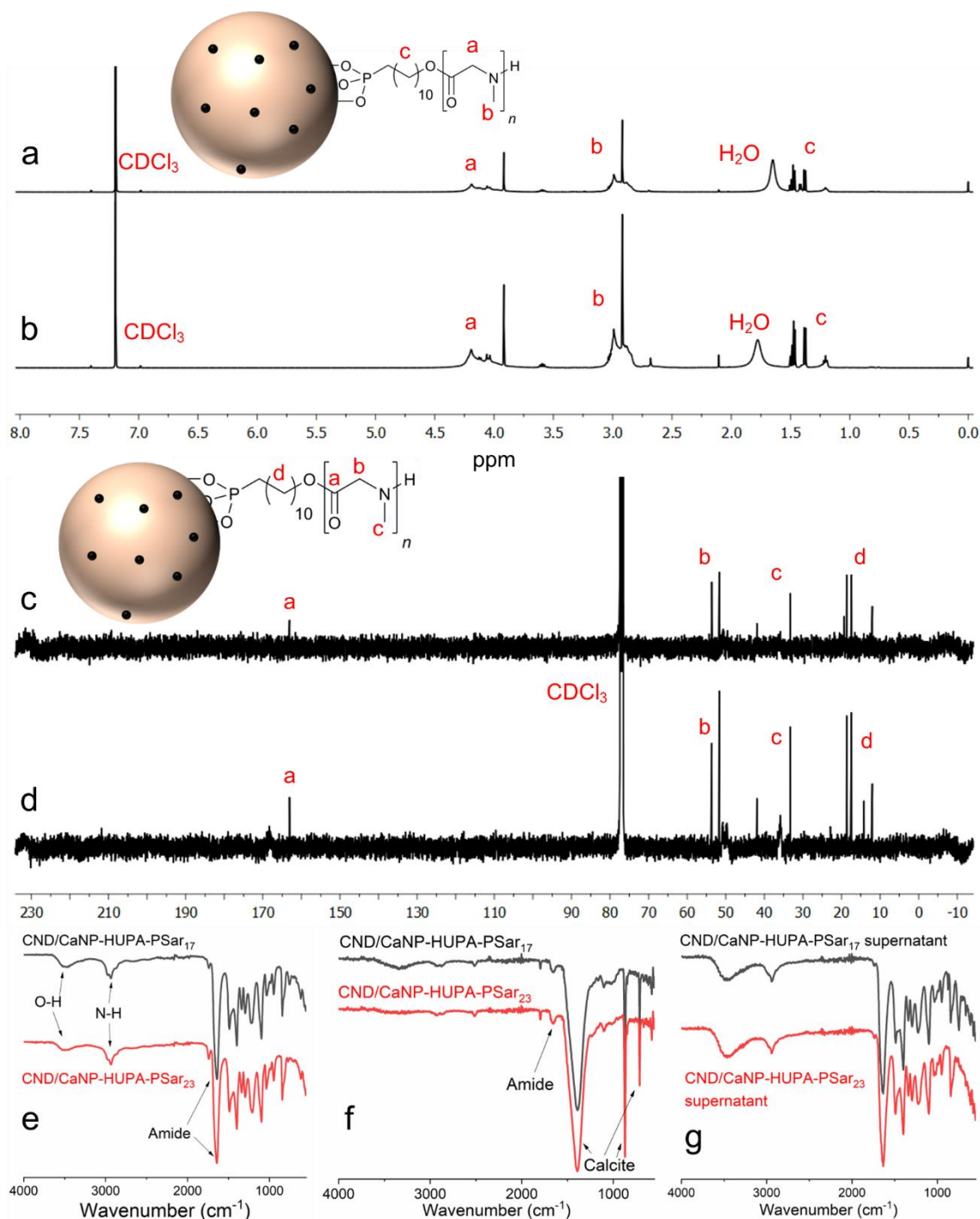


**Figure 4.9** <sup>1</sup>H NMR spectra of HUPA-PSar<sub>17</sub> (a) and HUPA-PSar<sub>23</sub> (b) (500 MHz, CDCl<sub>3</sub>), <sup>13</sup>C NMR spectra of HUPA-PSar<sub>17</sub> (c) and HUPA-PSar<sub>23</sub> (d) (125 MHz, CDCl<sub>3</sub>), and FTIR spectra of the HUPA-PSar polymers (e), CND/CaNP-HUPA-PSar nanocomposites (f) and dried supernatants (g).

#### 4.3.2.4 TGA analysis of the nanocomposites

The extent of polymer grafting to CND/CaNPs was explored using TGA analysis (Figure 4.10). The thermal decomposition of CND/CaNPs occurred with a single

weight loss step between 600 °C and 700 °C, leaving a yield of 58% at 800 °C which corresponds to the loss of one formula unit CO<sub>2</sub> per formula unit CaCO<sub>3</sub>. In contrast, pure polymers ABPA-PPhe<sub>8</sub>-*b*-PSar<sub>105</sub> and HUPA-PSar<sub>95</sub> showed a dominant weight loss step which started between 250 °C and 350 °C and was completed at ~550 °C. Negligible char remained at 800 °C. Therefore, it was possible to determine the extent of polymer grafting by comparing the weight loss at lower (attributed to the polymer) and higher (attributed to CND/CaNPs) temperatures.

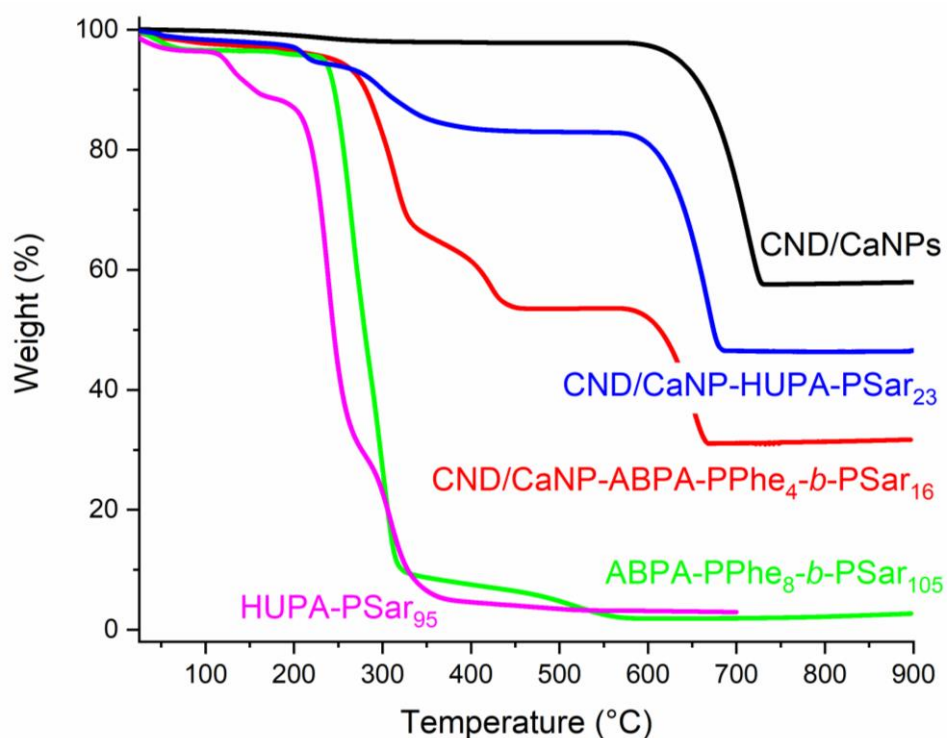


**Figure 4.10** TGA thermograms of CND/CaNPs, some CND/CaNP-polymer nanocomposites, and polymer analogues.

TGA data showed that the total organic material mass of CND/CaNP-ABPA-PPhe<sub>4</sub>-*b*-PSar<sub>16</sub> (grafting-from approach) and CND/CaNP-HUPA-PSar<sub>23</sub> (grafting-to approach) was 27% and 12%, respectively, suggesting that the grafting-to approach enabled more efficient polymer attachment to CND/CaNP surfaces (Table 4.3). Consequentially, nanocomposites formed by the grafting-from approach were advanced to controlled therapeutic release studies.

**Table 4.3** Summary of TGA data. The furnace temperatures recorded at 95%, 90% and 60% weight loss, and the char yields at 800 °C.

Sample	Temperature at wt.% (°C)			Char yield at 800 °C (wt.%)
	95%	90%	60%	
CND/CaNP	634	662	723	58
CND/CaNP-ABPA-PPhe <sub>4</sub> - <i>b</i> -PSar <sub>16</sub>	246	281	410	31
ABPA-PPhe <sub>8</sub> - <i>b</i> -PSar <sub>105</sub>	234	246	271	2
CND/CaNP-HUPA-PSar <sub>23</sub>	219	300	659	46
HUPA-PSar <sub>95</sub>	122	155	238	3

### 4.3.3 Nanocomposites as drug release vehicles

#### 4.3.3.1 Dispersion stability of the nanocomposites

Drug delivery vehicles intended for intravenous injection must form a stable dispersion for extended shelf-life prior to administration, and disperse in aqueous solution such as the bloodstream, post-administration. DLS analysis would allow the hydrodynamic diameter to be measured, but discussed previously is the unsuitability of CND/CaNPs to be sized by DLS due to fluorescence causing interference (Section 4.3.1). CaNPs were synthesised without CNDs, and thus do not fluoresce or present afterglow, but may be sized using DLS. A nanocomposite was formed of these non-fluorescent CaNPs, CaNP-ABPA-PBLG<sub>18</sub>-*b*-PSar<sub>16</sub>, using the grafting-from technique, and its hydrodynamic diameter measured by DLS as being  $219.1 \pm 50.94$  nm in PBS buffer solution at pH 7.4 (Figure 4.4c-d). The same sample was re-analysed on DLS four days later, and Figure 4.4d shows the hydrodynamic diameter is still within error of the first measurement ( $274.2 \pm 68.08$  nm). This brief study demonstrates these nanocomposites may be stable in aqueous environments such as the bloodstream, and thus potentially suitable for utilisation as a drug delivery vehicle.

The effect of polymer grafting on enhancing the dispersibility and suspension stability of CND/CaNPs in water was then tested by time-resolved turbidimetry

studies. This analysis involved monitoring the absorbance at 450 nm every 60 seconds. Upon NP aggregation, the aggregates sank to the bottom of the cuvette and thus the clear (less turbid) solution results in a reduction in absorbance, monitored over time. Only 11% CND/CaNPs remained homogeneously dispersed in water after four hours, whereas 34% of CND/CaNP-ABPA-PPhe<sub>4</sub>-*b*-PSar<sub>16</sub> and 82% of CND/CaNP-HUPA-PSar<sub>23</sub> remained homogeneously dispersed in water after four hours (Figure 4.11). The increased stability of the suspension was attributed to the introduction of a hydrophilic PSar shell to the CND/CaNP surface. The difference in suspension stability enhancement between the two classes of nanocomposite may be linked to the differences in PSar chain length, and the extent of polymer grafting. Nonetheless, polymer grafting enhances the stability of CND/CaNP dispersions in water.

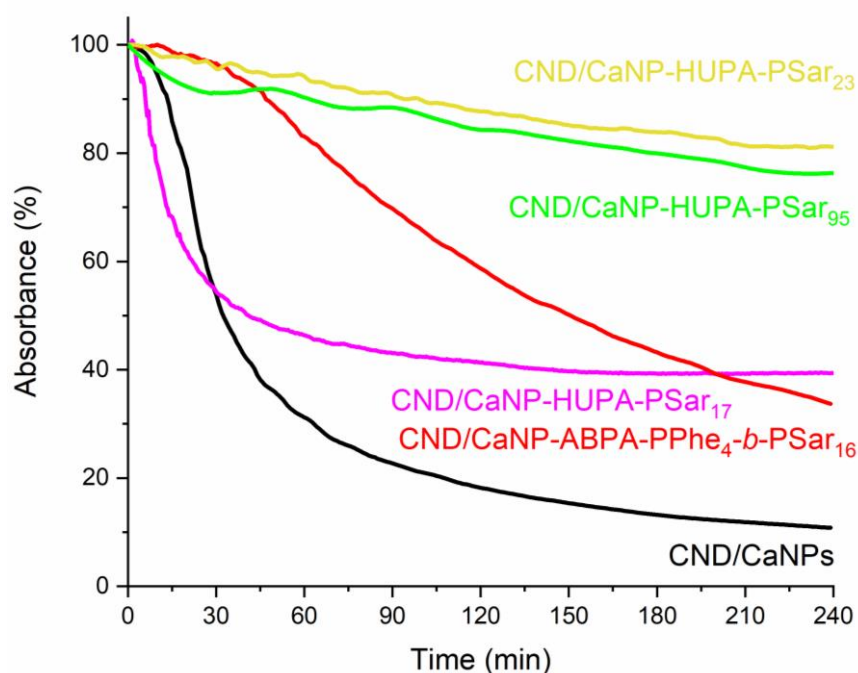


**Figure 4.11** Kinetic UV-vis absorbance of CND/CaNPs and CND/CaNP-polymer nanocomposites in water over four hours. All suspensions/solutions were at a concentration of 0.1 mg mL<sup>-1</sup> and absorbances were taken every 60 s at 450 nm.

#### 4.3.3.2 pH-responsive Dox delivery

Owing to the nanocomposites improved suspension stability over CND/CaNPs, CND/CaNP-ABPA-PPhe<sub>4</sub>-*b*-PSar<sub>16</sub> and CND/CaNP-HUPA-PSar<sub>23</sub> were

assessed for their ability to both retain and selectively release the chemotherapeutic Dox. The nanocomposites were suspended in pH 7.4 buffer solution and loaded with Dox as per Section 2.3.4 to 82% and 72% efficiency, respectively. Dox-loaded nanocomposite suspensions were then dialysed against pH 7.4 buffer solution while the Dox concentration in the surrounding dialysis medium was assayed over time by HPLC (Figure 4.12). Negligible Dox (0.0-0.1%) was released after 168 h from both nanocomposites, suggesting excellent retention of Dox under physiological pH conditions. It was also inferred that both the polymer shell remained intact and attached to the NP core, preventing Dox release, and the CND/CaNP core was protected from dissolution into the surrounding medium.

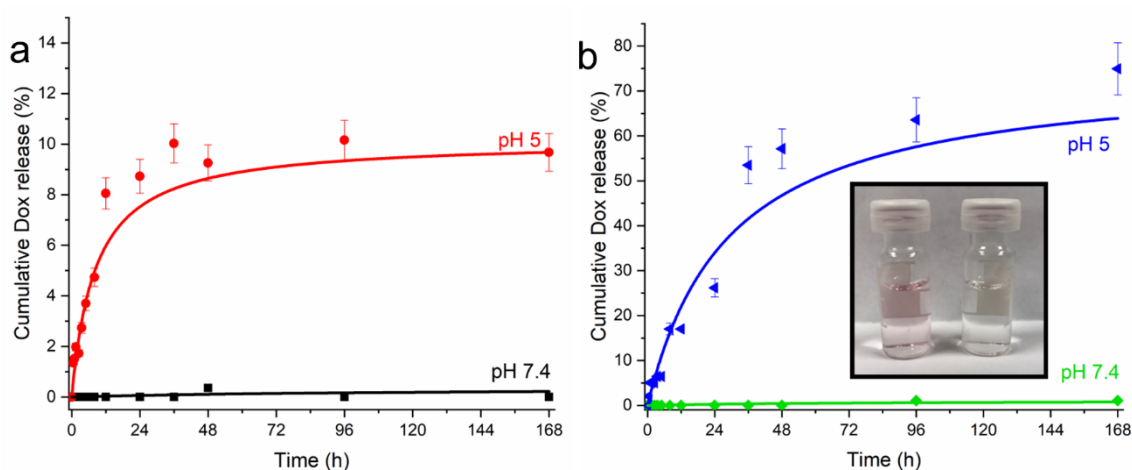


**Figure 4.12** (a) Cumulative amount of Dox released over time for CND/CaNP-ABPA-PPhE<sub>4</sub>-b-PSAr<sub>16</sub> in PBS buffer solution at pH 7.4 (■) and acetate buffer solution at pH 5 (●). (b) Cumulative amount of Dox released over time for CND/CaNP-HUPA-PSAr<sub>23</sub> in PBS buffer solution at pH 7.4 (◆) and acetate buffer solution at pH 5 (◄). Inset: buffer solutions outside the dialysis tubing of CND/CaNP-HUPA-PSAr<sub>23</sub> at pH 5 (left) and 7.4 (right) after 168 h.

To test the capability for the nanocomposites to release Dox as triggered by a solution pH change, Dox-loaded nanocomposite suspensions were also dialysed against a pH 5 acetate buffer solution. Only moderate Dox release from CND/CaNP-ABPA-PPhE<sub>4</sub>-b-PSAr<sub>16</sub> was anticipated due to the inability of acid to hydrolyse the polymer at such pH; Dox release may instead be driven by its enhanced solubility in the acidic environment, enabling some escape from the NP. In addition, some degradation of the CaNP core may be anticipated.

Accordingly, only 9.6% of the loaded Dox was released (Figure 4.12a). In contrast, Dox release from CND/CaNP-HUPA-PSar<sub>23</sub> was anticipated to be significant due to the presence of the acid-cleavable ester link between the HUPA and PSar blocks within the polymer shell. Studies revealed that 74.9% of the loaded Dox was released when the nanocomposites were maintained within pH 5 acetate buffer solution (Figure 4.12b). The pH-triggered release of Dox from both nanocomposites was mostly completed within the first 24 h of the experiment, indicating a restricted 'burst release' because of an initial large rate of release before reaching equilibrium. Furthermore, the release of Dox was also clearly demonstrated by the colourless-to-pink colour change observed in pH 5 acetate buffer dialysis medium, attributed to increasing Dox concentration. In contrast, no colour change was observed when pH 7.4 PBS buffer solution was used as the dialysis medium (Figure 4.12b, inset).

#### 4.3.3.3 pH-responsive afterglow

The ability to trace the activity of a drug delivery vehicle in real time is desirable for ensuring the therapeutic reaches the target site. Here, the nanocomposites feature a CND/CaNP core which exhibits a green afterglow after UV stimulation when intact, but loses this ability when dissolved and the CNDs are instead in aqueous solution. Therefore, introducing the nanocomposites to an acidic environment would not only trigger Dox release, it may enable nanocomposite tracing by the loss of afterglow behaviour due to the dissolution of the CaNP core and release of CNDs. Stroboscopy studies showed that the nanocomposite CND/CaNP-ABPA-PPhe<sub>4</sub>-*b*-PSar<sub>16</sub> retained afterglow when suspended in pH 7.4 PBS buffer solution (Figure 4.13a). Afterglow was also retained after the nanocomposites were recovered from solution and dried (Figure 4.13b). To determine afterglow retention in acidic solution, the same nanocomposites were suspended in pH 5 acetate buffer solution, stirred for 24 h and then dried. No afterglow was observed for any nanocomposite tested, which may be ascribed to some degradation of the CaNP core and subsequent release of CNDs (Figure 4.13c). This pH-responsive degradation of afterglow may provide a mechanism for composite tracing by the loss of afterglow. It should be noted, however, that

for effective transmission of light through living tissue, and thus for tracing *in vivo*, excitation with red light and emission in red/near-IR are required. Further, an optimised quantum yield is required to account for dilution, although ways of amplifying afterglow are an active area of research.<sup>29</sup> Nonetheless, the combination of pH-responsive afterglow and Dox release may offer a system for identifying and eliminating cancerous cells and tumours simultaneously.

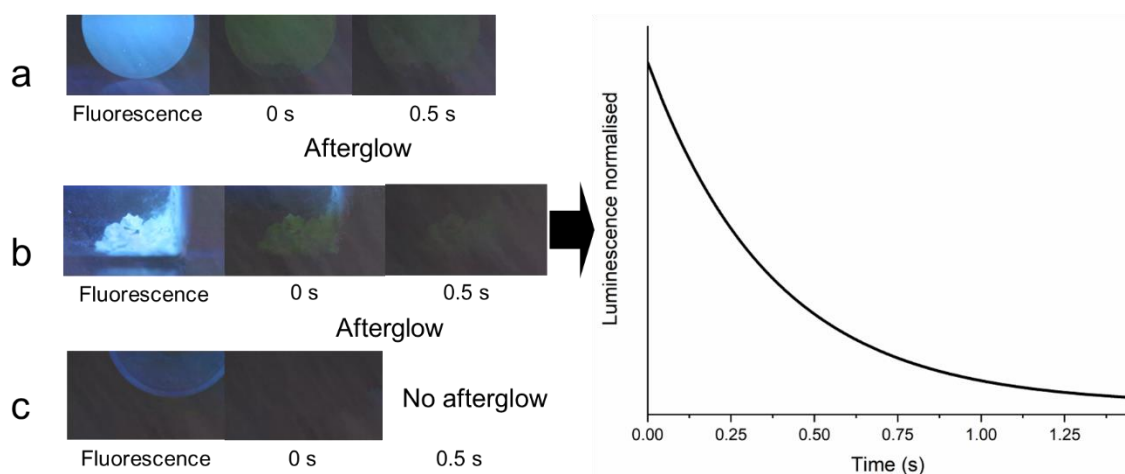


**Figure 4.13** Images determining the presence of afterglow of CND/CaNP-ABPA-PPhe<sub>4</sub>-*b*-PSar<sub>16</sub> in PBS buffer solution (a), CND/CaNP-ABPA-PPhe<sub>4</sub>-*b*-PSar<sub>16</sub> following removal of solution and drying (b), and CND/CaNP-ABPA-PPhe<sub>4</sub>-*b*-PSar<sub>16</sub> after being suspended in pH 5 acetate buffer solution (c). The normalised afterglow lifetime of CND/CaNP-ABPA-PPhe<sub>4</sub>-*b*-PSar<sub>16</sub> following removal from solution is also presented (right). Afterglow was triggered by irradiating the samples with UV light at 365 nm for a few seconds beforehand.

## 4.4 Conclusions

CND/CaNPs were synthesised and successfully surface-functionalised with amphiphilic block copolymers via a grafting-to or grafting-from approach. The reported grafted-from nanocomposites were synthesised by firstly functionalising CND/CaNPs with ABPA or HUPA, presenting an amine or hydroxyl group, respectively, to initiate NCA ROP. Alternatively, HUPA-PSar block copolymers were synthesised and grafted to CND/CaNPs by the terminal phosphonate functional group forming P-O-M bonds with CaNPs: the grafting-to approach. These synergistic CND/CaNP-polymer nanocomposites had good compatibility with aqueous media whilst retaining fluorescence and afterglow. The

nanocomposites were loaded with Dox at high efficiency and Dox release studies revealed that an acidic environment was able to promote Dox release, particularly when an ester link was incorporated within the polymer chain. The selectivity of the nanocomposites to release Dox in an acidic environment, but retain Dox when stored in a non-acidic environment, was significant and a key requirement for controlled drug delivery. Additionally, the nanocomposites demonstrated afterglow in pH 7.4 solution for approximately 1 s, but do not display afterglow when stored in an acidic environment. This could be optimised further as a tracing mechanism by seeking the loss of afterglow in target cells. With further optimisation, the simultaneous pH-responsive Dox delivery and pH-triggered loss of afterglow may enable these materials to be theranostic devices.

## 4.5 References

1. S. Manchun, C. R. Dass and P. Sriamornsak, *Life Sciences*, 2012, **90**, 381-387.
2. M. Thompson and C. Scholz, *Nanomaterials*, 2021, **11**, 1119.
3. R. Baumgartner, H. Fu, Z. Song, Y. Lin and J. Cheng, *Nature Chemistry*, 2017, **9**, 614-622.
4. J. Huang and A. Heise, *Chemical Society Reviews*, 2013, **42**, 7373-7390.
5. M. Khuphe, C. S. Mahon and P. D. Thornton, *Biomaterials Science*, 2016, **4**, 1792-1801.
6. H. Yu, N. Ingram, J. V. Rowley, S. Parkinson, D. C. Green, N. J. Warren and P. D. Thornton, *Journal of Materials Chemistry B*, 2019, **7**, 4217-4223.
7. T. Borase, M. Iacono, S. I. Ali, P. D. Thornton and A. Heise, *Polymer Chemistry*, 2012, **3**, 1267-1275.
8. M.-Q. Gong, J.-L. Wu, B. Chen, R.-X. Zhuo and S.-X. Cheng, *Langmuir*, 2015, **31**, 5115-5122.
9. S. Senapati, A. K. Mahanta, S. Kumar and P. Maiti, *Signal Transduction and Targeted Therapy*, 2018, **3**, 7.
10. V. Lionetti and S. Paddeu, in *Ultrasound contrast agents: Targeting and processing methods for theranostics*, eds. G. Paradossi, P. Pellegritti and A. Trucco, Springer Verlag, Milan, Italy, 2009, ch. Chapter 1, pp. 1-11.
11. G. Chen, H. Qiu, P. N. Prasad and X. Chen, *Chemical Reviews*, 2014, **114**, 5161-5214.
12. Z. Chen, H. Chun-Ying, M. S. Erin, M. L. Joseph and Y. L. Lih, *Nanotechnology*, 2017, **28**, 455201.
13. Z. Zhang, Z. Chen, L. Yuan, W. Chen, J. Yang, B. Wang, X. Wen, J. Zhang, L. Hu, J. A. Stride, G. J. Conibeer, R. J. Patterson and S. Huang, *Advanced Materials*, 2017, **29**, 1703214.
14. X. Gao, L. W. Chung and S. Nie, in *Methods in Molecular Biology - Quantum Dots: Applications in Biology*, 2007, vol. 374, pp. 135-145.

15. A. M. Derfus, W. C. W. Chan and S. N. Bhatia, *Nano Letters*, 2004, **4**, 11-18.
16. H. Li, Z. Kang, Y. Liu and S.-T. Lee, *Journal of Materials Chemistry*, 2012, **22**, 24230-24253.
17. Y. Fang, S. Guo, D. Li, C. Zhu, W. Ren, S. Dong and E. Wang, *ACS Nano*, 2012, **6**, 400-409.
18. Q. Zeng, D. Shao, X. He, Z. Ren, W. Ji, C. Shan, S. Qu, J. Li, L. Chen and Q. Li, *Journal of Materials Chemistry B*, 2016, **4**, 5119-5126.
19. F. Wang, Y.-h. Chen, C.-y. Liu and D.-g. Ma, *Chemical Communications*, 2011, **47**, 3502-3504.
20. L. Cao, S. Sahu, P. Anilkumar, C. E. Bunker, J. Xu, K. A. S. Fernando, P. Wang, E. A. Gulians, K. N. Tackett and Y.-P. Sun, *Journal of the American Chemical Society*, 2011, **133**, 4754-4757.
21. H. Li, X. He, Z. Kang, H. Huang, Y. Liu, J. Liu, S. Lian, C. H. A. Tsang, X. Yang and S.-T. Lee, *Angewandte Chemie International Edition*, 2010, **49**, 4430-4434.
22. Y. Chen, J. He, C. Hu, H. Zhang, B. Lei and Y. Liu, *Journal of Materials Chemistry C*, 2017, **5**, 6243-6250.
23. J. Tan, R. Zou, J. Zhang, W. Li, L. Zhang and D. Yue, *Nanoscale*, 2016, **8**, 4742-4747.
24. D. C. Green, M. A. Holden, M. A. Levenstein, S. Zhang, B. R. G. Johnson, J. Gala de Pablo, A. Ward, S. W. Botchway and F. C. Meldrum, *Nature Communications*, 2019, **10**, 206.
25. Y. Fan, P. Wang, Y. Lu, R. Wang, L. Zhou, X. Zheng, X. Li, J. A. Piper and F. Zhang, *Nature Nanotechnology*, 2018, **13**, 941-946.
26. X. Zhu, X. Liu, H. Zhang, M. Zhao, P. Pei, Y. Chen, Y. Yang, L. Lu, P. Yu, C. Sun, J. Ming, I. M. Ábrahám, A. M. El-Toni, A. Khan and F. Zhang, *Angewandte Chemie International Edition*, 2021, **60**, 23545-23551.
27. W. Li, S. Wu, X. Xu, J. Zhuang, H. Zhang, X. Zhang, C. Hu, B. Lei, C. F. Kaminski and Y. Liu, *Chemistry of Materials*, 2019, **31**, 9887-9894.
28. Y. Zhou, S. Lu, J. Zhi, R. Jiang, J. Chen, H. Zhong, H. Shi, X. Ma and Z. An, *Analytical Chemistry*, 2021, **93**, 6516-6522.
29. H. Yuan, L. Guo, Q. Su, X. Su, Y. Wen, T. Wang, P. Yang, M. Xu and F. Li, *ACS Applied Materials & Interfaces*, 2021, **13**, 27991-27998.
30. T. Kato, A. Sugawara and N. Hosoda, *Advanced Materials*, 2002, **14**, 869-877.
31. D. H. Keum, J. H. Mun, B. W. Hwang, J. Kim, H. Kim, W. Jo, D.-H. Ha, D.-W. Cho, C. Kim and S. K. Hahn, *Small*, 2017, **13**, 1602925.
32. World Health Organization, *Journal*, 2011.
33. Y. Lin and C.-M. Chan, in *Advances in Polymer Nanocomposites - Types and Applications*, ed. G. Fengge, Woodhead Publishing, Cambridge, U.K., 2012, ch. 3, pp. 55-90.
34. M. A. Osman and U. W. Suter, *Chemistry of Materials*, 2002, **14**, 4408-4415.
35. Z. Wang, *Journal of Applied Polymer Science*, 1996, **60**, 2239-2243.
36. Z. Demjén, B. Pukánszky, E. Földes and J. Nagy, *Journal of Colloid and Interface Science*, 1997, **190**, 427-436.
37. Z. Dong, L. Feng, W. Zhu, X. Sun, M. Gao, H. Zhao, Y. Chao and Z. Liu, *Biomaterials*, 2016, **110**, 60-70.
38. Y. Mima, Y. Hashimoto, T. Shimizu, H. Kiwada and T. Ishida, *Molecular Pharmaceutics*, 2015, **12**, 2429-2435.

39. S. Lassiaz, D. Labarre, A. Galarneau, D. Brunel and P. H. Mutin, *Journal of Materials Chemistry*, 2011, **21**, 8199-8205.
40. E. Ruiz-Agudo, D. Di Tommaso, C. V. Putnis, N. H. de Leeuw and A. Putnis, *Crystal Growth & Design*, 2010, **10**, 3022-3035.
41. W. El Malti, D. Laurencin, G. Guerrero, M. E. Smith and P. H. Mutin, *Journal of Materials Chemistry*, 2012, **22**, 1212-1218.
42. S. Sene, B. Bouchevreau, C. Martineau, C. Gervais, C. Bonhomme, P. Gaveau, F. Mauri, S. Begu, P. H. Mutin, M. E. Smith and D. Laurencin, *CrystEngComm*, 2013, **15**, 8763-8775.
43. M. Nalbach, A. Moschona, K. D. Demadis, S. Klassen, R. Bechstein and A. Kühnle, *Crystal Growth & Design*, 2017, **17**, 5867-5874.
44. L. Wang, L. Qin, C. V. Putnis, E. Ruiz-Agudo, H. E. King and A. Putnis, *Environmental Science & Technology*, 2016, **50**, 259-268.
45. Š. Gradišar, E. Žagar and D. Pahovnik, *ACS Macro Letters*, 2017, **6**, 637-640.
46. B. D. Cullity and S. R. Stock, *Elements of X-Ray Diffraction*, Prentice Hall, New Jersey, USA, 3rd edn., 2001.
47. N. Pierre-Pierre and Q. Huo, in *Recent Progress in Colloid and Surface Chemistry with Biological Applications*, American Chemical Society, 2015, vol. 1215, ch. 9, pp. 157-179.
48. S. Bhattacharjee, *Journal of Controlled Release*, 2016, **235**, 337-351.
49. H. Nebel, M. Neumann, C. Mayer and M. Epple, *Inorganic Chemistry*, 2008, **47**, 7874-7879.

## Chapter 5

### Novel route to PEG-*block*-polyalanine: tin-catalysed ring-opening polymerisation of alanine anhydride

#### Abstract

For the first time, stannous octoate-catalysed ring-opening polymerisation of alanine anhydride, a cyclic dipeptide of alanine, is reported initiated from PEG methyl ether. The synthesised PEG-*block*-polyalanine amphiphilic copolymers had high equivalences up to 36 alanine units, offering an alternative route to polyalanine synthesis avoiding alanine-*N*-carboxyanhydride. Uniform and stable nanoparticles were formed when the block copolymer was dispersed in aqueous solution, as evidenced by DLS and SEM. The nanoparticles were able to load the potent chemotherapeutic, doxorubicin (Dox), with efficiency up to 43%. Dox release studies were performed and PEG-*b*-polyalanine<sub>20</sub> released only 20% Dox at physiological pH (7.4) but released 73% Dox in acidic environments (pH 5). This stimuli-responsiveness with respect to pH offers these biocompatible polymers potential for use as drug delivery vehicles for chemotherapeutics.

#### 5.1 Introduction

L-Alanine (Ala, **1**) is a proteinogenic  $\alpha$ -amino acid, as discussed in Section 1.2.1, whereby the R group is a simple CH<sub>3</sub> group. Figure 1.2 shows Ala as a hydrophobic amino acid, and as such the homopolypeptide of Ala, polyalanine (PAla), is also hydrophobic. PAla forms  $\beta$ -sheet structures with high crystallinity and possess outstanding mechanical properties.<sup>1</sup> For example, silks from spiders and silkworms have excellent physical properties and contain relatively large equivalents of Ala in the protein chain (up to 22 residues, but typically 6-7).<sup>2</sup> On an equal weight basis, spider silks out-perform man-made materials including steel and Kevlar,<sup>3-4</sup> and it is understood that Ala contributes significantly to these excellent mechanical properties.<sup>2,5-6</sup> It has been shown that a general increase in

the amount of residues of Ala in a block in silk protein improves its toughness.<sup>5,7</sup> The synthesis of PAla, and copolymers thereof, is therefore a promising avenue to explore for synthetic fibres with record-breaking properties, or for biomaterials where rugged properties are required.

### **5.1.1 Problems encountered synthesising PAla via NCA ROP**

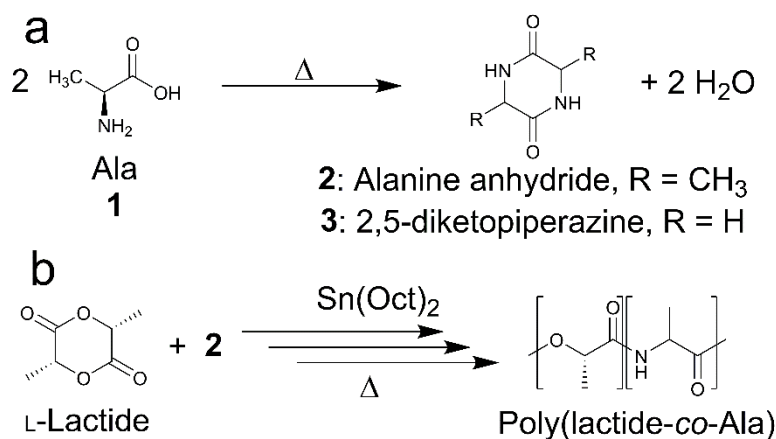
Section 1.2.2 described common routes to synthesise poly(amino acid)s (PAAs), namely solid-phase peptide synthesis, NCA ROP or protein biosynthesis. NCA ROP (Section 1.3.3) allows PAAs to be synthesised reliably with low dispersity and relatively easily; however high  $M_w$  PAla is difficult to synthesise via NCA ROP due to its low solubility in common solvents. This low solubility leads to PAla precipitating from solution prematurely during NCA ROP, inhibiting propagation and resulting in low equivalence.<sup>8-9</sup>

Moreover, PAla synthesis via NCA ROP requires the monomer Ala-NCA, frequently synthesised via the Fuchs-Farthing approach (Section 1.3.3.1). This reaction requires phosgene generation, which is of lethal toxicity and evolves highly corrosive HCl.<sup>10</sup> There are alternative methods of synthesising NCAs avoiding phosgene, such as using diphenyl carbonate,<sup>11</sup> or including mercapto analogues to NCAs, *N*-thiocarboxyanhydrides, but these still have other inherent issues such as a lower reactivity than NCAs.<sup>12-14</sup> Other routes have been explored to synthesise PAla, such as that by Baker and Numata who reported the synthesis of PAla via chemoenzymatic synthesis from alanine ethyl ether.<sup>15</sup> These other routes are also not straightforward and so an alternative route to high  $M_w$  PAla avoiding phosgene is urgently sought.

### **5.1.2 ROP of alanine anhydride**

The carboxylic acid functional group of one Ala molecule may react with the amine group of another under thermal treatment, forming a dipeptide which can

cyclise via a condensation reaction forming alanine anhydride, a cyclic dipeptide of Ala (3,6-dimethyl-2,5-piperazinedione, cyclo(Ala-Ala), **2**) (Scheme 5.1a).<sup>16-17</sup> Alanine anhydride is an example of a 2,5-diketopiperazine (**3**), which may also be synthesised on fused silica NPs,<sup>18-20</sup> and are also found in nature.<sup>21-22</sup>



**Scheme 5.1** Synthesis of alanine anhydride (a) and the synthesis of poly(lactide-co-Ala) (b).

Sn(Oct)<sub>2</sub> (stannous octoate, tin (II) 2-ethylhexanoate) is a highly effective catalyst for the ROP of L-lactide, and is low cost and stable on storage (Section 1.3.2.1).<sup>23-24</sup> Although Sn(Oct)<sub>2</sub> is slightly toxic to humans, as all soluble tin compounds are, it is approved by the US FDA as a food preservative.<sup>24-25</sup> Noomhorm and Tokiwa previously reported the synthesis of poly(lactide-co-Ala) via the ROP of L-lactide with alanine anhydride.<sup>26</sup> The authors used Sn(Oct)<sub>2</sub> as the catalyst with the ROP carried out in bulk, at 195 °C, and in sealed ampules (Scheme 5.1b), however only low M<sub>w</sub> polymers were obtained (5,130 Da).

### 5.1.3 PEG-*b*-PAIa block copolymers

PAIa copolymerised with PEG holds many useful potential applications, as the excellent mechanical properties of PAIa can be combined with the useful properties of PEG in biomedicine such as biocompatibility and hydrophilicity (Section 1.4). For example, implants and implant coatings require both biocompatibility and good mechanical properties.<sup>27</sup> Jeong *et al.* synthesised a

PEG-*b*-PAla<sub>7</sub>-azobenzene-PAla<sub>7</sub>-*b*-PEG triblock copolymer via NCA ROP followed by coupling with the azobenzene chromophore.<sup>28</sup> Although the authors demonstrated the copolymers stimuli-responsiveness to light and temperature, offering a potential drug delivery vehicle,<sup>29</sup> low equivalences of Ala (seven) was reported and laborious synthesis of Ala-NCA was required, hindering its commercialisation. Other PEG-PAla copolymers have been previously reported for synthetic spider silk<sup>30</sup> and tissue engineering, however only low Ala equivalencies are reported and/or low equivalence values and laborious Ala-NCA synthesis is required.<sup>31-35</sup>

#### 5.1.4 Summary

PAla is an attractive polymer to synthesise with high equivalence due to its high mechanical strength and crystallinity, yet is still a biodegradable and biocompatible PAA. Copolymers of PAla are also highly sought after, but it is difficult to obtain PAla with a high equivalence and without requiring Ala-NCA. To the best of this authors knowledge, the example by Noomhorm and Tokiwa of the synthesis of poly(lactide-*co*-Ala) is the only example of alanine anhydride ROP. More work is required to improve the equivalences and copolymerise with different monomers to form different polymer architectures. It is hypothesised that Sn(Oct)<sub>2</sub> may catalyse the ROP of alanine anhydride initiated from the terminal hydroxyl group of PEG, forming a PEG-*b*-PAla block copolymer. This hypothesis was investigated in this Chapter, and is the first report of alanine anhydride ROP initiated from PEG, enabling the inclusion of an ester link between the amphiphilic polymer blocks that is acid sensitive, and consequentially may be used for the acid-triggered release of guest molecules.

## 5.2 Experimental Details

### 5.2.1 Synthesis of PEG-*b*-PAla copolymers

The ROP of alanine anhydride was initiated from PEG methyl ether (5,000 Da  $M_w$ ), catalysed by  $\text{Sn}(\text{Oct})_2$ , and conducted in anhydrous dioxane at reflux. As a representative example (Table 5.1, record 1), PEG methyl ether (5,000 Da  $M_w$ , 0.5070 g, 0.1 mmol, 1 eq.) and alanine anhydride (0.2802 g, 2.0 mmol, 39 eq.) were weighed into an oven-dried,  $\text{N}_2$ -flushed, 3-necked RB flask. The reagents were suspended in anhydrous dioxane (30 mL) before  $\text{Sn}(\text{Oct})_2$  (0.05 mL, 0.06 g, 0.2 mmol, 2 eq.) was added via syringe. The suspension was stirred under  $\text{N}_2$  and heated to reflux. After being heated at reflux for ~30 minutes, all reagents were dissolved and a colourless solution formed. After being heated to reflux with stirring under  $\text{N}_2$  for six days, the reaction solution was cooled and the solution added dropwise to ice-cold diethyl ether (1:5 v/v). On addition to diethyl ether, a white precipitate formed which was collected by centrifugation (4,500 r.p.m., 30 minutes), washed three times in diethyl ether and dried in a vacuum oven at 40 °C overnight. To ensure no unreacted alanine anhydride was collected, the sample was re-dissolved in dioxane at room temperature (alanine anhydride does not dissolve in dioxane at room temperature), and the solution added dropwise to ice-cold diethyl ether. A white precipitate formed again which was collected by centrifugation (4,500 r.p.m., 30 minutes), washed three times in diethyl ether and dried in a vacuum oven at 40 °C.

### 5.2.2 Catalyst loading on kinetics investigation

To investigate the effects of catalyst loading on the kinetics of the reaction, two reaction systems were set up with different catalyst loadings. Each reaction was performed in the same manner as the dioxane method above (Section 5.2.1) with PEG methyl ether (5,000 Da  $M_w$ , 0.5070 g, 0.1 mmol, 1 eq.) and alanine anhydride (0.2801 g, 2.0 mmol, 39 eq.) in anhydrous dioxane (30 mL). To both reactions,  $\text{Sn}(\text{Oct})_2$  was added by syringe but with different amounts: to the first

0.05 mL (0.06 g, 0.2 mmol, 2 eq.) was added, and to the second 0.1 mL (0.1 g, 0.3 mmol, 3 eq.) was added. The reactions were stirred under N<sub>2</sub> and heated at reflux. At various time intervals the reactions were cooled to room temperature and stirring stopped. On cooling, a precipitate settled to the bottom of the reaction flask and a 1 mL aliquot of the dioxane solution was taken, with care to avoid disturbing and re-suspending the unreacted alanine anhydride. Stirring was then continued and the ROP reaction heated to reflux again. The dioxane aliquots collected were added to ice-cold diethyl ether (15 mL) and a white precipitate formed on addition. These precipitates were collected by centrifugation (4,500 r.p.m., 10 minutes), washed three times with diethyl ether and dried in a vacuum oven at 40 °C before <sup>1</sup>H NMR analysis.

### 5.2.3 NP formation and Dox release

#### 5.2.3.1 NP formation

PEG-*b*-PAla NPs were formed using the 'dropping-in' method (Section 2.3.3). Briefly, the polymer was dissolved in chloroform (1 mL, 10 mg mL<sup>-1</sup>) and added dropwise to a RB flask fitted with DI water (10 mL) under vigorous stirring. The mixture was stirred vigorously overnight in the open for the chloroform to evaporate, resulting in an aqueous polymer NP solution of concentration 1 mg mL<sup>-1</sup>.

#### 5.2.3.2 Dox loading

Dox-loaded NPs were formed in the same manner as above (Section 5.2.3.1) but with Dox free base (Section 2.3.4.1) *in situ*. To remove excess Dox, the Dox-loaded NP solution was transferred to dialysis tubing (2,000 Da MWCO) and dialysed against PBS buffer solution at pH 7.4. Aliquots of the PBS buffer solution outside the dialysis tubing were analysed by UV-vis spectrophotometry to

determine the amount of Dox leaching, and hence amount loaded, as per Section 2.3.4.2.

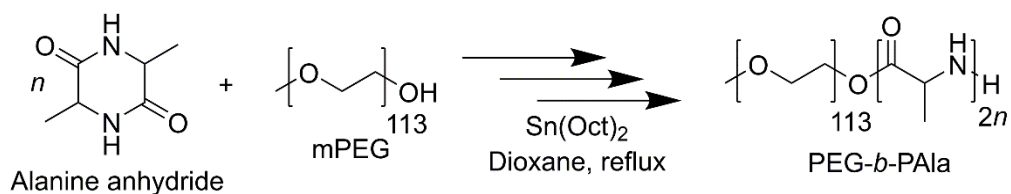
### 5.2.3.3 Dox release

Each Dox-loaded NP solution was split into two, with one half transferred to dialysis tubing and the other half transferred to separate dialysis tubing. One of these halves was dialysed against fresh PBS buffer solution at pH 7.4 whilst the other was dialysed against acetate buffer solution at pH 5. Dox release dialysis was conducted in the dark and incubated at 37 °C. Aliquots of the solution outside the dialysis tubing were taken and transferred to poly(methyl methacrylate) cuvettes for UV-vis spectrophotometry analysis for the amount of Dox releasing to be quantified as per Section 2.3.4.2. Once analysed, aliquots were returned to their respective buffer solutions.

## 5.3 Results and Discussion

### 5.3.1 Copolymer synthesis

A series of PEG(5,000)-*b*-PALa block copolymers were synthesised with the food-grade Sn(Oct)<sub>2</sub> as a catalyst (Table 5.1) (Scheme 5.2). Alanine anhydride dissolves in dioxane at elevated temperatures, but not at room temperature. After conducting the polymerisation reaction in dioxane at reflux, the colourless solution was cooled to room temperature and no alanine anhydride precipitated, indicating complete monomer consumption. To ensure there was no remaining alanine anhydride in the product, the collected polymer was re-dissolved in dioxane and precipitated in diethyl ether. <sup>1</sup>H NMR spectra of the washed polymers confirmed synthesis (Figure 5.1), and actual polymer equivalents were calculated by comparing the methyl ether CH<sub>3</sub> peak on PEG at 3.37 ppm with the PALa CH peak at 4.10 ppm.



**Scheme 5.2** Reaction scheme for the Sn(Oct)<sub>2</sub>-catalysed synthesis of PEG-*b*-PAla.

**Table 5.1** List of polymers synthesised with their expected and actual equivalence of Ala.

	Solvent	Initiator	Ala equivalents		Equivalence (%) <sup>a</sup>	Yield (%)
			Calculated	Actual <sup>b</sup>		
1	Dioxane	PEG(5,000)	38.9	36.0	93	54
2	Dioxane	PEG(5,000)	19.7	20.3	103	100
3	Dioxane	PEG(5,000)	9.9	3.9	39	92

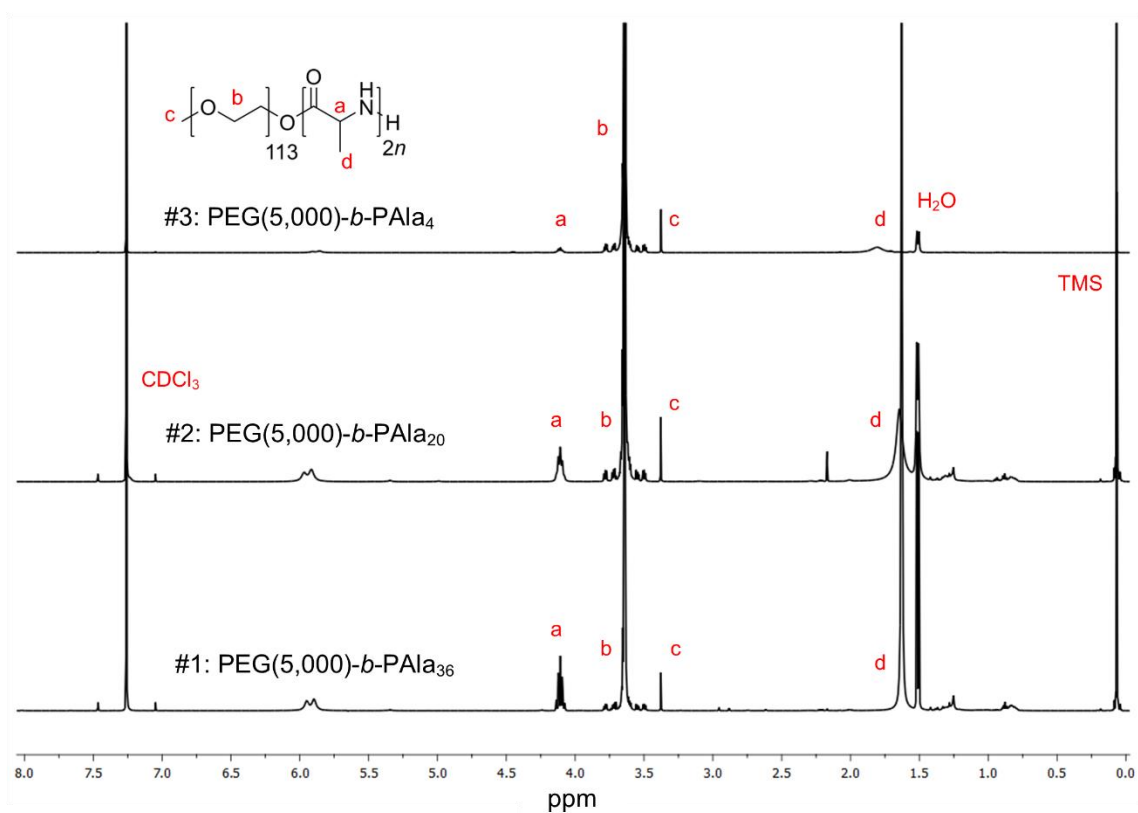


**Figure 5.1** <sup>1</sup>H NMR spectra of the PEG(5,000)-*b*-PAla copolymers (500 MHz, CDCl<sub>3</sub>).

<sup>a</sup> 100% \* actual/expected equivalence. <sup>b</sup> Calculated from <sup>1</sup>H NMR spectroscopy.

$^{13}\text{C}$  NMR spectra confirmed the synthesis of the block copolymers (Figure 5.2). The  $^{13}\text{C}$  NMR peaks at 169 ppm correspond with the carbonyl  $\text{C}=\text{O}$  group of PAla, the peak at 71 ppm corresponds with the  $\text{CH}_2$  groups of PEG, the peaks at 51 ppm are corresponding with the  $\text{CH}$  group of PAla, and finally a peak at 20 ppm corresponds with the  $\text{CH}_3$  group of PAla.

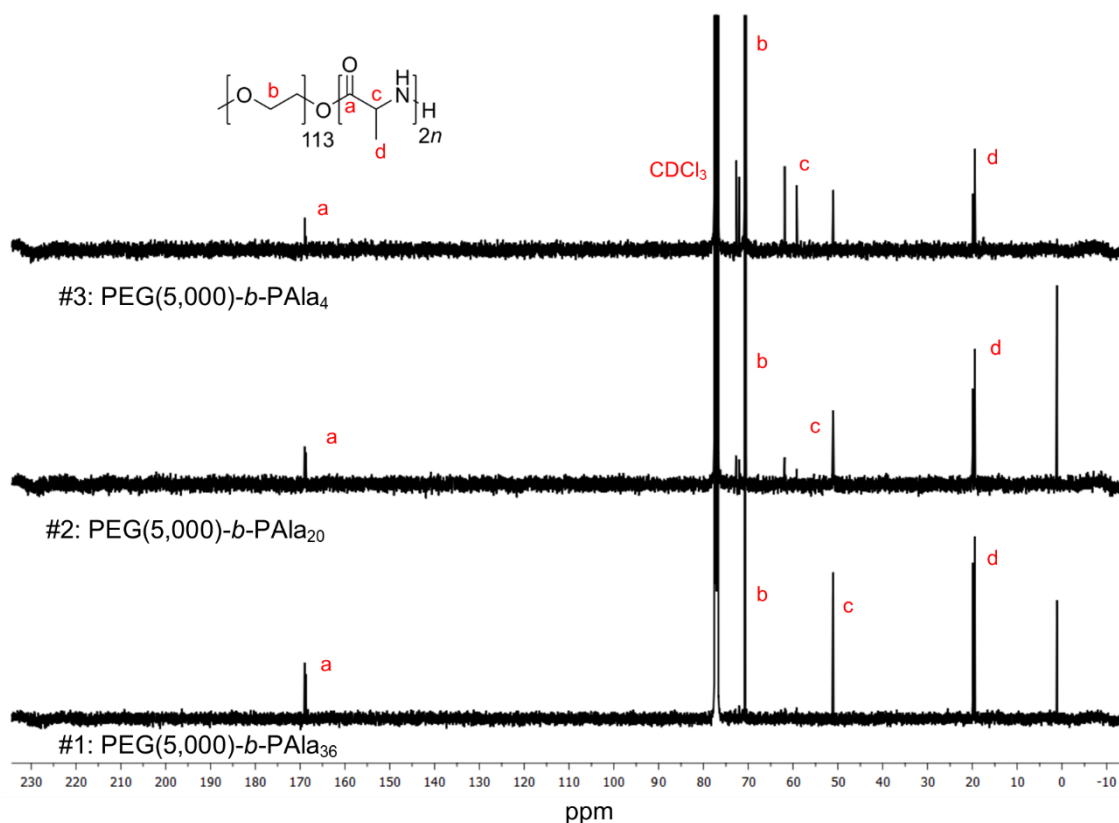


**Figure 5.2**  $^{13}\text{C}$  NMR spectra of the PEG(5,000)-*b*-PAla copolymers (125 MHz,  $\text{CDCl}_3$ ).

Polymer synthesis was also confirmed by FTIR spectroscopy (Figure 5.3a) with all copolymers possessing a peak at  $2881\text{ cm}^{-1}$  corresponding with the C-H functional groups in the structures of both PEG and PAla, and a peak at  $1681\text{ cm}^{-1}$  corresponding with the amide group in PAla. The crystallinity of the polymers were investigated on pXRD. As can be seen in Figure 5.3b, the copolymers are semicrystalline and they contain a peak with  $2\theta = 11.5^\circ$ , which is present in all copolymers, but not PEG(5,000).

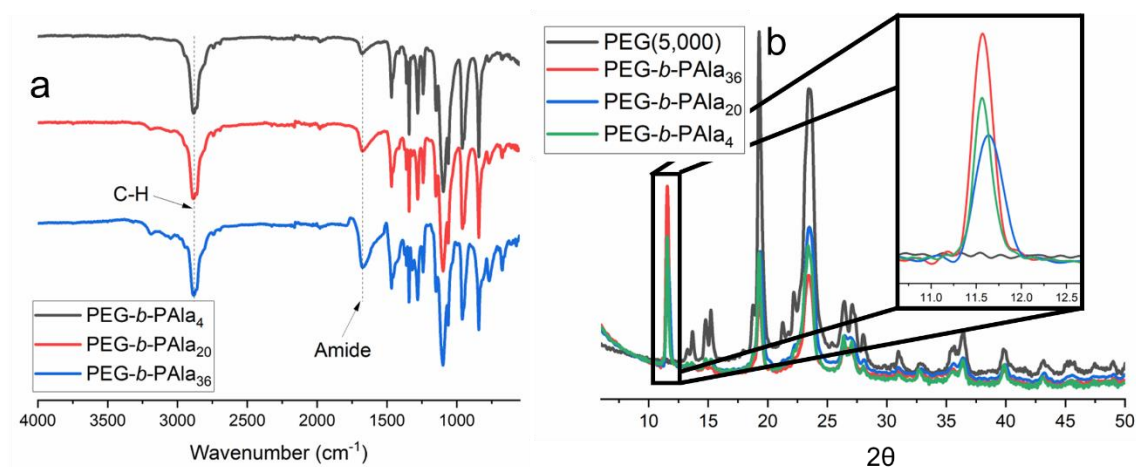


**Figure 5.3** (a) FTIR spectra and (b) pXRD patterns of the PEG-*b*-PAla polymers. Insert: close-up of pXRD pattern.

The effect of catalyst loading on the time to reach 100% equivalence was investigated with two different catalyst loadings: a 1.5:1 and 3.0:1 catalyst/initiator molar ratio. The equivalence was tracked by taking an aliquot of the polymerisation reaction mixture at pre-determined time intervals and analysing the collected sample with <sup>1</sup>H NMR spectroscopy. Figure 5.4 shows that when the catalyst loading is doubled, the time it takes to reach 100% equivalence reduces from nine days to approximately three days. The pseudo-first order behaviour is consistent with Sn(Oct)<sub>2</sub>-catalysed ROP reactions of other systems.<sup>36-38</sup> This conclusion demonstrates the tunability of the reported method to suit the application, as although a shorter polymerisation time is often desired, a significant molar amount of Sn(Oct)<sub>2</sub> catalyst could be undesirable for a biomedical application.

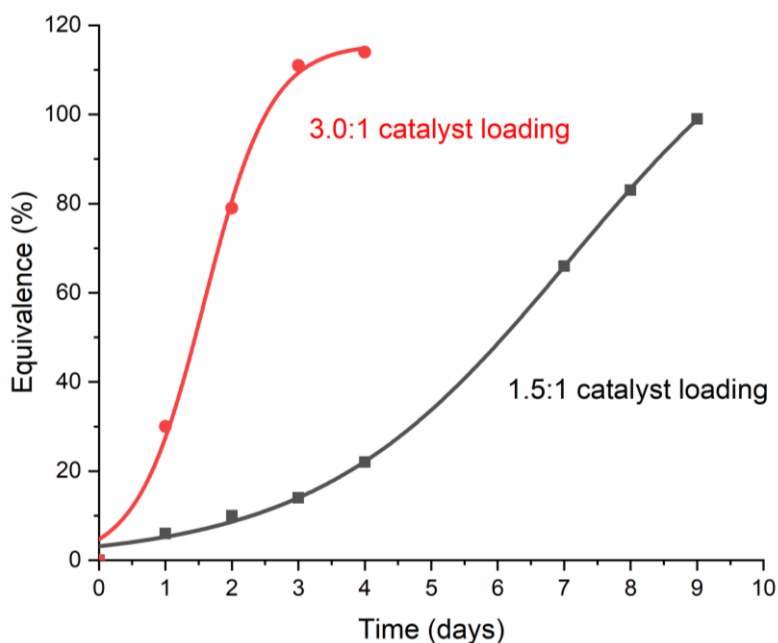


**Figure 5.4** Equivalence over time for the synthesis of PEG(5,000)-*b*-PAla with different catalyst loadings.

### 5.3.2 Polymer NP formation

The amphiphilic block copolymers were able to self-assemble using the ‘dropping-in’ method of NP formation (Section 2.3.3), whereby the polymers were dissolved in chloroform, added dropwise to PBS buffer solution under vigorous stirring, and the chloroform allowed to evaporate. Table 5.2 and Figure 5.5a show the hydrodynamic diameter ( $d_H$ ) of the NPs formed and their PDI values, determined by DLS. The PDI values reveal that the NPs are uniform in size. In order to determine if there was any observable trend in particle size with equivalence, the two parameters were plotted in Figure 5.5b which shows there is no obvious trend and the NPs are all in the 100 nm size order. The NPs were dried and imaged by SEM, whereby Figure 5.5c-d shows the NPs are globular in shape and in the nano scale. Analysis of the SEM images shows PEG(5,000)-*b*-PAla<sub>36</sub> forms NPs with an average particle size of  $52 \pm 10$  nm ( $n = 32$ ) and PEG(5,000)-*b*-PAla<sub>4</sub> has average particle sizes of  $76 \pm 14$  nm ( $n = 32$ ). As expected, the NP diameters are smaller from analysis of the SEM images compared to the  $d_H$  values calculated from DLS because of shrinkage from drying and being under a high vacuum in the SEM chamber.

**Table 5.2** Hydrodynamic diameters ( $d_H$ ) and PDI values of the PEG(5,000)-*b*-PAla polymers measured by DLS.

	Polymer	Hydrodynamic diameter ( $d_H$ ) (nm)	PDI
1	PEG(5,000)- <i>b</i> -PAla <sub>36</sub>	85.27 ± 15.97	0.282
2	PEG(5,000)- <i>b</i> -PAla <sub>20</sub>	122.5 ± 41.16	0.291
3	PEG(5,000)- <i>b</i> -PAla <sub>4</sub>	95.78 ± 20.67	0.290

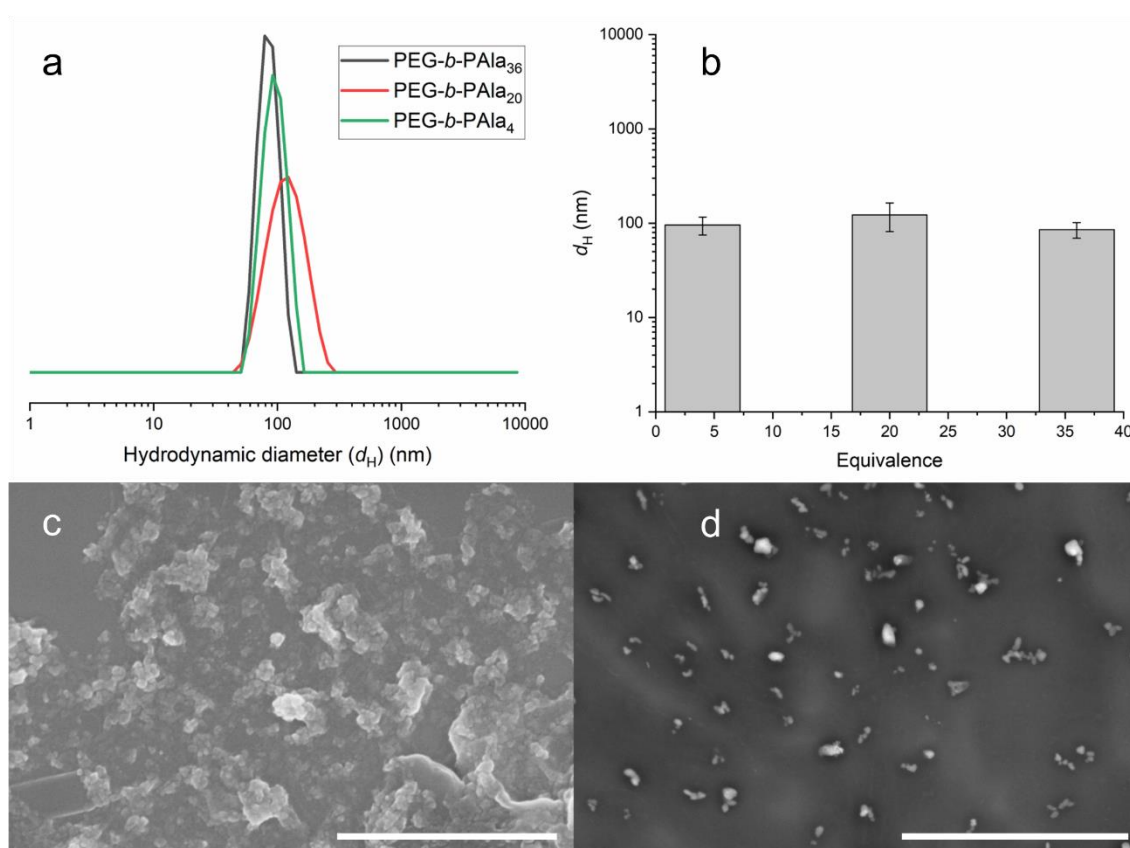


**Figure 5.5** (a)  $d_H$  sizes of the PEG-*b*-PAla polymers determined from DLS, and (b)  $d_H$  plotted against equivalence for the copolymers. (c) SEM images of PEG(5,000)-*b*-PAla<sub>36</sub> (scale bar 1  $\mu$ m) and (d) PEG(5,000)-*b*-PAla<sub>4</sub> (scale bar 2  $\mu$ m).

### 5.3.3 Dox release study of the polymers

The polymers produced possess an ester bond between the PEG and PAla block which is susceptible to acid hydrolysis. This ester functional group can be exploited to provide the polymer NPs with stimuli-responsiveness with respect to pH. A study on the pH-responsiveness of two of the NPs was carried out. PEG-

*b*-PAla<sub>4</sub> and PEG-*b*-PAla<sub>20</sub> NPs were formed using the dropping-in method (Section 5.3.2) but in the presence of Dox. Any excess Dox was washed away and Dox loading quantified using UV-vis spectrophotometry as per Section 2.3.4.2. The Dox loading content and efficiency were calculated from Equations (2.5) and (2.6), respectively, and are shown in Table 5.3. PEG-*b*-PAla<sub>20</sub> has a Dox loading efficiency of 43%, and PEG-*b*-PAla<sub>4</sub> a loading efficiency of 27%. This difference may be due to more Ala units in PEG-*b*-PAla<sub>20</sub>, enabling increased interaction with Dox.

**Table 5.3** Dox loading content and efficiency for PEG-*b*-PAla<sub>4</sub> and PEG-*b*-PAla<sub>20</sub>.

Polymer NP	Dox loading content (%)	Dox loading efficiency (%)
PEG- <i>b</i> -PAla <sub>4</sub>	5	27
PEG- <i>b</i> -PAla <sub>20</sub>	9	43

The Dox-loaded NPs were then dialysed against PBS buffer solutions at pH 7.4 and acetate buffer solutions at pH 5. Aliquots were taken at various time points and the amount of Dox released over time monitored using UV-vis spectrophotometry (Figure 5.6). PEG-*b*-PAla<sub>4</sub> released 78% Dox in pH 5 buffer solution but only 29% in pH 7.4 buffer solution, whilst PEG-*b*-PAla<sub>20</sub> released 73% in pH 7.4 buffer solution but only 20% in pH 7.4 buffer solution, after 96 hours. These polymers therefore display stimuli-responsiveness with respect to pH, releasing significantly less Dox when stored in pH 7.4 solution compared to when stored in pH 5 solution.

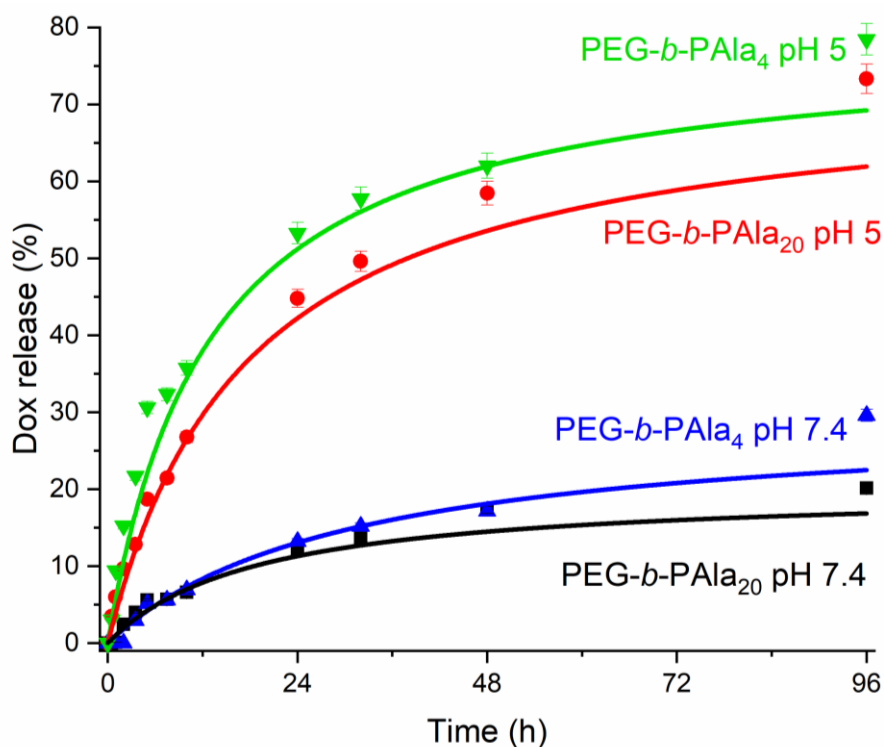


**Figure 5.6** Dox release study over time for PEG-*b*-PAla<sub>4</sub> and PEG-*b*-PAla<sub>20</sub> in pH 7.4 and pH 5 over 96 hours tracked by UV-vis spectrophotometry.

## 5.4 Conclusions

The ROP of alanine anhydride was initiated by the alcohol group of PEG methyl ether using Sn(Oct)<sub>2</sub> as the catalyst for the first time. The synthesis of PEG-*b*-PAla was confirmed by <sup>1</sup>H NMR, <sup>13</sup>C NMR and FTIR spectroscopies. Moreover, <sup>1</sup>H NMR revealed high equivalencies of Ala in the copolymer, and the amphiphilic copolymer was able to self-assemble and form stable NPs with small PDI values, as evidenced from DLS and SEM analysis. The potent chemotherapeutic Dox was loaded into the NPs with good efficiency. A release study of the loaded Dox was performed in buffer solutions of pH 7.4 (physiological pH) and pH 5, which revealed that the NPs displayed stimuli-responsiveness with respect to pH. Only 20-29% of the loaded Dox was released at pH 7.4, but 73-78% of loaded Dox was released at pH 5. This ability to extensively release Dox in acidic environments, and restrictively release Dox at physiological pH, offers these polymers potential as targeted drug delivery vehicles. Additionally, the reported synthesis of PAla avoiding intermediates such as Ala-NCA makes it easier for the

commercialisation of the polymer, introducing its high crystallinity and outstanding mechanical strength to industry.

## 5.5 References

1. K. Tsuchiya, H. Masunaga and K. Numata, *Biomacromolecules*, 2017, **18**, 1002-1009.
2. T. Asakura, Y. Tasei, A. Aoki and A. Nishimura, *Macromolecules*, 2018, **51**, 1058-1068.
3. O. S. Rabotyagova, P. Cebe and D. L. Kaplan, *Macromolecular Bioscience*, 2010, **10**, 49-59.
4. M. Heim, D. Keerl and T. Scheibel, *Angewandte Chemie International Edition*, 2009, **48**, 3584-3596.
5. S. Zhao, X. Ye, M. Wu, J. Ruan, X. Wang, X. Tang and B. Zhong, *International Journal of Molecular Sciences*, 2021, **22**, 1513.
6. K. Tsuchiya and K. Numata, *ACS Macro Letters*, 2017, **6**, 103-106.
7. T. Yoshioka, T. Tsubota, K. Tashiro, A. Jouraku and T. Kameda, *Nature Communications*, 2019, **10**, 1469.
8. Y. Y. Choi, J. H. Jang, M. H. Park, B. G. Choi, B. Chi and B. Jeong, *Journal of Materials Chemistry*, 2010, **20**, 3416-3421.
9. H. R. Kricheldorf, C. von Lossow and G. Schwarz, *Macromolecular Chemistry and Physics*, 2004, **205**, 918-924.
10. T. Endo and A. Sudo, *Biomedicines*, 2020, **8**, 317.
11. T. Endo and A. Sudo, *Polymer International*, 2020, **69**, 219-227.
12. D. Siefker, A. Z. Williams, G. G. Stanley and D. Zhang, *ACS Macro Letters*, 2018, **7**, 1272-1277.
13. J. Cao, D. Siefker, B. A. Chan, T. Yu, L. Lu, M. A. Saputra, F. R. Fronczek, W. Xie and D. Zhang, *ACS Macro Letters*, 2017, **6**, 836-840.
14. T. Xue, Z. Song, Y. Wang, B. Zhu, Z. Zhao, Z. Tan, X. Wang, Y. Xia and J. Cheng, *Macromolecules*, 2020, **53**, 6589-6597.
15. P. J. Baker and K. Numata, *Biomacromolecules*, 2012, **13**, 947-951.
16. E. Alizadeh, D. Gschliesser, P. Bartl, M. Hager, A. Edtbauer, V. Vizcaino, A. Mauracher, M. Probst, T. D. Märk, S. Ptasińska, N. J. Mason, S. Denifl and P. Scheier, *The Journal of Chemical Physics*, 2011, **134**, 054305.
17. C. J. Dinsmore and D. C. Beshore, *Tetrahedron*, 2002, **58**, 3297-3312.
18. C. Guo, J. S. Jordan, J. L. Yarger and G. P. Holland, *ACS Applied Materials & Interfaces*, 2017, **9**, 17653-17661.
19. M. Meng, L. Stievano and J.-F. Lambert, *Langmuir*, 2004, **20**, 914-923.
20. J.-F. Lambert, M. Jaber, T. Georgelin and L. Stievano, *Physical Chemistry Chemical Physics*, 2013, **15**, 13371-13380.
21. K. Zhao, R. Xing and X. Yan, *Peptide Science*, 2021, **113**, e24202.
22. A. D. Borthwick, *Chemical Reviews*, 2012, **112**, 3641-3716.
23. S. M. Weidner and H. R. Kricheldorf, *Macromolecular Chemistry and Physics*, 2018, **219**, 1800445.
24. H. R. Kricheldorf and S. M. Weidner, *Polymer Chemistry*, 2020, **11**, 5249-5260.

25. S. M. Weidner, A. Meyer, J. Falkenhagen and H. R. Kricheldorf, *European Polymer Journal*, 2021, **153**, 110508.
26. C. Noomhorm and Y. Tokiwa, *ScienceAsia*, 2008, **34**, 43-47.
27. B. S. Thorat Gadgil, N. Killi and G. V. N. Rathna, *MedChemComm*, 2017, **8**, 1774-1787.
28. S. Y. Jeong, H. J. Moon, M. H. Park, M. K. Joo and B. Jeong, *Journal of Polymer Science Part A: Polymer Chemistry*, 2012, **50**, 3184-3191.
29. S. Hehir and N. R. Cameron, *Polymer International*, 2014, **63**, 943-954.
30. O. Rathore and D. Y. Sogah, *Journal of the American Chemical Society*, 2001, **123**, 5231-5239.
31. S. Peng, C.-W. Wu, J.-Y. Lin, C.-Y. Yang, M.-H. Cheng and I. M. Chu, *Materials Science and Engineering: C*, 2017, **76**, 181-189.
32. B. Yeon, M. H. Park, H. J. Moon, S.-J. Kim, Y. W. Cheon and B. Jeong, *Biomacromolecules*, 2013, **14**, 3256-3266.
33. M. H. Park, H. J. Moon, J. H. Park, U. P. Shinde, D. Y. Ko and B. Jeong, *Macromolecular Bioscience*, 2015, **15**, 464-472.
34. Y. Wang, Z. Jiang, W. Xu, Y. Yang, X. Zhuang, J. Ding and X. Chen, *ACS Applied Materials & Interfaces*, 2019, **11**, 8725-8730.
35. J. Sim, H. J. Lee, B. Jeong and M. H. Park, *Polymers*, 2021, **13**, 1042.
36. R. F. Storey and J. W. Sherman, *Macromolecules*, 2002, **35**, 1504-1512.
37. C.-S. Xiao, Y.-C. Wang, J.-Z. Du, X.-S. Chen and J. Wang, *Macromolecules*, 2006, **39**, 6825-6831.
38. S. J. Moravek, J. M. Messman and R. F. Storey, *Journal of Polymer Science Part A: Polymer Chemistry*, 2009, **47**, 797-803.

## Chapter 6

### Antimicrobial Dye-Conjugated Polyglobalide-Based Organogels

#### Preamble

This Chapter is based on work published as: J. V. Rowley, P. Wall, H. Yu, G. Tronci, D. A. Devine, J. J. Vernon and P. D. Thornton, "Antimicrobial Dye-Conjugated Polyglobalide-Based Organogels", *ACS Applied Polymer Materials*, 2020, **2** (7), 2927-2933.

#### Abstract

Disperse dyes bearing an alcohol group were firstly modified to present a pendant thiol group via a Steglich esterification. Secondly, the straightforward colouration of polyglobalide by the covalent grafting of a thiol-modified dye to afford a coloured polyester is reported. The coloured polymer could form physical organogels, and upon covalently cross-linking formed chemical organogels in a range of food-grade oils, and the fragrant and antimicrobial molecule 2-phenylethanol. Antimicrobial testing of the 2-phenylethanol-swollen chemical organogels revealed significant antimicrobial activity against both *Staphylococcus aureus* and *Escherichia coli*. The materials reported offer a range of potential applications, particularly as simple and cost-effective antimicrobial gels.

#### 6.1 Introduction

As previously discussed in Section 1.1, commodity polymers such as polyethylene and PET are typically non-biodegradable and the monomers originate from a non-renewable source. Globally, approximately 8.3 billion metric tonnes of polymer is manufactured.<sup>1</sup> In 2017 approximately 40% of polymers

produced were classified as being non-biodegradable and from a non-renewable source.<sup>2-3</sup> Additionally, inefficient colouration of commodity polymers because of the lack of suitable chemical functionality leads to coloured wastewater, an aesthetic, ecological and environmental issue (Section 1.1.3).<sup>4-5</sup> Consequentially, there is an urgent demand for the creation of renewable and degradable polymers that can be efficiently and permanently coloured and applied commercially.<sup>6-8</sup>

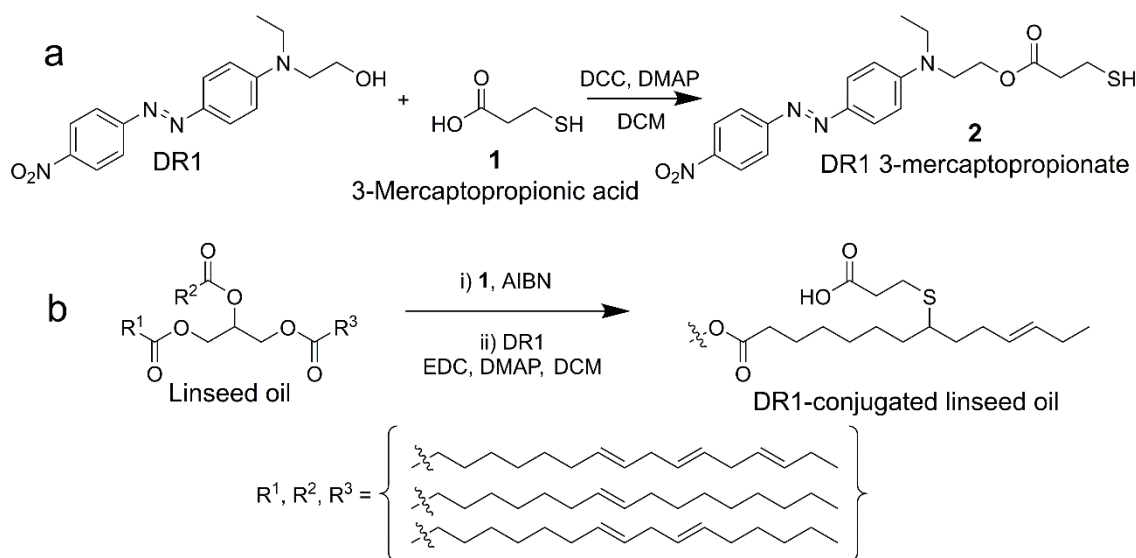
### 6.1.1 Polyglobalide (PGI)

Aliphatic polyesters have significant potential for use in numerous artifacts in sectors ranging from packaging to personal care products due to their degradability<sup>9</sup> and biocompatibility.<sup>10-13</sup> Additionally, many aliphatic polyesters can be created from renewable sources, such as sweet corn harvested to produce poly(lactic acid).<sup>14</sup> However, such polyesters often lack chemical functionality to enable chemical conjugation to the polymer backbone, restricting post-polymerisation functionalisation which may add value to the polymer.

Polyglobalide (PGI) is a noncytotoxic, potentially biodegradable, aliphatic polyester that has potential use within a biomedical setting.<sup>15-17</sup> Polymer synthesis is achieved by the enzymatic ROP (Section 1.3.2.2) of globalide (11/12-pentadecen-15-olide), a 16-membered cyclic lactone with two constitutional isomers: a C=C double bond at the eleven position and the other at the twelve position. Globalide is primarily used in the fragrance industry due to its musky fragrance and ability to release the aroma slowly.<sup>18-19</sup> Similar unsaturated cyclic macrolactones may be obtained from a renewable source, for instance, the essential oil from *Angelica archangelica*.<sup>20-21</sup> Crucially, globalide contains a C=C double bond which is transferred to the polymer and may be used for post-polymerisation functionalisation.<sup>22-24</sup>

## 6.1.2 Covalent dyeing of PGI

Reactive dyes that present thiol functionality are highly desirable owing to their capability to covalently couple to materials that present reactive C=C double bonds via efficient thiol-ene click chemistry reactions.<sup>25</sup> For example, Hayashi and Thornton chemically modified C.I. Disperse Red 1 (DR1) via a Steglich esterification reaction with 3-mercaptopropionic acid (**1**), yielding a thiol-bearing analogue (**2**, DR1 3-mercaptopropionate) (Scheme 6.1a).<sup>26</sup> Hayashi and colleagues used this chemistry to covalently conjugate DR1 to the C=C double bonds in linseed oil (Scheme 6.1b), for coloured, bio-derived, molecules which can potentially be applied as coatings.<sup>27</sup> This conversion from a disperse dye to a reactive dye holds promise for the efficient colouration of (macro)molecules that present C=C double bonds, such as PGI. Polymers coloured in this way will likely possess enhanced colour fastness compared to polymers coloured by a nonreactive dye that interacts with the substrate through non-covalent interactions.



**Scheme 6.1** (a) Conversion of DR1 into thiol-bearing DR1 and (b) covalent conjugation of DR1 to linseed oil.<sup>26-27</sup> DCC = *N,N*-dicyclohexylcarbodiimide; DMAP = 4-(dimethylamino)pyridine; AIBN = 2,2'-azobis(2-methylpropionitrile); EDC = 1-ethyl-3-(3-dimethylaminopropyl)carbodiimide.

### 6.1.3 Antimicrobial Organogels

The C=C double bonds of PGI may also be exploited for covalent cross-linking to yield a non-soluble material. The lack of polarity of PGI ensures that chemically cross-linked PGI may readily swell, but not dissolve, in a range of organic solvents, enabling the creation of organogels. Organogels are similar to hydrogels (Section 1.4.2) whereby the dispersant is an organic solvent or oil instead of an aqueous solution,<sup>28</sup> and have application in dye effluent removal,<sup>29</sup> oil spillage clean-up,<sup>30</sup> cosmetics,<sup>31</sup> and fluorescent displays.<sup>32</sup> Organogels are increasingly being employed as biomaterials due to their inherent stability, ease of preparation and capability to deliver guest molecules in a controlled manner.<sup>33-37</sup>

Organogels that aid the treatment of ailments caused or exacerbated by bacterial infection are extremely promising, and organogels with antimicrobial activity against *Escherichia coli*,<sup>38-40</sup> *Bacillus subtilis*,<sup>39, 41-43</sup> *Staphylococcus aureus*,<sup>44</sup> and *Candida albicans*<sup>45</sup> have been reported. Recently, Chen and Zhang developed a facile method of fabricating organogels of alginate, soy protein and corn oil.<sup>46</sup> Firstly, the authors formed an alginate/soy protein emulsion and conjugated the reagents via the Maillard reaction. On freeze-drying, an aerogel was obtained, and dipping the aerogel template into corn oil formed an organogel (Figure 6.1). Thymol, a strong antiseptic, was dissolved in the corn oil (5% thymol concentration) and the release of thymol from the organogel showed maximum antimicrobial efficiency of 53.9% against *E. coli* and 43.0% against *S. aureus* after 24 h.

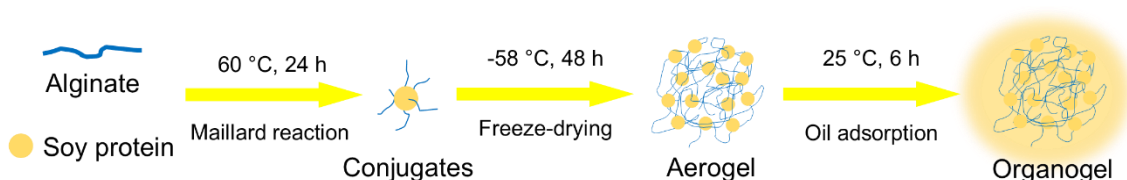


**Figure 6.1** Conjugation of alginate/soy protein via the Maillard reaction and organogel formation from the resulting aerogel by oil adsorption.<sup>46</sup>

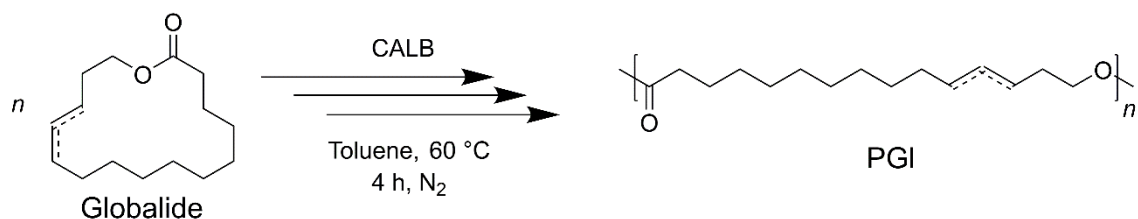
### 6.1.4 Summary

In this Chapter, the straightforward synthesis and colouration of PGI using thiol-modified DR1 and C.I. Disperse Blue 3 (DB3) is described to yield two permanently coloured polyesters. DR1 and DB3 were selected as two disperse dyes commonly used industrially, while the thiol-ene reaction was pursued to achieve coloured polymers and coloured covalently cross-linked polymer networks in one-step. Additionally, extensive cross-linking prevents the polymer from melting, rendering its use in recyclable packaging, which undergoes washing between use in warm solutions that may melt linear PGI, more feasible. The resulting thermoset polymers were able to form organogels when independently dispersed in a range of food-grade oils and the antimicrobial compound 2-phenylethanol. Finally, the antimicrobial activity of 2-phenylethanol-swollen organogels was tested against *S. aureus* and *E. coli*. It is envisioned that such materials hold great promise as potential biomaterials, rheology modifiers for personal care products, and antimicrobial gels.

## 6.2 Experimental Details

### 6.2.1 Synthesis of PGI

Globalide was polymerised as previously described (Scheme 6.2).<sup>47</sup> Briefly, globalide (2.11 g, 8.81 mmol) and CALB (recombinant lipase B from *Candida antarctica* immobilised on Immobead 150, recombinant from yeast) (0.44 g,  $\geq 2,000$  U g<sup>-1</sup>) were dissolved in anhydrous toluene (4.6 mL) in a Schlenk tube and stirred at 60 °C for four hours under a N<sub>2</sub> flow. To quench the reaction, DCM (10 mL) was added and CALB removed by vacuum filtration. The filtrate was added dropwise to ice-cold methanol (30 mL) to precipitate PGI, which was collected by vacuum filtration, washed with methanol, and dried *in vacuo* to yield an off-white crystalline polymer (yield 69%). FTIR ( $\nu_{\text{max}}$ , solid): 2918 cm<sup>-1</sup> (C-H), 2850 cm<sup>-1</sup> (C-H) and 1731 cm<sup>-1</sup> (ester).



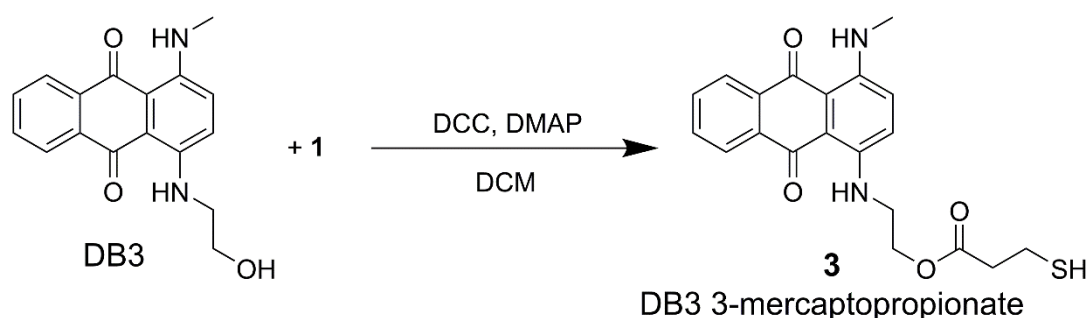
**Scheme 6.2** Reaction scheme for the CALB-catalysed ROP of globalide to synthesise PGI.

### 6.2.2 Synthesis of DR1 3-mercaptopropionate (**2**) and DB3 3-mercaptopropionate (**3**)

DR1 3-mercaptopropionate (**2**) was synthesised as previously reported (Scheme 6.1a).<sup>26</sup> Briefly, DR1 (1.04 g, 3.30 mmol), 4-dimethylaminopyridine (DMAP) (3 mg, 0.03 mmol), and 3-mercaptopropionic acid (**1**) (1.49 mL, 16.50 mmol) were mixed in anhydrous DCM (100 mL) and stirred at 0 °C under a N<sub>2</sub> flow. Over a ten minute period, a solution of *N,N*-dicyclohexyl-carbodiimide (DCC) (3.41 g, 16.50 mmol) in anhydrous DCM (30 mL) was added dropwise to the DR1 mixture and the reaction allowed to stir at 0 °C for two hours. HCl (0.5 M, 300 mL) was then added, forming a white precipitate, which was removed by filtration. The organic layer was washed with NaHCO<sub>3</sub> and then water, while the aqueous layer was washed with DCM before the organic layers were combined and dried over MgSO<sub>4</sub>. The solution was concentrated by rotary evaporator and purified by column chromatography (DCM) monitored by TLC (DCM). The eluents collected were precipitated in ice-cold hexane and collected by centrifugation (4,500 r.p.m., 15 min) as a red crystalline product (yield 68%).

<sup>1</sup>H NMR (400 MHz, CDCl<sub>3</sub>): δ 8.26 ppm (dt, Ar adjacent NO<sub>2</sub>), δ 7.85 ppm (tt, Ar), δ 6.74 ppm (dt, Ar), δ 4.28 ppm (t, CH<sub>2</sub> adjacent COO), δ 3.64 ppm (t, CH<sub>2</sub> adjacent amine), δ 3.47 ppm (q, CH<sub>2</sub> adjacent amine), δ 2.68 ppm (t, CH<sub>2</sub> adjacent C=O ester), δ 2.59 ppm (t, CH<sub>2</sub> adjacent thiol), δ 1.20 ppm (t, CH<sub>3</sub>). <sup>13</sup>C NMR (100 MHz, CDCl<sub>3</sub>): δ 171.5 ppm (ester), δ 156.7 ppm (Ar-N<), δ 151.2 ppm (Ar-N=N), δ 143.9 ppm (Ar-NO<sub>2</sub>), δ 126.3 ppm (Ar), δ 124.7 ppm (Ar), δ 122.7 ppm (Ar), δ 111.5 ppm (Ar), δ 61.6 ppm (-COO-), δ 48.8 ppm (C-N), δ 45.7 ppm (C-N), δ 38.4 ppm (-C-COO-), δ 19.6 ppm (C-SH), δ 12.3 ppm (C-C-N).

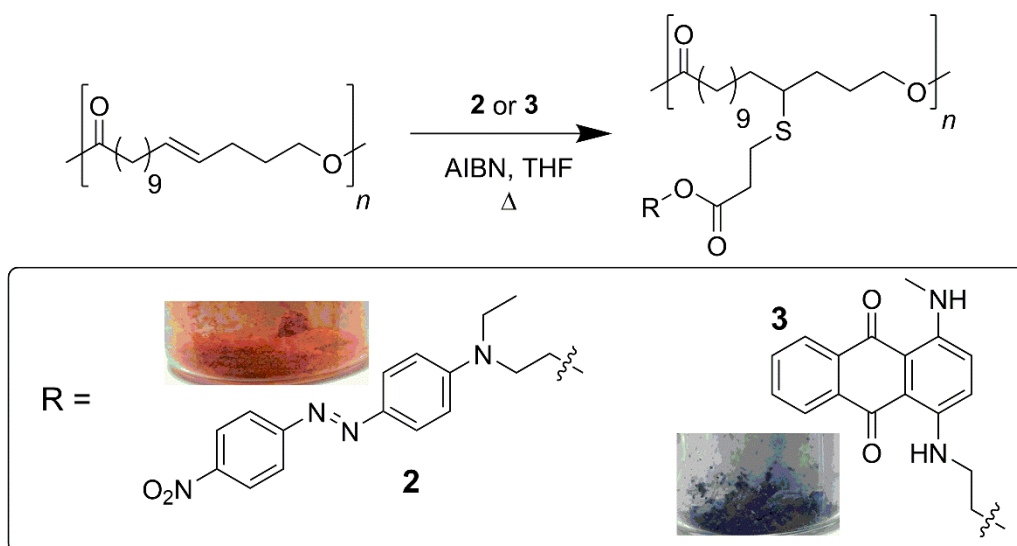
An analogous method was used to synthesise DB3 3-mercaptopropionate (**3**) (Scheme 6.3). DB3 (978 mg, 3.30 mmol), DMAP (3 mg, 0.03 mmol), and **1** (1.50 mL, 16.50 mmol) were combined with anhydrous DCM (80 mL). To this stirring DB3 mixture, a solution of DCC (3.41 g, 16.50 mmol) in anhydrous DCM (30 mL) was added dropwise over a ten minute period at 0 °C under a N<sub>2</sub> flow. After a further two hours of stirring at 0 °C, HCl (0.5 M, 200 mL) was added and the white precipitate that formed was removed by filtration. The filtrate was washed and purified as per the procedure above, yielding a fine blue powder (yield 9%).



**Scheme 6.3** Reaction scheme for the Steglich esterification of DB3 with 3-mercaptopropionic acid to afford DB3 3-mercaptopropionate (**3**).

### 6.2.3 Dyeing of PGI with DR1 3-mercaptopropionate or DB3 3-mercaptopropionate

PGI (120 mg, 0.01 mmol), **2** or **3** (12 mg, 0.04 mmol), and 2,2'-azobis(2-methylpropionitrile) (AIBN) (30 mg, 0.18 mmol) were dissolved in anhydrous THF (5 mL) and stirred at 60 °C under a N<sub>2</sub> flow (Scheme 6.4). After ~46 h, DCM (8 mL) was added and the solution added dropwise to ice-cold methanol (40 mL) to precipitate coloured product (red for **2** or blue for **3**), which was collected by centrifugation (4,500 r.p.m., 15 mins). The dyed polymer was then washed with methanol until the washings became colourless (yield 75%).



**Scheme 6.4** Thiol-ene coupling of PGI with **2** or **3** to yield PGI that is dyed red (left inset, photo of collected red PGI) or blue (right inset, photo of collected blue PGI).

## 6.2.4 PGI organogels

### 6.2.4.1 Physical PGI organogels

To PGI (50 mg), a collection of food-grade solvents (2-phenylethanol, safflower oil, linseed oil, olive oil, and corn oil) were independently added, and the suspensions sonicated to ensure thorough mixing. The mixtures were taken to and just beyond the point of maximum gelation, and the maximum point of gelation for each solvent was recorded.

### 6.2.4.2 Rheological analysis of gels formed

Rheological data were obtained on a TA Instruments AR1500ex rheometer fitted with a 40 mm 3° steel cone and operating an oscillation procedure at 25 °C with a constant strain rate of 0.05%.

### 6.2.4.3 Cross-linking PGI

Various PGI organogels were synthesised that contained various amounts of 2,2'-(ethylenedioxy)diethanethiol (EDT) cross-linkers. As a representative example, PGI (300 mg, 0.01 mmol), EDT (0.5 mL, 3.07 mmol), and AIBN (50 mg, 0.30 mmol) were dissolved in anhydrous THF (10 mL) in a 15 mL sample vial. After being left to stir gently with a magnetic stirrer bar at 60 °C under a flow of N<sub>2</sub> for ~26 h, a colourless gel had formed. The cross-linked polymer was dialysed against DI water (2,000 Da MWCO) and lyophilised.

Coloured cross-linked PGI was synthesised in a one-pot procedure. For example, PGI (290 mg, 0.01 mmol), **3** (1 mg, 0.003 mmol), and AIBN (50 mg, 0.30 mmol) were dissolved in anhydrous THF (8 mL). EDT (0.5 mL, 3.07 mmol) was then added to the blue-coloured THF solution at which point simultaneous cross-linking and dye conjugation reactions occurred by stirring at 60 °C under a flow of N<sub>2</sub>. The coloured, cross-linked, PGI was dialysed against DI water (2,000 Da MWCO) and lyophilised.

#### 6.2.4.4 Cross-linked PGI gelation

Coloured, cross-linked PGI (122 mg) was weighed into a small glass vial, and 2-phenylethanol was added until it no longer caused the cross-linked PGI to swell. The point before turning the vial upside down and the solvent that could be decanted were taken to be the maximum amount of solvent required to gel (730 mg). The degree of swelling was calculated to be 497.0 % by Equation (6.1).

$$\text{Degree of swelling} = 100\% * \frac{(\text{swollen mass} - \text{initial mass})}{\text{initial mass}} \quad (6.1)$$

### 6.2.5 Antimicrobial activity testing of the cross-linked organogels

#### 6.2.5.1 Initial sampling

The antimicrobial activity of the 2-phenylethanol-swollen organogels were tested against *E. coli* National Collection of Type Cultures (NCTC) 11954 and *S. aureus* NCTC 8532 strains. Organogels with concentrations of 84, 72, 60, and 48 mg mL<sup>-1</sup> in 2-phenylethanol were generated in both a colourless and blue-coloured formulation by casting in Corning 24-well plates. A cross-linked polymer (10 mg) in the absence of a solvent was tested as a control. The polymer-containing plates were UV-sterilised for 30 min at 254 nm prior to antibacterial testing. Polymer-free bacterial cultures acted as positive (growth) controls, while sterile broths functioned as negative controls.

Bacteria were cultured on Colombia blood agar (CBA) plates supplemented with 5% oxalated horse blood in 5% (v/v) CO<sub>2</sub> at 37 °C for 18 h. Single colonies were inoculated into 5 mL of brain heart infusion (BHI) broths, which were incubated at 37 °C while agitated at 150 r.p.m. (Thermo Scientific MaxQ 4450). Optical densities (OD<sub>600</sub>) of overnight cultures were measured to estimate the viable count of the undiluted suspension (based on calibration curve data). Inocula (500 µL) were added to polymer-containing wells and incubated overnight at 37 °C with gentle agitation (70 r.p.m., MaxQ 4450). Samples from these cultures were serially diluted in PBS solution and viable bacteria populations enumerated on incubated CBA, as previously discussed. All experiments were performed in biological triplicate with plate enumerations implemented on four separate occasions.

#### **6.2.5.2 Statistical analysis**

Statistical analysis was performed using IBM SPSS Statistics 25, and groups were compared by the Kruskal-Wallis test with the Bonferroni adjustment; \* $p < 0.05$ , \*\* $p < 0.01$ .

## 6.3 Results and Discussion

### 6.3.1 Polymer and dye synthesis

PGI was synthesised by the CALB enzyme-catalysed ROP of globalide. To maintain the activity of lipase B, the temperature of the reaction was limited to 70 °C. An off-white crystalline solid was produced and confirmed to be PGI by  $^1\text{H}$  (Figure 6.2a) and  $^{13}\text{C}$  NMR (Figure 6.2b) spectroscopy. APC analysis revealed the PGI produced has a  $M_n$  of 30,000 Da and a  $\bar{D}$  of 1.38 (Figure 6.3a), whilst DSC analysis found the PGI to have a melting point of 45 °C (Figure 6.3b).

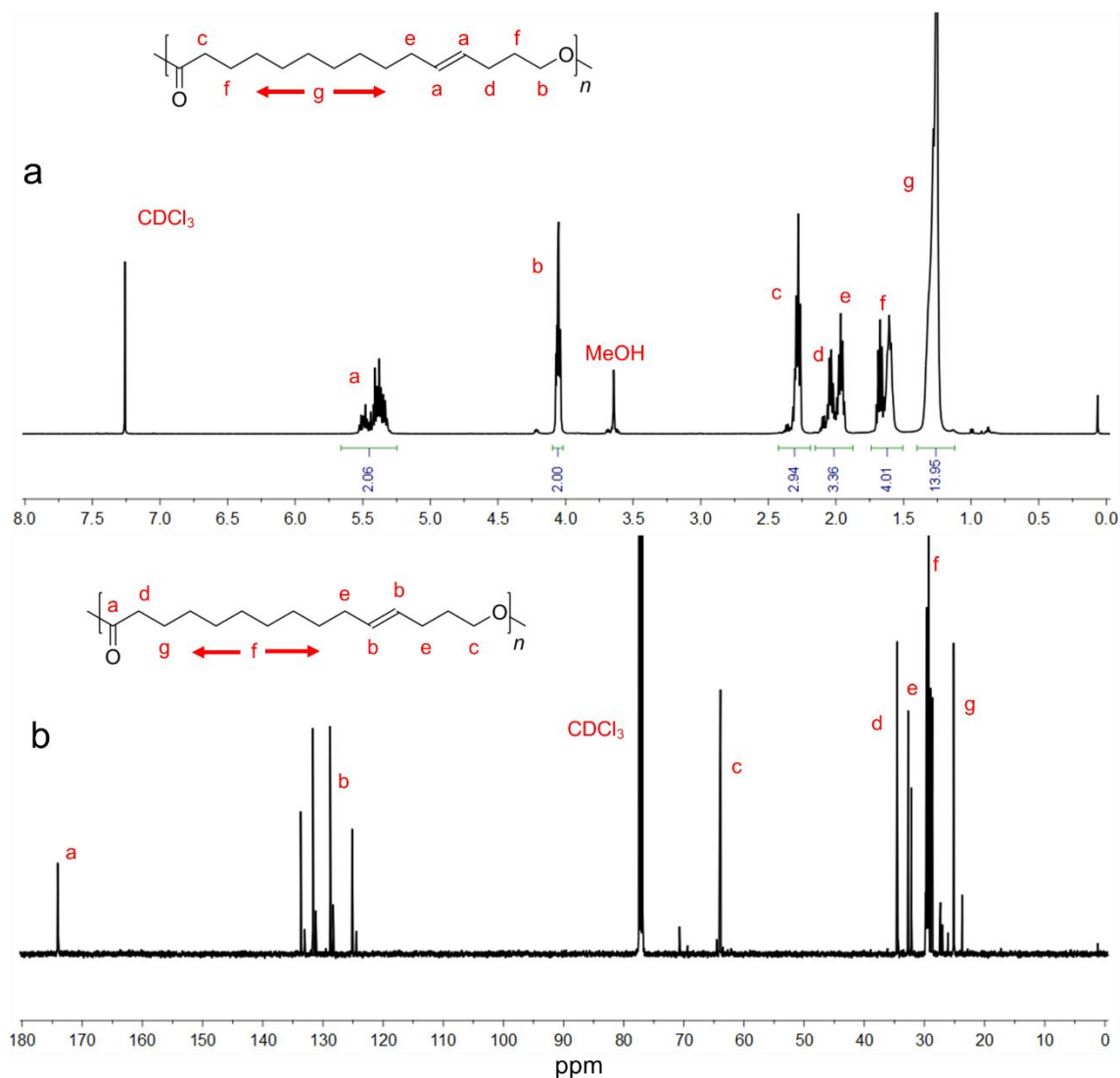


**Figure 6.2**  $^1\text{H}$  (a, 500 MHz,  $\text{CDCl}_3$ ) and  $^{13}\text{C}$  (b, 125 MHz,  $\text{CDCl}_3$ ) NMR spectra of PGI.

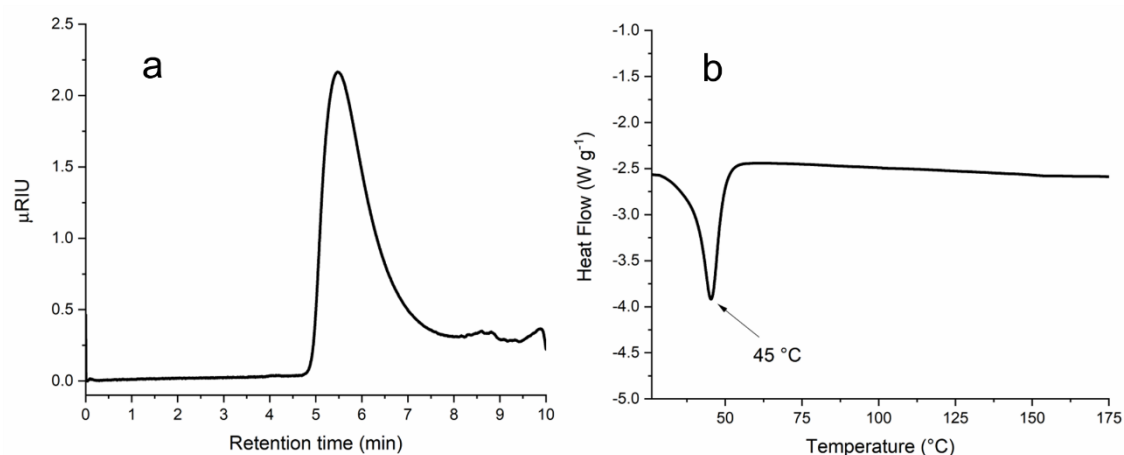


**Figure 6.3** APC chromatogram (a) and DSC thermogram (b) of PGI.

Thiol-bearing DR1 (DR1 3-mercaptopropionate) (**2**) and DB3 (DB3 3-mercaptopropionate) (**3**) were synthesised by Steglich esterification. The synthesis of **2** was confirmed by FTIR spectroscopy, and two further products that may be used for the colouration of PGI were also obtained from the reaction, DR1 bis(3-mercaptopropionate), and DR1 tris(3-mercaptopropionate) (Figure 6.4). All spectra reveal peaks corresponding to an S-H thiol stretch at  $2563\text{ cm}^{-1}$  and a C=O ester stretch at  $1721\text{ cm}^{-1}$ . The UV-vis absorbance spectrum of DR1 was near identical to those of **2** (Figure 6.4b), DR1 bis(3-mercaptopropionate) (Figure 6.4c), and DR1 tris(3-mercaptopropionate) (Figure 6.4d). DR1 revealed a maximum absorbance at 486 nm, whereas the thiol-functionalised derivatives had maximum absorptions at 476 nm, representing a hypsochromic shift.

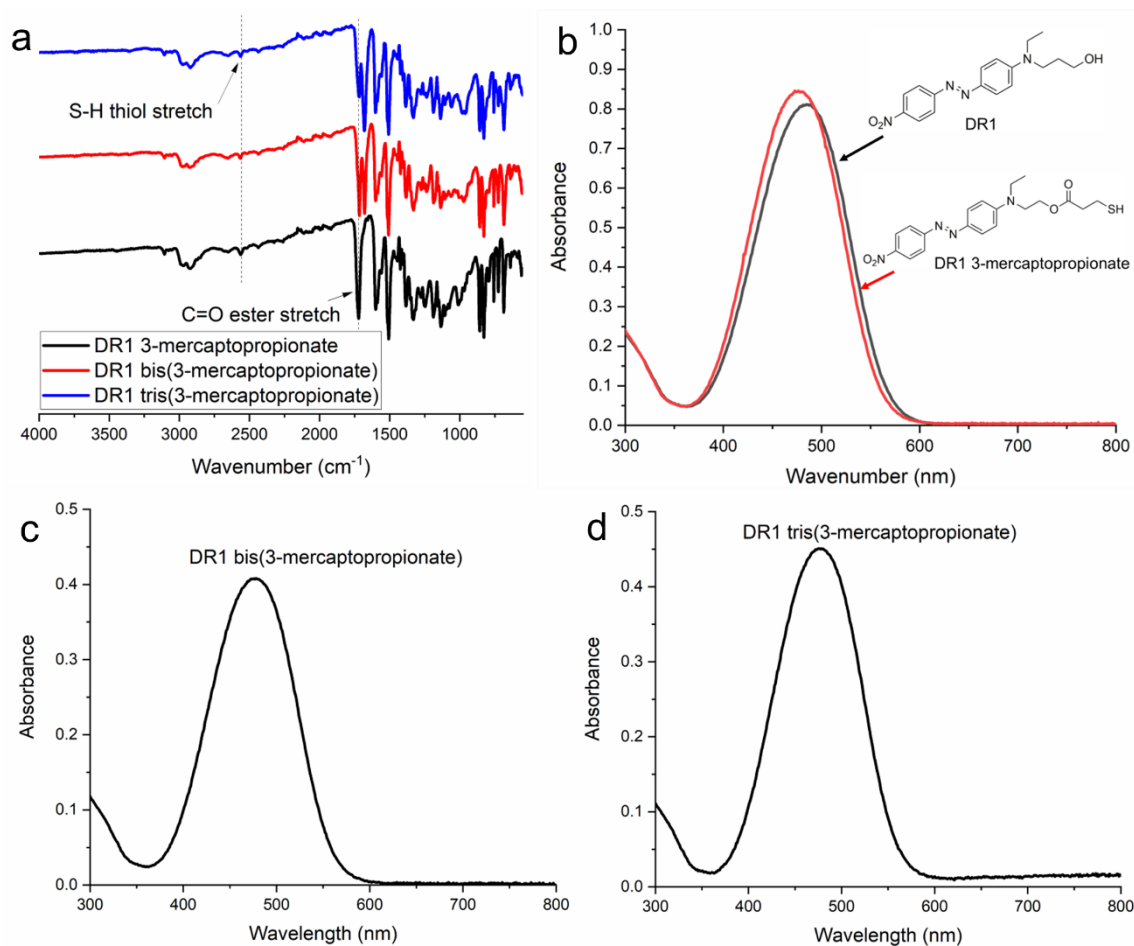


**Figure 6.4** (a) FTIR spectra of DR1 3-mercaptopropionate, DR1 bis(3-mercaptopropionate) and tris(3-mercaptopropionate); UV-vis absorbance spectra of (b) DR1 and DR1 3-mercaptopropionate, (c) DR1 bis(3-mercaptopropionate), and (d) DR1 tris(3-mercaptopropionate).

<sup>1</sup>H NMR spectroscopy was employed to analyse **2**, DR1 bis(3-mercaptopropionate) (Figure 6.5a), and DR1 tris(3-mercaptopropionate) (Figure 6.5b). The latter is particularly informative as the integration values of the peaks at 3.09 and 3.05 ppm have increased by a factor of two, confirming the successful formation of DR1 tris(3-mercaptopropionate). This trimer was not reported in the work by Hayashi and Thornton.<sup>26</sup> Yields of 41.4%, 20.1%, and 6.6% were obtained for **2**, DR1 bis(3-mercaptopropionate), and DR1 tris(3-mercaptopropionate), respectively (68.1% yield of the coloured material overall). All three products are suitable for use as a reactive dye in thiol-ene coupling reactions as they each contain a thiol group and azobenzene chromophore.

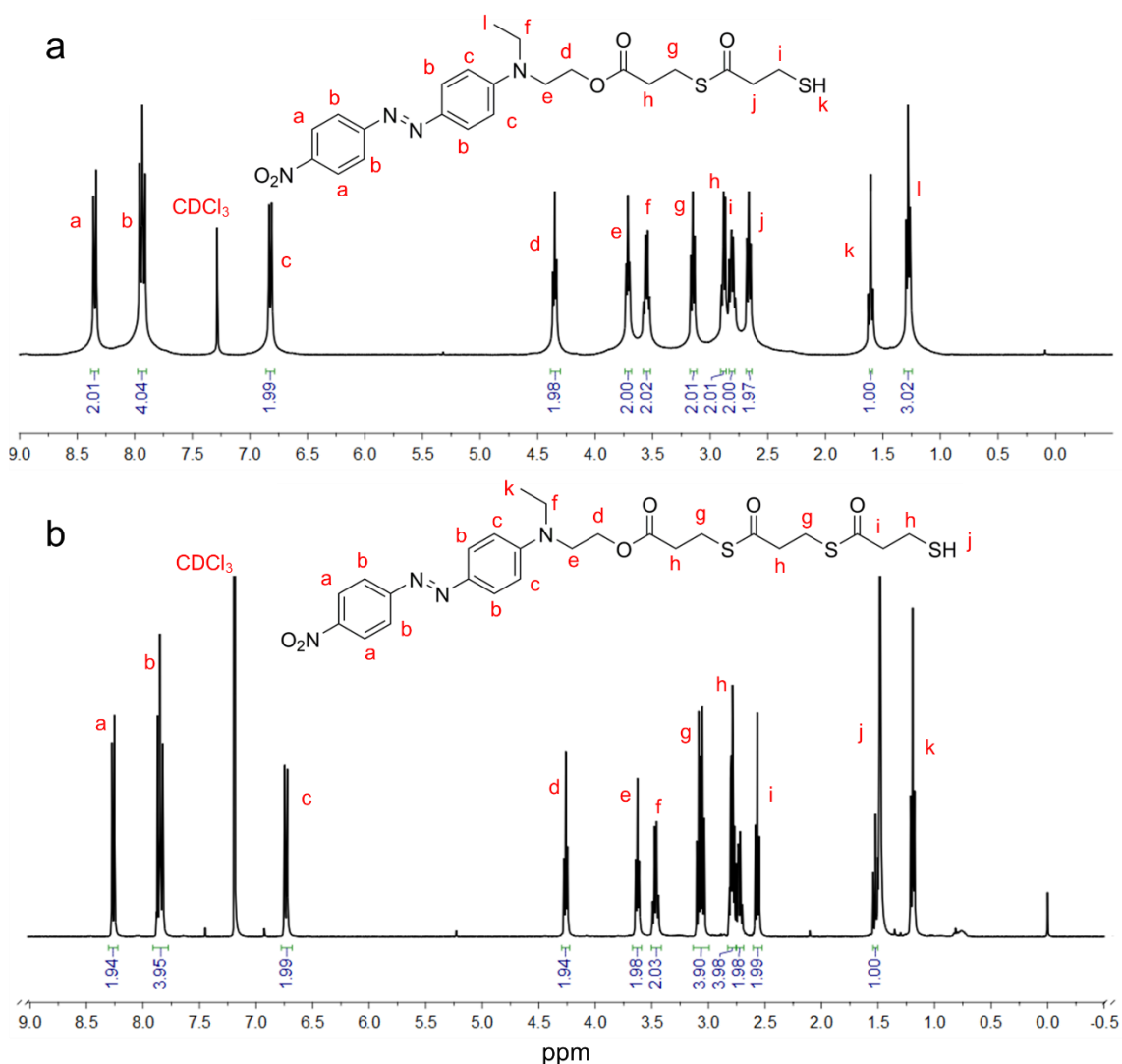


**Figure 6.5**  $^1\text{H}$  NMR spectra of DR1 bis(3-mercaptopropionate) (a) and DR1 tris(3-mercaptopropionate) (b) (400 MHz,  $\text{CDCl}_3$ ).

$^1\text{H}$  NMR spectroscopy was also used to confirm successful synthesis of **3** (Figure 6.6a). Notably, the peak at 1.60 ppm, which corresponds to the thiol proton, is absent from the  $^1\text{H}$  NMR spectrum of unmodified DB3. In addition, peaks at 2.73 and 3.13 ppm that originate from conjugated 3-mercaptopropionate are present in the spectrum of **3** but are lacking in that of DB3. FTIR analysis of **3** revealed a weak peak corresponding to the S-H thiol stretch at  $2567\text{ cm}^{-1}$  and a peak representing the C=O ester stretch at  $1739\text{ cm}^{-1}$  (Figure 6.6b). The UV-vis absorbance spectrum of **3** revealed maximum absorbance values of 554, 594, and 641 nm that are comparable to the spectrum of DB3, which has maximum absorbance values of 559, 599, and 646 nm (Figure 6.6c). Similar to that which occurred in the synthesis of **2**, the maximum absorbance values of DB3 hypsochromically shifted after esterification.

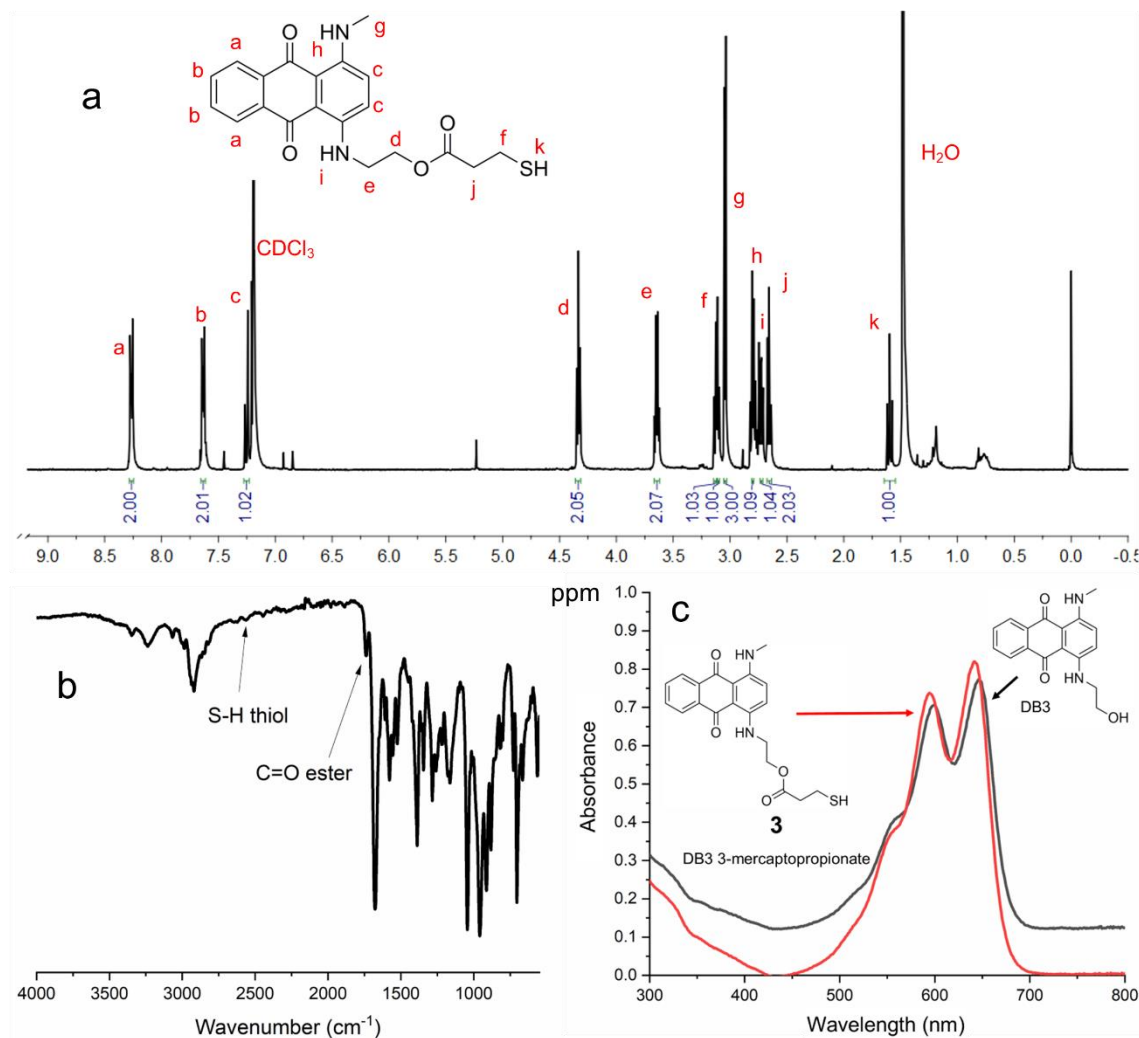


**Figure 6.6**  $^1\text{H}$  NMR (400 MHz,  $\text{CDCl}_3$ ) (a), FTIR (b) and UV-vis absorbance (c) spectra of DB3 3-mercaptopropionate.

### 6.3.2 Covalent conjugation of PGI with DR1 3-mercaptopropionate (2) and DB3 3-mercaptopropionate (3)

**2** and **3** were used to covalently dye PGI via thiol-ene coupling. After dyeing, the coloured polymer was washed thoroughly with methanol, a solvent that readily solubilises both modified dye molecules, until the washings were colourless to ensure any dye remaining was covalently bound to PGI.  $^1\text{H}$  NMR analysis confirmed the successful conjugation of **2** (Figure 6.7a) and **3** (Figure 6.7b) to PGI. Based on comparing the integrals of peaks corresponding to the methylene group adjacent to the terminal hydroxyl group of PGI (f for **2** or e for **3**) with peaks

corresponding to the aromatic groups of **2** (a-c) and **3** (a & b), dye conjugation to PGI was found to be ~2% for both dyes.

FTIR analysis of the polymer dyed with **2** revealed peaks that are attributed to PGI, and additional peaks at  $1604\text{ cm}^{-1}$ , corresponding to the azobenzene group on **2**, and  $1520\text{ cm}^{-1}$ , representing the  $\text{NO}_2$  asymmetric stretch of **2** (Figure 6.7c). The FTIR spectrum of PGI dyed with **3** contains the peaks that are attributed to PGI plus an additional peak at  $1677\text{ cm}^{-1}$ , which corresponds to the aromatic ketone of **3** (Figure 6.7c). It was found that the melting transition of PGI increased slightly from  $45\text{ }^\circ\text{C}$  for linear PGI (Figure 6.3b) to  $51\text{-}52\text{ }^\circ\text{C}$  for dyed PGI (Figure 6.7d). This increase in the melting point is likely due to restricted polymer flexibility as a result of the conjugated pendant groups.

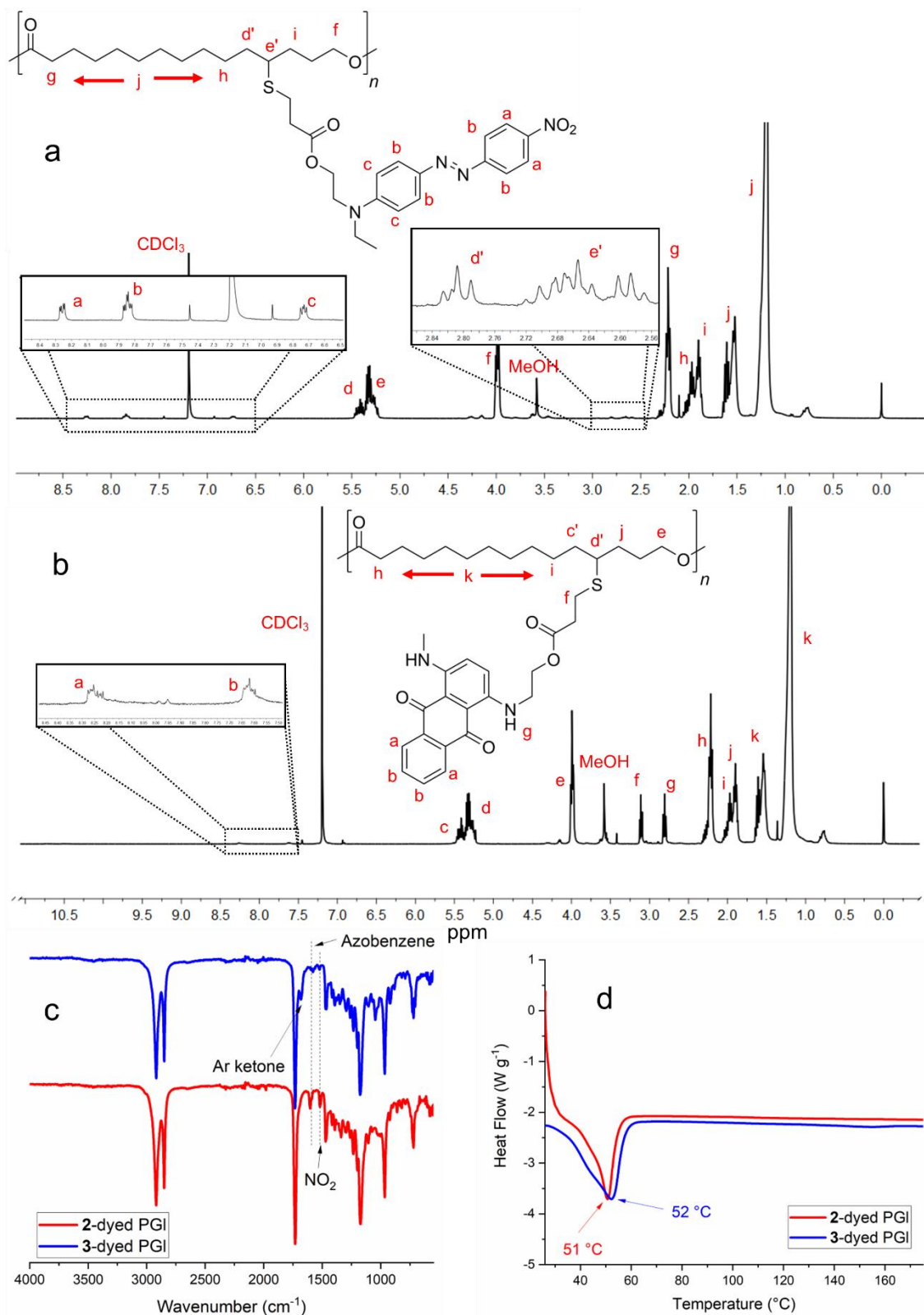


**Figure 6.7** Analysis of PGI dyed with **2** and **3**.  $^1\text{H}$  NMR (400 MHz,  $\text{CDCl}_3$ ) spectra of (a) **2**-dyed and (b) **3**-dyed PGI; (c) FTIR spectra of the dyed PGI; and (d) DSC thermogram of **2**- and **3**-dyed PGI.

### 6.3.3 PGI-based physical organogels

The capability of linear PGI to form physical organogels via organic solvent uptake was assessed using various nonaqueous solvents as the continuous phase (Table 6.1). 2-Phenylethanol was selected as it is a fragrant and antimicrobial molecule, and so, any gel formed has a potential application as a perfumed, antimicrobial gel.<sup>48</sup> The gel swollen in 2-phenylethanol was a physical gel, whereby the elastic modulus ( $G'$ ) exceeds the viscous modulus ( $G''$ ) at higher angular frequency owing to relative freedom of the polymer chains within the physically cross-linked network (Figure 6.8). The other oils tested are certified food grade, and so, gels formed have potential *in vivo* application. In all cases, self-supporting materials were formed with the lowest and highest quantity of polymer (disperse phase) required for organogel formation being when corn oil (11.3% PGI) and 2-phenylethanol (24.8% PGI) were used as the continuous phase (Table 6.1).

**Table 6.1** Minimum weight percentage of PGI required to form a self-supporting organogel in various continuous phases.

<b>Weight % of polymer required for gel formation</b>				
2-Phenylethanol	Safflower oil	Linseed oil	Olive oil	Corn oil
24.8	15.5	20.8	21.1	11.3

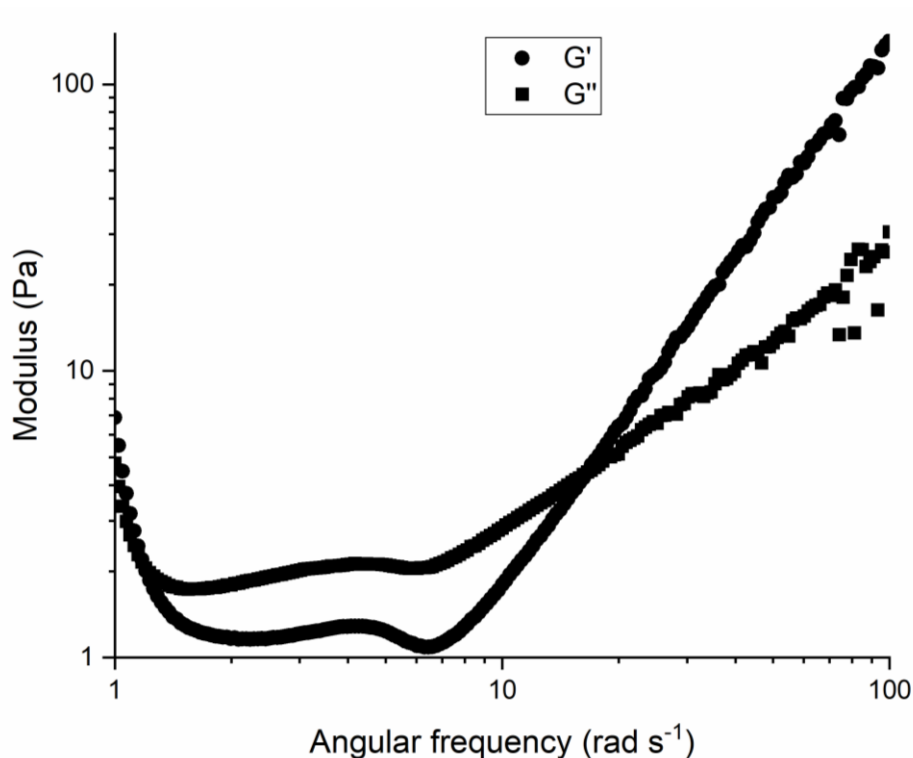


**Figure 6.8** Elastic ( $G'$ ) and viscous modulus ( $G''$ ) against angular frequency for PGI swollen in 2-phenylethanol.

### 6.3.4 PGI-based cross-linked chemical organogels

PGI was covalently cross-linked with EDT using thiol-ene coupling. Successful PGI cross-linking was confirmed by DSC analysis; the thermogram produced revealed an exothermic peak at 123 °C that is attributed to cross-linker degradation and lacked the sizable endothermic melting point at 45 °C that linear PGI possesses (Figure 6.9a). Such thermal stability is advantageous for using the materials in applications in which it must retain structural integrity at elevated temperatures, for instance, as a recyclable polymer that undergoes washing in hot liquids between uses. The cross-linked polymer was robust when handled.

The cross-linked polymer also holds great potential to form an organogel with increased mechanical properties when swollen in an organic continuous phase. Once more, 2-phenylethanol was probed to determine if it can form a chemical organogel that includes a fragrant antimicrobial molecule as the continuous phase (Table 6.2). Figure 6.9b demonstrates the solid-like behaviour of the

covalent gel, whereby values of the storage modulus are significantly increased with respect to those of the loss modulus, regardless of the angular frequency. The rheogram also shows the significantly increased storage modulus of this organogel compared with the non-cross-linked organogel (Figure 6.8). THF was also used to create organogels owing to its ability to readily solubilise linear PGI, rendering it ideal to demonstrate PGI cross-linking by organogel formation as linear PGI dissolves in THF, whereas cross-linked PGI should swell in THF.

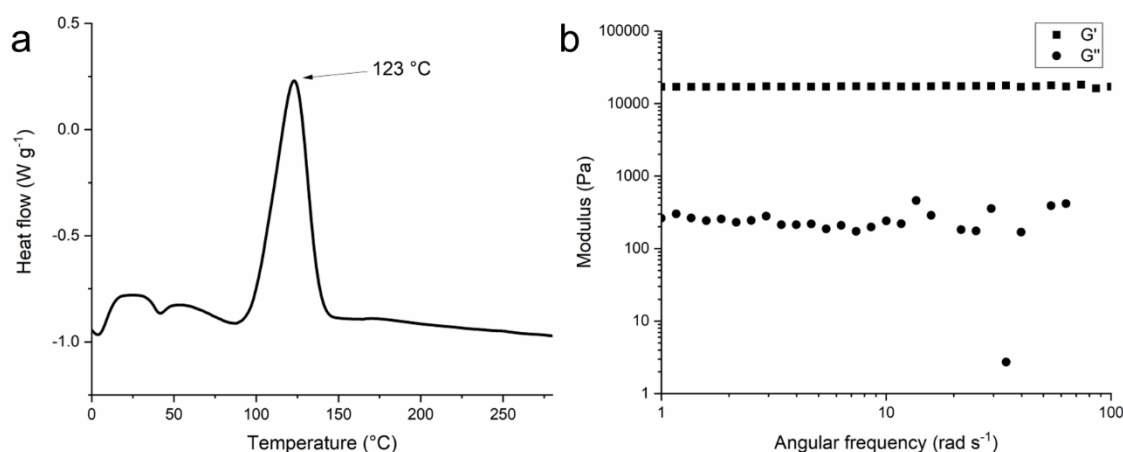


**Figure 6.9** (a) DSC thermogram for PGI cross-linked with EDT. (b) Average ( $n=6$ ) elastic ( $G'$ ) and viscous ( $G''$ ) modulus against angular frequency for PGI cross-linked with EDT and swollen in 2-phenylethanol.

**Table 6.2** PGI:EDT ratio, weight loss % of PGI in the organogels formed, and the solvent loss rate ( $\text{mL h}^{-1}$ ) of the organogels created in THF or 2-phenylethanol.

Sample	Polymer:Cross-linker ratio	THF		2-Phenylethanol	
		% PGI	Solvent loss	% PGI	Solvent loss
1	1:0.11	15	0.3	11	0.07
2	1:0.22	19	0.29	16	0.06
3	1:0.44	21	0.24	22	0.05
4	1:0.85	23	0.24	20	0.04

In general, as the PGI:EDT ratio converges to parity, the weight percentage of PGI in the organogels formed increases. This was anticipated as reduced gel

swelling typically corresponds to increased cross-link density. Organogels formed using 2-phenylethanol had a solvent loss rate, determined by organogel mass, of  $0.07 \text{ mL h}^{-1}$  over 24 h, which proved to be much lower to that of THF. 2-Phenylethanol retention capability provides the material with potential use as an antimicrobial gel that provides prolonged fragrance release; control over solvent loss ensures that the material does not dry prematurely. SEM analysis revealed that such structures possessed a porous morphology and so may also be feasibly deployed as scaffolds for a three-dimensional cell culture owing to the non-cytotoxic components of the material (Figure 6.10a). The porous morphology is also relevant when aiming to achieve an uptake of an antibacterial compound within the pores rather than only in the polymer-free volume.

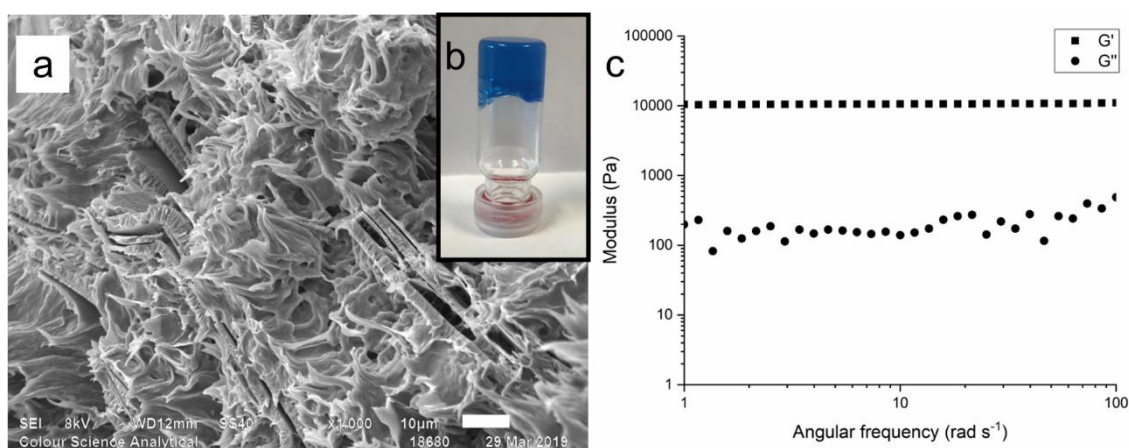


**Figure 6.10** (a) SEM micrograph of PGI cross-linked with EDT (scale bar represents  $10 \mu\text{m}$ ). (b) **3**-dyed PGI cross-linked with EDT and dispersed in 2-phenylethanol. (c) Average ( $n=7$ ) elastic ( $G'$ ) and viscous ( $G''$ ) modulus against angular frequency for PGI cross-linked with EDT, covalently dyed with **3** and swollen in 2-phenylethanol.

PGI was simultaneously dyed with **3** and cross-linked with EDT to yield a polymer that may form a blue organogel (Figure 6.10b). **3**-dyed and EDT-cross-linked PGI expanded to 497% of the original polymer mass when dispersed in 2-phenylethanol. Figure 6.10c demonstrates that this dyed organogel is stronger than the non-cross-linked organogel (Figure 6.8) as the  $G'$  value is much greater than the  $G''$  value. However, the  $G'$  value is less than that of the nondyed organogel (Figure 6.9b) ( $G'$  of  $\sim 17,000 \text{ P}$  and  $\sim 10,250 \text{ Pa}$  for the non-dyed and dyed organogels, respectively).

### 6.3.5 Antimicrobial activity of the chemical organogels

Finally, the antimicrobial activity of the blue-coloured and uncoloured chemically cross-linked 2-phenylethanol-swollen PGI-based organogels was assessed versus *S. aureus* and *E. coli*. Preliminary testing revealed comparable antimicrobial activity for all concentrations tested (Figure 6.11a-b); therefore, subsequent experiments focused only on the gel with the lowest solvent concentration (84 mg mL<sup>-1</sup>). Figure 6.11c-d shows the bacterial viability following incubations of *S. aureus* and *E. coli* in the positive growth control with the 2-phenylethanol-free PGI control and the coloured/non-coloured organogels. The antimicrobial effect of coloured and non-coloured PGI in the absence of 2-phenylethanol was minimal, but when swollen to form an organogel, the material displayed clear antimicrobial capabilities. As expected, there was no marked difference in the antimicrobial activity between cross-linked PGI dyed with or without **3**, although some difference was found when assessed against *S. aureus*.

Additionally, OD<sub>600</sub> readings were made of the suspensions incubated with the organogels. For *S. aureus*, the OD<sub>600</sub> values for both the colourless and dyed 84 mg mL<sup>-1</sup> organogel were reduced by >95% compared with the positive growth control (Figure 6.11e). Similarly, the OD<sub>600</sub> values for both *E. coli* organogels decreased by >97% from the positive growth control (Figure 6.11f), further demonstrating the pronounced antimicrobial capabilities of the reported organogels.

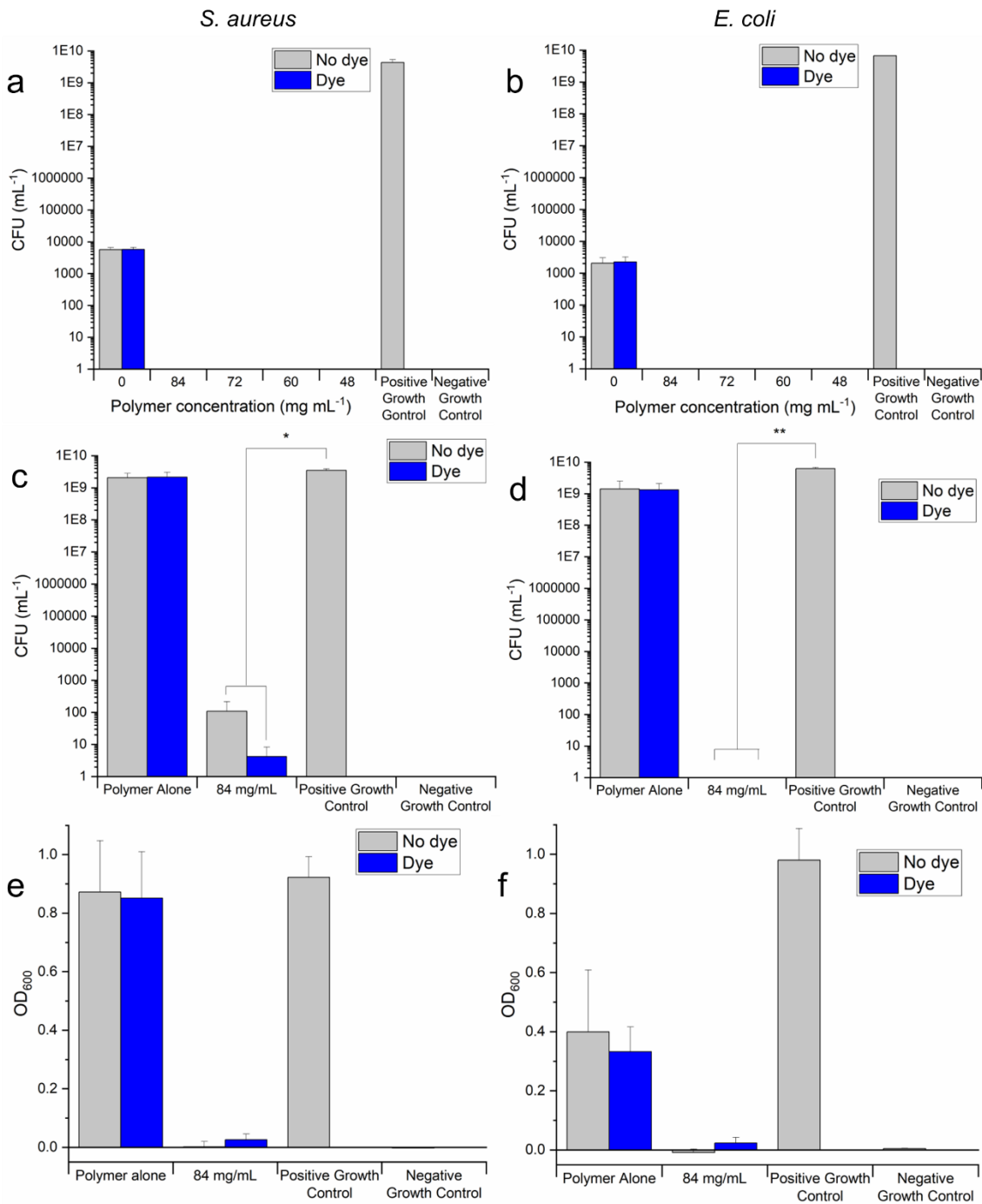


**Figure 6.11** Antimicrobial activities of the dyed and non-dyed cross-linked PGI organogels in 2-phenylethanol. Preliminary testing against a range of concentrations for *S. aureus* (a) and *E. coli* (b); subsequent experiments probing the bacterial viability at 84 mg mL<sup>-1</sup> for *S. aureus* (c) and *E. coli* (d); OD<sub>600</sub> readings of suspensions incubated with *S. aureus* (e) and *E. coli* (f).

## 6.4 Conclusions

The thiol modification of DR1 and DB3 was carried out to yield two reactive dyes that are able to colour (macro)molecules that possess C=C double bonds through covalent coupling. PGI, a biocompatible and potentially biodegradable polyester, was both coloured by such dyes and cross-linked via a one-step thiol-ene reaction to yield a nonsoluble polymer that lacks a melting point. Cross-linked PGI was used as the gelating component for various food-grade solvents, including the fragrant, food-grade molecule 2-phenylethanol. Chemically cross-linked PGI-based organogels that have 2-phenylethanol as the continuous phase demonstrate a predominantly elastic behaviour with an increased storage modulus with respect to both the loss and storage modulus of the 2-phenylethanol-swollen linear polymer. Such organogels display excellent antimicrobial activity against *S. aureus* and *E. coli*, regardless of dye conjugation to the cross-linked network. Consequentially, the PGI-based, 2-phenylethanol-containing organogels reported are highly promising candidates to be employed for the prolonged release of a fragrant molecule and as antimicrobial gels.

## 6.5 References

1. S. L. Wright and F. J. Kelly, *BMJ*, 2017, **358**, j4334.
2. M. Mishra, ed., *Encyclopedia of Polymer Applications*, CRC Press, Boca Raton, Florida U.S.A., 2019.
3. R. Geyer, J. R. Jambeck and K. L. Law, *Science Advances*, 2017, **3**, e1700782.
4. T. Salem, S. Uhlmann, M. Nitschke, A. Calvimontes, R.-D. Hund and F. Simon, *Progress in Organic Coatings*, 2011, **72**, 168-174.
5. J. V. Rowley, J. Exley, H. Yu, G. S. Mircale, A. S. Hayward and P. D. Thornton, *Chemical Communications*, 2020, **56**, 6360-6363.
6. T. P. Haider, C. Völker, J. Kramm, K. Landfester and F. R. Wurm, *Angewandte Chemie International Edition*, 2019, **58**, 50-62.
7. S. M. Burkinshaw, K. Liu and G. Salihu, *Dyes and Pigments*, 2019, **171**, 106367.
8. A. Murcia-Salvador, J. A. Pellicer, M. I. Fortea, V. M. Gómez-López, M. I. Rodríguez-López, E. Núñez-Delicado and J. A. Gabaldón, *Polymers*, 2019, **11**, 1003.

9. I. Grizzi, H. Garreau, S. Li and M. Vert, *Biomaterials*, 1995, **16**, 305-311.
10. G. Guidotti, M. Soccio, V. Siracusa, M. Gazzano, E. Salatelli, A. Munari and N. Lotti, *Polymers*, 2017, **9**, 724.
11. D. da Silva, M. Kaduri, M. Poley, O. Adir, N. Krinsky, J. Shainsky-Roitman and A. Schroeder, *Chemical Engineering Journal*, 2018, **340**, 9-14.
12. S. Bi, B. Tan, J. L. Soule and M. J. Sobkowicz, *Polymer Degradation and Stability*, 2018, **155**, 9-14.
13. G. Becker and F. R. Wurm, *Chemical Society Reviews*, 2018, **47**, 7739-7782.
14. R. Auras, B. Harte and S. Selke, *Macromolecular Bioscience*, 2004, **4**, 835-864.
15. I. van der Meulen, M. de Geus, H. Antheunis, R. Deumens, E. A. J. Joosten, C. E. Koning and A. Heise, *Biomacromolecules*, 2008, **9**, 3404-3410.
16. A. E. Polloni, V. Chiaradia, E. M. Figura, J. P. De Paoli, D. de Oliveira, J. V. de Oliveira, P. H. H. de Araujo, C. J. A. B. Sayer and Biotechnology, *Applied Biochemistry and Biotechnology*, 2018, **184**, 659-672.
17. I. van der Meulen, Y. Li, R. Deumens, E. A. J. Joosten, C. E. Koning and A. Heise, *Biomacromolecules*, 2011, **12**, 837-843.
18. H. Surburg and J. Panten, *Common fragrance and flavor materials: preparation, properties and uses*, Wiley, Weinheim, 5th edn., 2006.
19. P. Kraft and W. Eichenberger, *European Journal of Organic Chemistry*, 2004, **2004**, 354-365.
20. M. Claudino, I. van der Meulen, S. Trey, M. Jonsson, A. Heise and M. Johansson, *Journal of Polymer Science Part A: Polymer Chemistry*, 2012, **50**, 16-24.
21. A. S. Williams, *Synthesis*, 1999, **1999**, 1707-1723.
22. Z. Ates, P. D. Thornton and A. Heise, *Polymer Chemistry*, 2011, **2**, 309-312.
23. C. L. Savin, C. Peptu, Z. Kroneková, M. Sedlačik, M. Mrlik, V. Sasinková, C. A. Peptu, M. Popa and J. Mosnáček, *Biomacromolecules*, 2018, **19**, 3331-3342.
24. C. Guindani, M.-L. Frey, J. Simon, K. Koynov, J. Schultze, S. R. S. Ferreira, P. H. H. Araújo, D. de Oliveira, F. R. Wurm, V. Mailänder and K. Landfester, *Macromolecular Bioscience*, 2019, **19**, 1900145.
25. T. Fuoco and A. Finne-Wistrand, *Polymer Reviews*, 2020, **60**, 86-113.
26. T. Hayashi and P. D. Thornton, *Dyes and Pigments*, 2015, **121**, 235-237.
27. T. Hayashi, A. Kazlauciusas and P. D. Thornton, *Dyes and Pigments*, 2015, **123**, 304-316.
28. M. Khuphe, B. Mukonoweshuro, A. Kazlauciusas and P. D. Thornton, *Soft Matter*, 2015, **11**, 9160-9167.
29. M. Chetia, S. Debnath, S. Chowdhury and S. Chatterjee, *RSC Advances*, 2020, **10**, 5220-5233.

30. Z. Khayat and H. Zali-Boeini, *Soft Materials*, 2019, **17**, 150-158.
31. P. Kirilov, S. Rum, E. Gilbert, L. Roussel, D. Salmon, R. Abdayem, C. Serre, C. Villa, M. Haftek, F. Falson and F. Pirot, *International Journal of Cosmetic Science*, 2014, **36**, 336-346.
32. Y.-M. Zhang, W. Zhu, W.-J. Qu, K.-P. Zhong, X.-P. Chen, H. Yao, T.-B. Wei and Q. Lin, *Chemical Communications*, 2018, **54**, 4549-4552.
33. A. Vintiloiu and J.-C. Leroux, *Journal of Controlled Release*, 2008, **125**, 179-192.
34. H. Zheng, L. Deng, F. Que, F. Feng and H. Zhang, *Colloids and Surfaces A: Physicochemical and Engineering Aspects*, 2016, **502**, 19-25.
35. M. Dai, L. Bai, H. Zhang, Q. Ma, R. Luo, F. Lei, Q. Fei and N. He, *International Journal of Pharmaceutics*, 2020, **576**, 119027.
36. S. Uzan, D. Barış, M. Çolak, H. Aydın and H. Hoşgören, *Tetrahedron*, 2016, **72**, 7517-7525.
37. C. L. Esposito, P. Kirilov and V. G. Roullin, *Journal of Controlled Release*, 2018, **271**, 1-20.
38. V. K. Singh, A. Anis, I. Banerjee, K. Pramanik, M. K. Bhattacharya and K. Pal, *Materials Science and Engineering: C*, 2014, **44**, 151-158.
39. V. K. Singh, K. Pal, D. K. Pradhan and K. Pramanik, *Journal of Applied Polymer Science*, 2013, **130**, 1503-1515.
40. V. K. Singh, K. Pal, I. Banerjee, K. Pramanik, A. Anis and S. M. Al-Zahrani, *European Polymer Journal*, 2015, **68**, 326-337.
41. V. K. Singh, I. Banerjee, T. Agarwal, K. Pramanik, M. K. Bhattacharya and K. Pal, *Colloids and Surfaces B: Biointerfaces*, 2014, **123**, 582-592.
42. D. Satapathy, D. Biswas, B. Behera, S. S. Sagiri, K. Pal and K. Pramanik, *Journal of Applied Polymer Science*, 2013, **129**, 585-594.
43. B. Behera, S. S. Sagiri, K. Pal and A. Srivastava, *Journal of Applied Polymer Science*, 2013, **127**, 4910-4917.
44. H. Yu, P. Zeng, Y. Liang, X. Chen, H. Hu, L. Wen and G. Chen, *International Journal of Pharmaceutics*, 2020, **574**, 118846.
45. S. M. Querobino, N. C. de Faria, A. A. Vigato, B. G. M. da Silva, I. P. Machado, M. S. Costa, F. N. Costa, D. R. de Araujo and C. Alberto-Silva, *Materials Science and Engineering: C*, 2019, **99**, 1350-1361.
46. K. Chen and H. Zhang, *ACS Applied Materials & Interfaces*, 2020, **12**, 7795-7804.
47. Z. Ates and A. Heise, *Polymer Chemistry*, 2014, **5**, 2936-2941.
48. Y.-J. Zhu, H.-T. Zhou, Y.-H. Hu, J.-Y. Tang, M.-X. Su, Y.-J. Guo, Q.-X. Chen and B. Liu, *Food Chemistry*, 2011, **124**, 298-302.

## Chapter 7

### Covalent colouration of an amphiphilic polyester by *in situ* chromophore creation for advanced laundry formulations

#### Preamble

This Chapter is based on work published as: J. V. Rowley, J. Exley, H. Yu, G. S. Mircale, A. S. Hayward and P. D. Thornton, "Covalent polyester colouration by *in situ* chromophore creation", *Chemical Communications*, 2020, **56** (47), 6360-6363.

#### Abstract

Limited quantities of *N*-phenyldiethanolamine included in the step-growth polymerisation reaction mixture afforded an amphiphilic block copolymer of PET-PEG with an aromatic amine capable of sequential diazotisation and azo coupling reactions. Uniquely, the chromophore is created only upon successful polymer modification with a non-coloured molecule, 2-amino-3,5-dinitrothiophene (*in situ* colouration), which confirms successful polymer adaption and ensures that coloured waste is not produced. The method of permanent colouration, which may feasibly be applied for the colouration of a wide-range of step-growth polyesters, yielded a polymer capable of preventing indigo dye deposition onto a range of fabrics, offering potential use within advanced laundry formulations.

## 7.1 Introduction

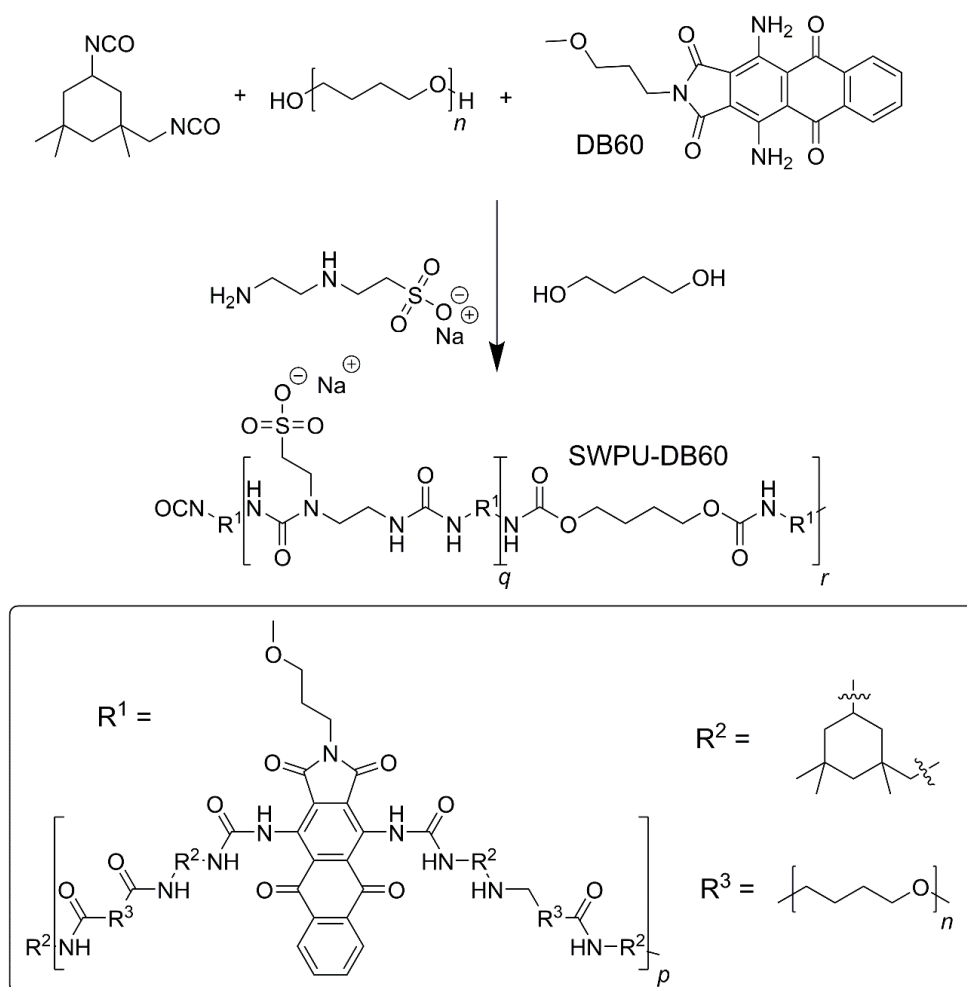
### 7.1.1 Traditional methods of dyeing PET and associated issues

Polyesters such as PET are the most widely used material in the textiles industry.<sup>1</sup> PET is the most important synthetic fibre in terms of production volume because of its excellent properties including high tensile strength, low cost, good barrier properties and high thermal stability (Section 1.1.1).<sup>2-3</sup> PET, and other commodity polymers produced by step-growth polymerisations, are coloured in order to add value, but the polymers lack suitable chemical functionality to enable efficient dyeing.<sup>4-7</sup> Consequentially, PET is commonly dyed using disperse dyes and frequently necessitates the inclusion of dispersants, carriers, thickeners, and reducing agents as auxiliaries to achieve effective polymer colouration, as discussed in Section 1.1.3.<sup>8-10</sup> PET colouration is difficult to achieve and the process is typically conducted in aqueous solution at 130 °C under pressure.<sup>1</sup> Colour is imparted by the disperse dyes being dissolved in the PET, with dye-fibre affinity generally involving van der Waals interactions, dipolar forces, hydrogen bonding, and potentially  $\pi$ - $\pi$  interactions between aromatic groups on the dye and PET repeat units.<sup>11</sup>

Coloured wastewater is produced in the dyeing process that creates acute aesthetic, ecological and environmental problems.<sup>12-15</sup> Globally, the textile industry consumes approximately 460,000 metric tonnes of dyes and pigments annually.<sup>16</sup> Between 10-25% material loss is incurred during conventional textile dyeing, and 2-20% of this is directly discharged as effluent into the environment, equating to 9,200-92,000 metric tonnes released into the environment every year.<sup>17-18</sup> As disperse dye molecules do not covalently bind to the polymer substrate, long-term colouration is restricted by the disassociation of non-bound dye molecules over time.<sup>19</sup>

Covalently grafting dye molecules provides permanent substrate colouration,<sup>20-21</sup> and covalent colouration of step-growth polymers may proceed using dye

molecules that form the terminal group of polymers,<sup>22</sup> or by incorporating a difunctional dye within a step-growth polymerisation.<sup>23</sup> Recently, Hu *et al.* incorporated C.I. Disperse Blue 60 (DB60) within a step-growth polymerisation reaction of sulfonated waterborne polyurethane (SWPU), forming a dark purple-coloured SWPU-DB60 conjugate (Scheme 7.1).<sup>24</sup> Because the dye is bound to the polymer chain, the material demonstrated excellent colour fastness, with 8.7% and 34.1% dye migration for SWPU-DB60 and SWPU + DB60, respectively. The authors used this coloured polymer to impart colour onto polyester fabrics. However, such methods use a dye molecule that may be transferred to coloured effluent and/or are restricted by the extent of dye incorporation possible. Consequentially, straightforward methods to covalently include dye molecules within step-growth commodity polymers that lack pendant functional groups, in the absence of coloured effluent generation, are urgently sought.



**Scheme 7.1** Step-growth polymerisation process for the synthesis of SWPU-DB60.<sup>24</sup>

### **7.1.2 Soil release polymers (SRPs) and optical brighteners in advanced laundry formulations**

Polyesters may be employed within laundry detergent formulations as soil release polymers (SRPs), which aid the diffusion of water into the soil-fabric interface, decrease soil adsorption onto fabric surfaces, and reduce soil redeposition onto fabrics.<sup>25-28</sup> These materials are advantageous in all laundry care formulations, and crucial for low temperature laundering.<sup>29</sup> SRPs must be amphiphilic to fulfil this role;<sup>30</sup> the hydrophile ensures the dispersibility of the SRP in aqueous solution, whilst the lipophile facilitates the interaction of the SRP with the soil prior to soil removal from the garment.<sup>31</sup>

As white fabric ages it adopts a yellow shade that remains following laundering.<sup>32-34</sup> Attempts have been made to counter this discolouration by the addition of trace quantities of blue dye, typically ultramarine blue.<sup>32</sup> In modern times, such agents have adopted the synonymous terms optical brighteners and fluorescent whitening agents, with their primary purpose being the absorption of UV light and the fluorescence of blue light.<sup>35-37</sup> Optical brighteners coupled to SRPs are a desirable prospect for use in advanced laundry formulations. The use of a polymeric dye delivery vehicle may increase efficiency, homogeneity, and the level of control over the dye interaction with the fabric surface.<sup>32,38-40</sup> However, common dye-SRP approaches tend to yield high percentages of unattached dye either because the disperse dye used has not been able to react with the SRP, or has undergone hydrolysis prior to conjugation with the SRP (Figure 7.1).<sup>41</sup> Consequentially, coloured wastewater is produced and the diffusion of dyes from fabric over time is a likely prospect.

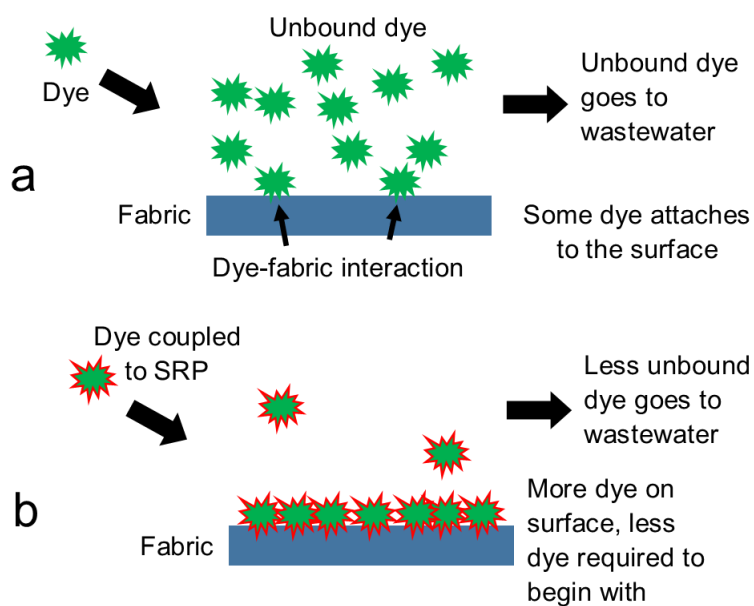


**Figure 7.1** Diagrams showing (a) the difference between dyeing polyester fabric using a disperse dye, and (b) dyeing polyester fabric with a disperse dye coupled to a SRP.

### 7.1.3 Summary

Combining a blue dye that acts as an optical brightener with a SRP yields a material that holds great promise for application in advanced laundry applications. Such active ingredient may prevent fabric staining and discolouration, and simultaneously impart brilliance to white fabrics. However, the permanent and extensive colouration of polymers that inherently lack repeat unit functionality is challenging. Additionally, the non-covalent coupling of dye molecules to a polymer backbone results in inevitable non-coupling of dye molecules, leading to coloured wastewater and high lightfastness of the coloured material.

Reported is the permanent colouration of an amphiphilic PET-PEG copolymer through innovative *in situ* chromophore creation. The simple addition of limited quantities of *N*-phenyldiethanolamine to the step-growth polymerisation reaction mixture yields a polymer that contains an aromatic amine capable of undergoing sequential diazotisation and azo coupling reactions. Resultantly, the polymer only becomes coloured following chromophore formation upon azo bond formation,

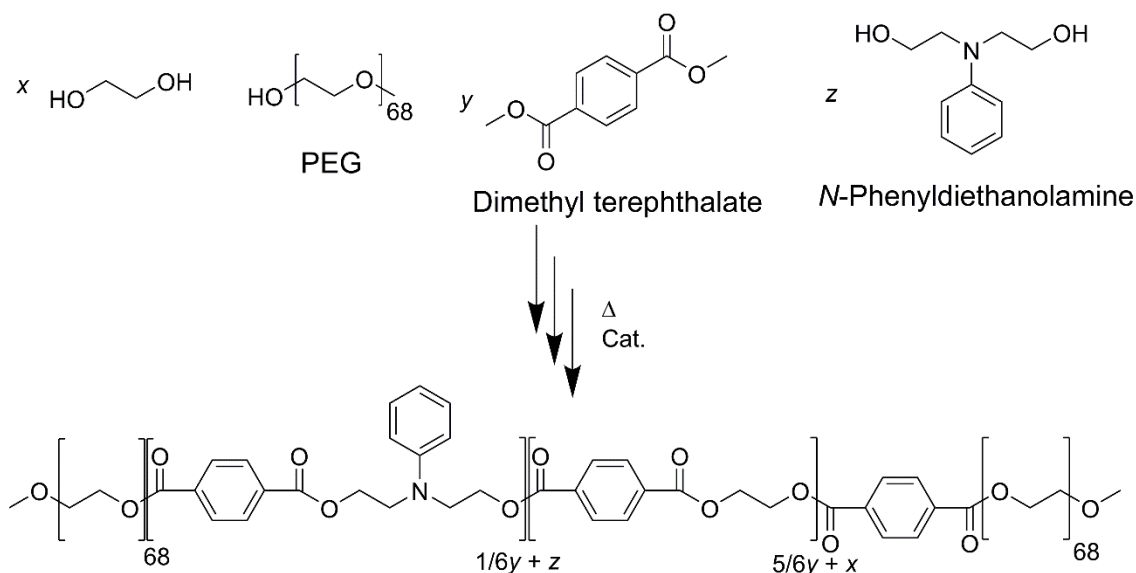
and the successful conjugation of a non-coloured molecule. Although the effectiveness of the polymers created within the context of laundry detergent active ingredients is demonstrated, the following novel method of polymer colouration has wide-ranging potential for the effective colouration of a wide variety of commodity step-growth polyesters.

## 7.2 Experimental Details

### 7.2.1 Synthesis of P1

Into a 3-necked RB flask, PEG monomethyl ether (3,000 Da, 9.99 g, 3.33 mmol, 1.5 eq.), dimethyl terephthalate (3.60 g, 18.54 mmol, 8.2 eq.), ethylene glycol (1.12 g, 18.04 mmol, 8.0 eq.), *N*-phenyldiethanolamine (0.41 g, 2.26 mmol, 1.0 eq.), antimony trioxide (0.03 g, 0.10 mmol, 0.04 eq.), calcium acetate monohydrate (0.03 g, 0.17 mmol, 0.08 eq.) and butylated hydroxytoluene (0.02 g, 0.09 mmol, 0.04 eq.) were weighed. A magnetic stirrer bar was fitted and the bulk polymerisation reaction stirred and heated to 210 °C. The flask was fitted with a distillation apparatus and the polymerisation reaction was conducted with a flow of N<sub>2</sub> over seven days (Scheme 7.2). The crude polymer was purified by dialysis (2,000 Da MWCO) against DI water and **P1** collected by lyophilisation prior to analysis (yield 72%).

166



**Scheme 7.2** Reaction scheme for the step-growth synthesis of **P1**.

### 7.2.2 Simulated dye transfer inhibition of **P1**

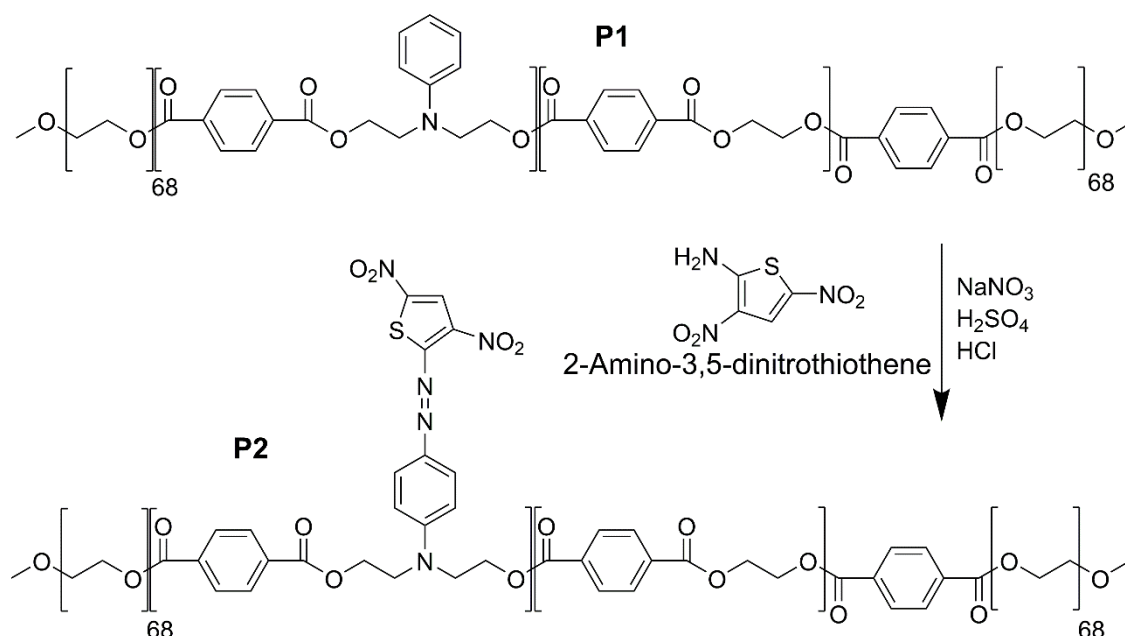
A GyroWash TestWise Touch laundrometer was used to assess the capability of **P1** to reduce dye transfer from an indigo test fabric to a range of test fabrics, and thus its suitability as a SRP. A  $0.1 \text{ mg mL}^{-1}$  solution of **P1** in DI water (50 mL) was prepared and transferred to a laundry test capsule along with a multifibre swatch. The multifibre swatch was composed of strips of regenerated cellulose, cotton, wool, nylon, polyester and acrylic. An indigo dye bleed was introduced to the laundry test capsule in the form of a piece of fabric dyed with indigo dye the same size as the multifibre swatch. 25 stainless steel ball bearings were added to the laundry test capsule to aid the simulation of the mechanical action of a domestic laundry setting. The sample was then washed at  $40 \text{ }^\circ\text{C}$  at a rotation of 40 r.p.m. for 30 minutes.

The colour change of the various test fabrics was measured using a Spectraflash DataColor spectrophotometer providing  $L^*a^*b^*$  colour system values, before and after washing in the laundrometer. Measurements were made under D65 lighting. The colour difference,  $\Delta E$ , was calculated from Equation (7.1). The washings in the presence and absence of **P1** were all performed in triplicate and the average  $\Delta E$  value is presented.

$$\Delta E = \sqrt{(\Delta L *)^2 + (\Delta a *)^2 + (\Delta b *)^2} \quad (7.1)$$

### 7.2.3 Synthesis of P2: conjugation of 2-amino-3,5-dinitrothiophene to P1

A RB flask was fitted with a magnetic stirrer bar and cooled in ice before sodium nitrite (0.48 g, 6.96 mmol) was weighed and dissolved slowly in concentrated sulfuric acid (6 mL). To the stirring sodium nitrite solution, a solution of propionic acid (3 mL) in acetic acid (18 mL) was added slowly over a 20 minute period with stirring at 0 °C. To the stirring solution, 2-amino-3,5-dinitrothiophene (1.2 g, 6.34 mmol) was added slowly. After 30 minutes of stirring at 0 °C, a solution of **P1** (0.5 g, 0.05 mmol) in DI water (20 mL) was transferred slowly followed by concentrated HCl (2 mL). The blue coloured solution was stirred for a further hour at 0 °C to ensure the reaction was complete before being washed by dialysis (2,000 Da MWCO) and **P2** collected by lyophilisation (Scheme 7.3) (yield 60%).



**Scheme 7.3** Reaction scheme for the colouration of **P1** to yield **P2**.

## 7.2.4 Tests of P2 in laundry applications

### 7.2.4.1 Test for the extent of blue colour release from P2 and a conventional polymer-dye

A conventional polymer-dye<sup>38</sup> and **P2** were independently dissolved in DI water and the deep blue coloured solutions transferred to dialysis tubing. The solutions were dialysed against DI water and the extent of release monitored by analysing aliquots of the media outside the dialysis membrane on a UV-vis spectrophotometer. The amount released was quantified by preparing a calibration curve of known concentrations of pure unreacted/monomeric dye precursors (Figure 7.2).

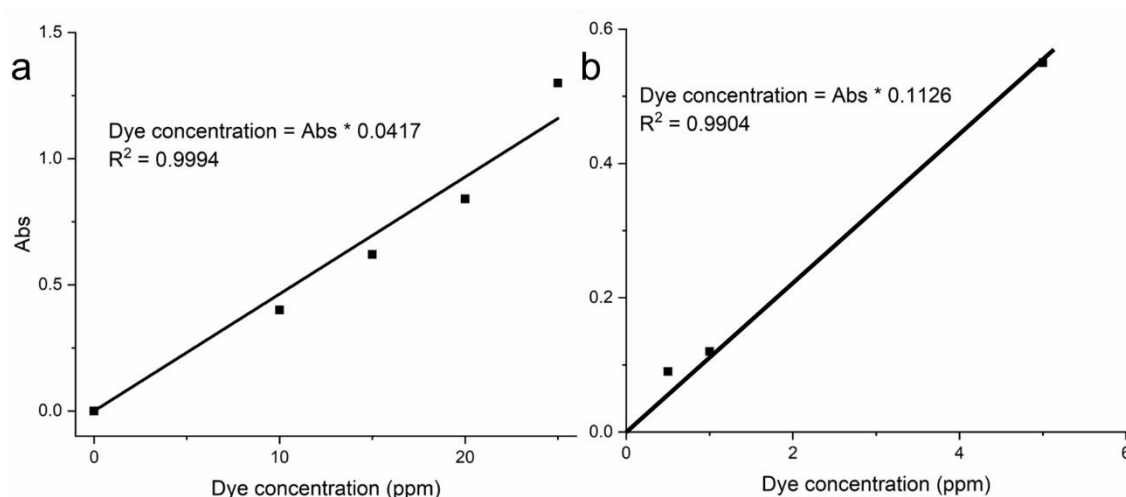


**Figure 7.2** Calibration curves for known concentrations of pure unreacted/monomeric dye precursors for a conventional polymer-dye (a) and **P2** (b).

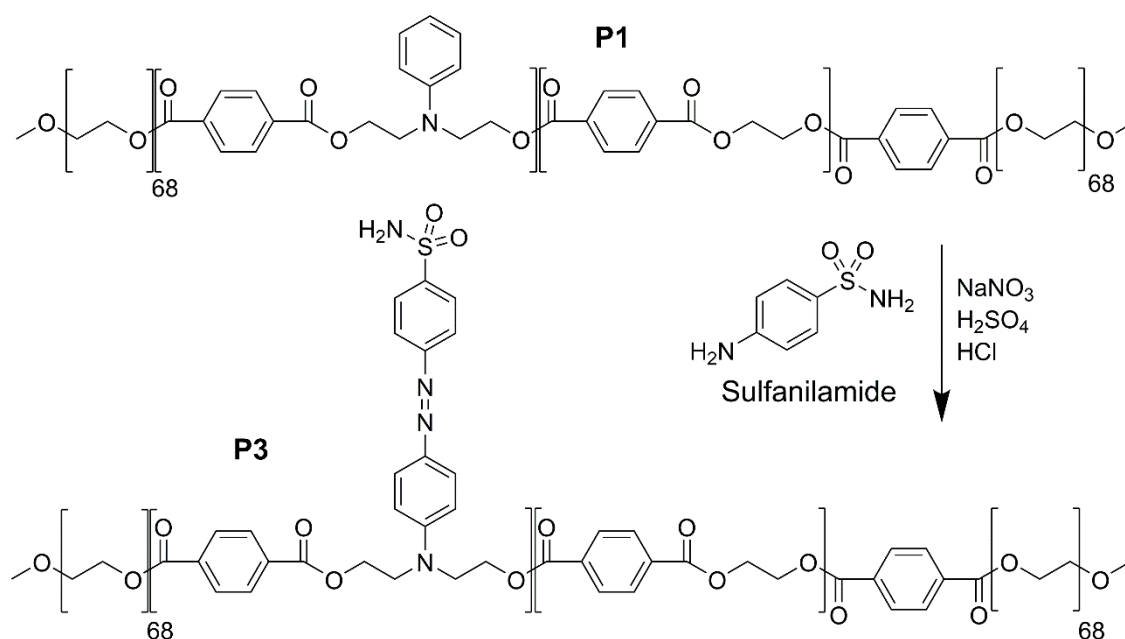
### 7.2.4.2 Test for the consistency of blue colouration to fabrics

Using the same laundrometer test conditions as Section 7.2.2, a solution of **P2** ( $0.1 \text{ mg mL}^{-1}$ ) in DI water (50 mL) was assessed in the presence of test fabric using the laundrometer, but in the absence of an indigo dye bleed. The same test was performed for a commercial polymer-dye conjugate to determine any

difference in fabric colouration when the fabric undergoes simulated laundering, independently in the presence of **P2** and a patented polymer-dye conjugate.<sup>38</sup> The colour difference of the fabric pre- and post-laundering was calculated using Equation (7.1).

### 7.2.5 Synthesis of **P3**: sulfanilamide conjugation to **P1**

Analogous to the synthesis of **P2** above (Section 7.2.3), a solution of propionic acid (3 mL) in acetic acid (18 mL) was added slowly to a solution of sodium nitrite (0.48 g, 6.96 mmol) in concentrated sulfuric acid (6 mL) at 0 °C. Sulfanilamide (1.09 g, 6.33 mmol) was added slowly at 0 °C and left to stir for 30 minutes for the reaction to complete. A solution of **P1** (0.69 g, 0.07 mmol) in DI water (20 mL) was then transferred slowly to the sulfanilamide solution followed by concentrated HCl (2 mL). The dark red coloured solution was stirred for a further hour at 0 °C before being washed by dialysis (2,000 Da MWCO) and **P3** collected by lyophilisation (Scheme 7.4) (yield 90%).



**Scheme 7.4** Reaction scheme for the conjugation of sulfanilamide to **P1** forming **P3**.

## 7.3 Results and Discussion

### 7.3.1 Amphiphilic PET-PEG synthesis and capability to be a SRP

To achieve the aim of covalent step-growth polymer colouration, an amphiphilic polymer containing central ethylene terephthalate repeat units, terminated by hydrophilic PEG blocks (Figure 7.3a),<sup>38</sup> was synthesised and modified to include an aniline group (Figure 7.3b) (**P1**). It was envisaged that the aniline group may act as a handle for polymer modification by diazonium formation at the site marked on Figure 7.3 with a red star, and subsequent azo coupling reactions. With the target application of producing a SRP in mind, it was hypothesised that the hydrophobicity provided by the central polyester units facilitates soil-polymer and/or fabric-polymer interactions, whilst the terminal, hydrophilic PEG units enable the polymer to disperse in aqueous solution.

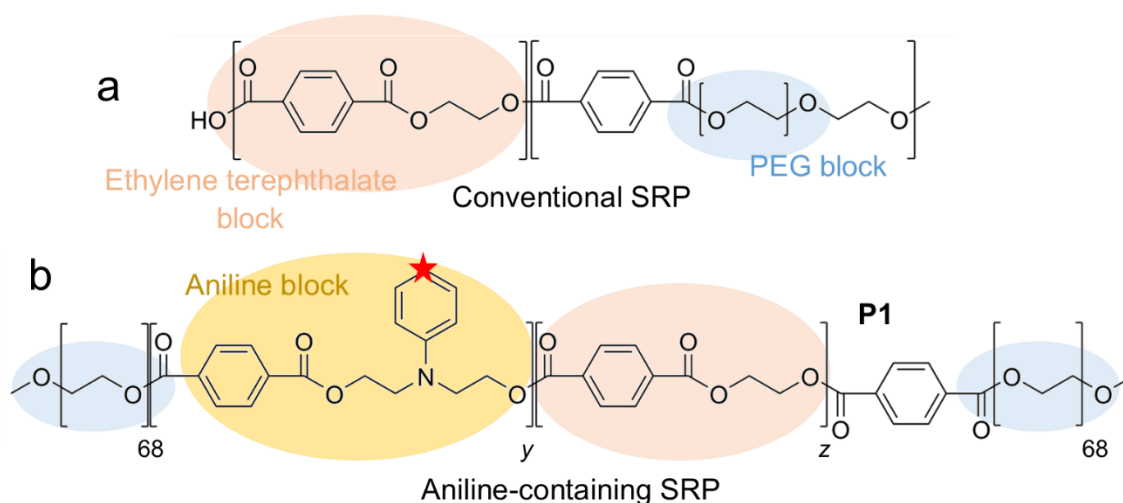


**Figure 7.3** Conventional<sup>38</sup> (a) vs. aniline-containing SRP (**P1**) (b).

The polymerisation to produce **P1** occurred over seven days at 210 °C, far exceeding the time required to commercially produce PET. This excess time is due to experimental constraints, but it is envisaged that aniline-containing polyesters may be readily produced on an industrial scale following a procedure analogous to that of commercial PET (Section 1.1.1.1). Successful synthesis of the aniline-containing polymer backbone was confirmed by <sup>1</sup>H NMR spectroscopy

(Figure 7.4a). Peaks corresponding to the protons of PEG are present between 3.24 and 3.89 ppm, and peaks corresponding to the ethylene glycol group in the terephthalate group appear between 4.43 and 4.53 ppm. The protons corresponding to *N*-phenyldiethanolamine are represented by peaks between 6.63 and 7.17 ppm, 3.90 and 3.95 ppm, and 4.62 and 4.71 ppm whilst peaks corresponding to the aromatic groups of the terephthalate group appear between 7.89 and 8.14 ppm. Theoretically, there are six times as many terephthalate groups to *N*-phenyldiethanolamine groups in the polymer formed, which was confirmed by comparing the integrals of the peaks corresponding to *N*-phenyldiethanolamine with the integrals of the aromatic protons corresponding to the terephthalate group.

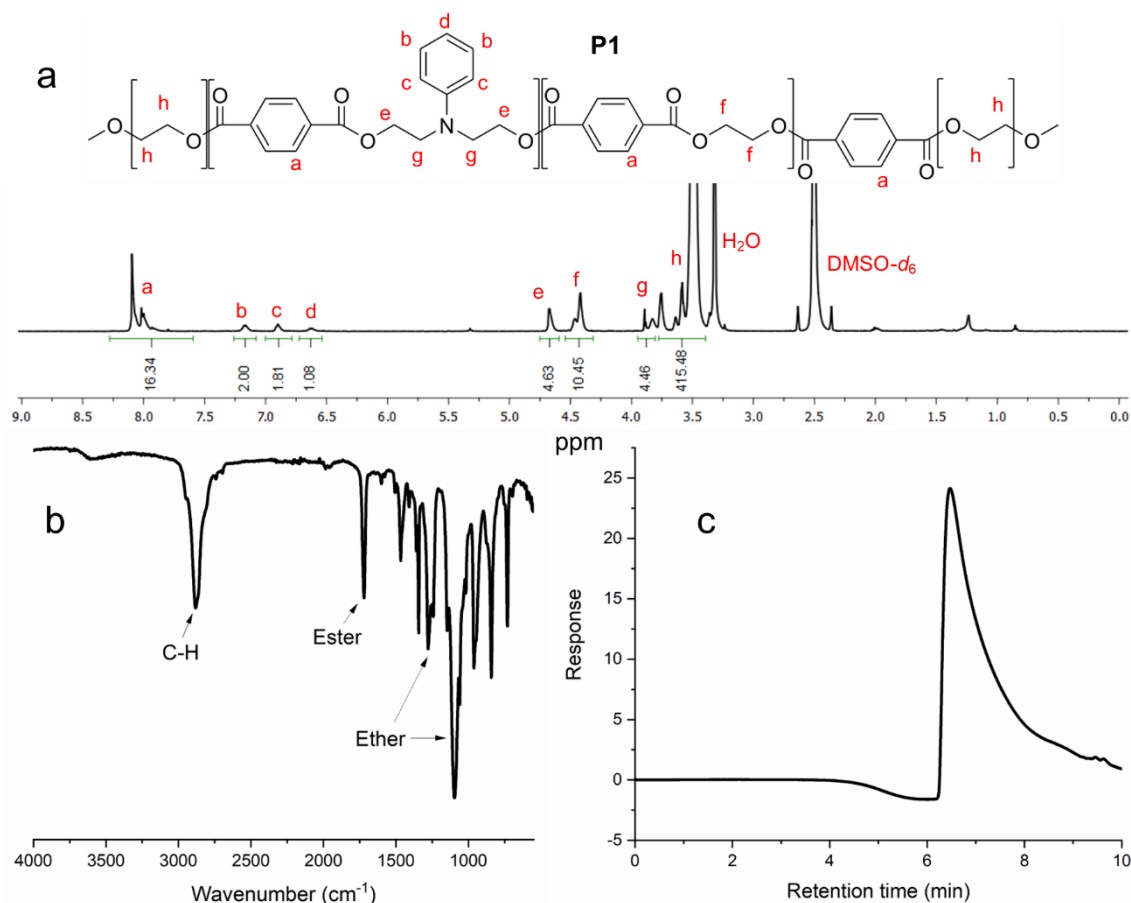


**Figure 7.4** <sup>1</sup>H NMR spectra (a) (500 MHz, DMSO-*d*<sub>6</sub>), FTIR spectra (b), and APC chromatogram (c) of P1.

FTIR spectroscopy confirmed the presence of both ester and ether bonds within P1 (Figure 7.4b). In addition, aromatic peaks may be assigned within the

fingerprint region at  $842\text{ cm}^{-1}$  and  $731\text{ cm}^{-1}$ . APC revealed that the polymer possessed  $M_w$  and  $M_n$  values of  $10,000\text{ g mol}^{-1}$  and  $7,300\text{ g mol}^{-1}$ , respectively (Figure 7.4c). The  $\bar{D}$  of step-growth polymers such as PET are  $\geq 2$ ,<sup>42</sup> but **P1** presented a lower  $\bar{D}$  of 1.4 because of the terminal PEG groups bringing more uniformity to the system.

To determine the effectiveness of **P1** as an SRP, the polymer was tested for its capability to inhibit the transfer of indigo dye to a variety of common fabrics. An aqueous solution of **P1** was prepared and added to a laundrometer together with an indigo dye bleed and strips of fabric (cellulose, cotton, wool, nylon, polyester and acrylic). Domestic laundry washing was then simulated at  $40\text{ }^\circ\text{C}$  for 30 minutes in triplicate. A control simulated wash was also conducted in triplicate under the same conditions but without **P1**. The colour of the fabrics was measured using a spectrophotometer providing  $L^*a^*b^*$  colour system values before and after washing. The colour difference,  $\Delta E$ , was calculated as per Equation (7.1), whereby the lower the change in colour of the fabric after washing, the greater the extent of the polymer's capability to prevent dye transfer to the particular fabric type. The minimal addition of **P1** to the simulated wash (only  $0.1\text{ mg mL}^{-1}$  of **P1** in  $50\text{ mL}$  DI water) vastly inhibited dye transfer to fabric during simulated washing, compared to when the polymer was absent (Figure 7.5). Dye transfer to nylon, polyester and woollen fabrics was particularly restricted when **P1** was included in the wash, compared to washes performed in the absence of the polymer. Such differences are clearly visible to the human eye. These results demonstrate the inclusion of *N*-phenyldiethanolamine into the polymer backbone do not negatively affect **P1**'s ability as a SRP.

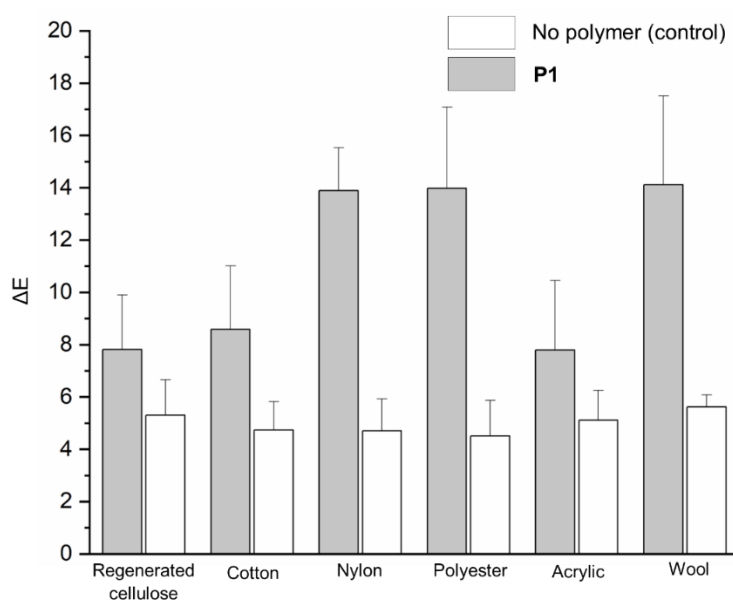


**Figure 7.5** The colour difference,  $\Delta E$ , of various fabrics before and after simulated washing with an indigo dye bleed in the absence (control) and presence of **P1**.

### 7.3.2 Colouration of **P1** and fabric dyeing ability

Permanent, covalent, colouration of **P1** to yield a blue polymer (**P2**) was achieved and the resulting polymer was characterised by  $^1\text{H}$  NMR spectroscopy (Figure 7.6a). Peaks corresponding to the protons of PEG are present between 3.41 and 3.58 ppm, and peaks corresponding to the ethylene glycol group in the terephthalate group appear between 4.34 and 4.53 ppm, much like **P1** above. The protons corresponding to *N*-phenyldiethanolamine are represented by peaks between 7.00 and 7.12 ppm, 3.89 and 4.01 ppm, and 4.61 and 4.70 ppm whilst peaks corresponding to the aromatic groups of the terephthalate, *N*-phenyldiethanolamine and 2-amino-3,5-dinitrothiophene groups appear between 7.73 and 8.13 ppm. The FTIR spectrum of **P2** (Figure 7.6b) was similar to that of **P1**, but UV-vis absorbance spectrophotometry shows a strong  $\lambda_{\text{max}}$  of 640 nm (Figure 7.6c).

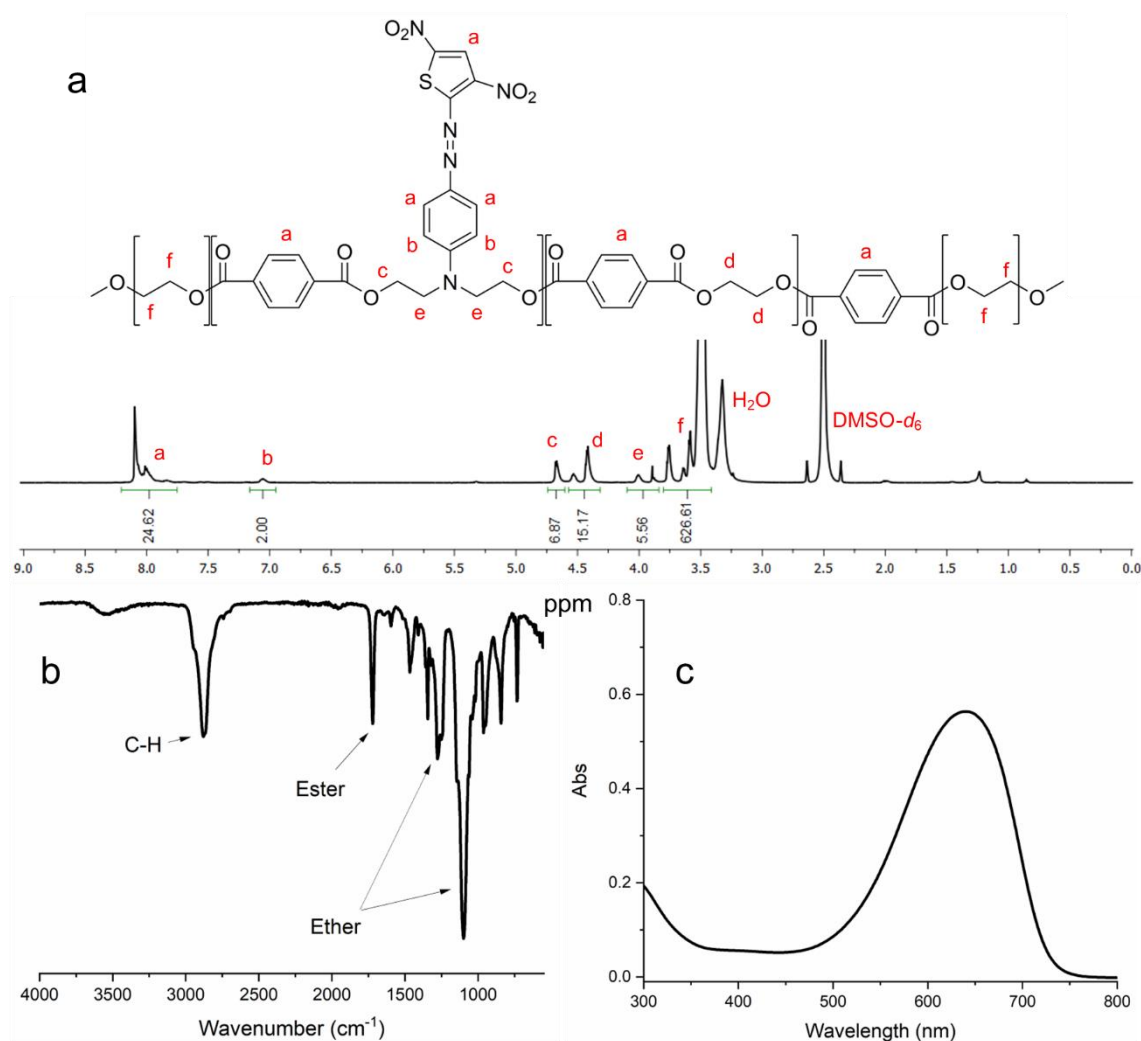


**Figure 7.6** <sup>1</sup>H NMR (500 MHz, DMSO-*d*<sub>6</sub>) (a), FTIR (b), and UV-vis absorbance spectra (c) of P2.

The extent of blue dye release from the polymer into aqueous solution post-dyeing was monitored by UV-vis spectrophotometry to determine if the system proposed restricts the unwanted release of dye molecules to solution. Using readily available materials, the recreation of commercially-available polymer-dye material that is suggested as an optical brightener was realised for comparison.<sup>38</sup> This comparative material follows the conventional approach of binding reactive dye molecules to an active acceptor site on the polymer, in this case the primary alcohol of the PEG block. Dialysis (membrane diffusion) was employed to resolve low molecular weight coloured components from both coloured polymers. The absorbance spectra of the outer dialysis media were solved against a calibration curve (Figure 7.2) to calculate the concentration of rogue dye present in the dye-polymer raw material. The conventional and novel approaches to coloured SRPs

were found to contain unreacted dye contents of 18% and 2.3%, respectively (Figure 7.7), emphasising the effectiveness of the proposed method of polymer colouration.

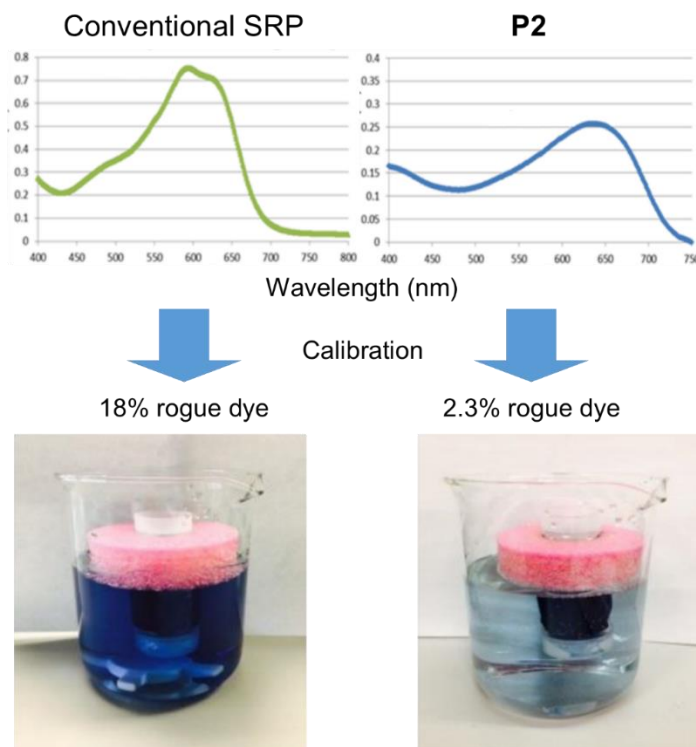


**Figure 7.7** UV-vis absorbance spectra of the media outside the dialysis membrane for conventional and this novel approach.

It is important that dyeing moieties, such as optical brighteners, uniformly deposit on fabric to avoid discrepancies in the colour delivered (vs. intended) across mixed loads containing a variety of fabric types. The dye delivery of **P2** and a commercially reported polymer-dye conjugate<sup>38</sup> were compared by adding the optical brighteners independently to a laundrometer with cotton or polyester fabric and no dye bleed. The colour difference was calculated as per Equation (7.1) and the tests repeated to enable the consistency of dyeing to be quantified. Dye delivery to cotton and polyester were more consistent when **P2** was employed, compared to the conventional polymer-dye conjugate (Figure 7.8a). The same laundrometer tests were repeated with mixed washing loads containing cotton, polycotton and polyester fabrics, and it was found that **P2** delivered significantly more consistent dyeing to the range of fabrics compared to the commercially reported polymer-dye conjugate (Figure 7.8b).

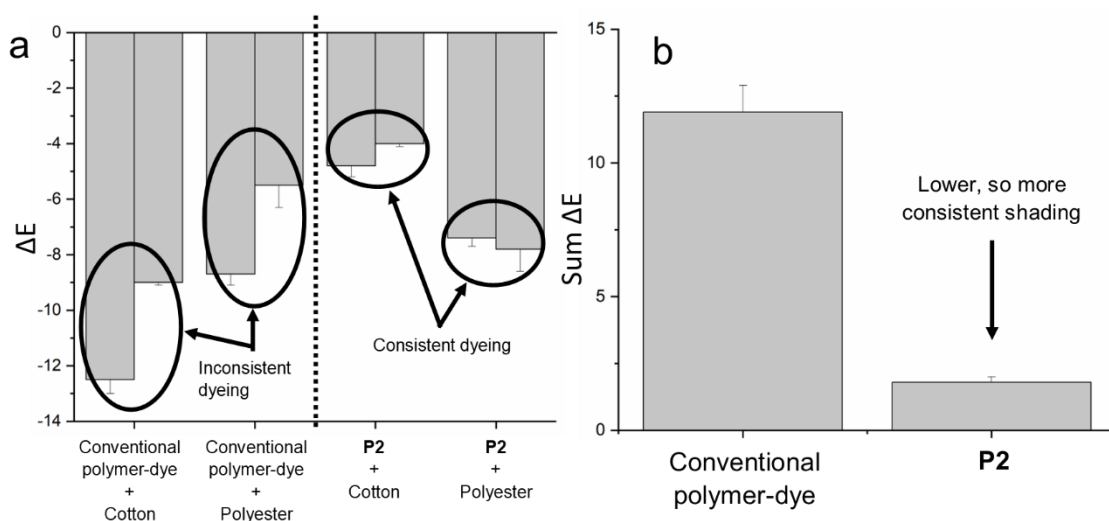


**Figure 7.8** (a) Graph comparing the consistency of dye deposition onto cotton and polyester for a commercial unmodified polymer-dye and **P2**. (b) Graph comparing the consistency of the shading across a mixed washing load containing cotton, polycotton and polyester.

### 7.3.3 Sulfanilamide conjugation to P1

To demonstrate the versatility that the reported method of polymer colouration has, the conjugation of sulfanilamide to uncoloured **P1** was done to afford a red coloured polymer (**P3**), confirmed by UV-vis absorbance spectrophotometry in water with a  $\lambda_{\max}$  of 438 nm (Figure 7.9a). The azo coupling reaction proceeded to yield a red solution immediately upon sulfanilamide addition to the polymer-containing solution (Figure 7.9a inset). The polymer had a similar FTIR spectrum to that of **P1** (Figure 7.9b vs. Figure 7.4b).  $^1\text{H}$  NMR spectroscopy (Figure 7.9c) was used to confirm successful polymer synthesis, and further demonstrate how the inclusion of limited amounts of *N*-phenyldiethanolamine within a step-growth polymerisation reaction enables facile polymer colouration. Figure 7.9c shows peaks corresponding to the protons of PEG are present between 3.39 and 3.78 ppm, and peaks corresponding to the ethylene glycol group in the terephthalate group appear between 4.30 and 4.45 ppm. The protons corresponding to *N*-phenyldiethanolamine are represented by peaks between 7.00 and 7.51 ppm, 4.61 and 4.71 ppm, and 3.92 and 4.05 ppm whilst peaks corresponding to the aromatic groups of the terephthalate and sulfanilamide groups appear between

7.72 and 8.12 ppm. Sulfanilamide has a characteristic secondary amide group  $\text{H}_2\text{N-SO}_2$ - between 4.50 and 4.57 ppm.

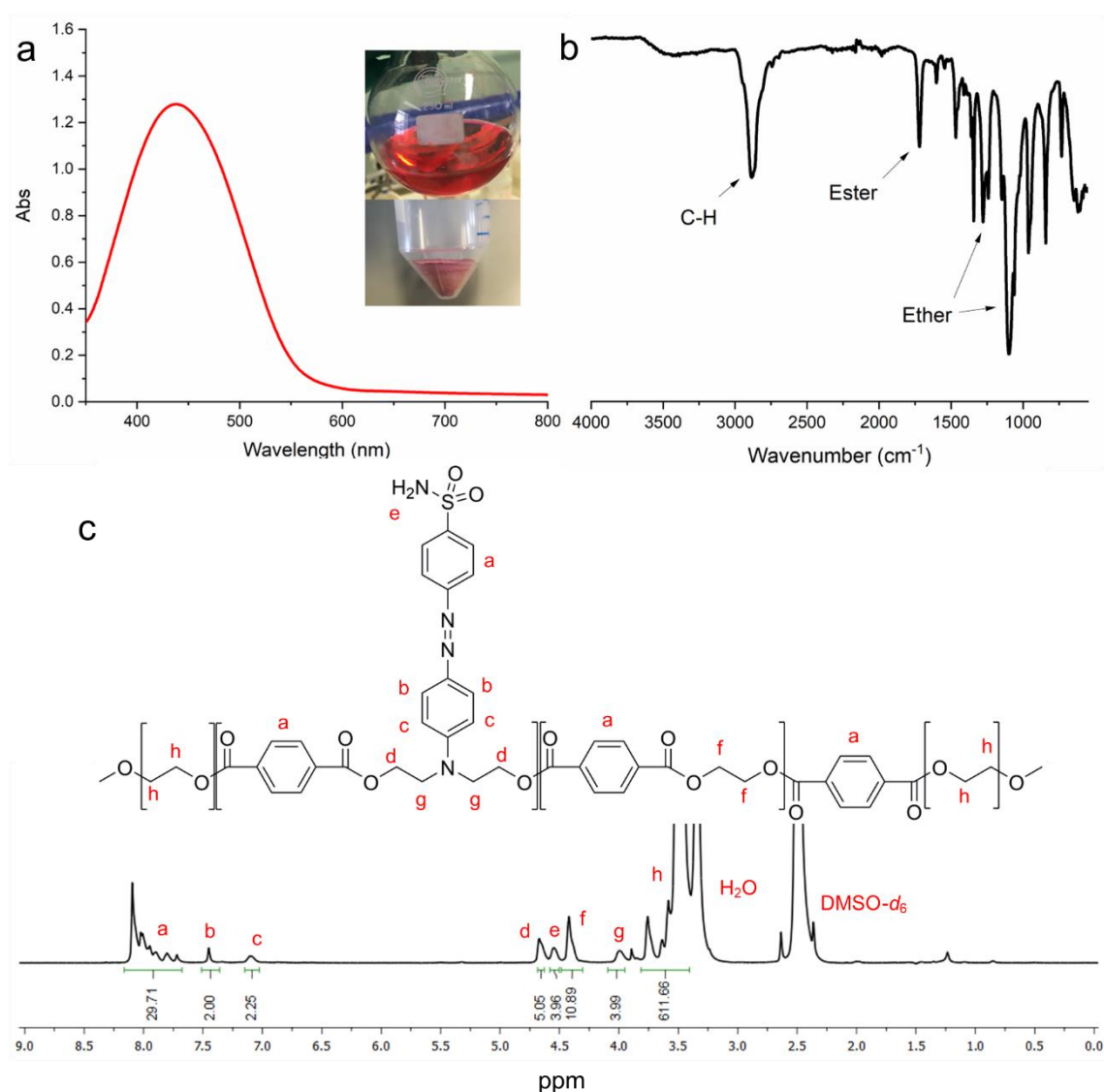


**Figure 7.9** UV-vis absorbance (a), FTIR (b), and  $^1\text{H}$  NMR (500 MHz,  $\text{DMSO-d}_6$ ) (c) spectra of **P3**. Inset = during the conjugation, a red solution formed from which a red coloured polymer precipitated.

Crucially, colouration of the polymer only occurred upon the creation of the azo group following the covalent coupling of sulfanilamide. The relative ease of **P1** colouration ensured that scaled-up production within an industrial setting is anticipated to be straightforward. Additionally, sulfanilamide has presented good antifungal activity,<sup>43</sup> and as such it is anticipated **P3** could also demonstrate antifungal activity, but this was not explored.

## 7.4 Conclusions

An innovative method for the colouration of polymers produced by step-growth polymerisations involving dicarboxylic acid monomers, for instance polyesters, is demonstrated. The incorporation of limited amounts of *N*-phenyldiethanolamine within the step-growth polymerisation process provides a molecular handle for prompt polymer colouration by straightforward azo coupling. This mode of permanent colouration ensures that a very limited amount of unbound dye molecules is expelled from the polymer post-synthesis. Initially, a water-soluble polymer that presented a blue hue was created and found to be effective as a vehicle as an optical brightener, offering enhanced performance against a range of fabric types vs. a commercially reported polymer-dye conjugate. Accordingly, the polymer has significant promise for incorporation within advanced laundry care formulations to maintain the perception of whiteness of laundered items. The versatility of the mechanism of colour creation was demonstrated by the coupling of sulfanilamide to the uncoloured polymer, yielding a red polymeric product. It is envisaged that the simplistic method of polymer derivatisation and permanent colouration reported may be applied to a wide-range of polyesters created by step-growth polymerisation.

## 7.5 References

1. S. Yoon, B. Choi, M. M. Rahman, S. Kumar, S. M. Mamun Kabir and J. Koh, *Materials*, 2019, **12**, 4209.
2. X. Gong, X. Chen and Y. Zhou, in *High-Performance Apparel*, eds. J. McLoughlin and T. Sabir, Woodhead Publishing, 2018, ch. 4, pp. 75-112.
3. S. Zekriardehani, S. A. Jabarin, D. R. Gidley and M. R. Coleman, *Macromolecules*, 2017, **50**, 2845-2855.
4. J.-h. Choi and W.-y. Seo, *Fibers and Polymers*, 2006, **7**, 270-275.
5. S. M. Burkinshaw and D. S. Jeong, *Dyes and Pigments*, 2012, **92**, 1025-1030.
6. T. Salem, S. Uhlmann, M. Nitschke, A. Calvimontes, R.-D. Hund and F. Simon, *Progress in Organic Coatings*, 2011, **72**, 168-174.
7. A. D. Broadbent, *Basic Principles of Textile Colouration*, Society of Dyers and Colourists, Bradford, U.K., 2001.
8. T. Hussain, M. Tausif and M. Ashraf, *Journal of Cleaner Production*, 2015, **108**, 476-483.

9. S. M. Burkinshaw, J. Howroyd, N. Kumar and O. Kabambe, *Dyes and Pigments*, 2011, **91**, 340-349.
10. S. M. Burkinshaw, K. Liu and G. Salihu, *Dyes and Pigments*, 2019, **171**, 106367.
11. R. M. Christie, *Colour Chemistry*, Royal Society of Chemistry, 2nd edn., 2015.
12. A. Murcia-Salvador, J. A. Pellicer, M. I. Fortea, V. M. Gómez-López, M. I. Rodríguez-López, E. Núñez-Delicado and J. A. Gabaldón, *Polymers*, 2019, **11**, 1003.
13. G. Moussavi and M. Mahmoudi, *Journal of Hazardous Materials*, 2009, **168**, 806-812.
14. P. Huang, D. Xia, A. Kazlauciusas, P. Thornton, L. Lin and R. Menzel, *ACS Applied Materials & Interfaces*, 2019, **11**, 11961-11969.
15. S. J. Boardman, R. Lad, D. C. Green and P. D. Thornton, *Journal of Applied Polymer Science*, 2017, **134**, 44846.
16. T. Marchis, P. Avetta, A. Bianco-Prevot, D. Fabbri, G. Viscardi and E. Laurenti, *Journal of Inorganic Biochemistry*, 2011, **105**, 321-327.
17. T. Chiong, S. Y. Lau, Z. H. Lek, B. Y. Koh and M. K. Danquah, *Journal of Environmental Chemical Engineering*, 2016, **4**, 2500-2509.
18. Z. Carmen and S. Daniela, in *Organic Pollutants: Ten Years After the Stockholm Convention - Environmental and Analytical Update*, eds. T. Puzyn and A. Mostrag-Szlichtyng, IntechOpen, Rijeka, Croatia, 2012, ch. 3, pp. 55-86.
19. G. Mock, in *Synthetic Fibre Dyeing*, ed. C. Hawkyard, Society of Dyers and Colourists, Bradford, U.K., 2004, ch. 2, pp. 45-81.
20. T. Hayashi and P. D. Thornton, *Dyes and Pigments*, 2015, **121**, 235-237.
21. J. V. Rowley, P. Wall, H. Yu, G. Tronci, D. A. Devine, J. J. Vernon and P. D. Thornton, *ACS Applied Polymer Materials*, 2020, **2**, 2927-2933.
22. E. Zamani, H. Shaki, M. Rafizadeh, A. Khosravi and M. Pilehkouhi, *Fibers and Polymers*, 2017, **18**, 1431-1437.
23. X.-h. Hu, X. Liu, M.-l. Liu and G. Li, *Reactive and Functional Polymers*, 2018, **132**, 1-8.
24. X. Hu, M. Li, Y. Xian, X. Liu, M. Liu, G. Li, P. Hu and C. Cheng, *Journal of Applied Polymer Science*, 2020, **137**, 48862.
25. E. Kissa, in *Detergency: Theory and Technology*, eds. W. G. Cutler and E. Kissa, Marcel Dekker Inc., New York, USA, 1986, vol. 20, ch. 5, pp. 333-370.
26. B. S. Butola, in *Polyesters and Polyamides*, eds. B. L. Deopura, R. Alagirusamy, M. Joshi and B. Gupta, Woodhead Publishing, Cambridge, UK, 2008, ch. 12, pp. 325-353.
27. A. Valentini, S. Bakalis, K. Gkatzionis, G. Palazzo, N. Cioffi, C. D. Franco, E. Robles, A. Brooker and M. M. Britton, *Industrial & Engineering Chemistry Research*, 2019, **58**, 14839-14847.
28. S. J. Boardman, A. S. Hayward, N. J. Lant, R. D. Fossum and P. D. Thornton, *Journal of Applied Polymer Science*, 2020, **138**, 49632.
29. L. Cotton, A. S. Hayward, N. J. Lant and R. S. Blackburn, *Dyes and Pigments*, 2020, **177**, 108120.
30. A. J. O'Lenick Jr., *Journal of Surfactants and Detergents*, 1999, **2**, 553-557.
31. US4427557, 1984.

32. E. Smoulders and E. Sung, in *Ullmann's Encyclopedia of Industrial Chemistry*, eds. B. Elvers and G. Bellussi, Wiley-VCH, Weinheim, Germany, 2012, DOI: 10.1002/14356007.o15\_o13.
33. I. Castro, E. Ekinici, X. Huang, H. A. Cheaito, Y.-H. Ahn, J. Olivero-Verbel and Q. P. Dou, *Journal of Cellular Biochemistry*, 2019, **120**, 14065-14075.
34. H. Salas, C. Gutiérrez-Bouzán, V. López-Grimau and M. Vilaseca, *Materials*, 2019, **12**, 785.
35. R. Chen, J. Qu, Q. Zhao and J. He, *Fibers and Polymers*, 2014, **15**, 1915-1920.
36. Q. Zhao, J. Sun, B. Liu and J. He, *Cellulose*, 2014, **21**, 2937-2950.
37. Z. Fang, F. Wu, L. Lin, Q. Qin, C. Au, Q. Tao, X. Li, D. Yu and B. Yi, *Journal of Applied Polymer Science*, 2019, **136**, 47635.
38. WO2011098355, 2011.
39. US20190241840, 2019.
40. US20070277327, 2007.
41. W. Bertleff, P. Neumann, R. Baur and D. Kiessling, *Journal of Surfactants and Detergents*, 1998, **1**, 419-424.
42. M. V. Pergal and M. Balaban, in *Polyethylene Terephthalate: Uses, Properties and Degradation*, ed. N. A. Barber, Nova Science Publishers, New York, U.S.A., 2017, ch. 1, pp. 1-102.
43. I. Mishra, R. Mishra, S. Mujwar, P. Chandra and N. Sachan, *Journal of Heterocyclic Chemistry*, 2020, **57**, 2304-2329.

## Concluding Remarks and Future Works

This Thesis has described advances in the synthesis and applications of PAAs and polyesters. A novel route to the synthesis of PAla with high equivalence was proposed avoiding Ala-NCA, and the covalent dyeing of polyesters including PGI and PET-containing polymers was described. Advanced uses of PAAs include NPs for targeted chemotherapy treatment, a potentially theranostic device, and phosphonate-terminated polymers to improve the aqueous compatibility of metal NPs. Polyesters for advanced laundry formulations and for antimicrobial organogels have also been described in this Thesis.

Chapter 3 described the synthesis of an amphiphilic PSar with a terminal phosphonate group. The polymer is able to self-assemble into a polymeric NP which can uptake and selectively release Dox to acidic environments. Additionally, the phosphonate group allows these polymers to form P-O-M bonds with metals, and this was demonstrated by improving the aqueous compatibility of TiO<sub>2</sub>-NPs. Other PSar initiators which possess phosphonate functional groups could be investigated, such as ((hydroxy-2-naphthylmethyl)phosphonic acid, or bisphosphonates, for example. The applications of the P-O-M bond-forming ability could also be investigated further, such as for metal scavenging or corrosion inhibition. Chapter 4 further developed the P-O-M bond-forming ability to improve the aqueous compatibility of fluorescent and phosphorescent CaNPs with amphiphilic PSar-based PAAs. The reported materials show early promise as theranostic devices to acidic environments such as tumours, with pH-responsive Dox delivery and afterglow. Optimisation of these materials to further improve the pH stimuli-responsiveness or bioimaging ability with NIR-fluorescent CNDs would bring these materials closer to the clinic, as well as cell viability assays against healthy cells and tumour cells.

In Chapter 5, PAla was synthesised via ROP of alanine anhydride from PEG methyl ether and catalysed by Sn(Oct)<sub>2</sub> for the first time. A high equivalence PAla was prepared, offering an alternative route to PAla avoiding Ala-NCA, and thus the commercialisation of PAla is closer to realisation. The amphiphilic PEG-*b*-

PAla polymers were able to self-assemble into NPs and Dox was loaded with high efficiency. The NPs were stimuli-responsive with respect to pH, which offers these biocompatible polymers potential use as chemotherapeutic delivery vehicles. The efficacy of the reported NPs could be tested against live cells. To explore the mechanical properties of PAla, the ROP of alanine anhydride by  $\text{Sn}(\text{Oct})_2$  but initiated by other alcohols, such as small molecule alcohols rather than macroinitiators, could be investigated. The resulting PAla (with no macroinitiator) could then be subjected to mechanical testing such as tension and tear strength testing. These large  $M_w$  PAla polymers may be spun into fibres and potentially woven together for a material with potentially excellent mechanical properties and is biodegradable.

Chapter 6 described the straightforward colouration of PGI by the covalent grafting of a thiol-modified dye. Chemical organogels were formed upon covalent cross-linking, and the 2-phenylethanol-swollen organogel revealed significant antimicrobial activity against both *S. aureus* and *E. coli*. The biodegradability and biocompatibility of PGI and cross-linked PGI needs further exploration in order for the materials to be used in practice. In Chapter 7, the addition of limited amounts of *N*-phenyldiethanolamine within the step-growth polymerisation reaction mixture of PET-PEG afforded a handle for sequential diazotisation and azo coupling reactions. *In situ* chromophore creation was demonstrated resulting in permanent colouration and ensures that coloured wastewater is not produced. The dyed PET-PEG copolymer showed potential use in advanced laundry formulations as a soil release polymer and an optical brightener. The method of permanent colouration may feasibly be applied for the colouration of a wide range of step-growth polyesters, and so optimisation of such for different polyesters should be investigated. Additionally, other aromatic amines could be explored to increase the range of colours possible with this process. Sulfanilamide conjugation to the polyester may impart antifungal and/or antimicrobial activity to the polymer, which could also be investigated.

## List of Publications

1. H. Yu, N. Ingram, J. V. Rowley, S. Parkinson, D. C. Green, N. J. Warren and P. D. Thornton, “Thermoresponsive polysarcosine-based nanoparticles”, *Journal of Materials Chemistry B*, 2019, **7**, 4217-4223. Associated correction: 2019, **7**, 7795.
2. J. V. Rowley, J. Exley, H. Yu, G. S. Mircale, A. S. Hayward and P. D. Thornton, “Covalent polyester colouration by *in situ* chromophore creation”, *Chemical Communications*, 2020, **56**, 6360-6363.
3. H. Yu, J. V. Rowley, D. C. Green and P. D. Thornton, “Fucose-modified thermoresponsive poly(2-hydroxypropyl methacrylate) nanoparticles for controlled doxorubicin release from an injectable depot”, *Materials Advances*, 2020, **1**, 1293-1300.
4. H. Yu, N. Ingram, J. V. Rowley, D. C. Green and P. D. Thornton, “Meticulous Doxorubicin Release from pH-Responsive Nanoparticles Entrapped within an Injectable Thermoresponsive Depot”, *Chemistry – A European Journal*, 2020, **26**, 13352-13358.
5. J. V. Rowley, P. Wall, H. Yu, G. Tronci, D. A. Devine, J. J. Vernon and P. D. Thornton, “Antimicrobial Dye-Conjugated Polyglobalide-Based Organogels”, *ACS Applied Polymer Materials*, 2020, **2**, 2927-2933.
6. J. V. Rowley, P. A. Wall, H. Yu, M. J. Howard, D. L. Baker, A. Kulak, D. C. Green and P. D. Thornton, “Triggered and monitored drug release from bifunctional hybrid nanocomposites”, *Polymer Chemistry*, 2022, **13**, 100-108.